USAAMRDL-TR-76-18

12

FEASIBILITY ANALYSIS FOR A MICROWAVE DEICER FOR HELICOPTER ROTOR BLADES

Mechanics Research, Inc.
Electronics Systems Division
7929 Westpark Drive,
McLean, Va. 22101

May 1977

Prepared for

EUSTIS DIRECTORATE
U. S. ARMY AIR MOBILITY RESEARCH AND DEVELOPMENT LABORATORY
Fort Eustis, Va. 23604

EUSTIS DIRECTORATE POSITION STATEMENT

This report provides a theoretical demonstration of the technical feasibility of deicing helicopter rotor blades via microwave heating. The microwave concept appears to offer significant cost and weight advantages over existing electrothermal systems; however, the estimates of system power requirements and individual component efficiencies that directly relate to system weight and cost are subject to laboratory verification. Two practical aspects of a microwave deicer that must ultimately be addressed are: (1) development or identification of a dielectric material that can serve the dual purpose of an erosion shield and surface waveguide and (2) testing to demonstrate any effects that such a concept will have on radar cross section and detectability of a helicopter. It is believed that both of these areas can be adequately addressed during the design and development phase.

The microwave deicing concept described herein will be considered along with other candidate advanced blade ice protection techniques for further research and development, the ultimate goal being a reliable, lightweight, low-cost rotor blade ice protection system for Army helicopters.

Mr. Gene A. Birocco of the Military Operations Technology Division served as project engineer for this effort.

UNCLASSIFIED

SECURITY CLASSIFICATION OF THIS PAGE *(When Data Entered)*

REPORT DOCUMENTATION PAGE	READ INSTRUCTIONS BEFORE COMPLETING FORM
1. REPORT NUMBER (14) USAAMRDL-TR-76-18 (12)	2. GOVT ACCESSION NO.	3. RECIPIENT'S CATALOG NUMBER (9)
4. TITLE *(and Subtitle)* (6) FEASIBILITY ANALYSIS FOR A MICROWAVE DEICER FOR HELICOPTER ROTOR BLADES.	5. TYPE OF REPORT & PERIOD COVERED Final Report,
	6. PERFORMING ORG. REPORT NUMBER
7. AUTHOR(s) (10) Bertram Magenheim and Frank Hains	8. CONTRACT OR GRANT NUMBER(s) (15) DAAJ02-75-C-0042 new
9. PERFORMING ORGANIZATION NAME AND ADDRESS Mechanics Research, Inc., Electronic Systems Division, 7929 Westpark Drive, McLean, Virginia 22101	10. PROGRAM ELEMENT, PROJECT, TASK AREA & WORK UNIT NUMBERS (16) 63209A 1F263209DB38 00 019 EK
11. CONTROLLING OFFICE NAME AND ADDRESS Eustis Directorate, U.S. Army Air Mobility Research and Development Laboratory Fort Eustis, Virginia 23604 (11)	12. REPORT DATE May 1977 (12) 04
	13. NUMBER OF PAGES 278
14. MONITORING AGENCY NAME & ADDRESS *(if different from Controlling Office)* (12) 280 P.	15. SECURITY CLASS. *(of this report)* UNCLASSIFIED
	15a. DECLASSIFICATION/DOWNGRADING SCHEDULE

16. DISTRIBUTION STATEMENT *(of this Report)*

Approved for public release; distribution unlimited.

17. DISTRIBUTION STATEMENT *(of the abstract entered in Block 20, if different from Report)*

18. SUPPLEMENTARY NOTES

19. KEY WORDS *(Continue on reverse side if necessary and identify by block number)* Analysis, Feasibility, Helicopters, Rotors, Blades, Microwaves, Ice, Adhesion, Surface Waveguides, Dielectrics, Heat, Dissipation, Cost, Weight, Power

20. ABSTRACT *(Continue on reverse side if necessary and identify by block number)*

An analysis of the feasibility of utilizing microwave energy to deice helicopter rotor blades is presented. The analysis is based upon the coupling of microwave energy to the ice layers by means of dielectric surface waveguides coating the leading edge of the rotor blades where the ice accumulates. The thickness of the dielectric coating is adjusted by design so that in the ice-free condition a loosely bound surface wave may propagate along the coating with only minor losses. As the ice accumulates,

DD FORM 1 JAN 73 1473 EDITION OF 1 NOV 65 IS OBSOLETE

UNCLASSIFIED

SECURITY CLASSIFICATION OF THIS PAGE *(When Data Entered)*

4-10316 LB

tending to thicken the surface waveguide, the surface wave, becoming more tightly bound, undergoes higher losses, dissipating much of its energy in the lossy ice layer. The dissipation of energy in the ice raises its temperature above the level required for breaking its bond to the blade, which occurs before any melting takes place. The analysis considers four major topics: 1) the properties of surface waveguides, including dielectrics suitable electrically and mechanically for rotor blades and the dielectric properties of rotor ice; 2) dissipation and heat distribution theory; 3) the problems associated with coupling microwave energy to the surface waveguides; and 4) the typical and preliminary configuration, and the cost of installing microwave deicers in UH-1 helicopters in production quantities.

PREFACE

This report presents the results of an analysis of the feasibility using microwave energy for deicing helicopter rotor blades. The program was conducted by Mechanics Research, Inc., Electronic Systems Division, under contract DAAJ02-75-C-0042 to the Eustis Directorate, U.S. Army Air Mobility Research and Development Laboratory (USAAMRDL), Fort Eustis, Virginia. The technical monitor of the project for USAAMRDL was Mr. G. Birocco. The Mechanics Research, Inc., program was under the direction of Mr. B. Magenheim, Project Manager. Personnel contributing to the program included Messrs. F. Hains and L. Withers.

SUMMARY

The purpose of this analysis was to determine the feasibility of deicing helicopter rotor blades with microwave energy. The major benefits sought were:

- Low Power Consumption
- Low Weight
- Low Cost
- High Reliability
- High Maintainability

These benefits are not to be gained at the expense of any countermeasure goals.

It is believed, on the basis of this analysis, that the deicing of helicopter rotor blades with microwave energy is feasible and the major goals listed above are achievable. A summary of the expected results is presented in the following table. This summary indicates potentially significant improvements in the state of the rotor blade deicing art.

Summary of Findings - Microwave Deicer for UH-1 Helicopter Rotor Blades

OPERATING FREQUENCY	RECURRING COST	INCREMENTAL[1] WEIGHT	PRIME POWER CONSUMPTION
2,450 MHz	< $10,000	35.5 lbs.	< 1500 Watts
5,850 MHz	< $10,000	51 lbs.	< 1500 Watts
22,125 MHz	< $16,000	49 lbs.	< 2000 Watts

[1]"Incremental weight" means the weight increase above the basic weight of a UH-1 with no rotor blade deicing. It includes a weight savings due to the replacement of the existing heavy metallic erosion shield with a lightweight dielectric deicer boot that will function adequately as an erosion shield

THE CONFIGURATION AND THE RELIABILITY AND MAINTAINABILITY OF THE MICROWAVE DEICER

A block diagram and the preliminary illustrations of the microwave deicer are shown in Figures 51 through 69. The deicer boot is seen to be nothing more than a highly erosion-resistant dielectric layer with suitable microwave couplers that can be placed either at the root or tip end of the blade. The simplicity of the design will translate into increased reliability and maintainability.

Initial designs do not anticipate any sophisticated controllers. It is expected that there will be no need for zone cycling as in thermal deicers. It is believed that the power economy and deicing sequence achieved with cyclic electro thermal deicers are achieved inherently in the microwave deicer. A sequencer may be desirable that would periodically turn the microwave generator on and off during deicing and would be contained within the tube power supply.

With the exception perhaps of the feeder (waveguide mounted in the transmission shaft) and deicer boot, all parts are field replaceable. All electronics are particularly unsophisticated and can be trouble-shot in the field with minimal training.

MICROWAVE DEICER BOOT EROSION RESISTANCE AND DIELECTRIC PROPERTIES

Section 2.0 identifies dielectric materials which satisfy the dual requirements of providing satisfactory dielectric properties and the necessary sand, dust and rain erosion resistance. In particular, attention is directed to the dielectric "alumina", a material exhibiting the required dielectric properties and one which has been used routinely as an erosion shield for propellers. This material, perhaps in combination with high molecular weight polyethelene, should provide erosion shields equivalent to or better than nickel at a considerably lower weight penalty. The rain erosion characteristics of Alumina, Lennite, Polyurethane and Nickel are analyzed in Section 2.0 and significant results are presented in Figures 17, 18 and 19.

COUNTERMEASURE CONSIDERATIONS

Detectability

In general, deicers are seldom on: they are turned on during icing conditions only and then only at the discretion of the pilot. Any radiation from the microwave deicer will be unintentional. The design will be such as to eliminate or minimize radiation. All attempts will be made to insure that the rotor is not a good antenna. All these measures will be combined to produce low probability of intercept by a high gain, scanning, enemy receiver.

Climatic conditions that exist when icing occurs are the same as those that provide some attenuation of microwave signals. In addition, deicers that operate at 22,125 MHz fall in the oxygen water-vapor absorption bands, where any leakage signal will undergo heavy attenuation, practically eliminating the probability of intercept.

Radar Cross-section

There will be no effect on the radar cross-section in the case of metal rotor blades. Some investigators believe that coating parts of the metal blade with dielectrics will reduce the radar cross-section if done properly.

In the case of composite blades, since the dielectric deicer boots can be made by design to be transparent they will permit the utilization of many of the radar cross-section reduction techniques contemplated and discussed in the literature.

RECOMMENDATIONS

Initiate a program that will result in a microwave deicer prototype suitable for flight testing. This will include the following phased tasks:

1) Demonstrate performance of surface waveguides in the laboratory by building and testing experimental surface waveguides as defined in Task 1a, Appendix C.

2) After successful design of the experimental surface waveguides, use them to demonstrate the shedding of statically grown ice layers in the laboratory as described in Task 2a of Appendix C.

3) After successful completion of Task 2a, use the experimental surface waveguides to shed droplet impact ice loaded by centrifugal force in a whirling arm experiment validating the power requirement predictions of Section 3. Tests are described in Task 2c, Appendix C.

4) Enter into a full scale microwave deicer prototype development program resulting in a microwave deicer for full scale flight testing. The prototype should be capable of retrofitting existing helicopters as well as for use in future helicopters.

EXPERIMENTAL FREQUENCIES

It is recommended that initial experimental frequencies be close to 22,125 MHz. This will permit experimental establishment of feasibility as well as take advantage of existing microwave distribution hardware developed originally for helicopter rotor radar and described in Section 7, as well as existing tube technology. Conclusions drawn at this frequency are applicable to other frequencies as well.

TABLE OF CONTENTS

Page

LIST OF ILLUSTRATIONS

LIST OF TABLES

SECTION 1

INTRODUCTION TO THE MICROWAVE DEICING CONCEPT

The basic concept studied in this feasibility analysis is the use of a surface waveguide, composed of a thin layer of a stable dielectric material that has approximately the same dielectric constant as ice, for deicing the surface to which it is applied (Figure 1).

In the ice-free condition, microwave power injected into the surface waveguide will propagate down the dielectric slab, with relatively little loss of power, by successive reflections off its boundaries in what has been termed a "trapped mode". This requires that the angle of incidence of the microwaves on the air-dielectric interface exceed the critical angle, θ_c, for total reflection. As layers of ice begin to form on the dielectric surface, they will have the effect of thickening the surface waveguide so that microwave energy will be able to penetrate the ice layer and be totally reflected at the ice-air interface (Figure 1). The ice layers containing the microwave energy will be subject to dielectric heating by dissipation of the microwave energy and will experience a temperature rise. Only the ice will experience appreciable heating, the ice itself providing the mechanism for converting microwave energy to heat. In the conventional thermal deicing system, electrical energy is converted to heat in resistive heater pads that line the entire leading edge of the rotor blade; the entire leading edge of the blade is heated, including portions where there may not be any ice.

The high efficiency of the microwave deicer depends upon the following considerations:

1) The microwave technique provides a means of efficiently directing energy only to the existing ice. The blade itself is not heated. If there is no ice, there will be only minor heating of the blade.

2) The motion of the blade produces significant aerodynamic heating of the ice and the blade, particularly near the tip.

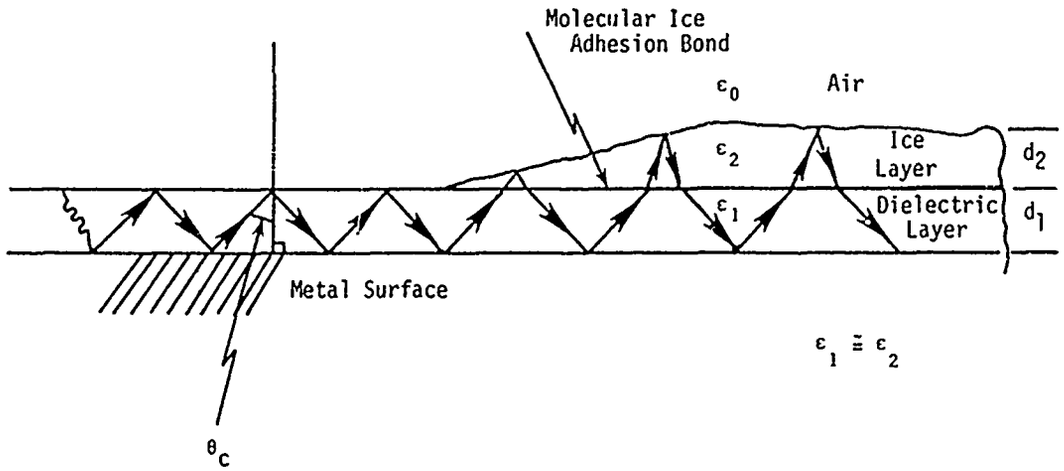

ε_0 = dielectric constant of air

ε_2 = dielectric constant of ice

ε_1 = dielectric constant of dielectric layer

d_1 = thickness of dielectric layer

d_2 = thickness of ice layer

Figure 1. Guidance of microwave energy by composite ice-dielectric surface waveguide

3) The large centrifugal force exerted on the ice layers provides a significant energy source tending to dislodge the ice. Even with aerodynamic heating, however, this force is insufficient to break the ice adhesion bond but becomes sufficient upon the application of relatively small quantities of microwave energy.

4) The use of hard, smooth, erosion-resistant dielectric coatings, such as Alumina, significantly reduces the strength of the ice adhesion bond, resulting in lower microwave power requirements.

5) Microwave heating is very rapid and is localized to the vicinity of the adhesion layer. The rate at which the ice is heated can be controlled by pulsing. The loss of heat by conduction is a relatively slow process so that there is a very rapid net gain in heat.

The estimate of prime power requirements to shed ice on two UH-1 rotor blades, based upon the above assumptions, is computed in Section 3 and is illustrated in Figure 2, where it can be seen to be an order of magritude less than that required by an equivalent thermal deicer.

An additional consideration that will improve the deicing efficiency is the shape of the power density curve of the microwave mode. Many modes may exist on the surface waveguide. In Section 2, two modes (the TE_1 and TM_0 modes) are identified as being particularly advantageous. A cross-section of the surface waveguide with various thicknesses of ice, showing the power density versus ice accretion, is illustrated in Figures 3 and 4 for the TE_1 and TM_0 modes respectively. As can be seen from these figures, both of these modes are only loosely bound to the surface guide when no ice layer exists; e.g., most of the energy contained in the mode is propagated in the air region immediately adjacent and parallel to the surface guide. This loose binding accounts for the low attenuation constant exhibited by these modes when no ice exists. As the ice layers accumulate, thickening the surface guides, the modes become more tightly bound with larger fractions of the power being propagated within the composite ice-dielectric surface guide. Under these conditions the attenuation constant, the energy dissipated per inch, rises rapidly, the major portion of energy being dissipated in the ice, which has a higher loss tangent than the stable

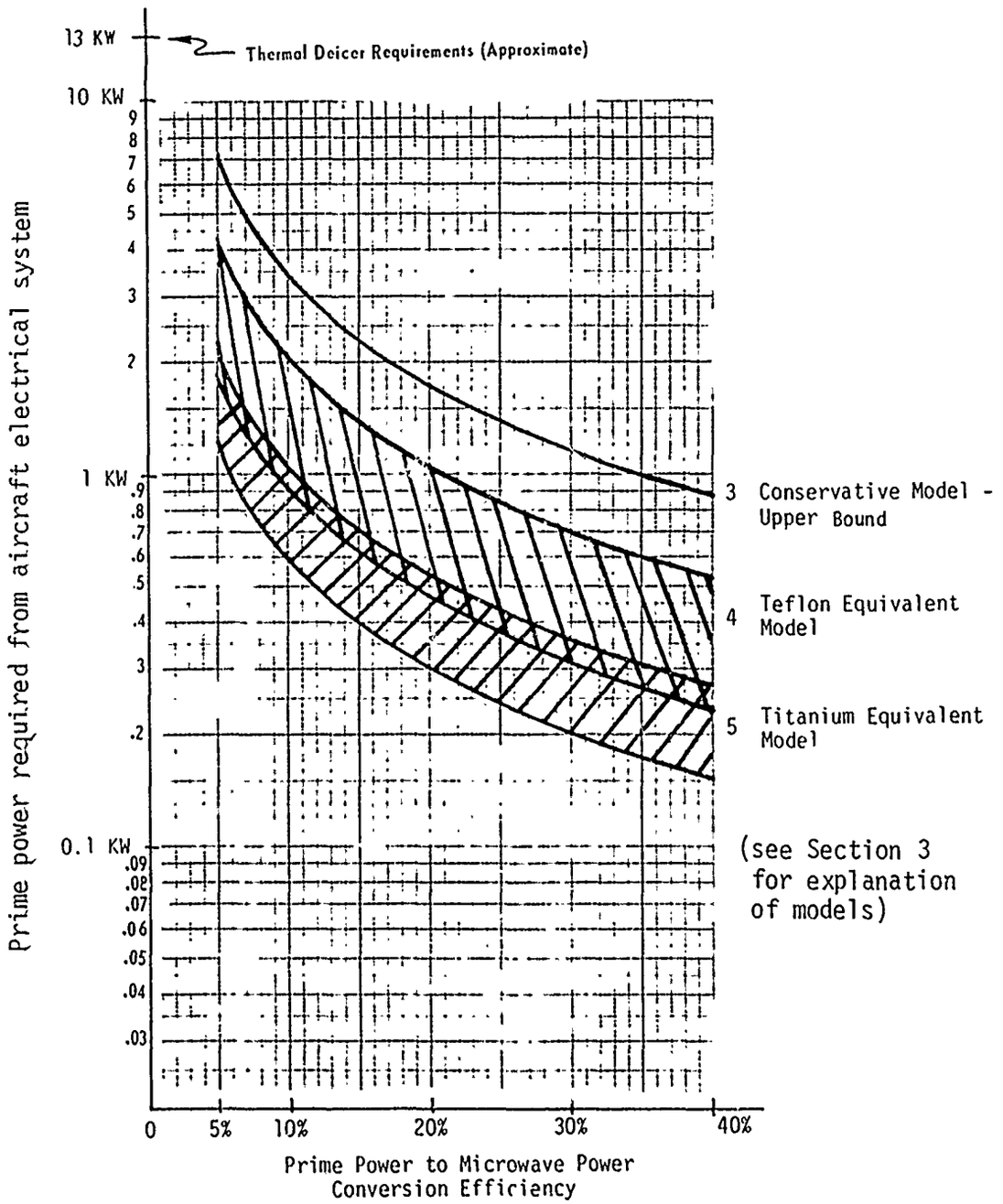

Figure 2. Estimated prime power required to shed ice on two UH-1 rotor blades
T_∞ = -20.9°C

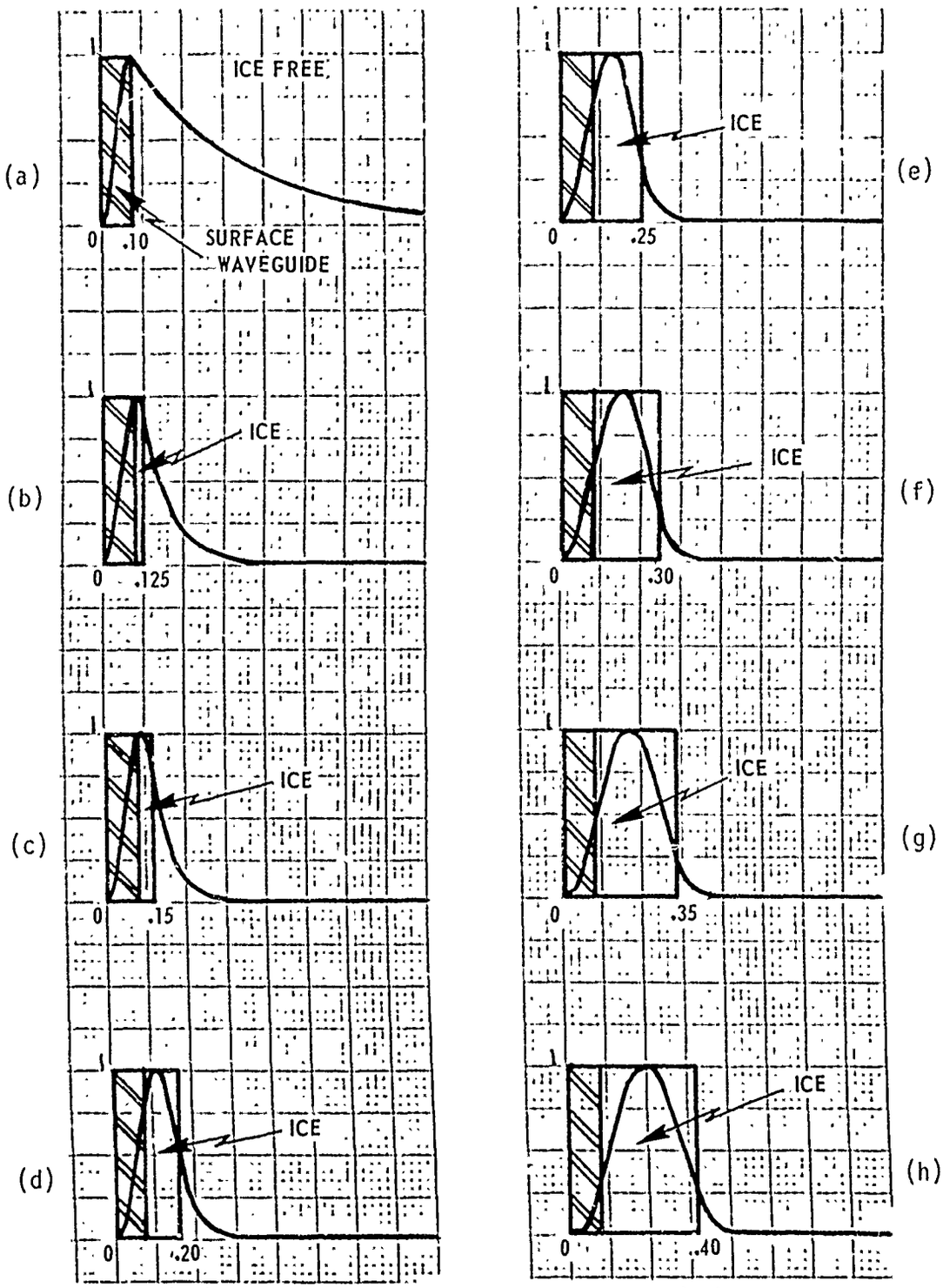

(Note: ordinate of each graph is normalized power density)

Figure 3. Calculated power density versus ice accretion on a dielectric surface waveguide, TE_1 mode (f = 22,125 MHz)

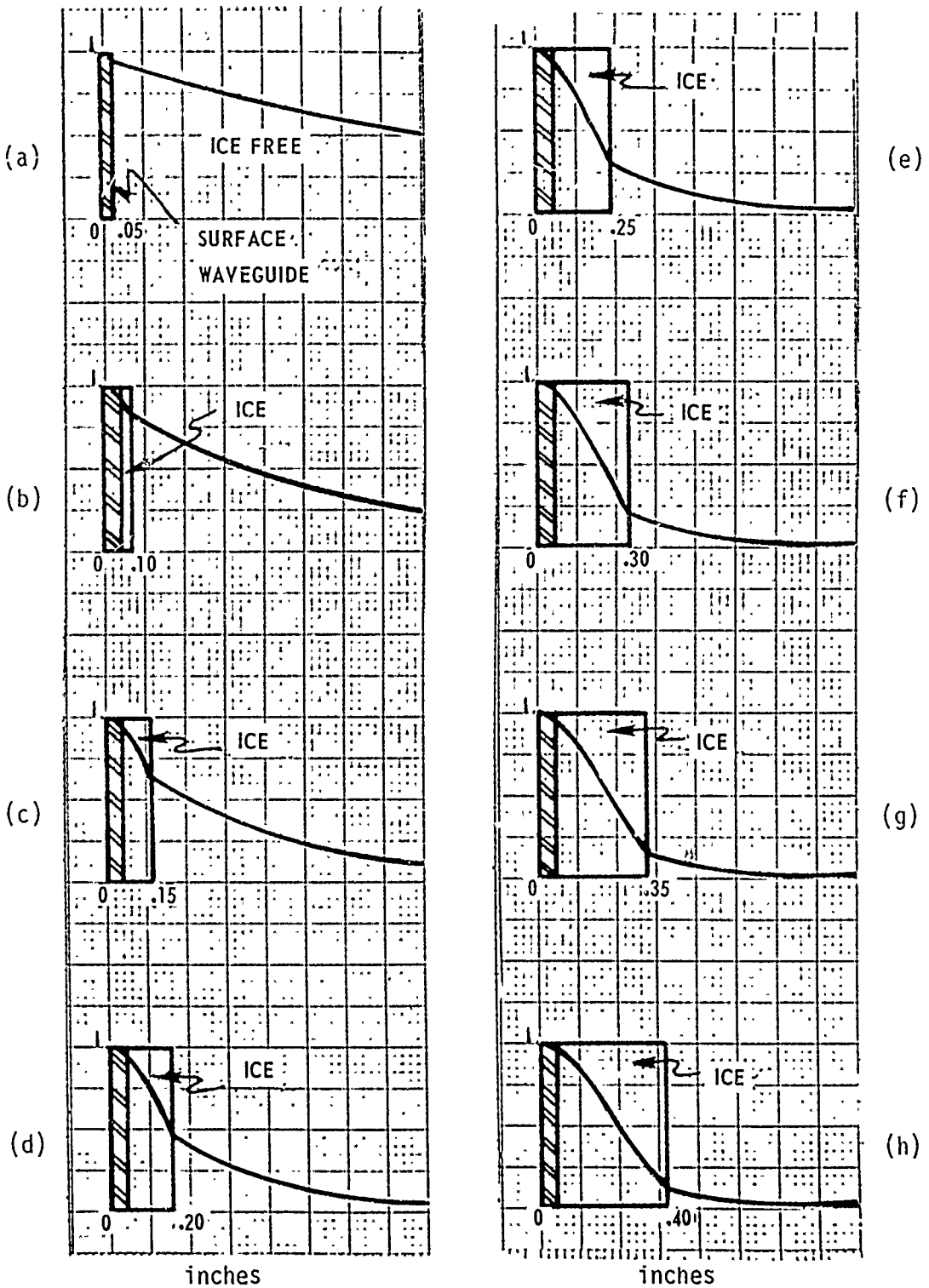

(Note: ordinate of each graph is normalized power density)

Figure 4. Calculated power density versus ice accretion on a dielectric surface waveguide, TM_0 mode (f = 5,850 MHz)

dielectric substrate. An illustration of the rapid increase in attenuation with ice accretions, as calculated in Section 3, is shown in Figures 5 and 6 for the TE_1 and TM_0 modes respectively.

The TE_1 mode has another interesting characteristic which should be noted. From Figure 3 it can be seen that when no ice exists, the power density reaches a peak just inside the dielectric to air interface. As the ice accumulates, this peak moves into the ice layers but stays close to the ice adhesion bond. This mode may thus be used to direct microwave energy primarily to the dielectric regions containing the dielectric to ice interface, having the effect of rapidly heating the interface causing the ice to shed more quickly than otherwise.

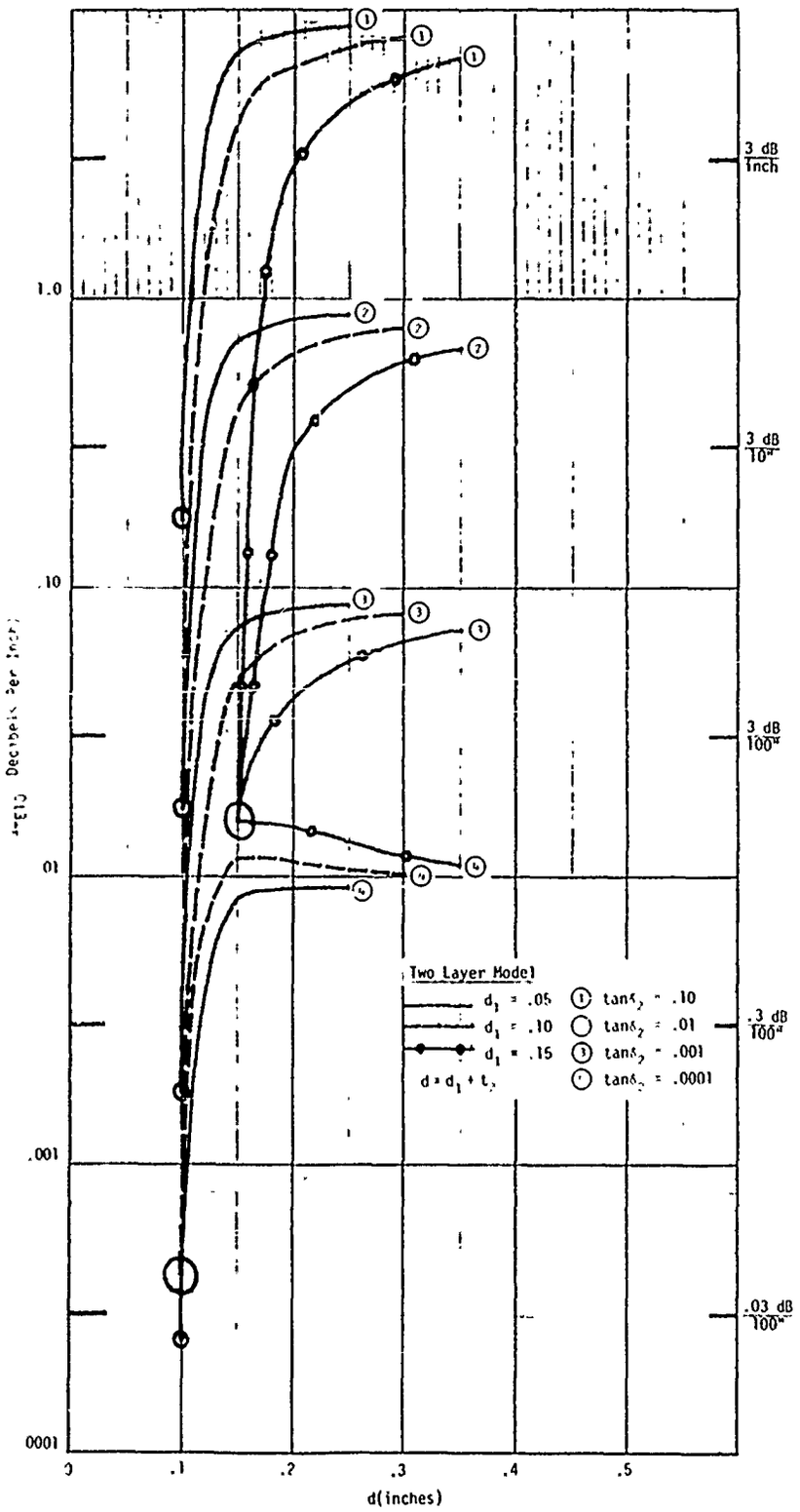

Figure 5. Attenuation versus thickness of dielectric for TE_1 odd mode
f = 22,125 MHz, ε_1 = 2.8, $\tan\delta_1$ = .0002

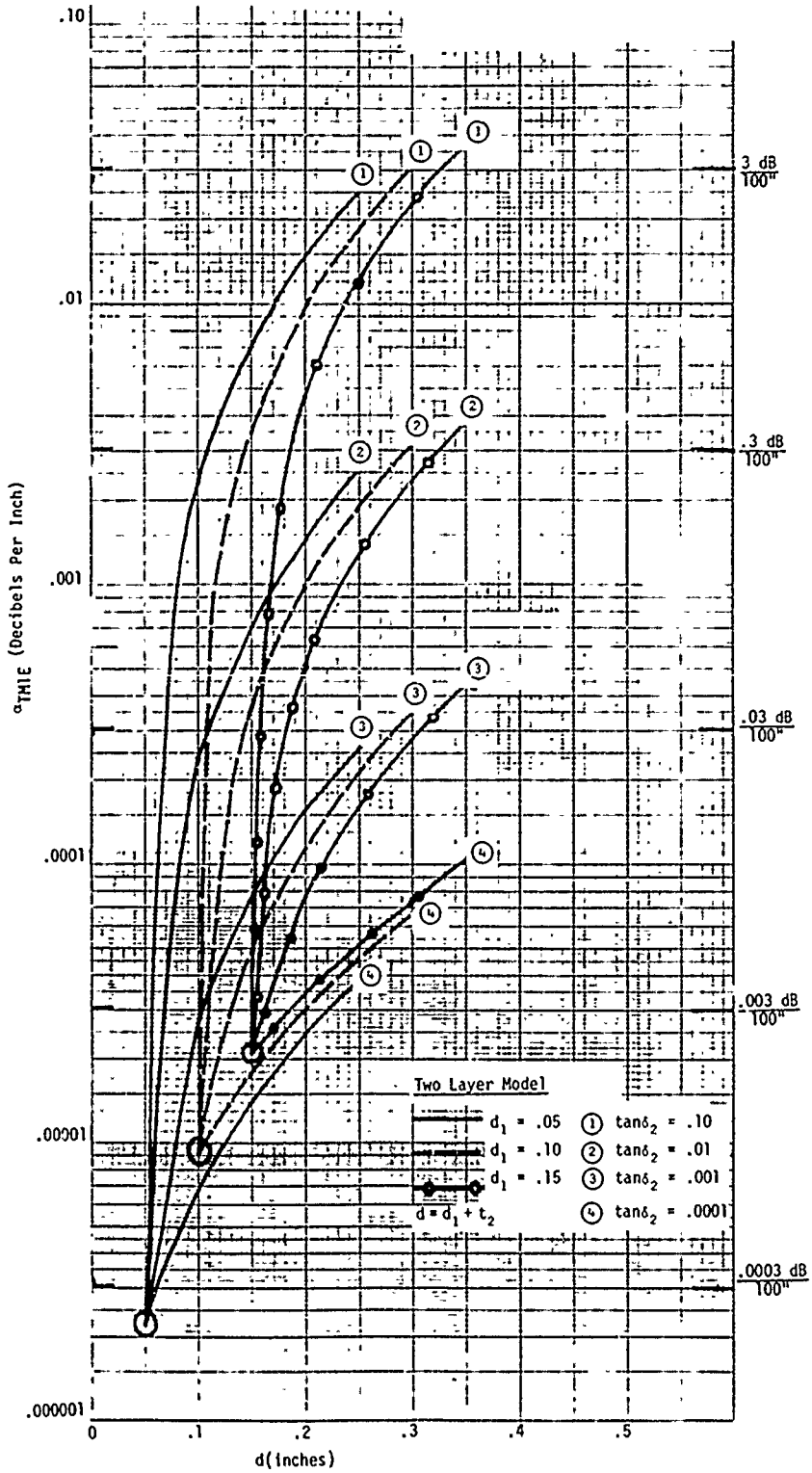

Figure 6. Attenuation versus thickness of dielectric for TM_0 mode
f = 2,450 MHz, ε_1 = 2.8, $\tan\delta_1$ = .0002

SECTION 2

PHASE I - SURFACE WAVEGUIDES

QUALITATIVE DISCUSSION OF SURFACE WAVEGUIDES

Most readers are probably familiar with rectangular or coaxial waveguides; these structures are formed from closed, cylindrical metal tubes. Probably fewer readers are familiar with surface waveguides, which are open boundary structures capable of guiding an electromagnetic wave along a surface. These structures are capable of supporting waves which are intimately bound to the surface of the structure, the wave propagating in a direction parallel to the surface with relatively little loss; hence it is named a surface waveguide. The fields are characterized by an exponential decay in the direction normal to the surface.

There are many surface structures which are capable of supporting surface waves; some are illustrated in Figure 7. This study has placed emphasis on the dielectric slab and dielectric-coated metal plane surface waveguide (a, b and f, Figure 7) simply because they appear to be compatible with the kinds of surfaces and shapes encountered on metal or composite helicopter rotor blades. Other structures illustrated in Figure 7 behave in a similar manner and may have other deicing applications.

A very satisfying physical view of dielectric slab surface waves is given in Figure 1. Wave propagation in a dielectric slab requires that the angle of incidence of the propagating wave on the air-dielectric interface exceed the critical angle. While this point of view is correct and may be made to give exact quantitative relationships, it is more convenient to describe these surface waves as wave solutions to Maxwell's equations. This mathematical treatment, which is used here, is presented in Appendix A.

Many modes of propagation may exist in dielectric slab lines. The reader interested in the general treatment of these modes is referred to Appendix A and References 1 and 2. Modes of propagation identified in

[1]R. Collin, Field Theory of Guided Waves, New York: McGraw-Hill, 1960.

[2]Ramo, Whinnery and Van Duzer, Fields and Waves in Communication Electronics, New York: John Wiley & Sons, 1965.

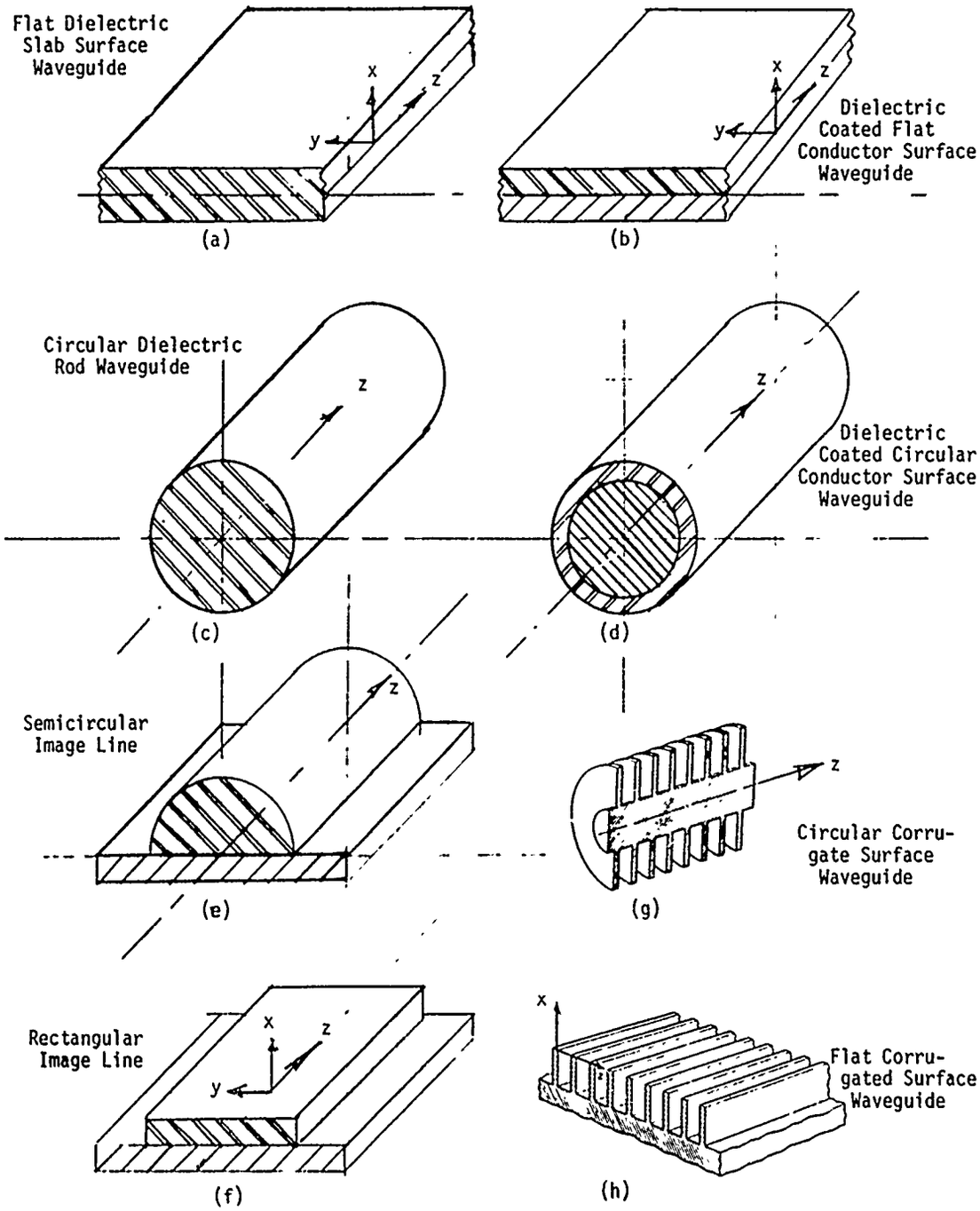

Figure 7. Some structures capable of supporting surface waves

Notes: Double cross hatch = dielectric
Single cross hatch = metal
z = direction of propagation

this study as being of interest to deicing helicopter rotor blades are the TM_0, TM_1, TE_0 and TE_1 modes, the field amplitudes of which are illustrated in Figure 8. The left column of Figure 8 illustrates amplitudes of the mode fields in the dielectric slab line while the right column illustrates them on dielectric coated metal planes. It is noted from the right hand column that the presence of the metal surface suppresses the TM_1 and TE_0 modes since these modes require a finite value of tangential electric field strength at the metal surface.

The direction of propagation of the wave is, by convention, always in the z direction, as indicated by the rectangular coordinates on the left side of Figure 8. The x direction is always normal to the slab, and the y direction parallel to the slab. The x-y plane is always the transverse plane.

It should be noted from Figure 8 that evanescent fields exist outside the dielectric that decay exponentially away from it in the x direction, there being no flow of power in this direction. Not all of the energy propagating in the z direction is trapped within the dielectric; some power flow takes place in the air adjacent and parallel to the dielectric in the evanescent fields.

A loosely bound surface wave is one in which more energy flows in the air region than in the dielectric region, whereas a tightly bound wave is one in which more energy is trapped in the dielectric than in the air. Loosely and tightly bound waves are illustrated in a and h, respectively, of Figure 3 for TE_1 modes and a and h of Figure 4 for TM_0 modes. Figures 3 and 4 are computer generated plots of the power flow densities of the TE_1 and TM_0 modes as functions of dielectric thickness (see Equations A-2, A-4, A-10 and A-12 of Appendix A). In loosely bound waves (Figure 3(a)), since most of the energy flow takes place in the air where there is little if any dissipative loss, the attenuation constant is low. As the dielectric thickens, the wave becomes tightly bound (Figure 3(h)), and most of the energy flow is trapped in the dielectric where dissipation may occur, depending upon the loss tangent of the dielectric. Under these conditions, the attenuation constant is high. Thus, as the dielectric thickens, the

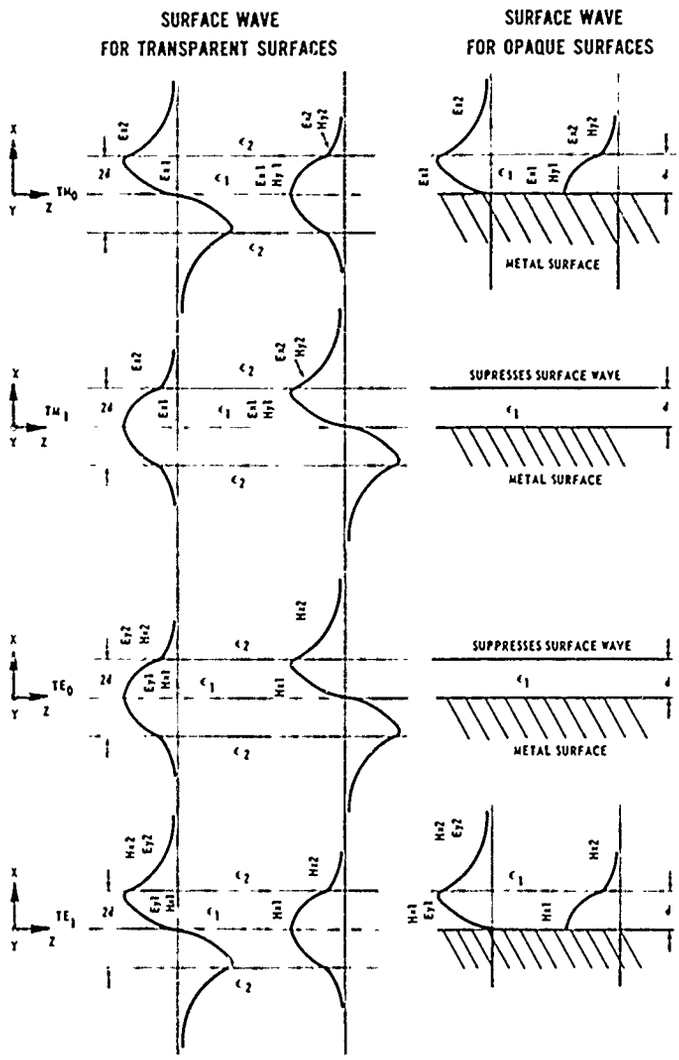

Figure 8. Possible modes of propagation of surface guided waves in dielectric slabs

(Electric and magnetic field strength symbols defined in table of symbols)

attenuation increases rapidly from very low values, leveling off at a very high value (illustrated in Figures 9 through 14) as the wave becomes almost totally trapped. The curves of Figures 9 through 14 were derived with analytical techniques, developed in Appendix A, which permit the computation of the attenuation constant as a function of dielectric thickness, loss tangent and frequency.

Illustrations of the field configurations for the TM_0 and TE_1 modes in a dielectric-slab surface guide are given in Figure 15. These are obtained directly from Equations A-2, A-4, A-10 and A-12 (Appendix A) and show the evanescent fields which exist in the air adjacent to the dielectric and which transmit much of the energy when the waves are loosely bound. These fields tend to collapse as the dielectric thickens and the wave becomes tightly bound.

Cut-Off Properties of Surface Waveguides

The cut=off frequencies of all of the modes in a surface waveguide are found using Equation A-28. Unlike rectangular waveguides, the lowest ordered modes, the TM_0 and TE_0, have no low frequency cutoff. All higher modes have cut-off frequencies below which no propagation can occur. The required thickness of the base dielectric is a function of mode, frequency and dielectric constant. Ideally all microwave frequencies may find use but 2.45, 5.85 and 22 GHz have been designated by the FCC for heating and are non-interfering and therefore of interest to deicing. The required thickness of dielectric to permit the propagation of the TE_1 mode at these frequencies is given in Figure 16 as a function of dielectric constant.

A QUANTITATIVE DESCRIPTION OF SURFACE WAVES AND WAVEGUIDES

Basic surface waveguide theory is developed in Appendix A. This appendix also identifies the field equations of the four modes of propagation in a dielectric-slab surface waveguide, the TM_0, TM_1, TE_0 and TE_1 modes. From these field equations, the power transfer and attenuation equations are developed.

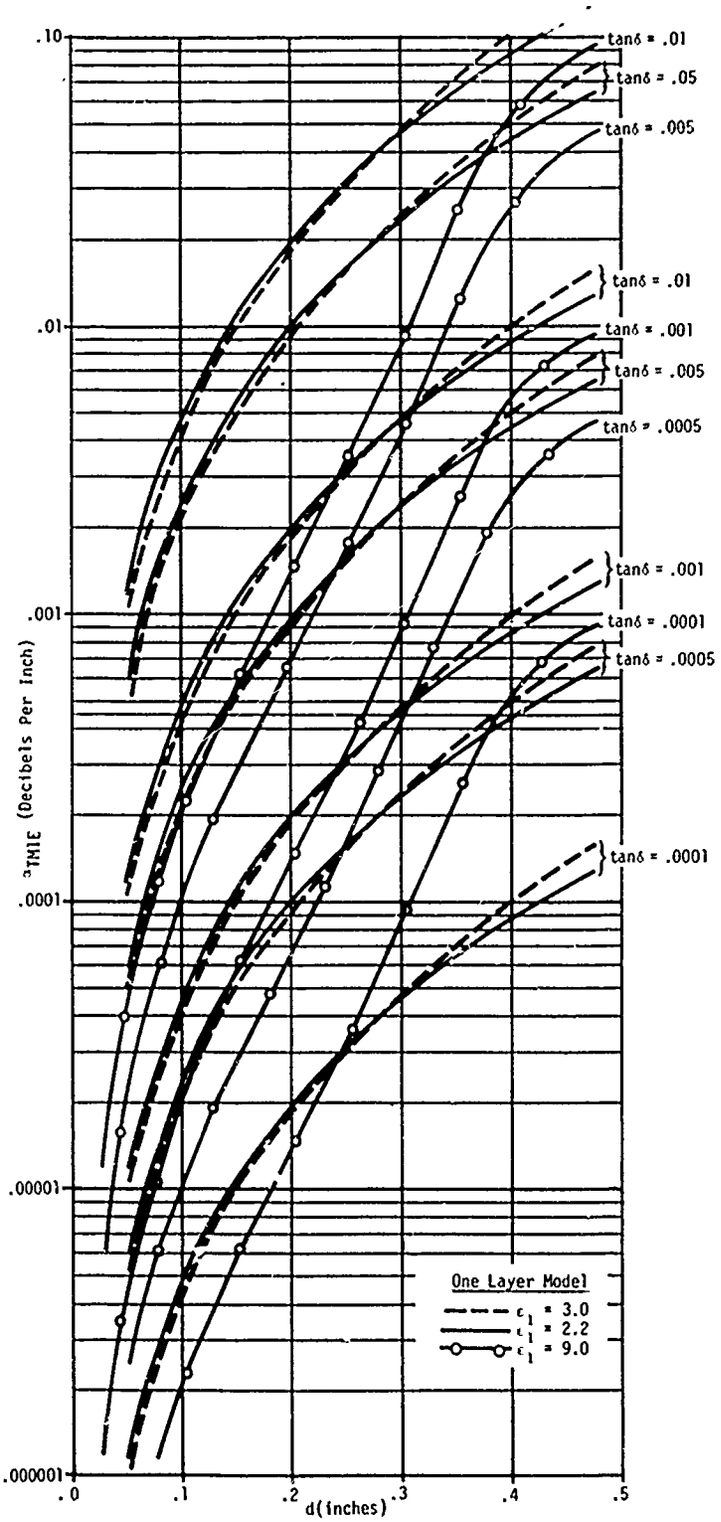

Figure 9. Attenuation versus thickness of dielectric for TM even mode, f = 2,450 MHz

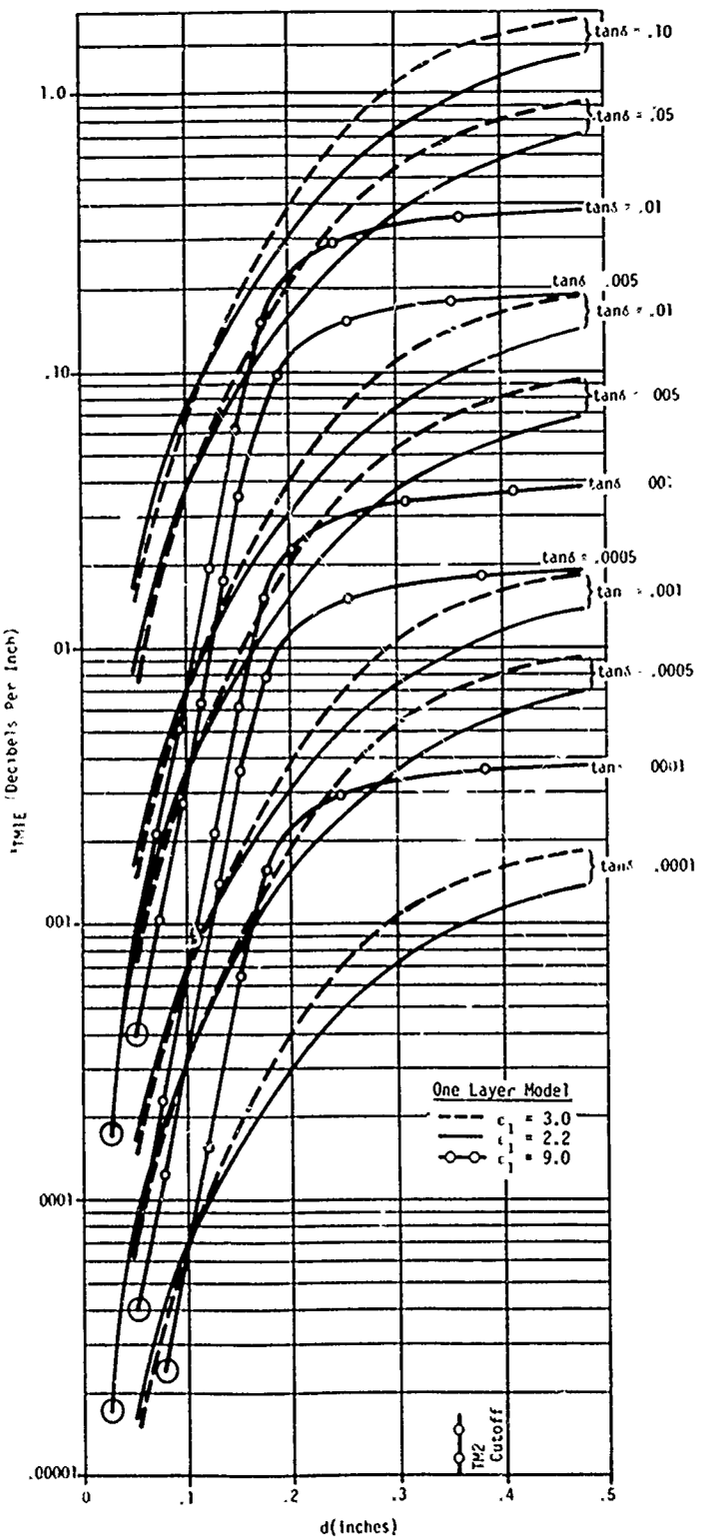

Figure 10. Attenuation versus thickness of dielectric for TM even mode
f = 5,850 MHz

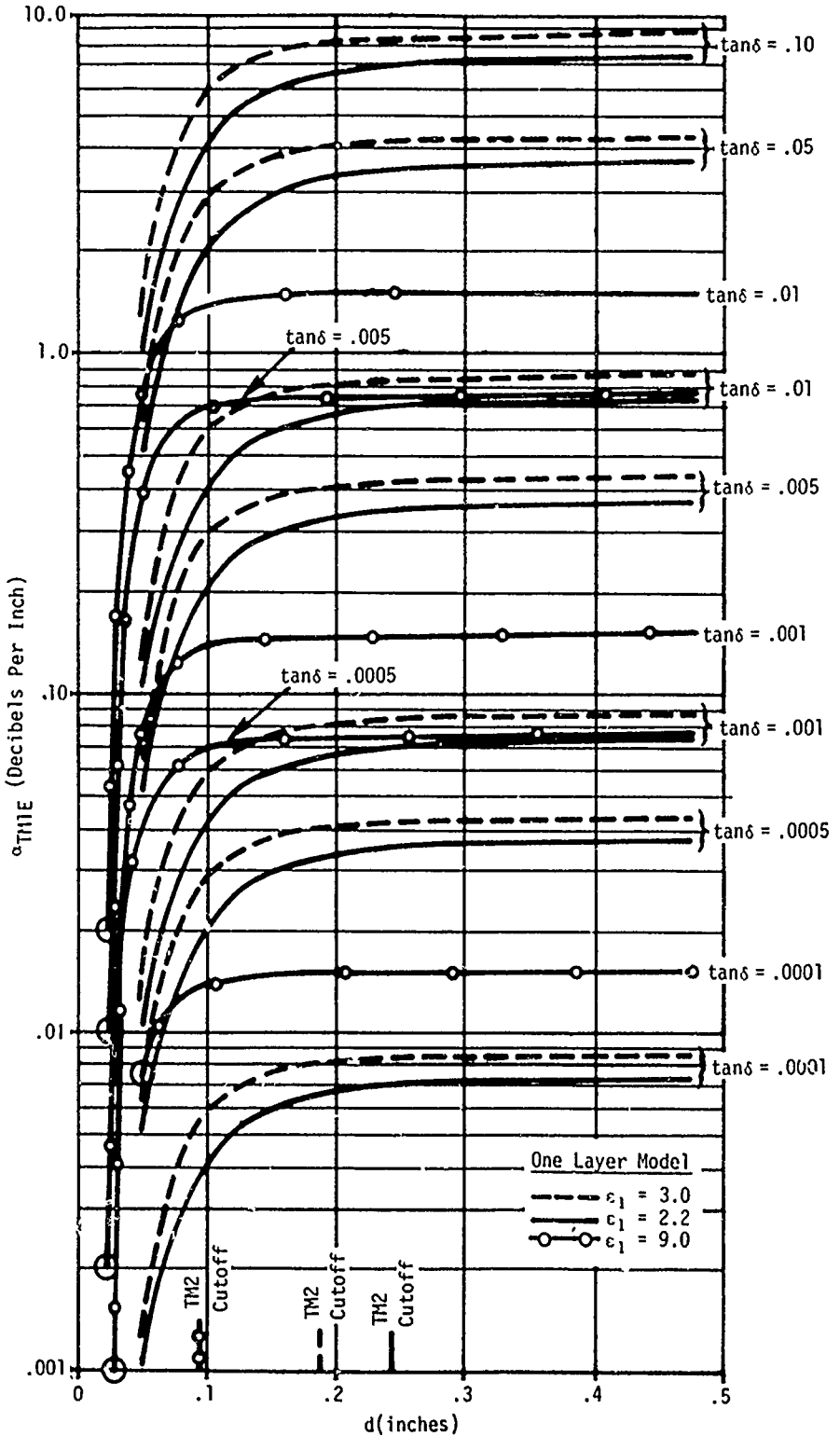

Figure 11. Attenuation versus thickness of dielectric for TM even mode, f = 22,125 MHz

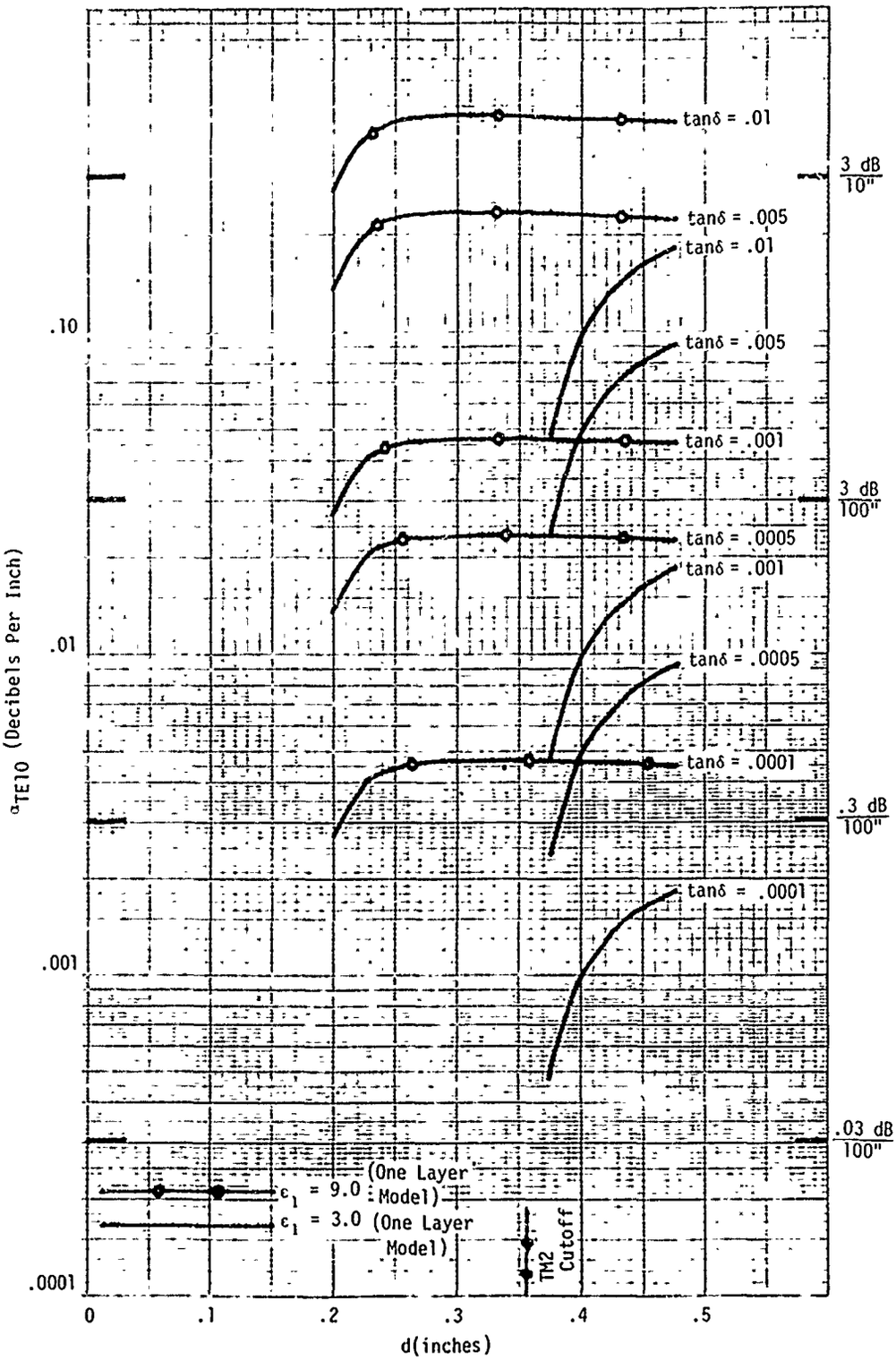

Figure 12. Attenuation versus thickness of dielectric for TE odd mode, f = 5,850

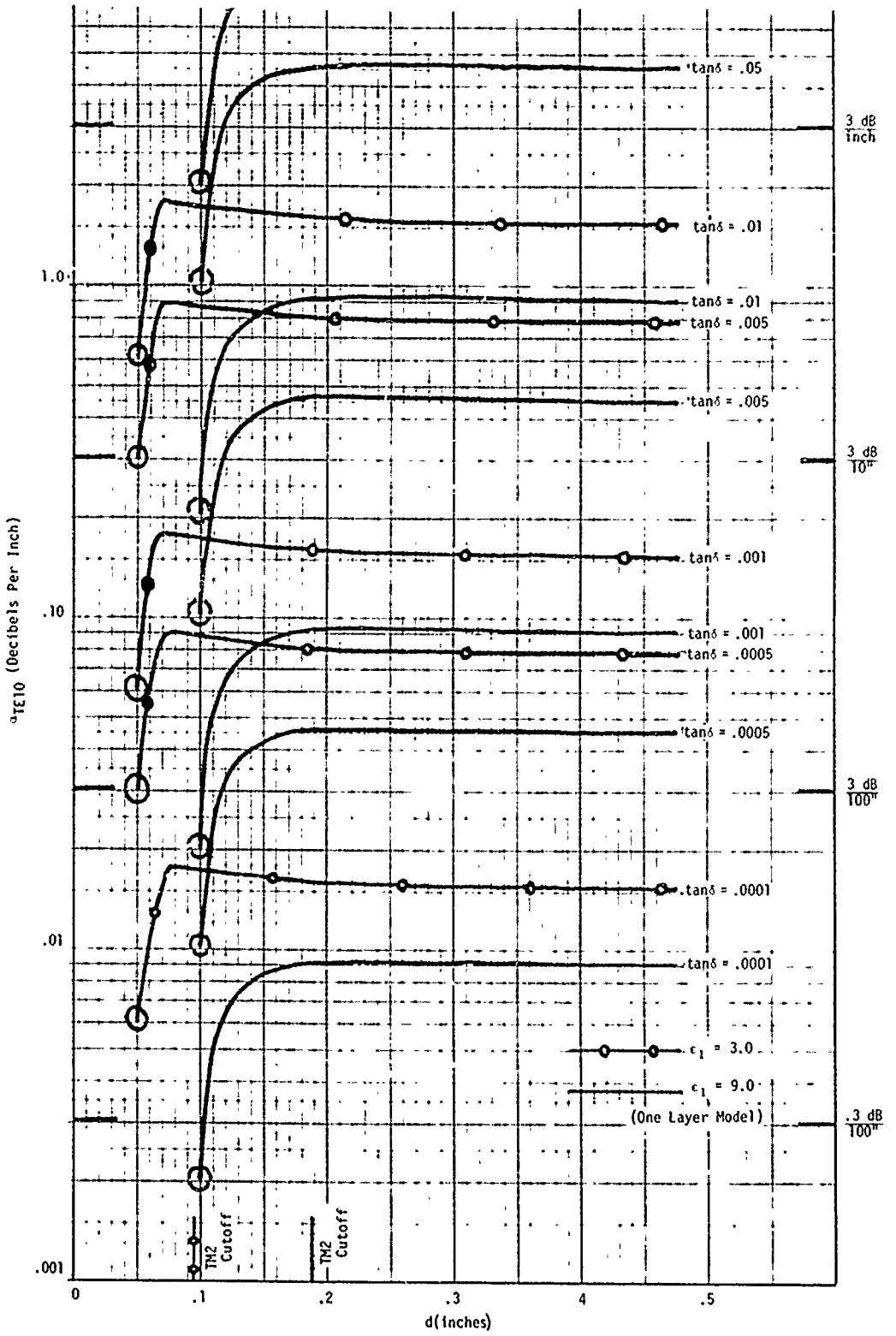

Figure 13. Attenuation versus thickness of dielectric for TE odd mode, f = 22,125 MHz

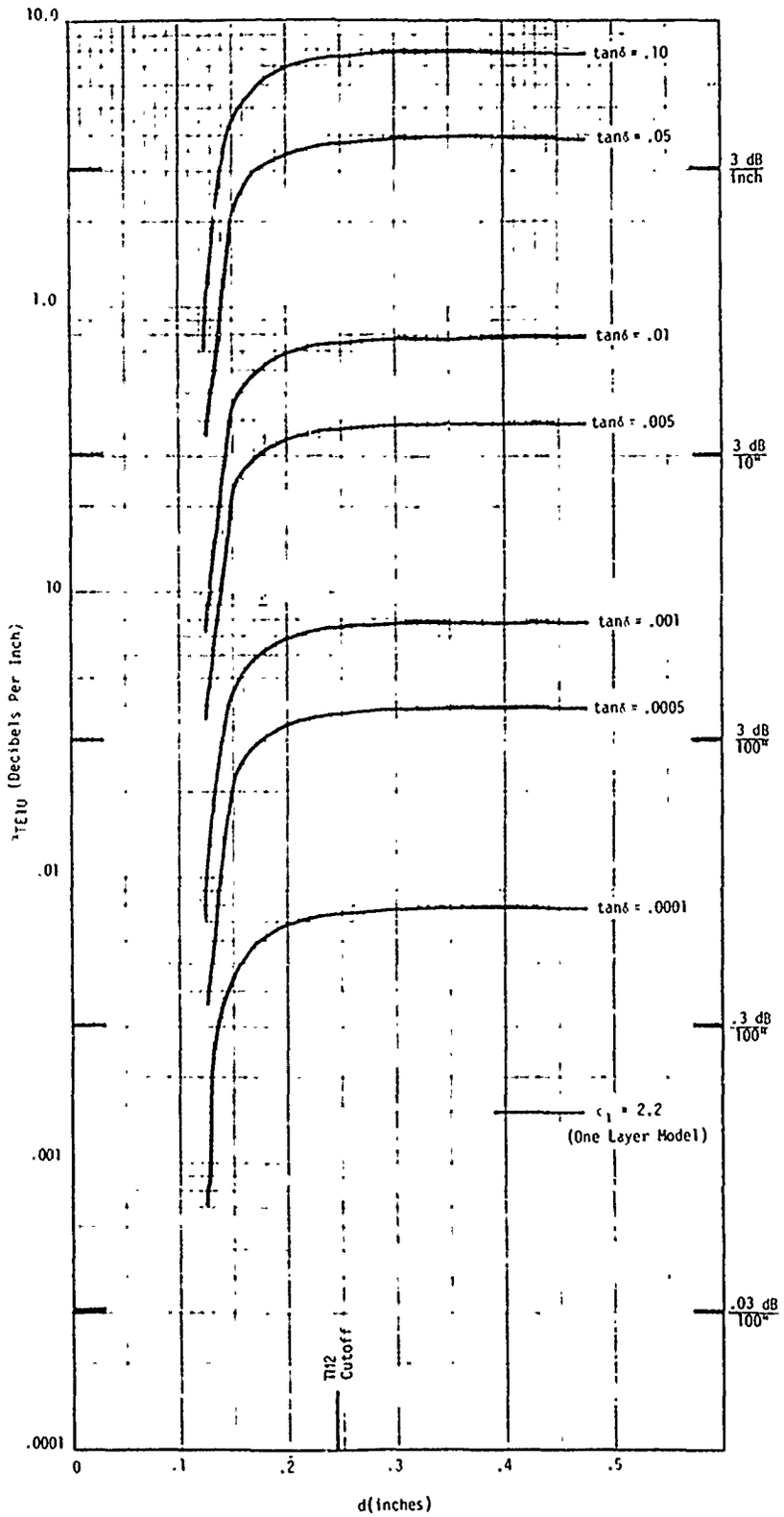

Figure 14. Attenuation versus thickness of dielectric for TE odd mode, f = 22,125 MHz

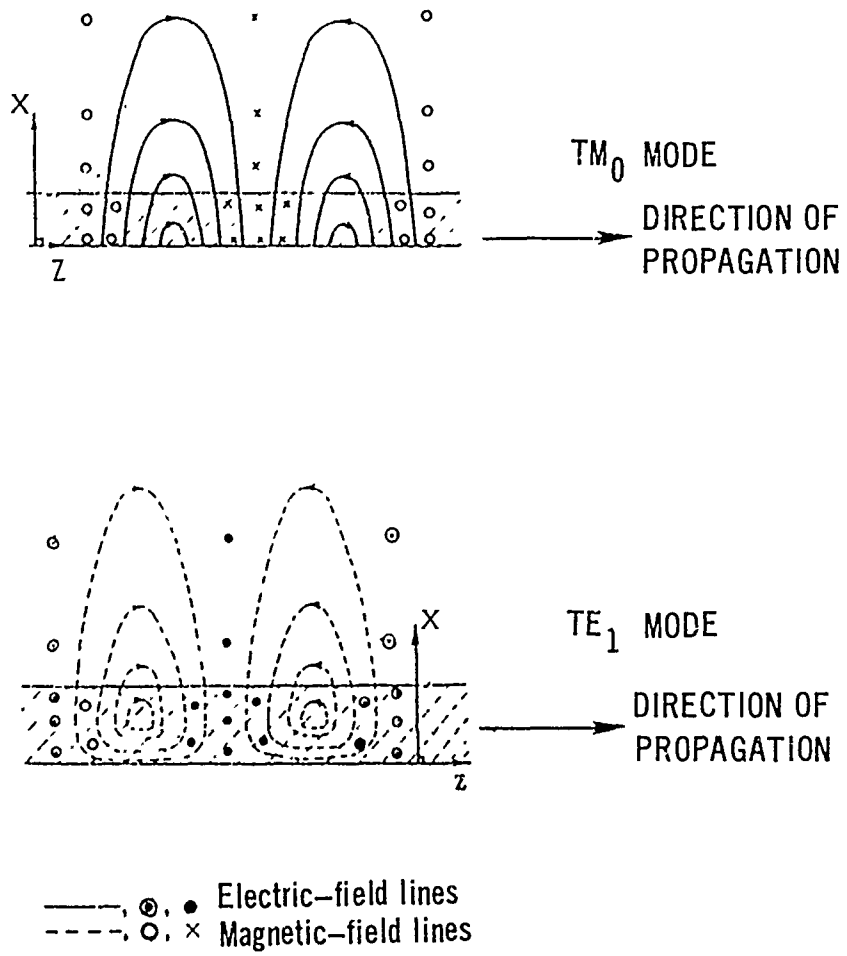

Figure 15. Electric and magnetic field lines for the TM_0 and TE_1 modes in dielectric-slab surface waveguides

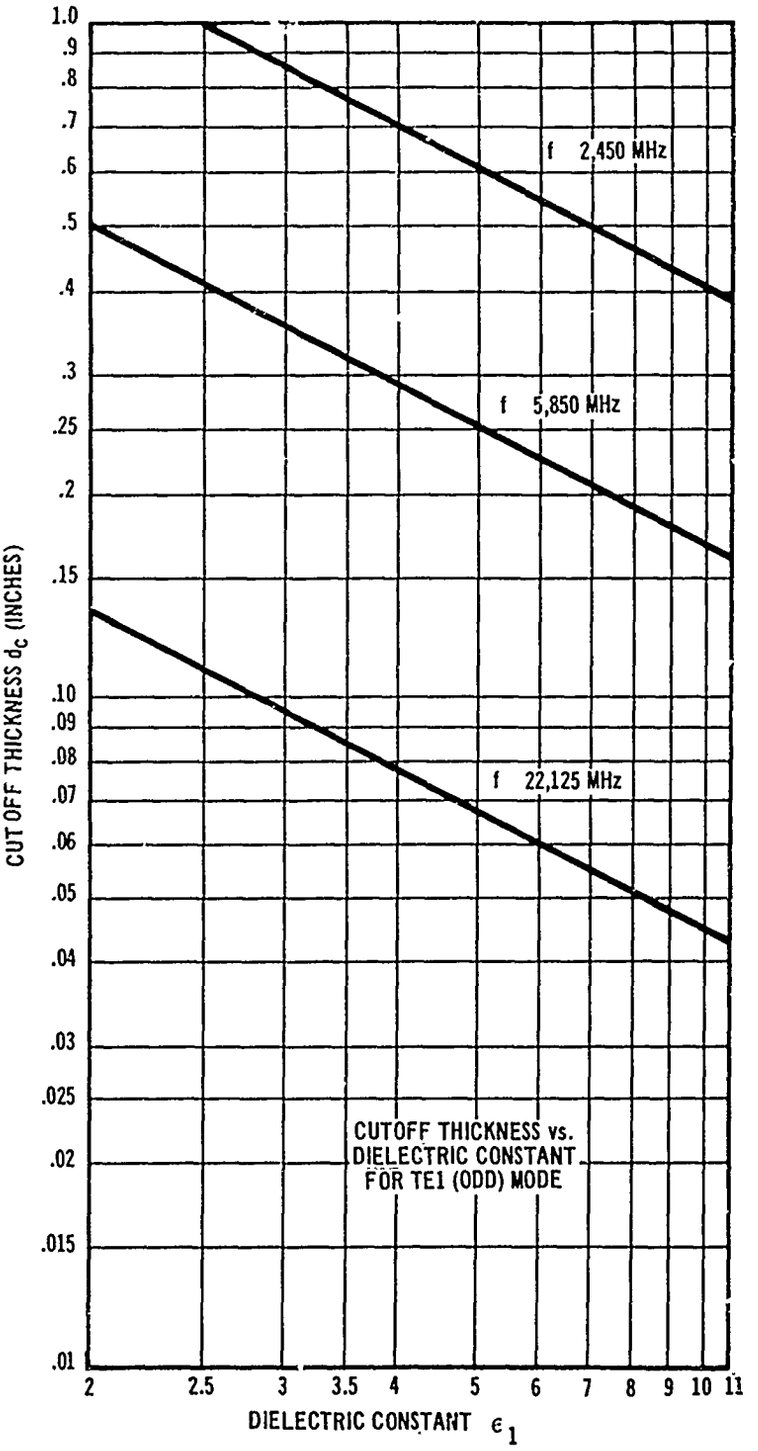

Figure 16. Cutoff thickness versus dielectric constant for TE_1 mode

Using these equations, a computer program was developed that computes the following parameters, completely describing surface waveguide behavior.

TABLE 1. SURFACE WAVEGUIDE PARAMETERS

1	Propagation Constant	β_z
2	Transverse field eigen values	
	Inside dielectric	k_x
	Outside dielectric	K_x
3	Attenuation Constant	α
4	Cut-off frequency	f_c
5	Ratio of power transmitted inside to outside dielectric	P_r
6	Guide Wavelength	λ_g
7	Free space wavelength	λ_o
8	Wavelength in dielectric 1	λ_1
9	Wavelength in dielectric 2	λ_2

The program was used to perform the following tasks:

1) Examination of parameters of Table 1 over the following range of surface waveguides:
   - Frequency f: $f_c \leq f \leq (f_c + 40\ \text{GHz})$

     f_c = cut-off frequency of guide
   - Slab Thickness d: $0.025_{in} \leq d \leq 0.5_{in}$
   - Dielectric Constant ε_1: $1.5 \leq \varepsilon_1 \leq 9.0$
   - Loss Tangent: $.01 \geq \tan\delta \geq .0001$
2) Examination of the parameters of Table 1 in the frequency bands presently assigned to microwave ovens by the FCC, 2450 MHz, 5850 MHz and 22, 125 MHz, for the same values of slab thickness, dielectric constant and loss tangent as in Task 1.

3) Examination of the attenuation characteristics of the TM_0 and TE_1 mode for a three dielectric layer surface waveguide model in which the loss tangent of each layer is different: the bottom layer being the base, low loss layer; the middle layer representing a thin erosion protection coating when required (such as polyurethan); and the top layer being the ice. The results of this program are presented graphically in Figures 27 through 44. It was assumed that the dielectric constant (real part) was the same for each layer. This program thus permits the computation of the microwave power dissipated in each layer, including the ice layer.

4) Generation of plots of the power density of the TM_0 and TE_1 modes as functions of dielectric thickness. These plots are illustrated in Appendix F for 2450 MHz, 5850 MHz, and 22,125 MHz, and demonstrate the unique property of the TE_1 mode of reaching a maximum close to the surface of the guide where the ice layers will adhere. It was in such plots that this property was first identified. The plots can be utilized to determine the degree of binding of the surface wave.

DIELECTRIC MATERIALS FOR SURFACE WAVEGUIDES AND ROTOR BLADE EROSION SHIELDS

The dielectric material for use in the microwave deicer boot must satisfy the dual requirements of providing satisfactory dielectric properties and resistance to sand, dust and rain erosion.

Dielectric Properties of Candidate Materials

A summary of the dielectric properties of candidate materials is given in Table 2. Low-loss surface waveguides can be constructed from all of the materials listed. Polyurethane is included because of its possible use as an erosion coating for other materials. Alumina can be used as a surface waveguide by itself or possibly as an erosion coat for other materials to which it is applied. Thirteen possible combinations of candidate materials are listed in Table 3.

TABLE 2. CANDIDATE DIELECTRIC MATERIALS FOR USE IN SURFACE WAVEGUIDES

MATERIAL		MFR's. DESCRIPTION	TRADE NAME	REF.		1 MHz	1 GHz	3 GHz	10 GHz	25 GHz	MANUFACTURER
Polyethelene (Polyolefin)	1	Irradiated High Density Polyolefin Laminate	Polyguide	3	ϵ_1 tanδ	2.320 .0002	-- --	2.3205 0.00021	2.3215 .0005	-- --	Electronized Chemical Corp.
	2	--	--	4	ϵ_1 tanδ	2.26 <.0002	-- --	2.26 0.00031	-- --	2.26 0.0006	
	3	--	--	5	ϵ_1 tanδ	2.3 <0.0003	2.3 0.0003	-- --	-- --	-- --	--
	4	Ultra-High Molecular Weight Polyethelene(Polyolefin)	Lennite	6	ϵ_1 tanδ	2.3 <.0002	-- --	-- --	-- --	-- --	Westlake Plastics
Quartz	5	High Quartz Fiber Silicone Resin Laminate	Alpha Quartz	7	ϵ_1 tanδ	-- --	-- --	-- --	2.93 0.00098	-- --	Alpha Associates
	6	Fuzed Quartz 100% S_iO_2	--	4	ϵ_1 tanδ	3.78 .0001	3.78 .0002	3.78 .00006	3.78 .0001	3.78 .00025	--
Polyurethane	7	Polyurethane Coatings	Astro-Coat	8	ϵ_1 tanδ	-- --	-- --	-- --	3.16 0.059	-- --	Olin Mathison
	8	--	--	3	ϵ_1 tanδ	5.8 .03-.04	-- --	-- --	-- --	-- --	--
Fiberglass Laminates	9	Epoxy Glass Laminates	--	5	ϵ_1 tanδ	4.4 .022	4.35 .019	-- --	-- --	-- --	--
	10	Silicone Glass Laminates	--	5	ϵ_1 tanδ	-- .002	4.2-4.3 .005-.004	-- --	-- --	-- --	--
	11	--	D-Glass Fiber	9 & 5	ϵ_1 tanδ	3.56 .0005	-- --	-- --	4.0 .003	-- --	Owens Corning
	12	--	E-Glass Fiber	9 & 5	ϵ_1 tanδ	6.33 .001	-- --	-- --	6.1 .006	-- --	Owens Corning
	13	--	S&S2 Glass Fiber	9 & 5	ϵ_1 tanδ	5.34 .002	-- --	-- --	5.3 .007	-- --	Owens Corning
	14	--	E-Glass Silicone Resin	7	ϵ_1 tanδ	-- --	-- --	-- --	3.946 0082	-- --	Owens Corning
	15	--	D-Glass Silicone Resin	7	ϵ_1 tanδ	-- --	-- --	-- --	3.6 .002	-- --	Owens Corning
Ceramics	16	Aluminum Oxide AL_2O_3	Alumina Alismag 753 L-724	5	ϵ_1 tanδ	9.4 .0001	-- --	-- --	-- --	8.9 .0001	--
			Alumina	4	ϵ_1 tanδ	8.8 .00033	-- --	8.79 .001	-- --	-- --	--
			Alumina Saphire	10 & 11	ϵ_1 tanδ	8.6 <.001	-- --	-- --	-- --	8.6 .001	Linde Air

TABLE 3. CANDIDATE MATERIALS WITH AND WITHOUT EROSION COATS

	(a)	(b)	(c)
1	Ultra-High Molecular Weight Polyethelene Erosion Coat	With 12 Mil Polyurethane Erosion Coat	With Alumina Erosion Coat
2	Irradiated, High-Density Polyolefin Laminate Polyguide	With 12 Mil Polyurethane Erosion Coat	With Alumina Erosion Coat
3	High Quartz Fiber Silicone Resin Laminate - Alphaquartz	With 12 Mil Polyurethane Erosion Coat	With Alumina Erosion Coat
4	Glass Laminate Silicone Resin Fiberglass	With 12 Mil Polyurethane Erosion Coat	With Alumina Erosion Coat
5	Alumina Aluminum Oxide	----	----

Erosion Properties of Candidate Materials

The non-metallic materials that possess suitable dielectric characteristics for a microwave deicer may also be susceptible to erosion damage from rain, sand or dust. It is therefore necessary to select a coating that not only has the required electrical properties, but is also erosion resistant and can serve as a protective coating for the substrate.

Three promising candidate materials were identified: Alumina, Lennite and Polyurethane. Lennite is the trade name for a new, high molecular weight polyethylene manufactured by Westlake Plastics Corporation. Lennite is expected to perform better than nickel in sand erosion, but worse than nickel in rain erosion. The hoped-for result is a material that performs better than polyurethane for a combination of exposure to both sand and rain.

Most of the present literature on the erosion of protective coatings is experimental in nature and deals with the measurement of weight loss under a specific set of test conditions. The erosion from solid particles, such as sand, dust, or snow, is not as well understood as rain erosion where a detailed, semi-empirical model is available. The Springer Model was first developed for analyzing the erosion of coated homogeneous materials and later extended to coated composite materials.[12,13] The model considers the stress wave pattern induced by the water hammer pressure from a droplet during its residence time on the coating. Depending on the relative impedance between the coating and substrate, the stress at the coating-substrate surface can either be higher or lower than the corresponding value without a coating. Details of the model and the basic equations are presented in Appendix E.

[12]G.S. Springer, et al., "Analysis of Rain Erosion of Coated Materials," Technical Report AFML-TR-73-227, September 1973 (DDC No. AD 769448).

[13]G.S. Springer, et al., "Analysis of Rain Erosion of Coated and Uncoated Fiber Reinforced Composite Materials," Technical Report AFML-TR-74-180, August 1974 (DDC No. ADA001086).

A computer code called REM (rain erosion model) was developed from the equations in Appendix E to obtain the rain erosion characteristics of coating materials chosen as candidates for a surface waveguide. The input to the program consists of the physical properties of the waveguide and parameters which describe the rain environment. The input quantities for the rain environment are: (See table of symbols, Appendix E.)

- R_i rainfall rate
- d droplet diameter
- A altitude
- V impingement velocity
- θ impingement angle

The remaining input quantities, which are related to the physical properties of the waveguide, are:

- C_c speed of sound in the coating
- H coating thickness
- ρ_c coating density
- ν Poisson's ratio for coating
- S_u ultimate tensile strength of coating
- C_s speed of sound in the substrate
- ρ_s substrate density

The output quantities are:

- t_i incubation time
- t_c time required to erode coating
- t_f total time to erode coating from initial droplet impact
- E erosion rate
- E_{max} erosion rate with droplet impact normal to the surface

The ultimate strengths and impedances of several materials of practical interest are shown in Table 4. Four coating materials were selected for analysis: nickel, polyurethane, Lennite (ultra-high molecular weight polyethylene), and Alumina. Although nickel cannot be used as a surface waveguide, it is listed here for comparison because of its current use as an erosion shield. Aluminum and epoxy glass are the two substrate materials considered in this study.

TABLE 4. ULTIMATE TENSILE STRENGTH AND IMPEDANCE

MATERIAL	Ultimate Strength S_u(KN/m^2)	Impedance z(Kg/m^2 - sec)
Alumina	220. x 10^3	21.6 x 10^6
Aluminum	---	14.0 x 10^6
Epoxy Glass	---	4.18 x 10^6
Lennite (Polyethelene)	46.9 x 10^3	2.16 x 10^6
Nickel	317. x 10^3	40.9 x 10^6
Polyurethane	57. x 10^3	0.271 x 10^6
Water	---	1.46 x 10^6

Of the materials listed, nickel has the highest ultimate tensile strength and largest impedance. Polyurethane has the lowest ultimate tensile strength and also the lowest impedance. It is the only material considered that has an impedance lower than water.

The type of stress* on the substrate surface depends only on the impedances of the coating and the substrate material relative to that of water. Although four combinations of impedance are possible, only three of the cases listed in Appendix E occur for the coating-substrate combinations considered here.

*See Appendix E for full definition.

Table 5 lists the type of substrate stress that results from each combination of coating and substrate materials. The substrate stress is increased above the no-coating value only in the case of Lennite. The impedance of Lennite lies between that of the substrate (either aluminum or epoxy glass) and water, and leads to a Case III type of substrate stress distribution. With a polyurethane coating, a Case II type of distribution with lower substrate stress is formed because its impedance is lower than that of water and the substrate. Alumina and nickel coatings have impedances higher than either the substrate or water so that a Case I type of distribution with lower substrate stress is formed. For a microwave deicer, only polyurethane and Alumina coatings lead to reduced substrate stresses.

Computations were made with the REM code with each of the eight coating-substrate combinations listed in Table 5. The rain intensity was 1 inch/hour at an altitude of 1 km. The coating was subjected to normal impact from 2-mm droplets impinging at 500 mph.

TABLE 5. TYPE OF SUBSTRATE STRESS DISTRIBUTION FOR VARIOUS COATING-SUBSTRATE COMBINATIONS

COATING	SUBSTRATE
	ALUMINUM OR EPOXY GLASS
Polyurethane	Case II, substrate stress reduced
Lennite	Case III, substrate stress increased
Alumina	Case I, substrate stress reduced
Nickel	Case I, substrate stress reduced

The incubation time, defined as the interval from initial droplet impact to the first indication of mass loss, is shown in Figure 17. When the substrate is aluminum, an Alumina coating performs better than a nickel coating. The incubation time for Alumina is about 6×10^4 minutes and is relatively insensitive to the coating thickness. A polyurethane coating has an incubation time that increases rapidly with coating thickness. When the thickness is greater than 60 mils, polyurethane has a longer incubation time than Alumina. Lennite has an incubation time of less than 8 minutes and probably should not be used as a protective coating for aluminum helicopter blades in areas of peak erosion.

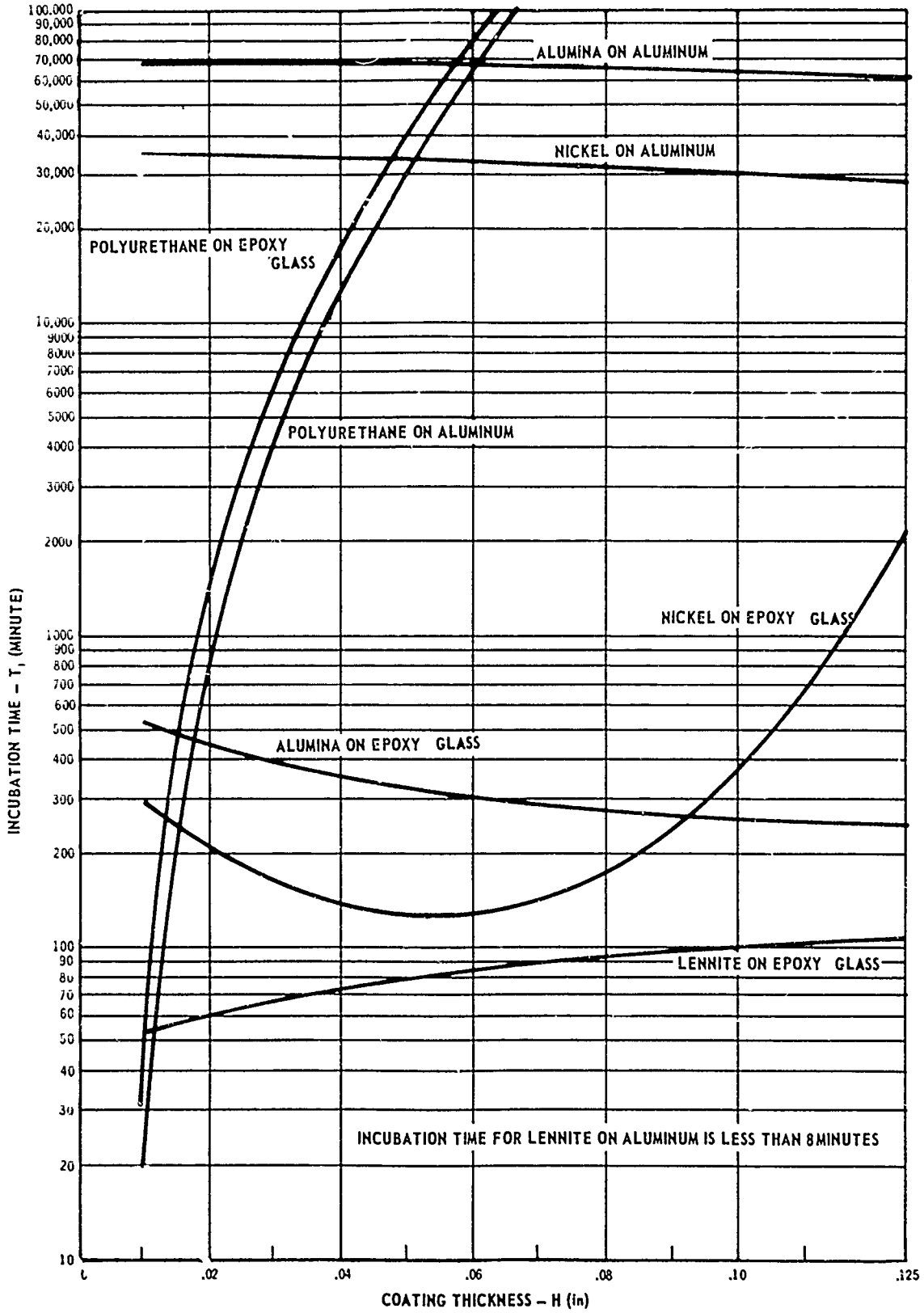

Figure 17. Incubation as a function of coating thickness

The results in Figure 17 are different when the substrate is epoxy glass. Lennite and polyurethane perform better on epoxy glass than on aluminum, while Alumina and nickel perform worse than on aluminum. Alumina has a longer incubation time than nickel for coating thicknesses less than 90 mils, while polyurethane performs better than both nickel and Alumina when its thickness exceeds 15 mils. Although thick polyurethane coatings are predicted to have good erosion resistance, they also have a relatively high loss tangent and may produce higher losses in the surface waveguide, reducing its efficiency when thicker than about 15 mils.

At the end of the incubation period, the coating materials begin to erode at constant rates, given in Figure 18. The coating materials with long incubation times also have lower erosion rates, so that the curves in Figure 18 are inverted from those in Figure 17. Of the materials considered here, Alumina has the lowest erosion rate for thin coatings, and polyurethane has the lowest erosion rate for thick coatings. Alumina has a lower erosion rate than nickel for both aluminum and epoxy glass substrates.

The total erosion time is the sum of the incubation time and the time to erode through the coating. It gives an indication of the total effectiveness of the coating as a protective shield. The total erosion times shown in Figure 19 are similar to the incubation times shown in Figure 17. As with incubation times, Alumina performs best for thin coatings and polyurethane for thicker coatings. In actual practice, however, a coating would be replaced before the end of its effective incubation time.

The above results were based on the assumptions of normal impact and steady state conditions. There are a number of factors that tend to increase the effectiveness of a particular coating when used on a helicopter blade. The rain droplets impinge on the surface at various angles because of the curvature of the surface of the blade and aerodynamics of flow field. Figure 20 shows the increase in incubation time over the minimum value at normal impingement. When the impingement angle is increased from zero to 26 degrees, the incubation time is doubled. Likewise, the erosion rate also decreases rapidly with oblique impingement, as shown in Figure 21.

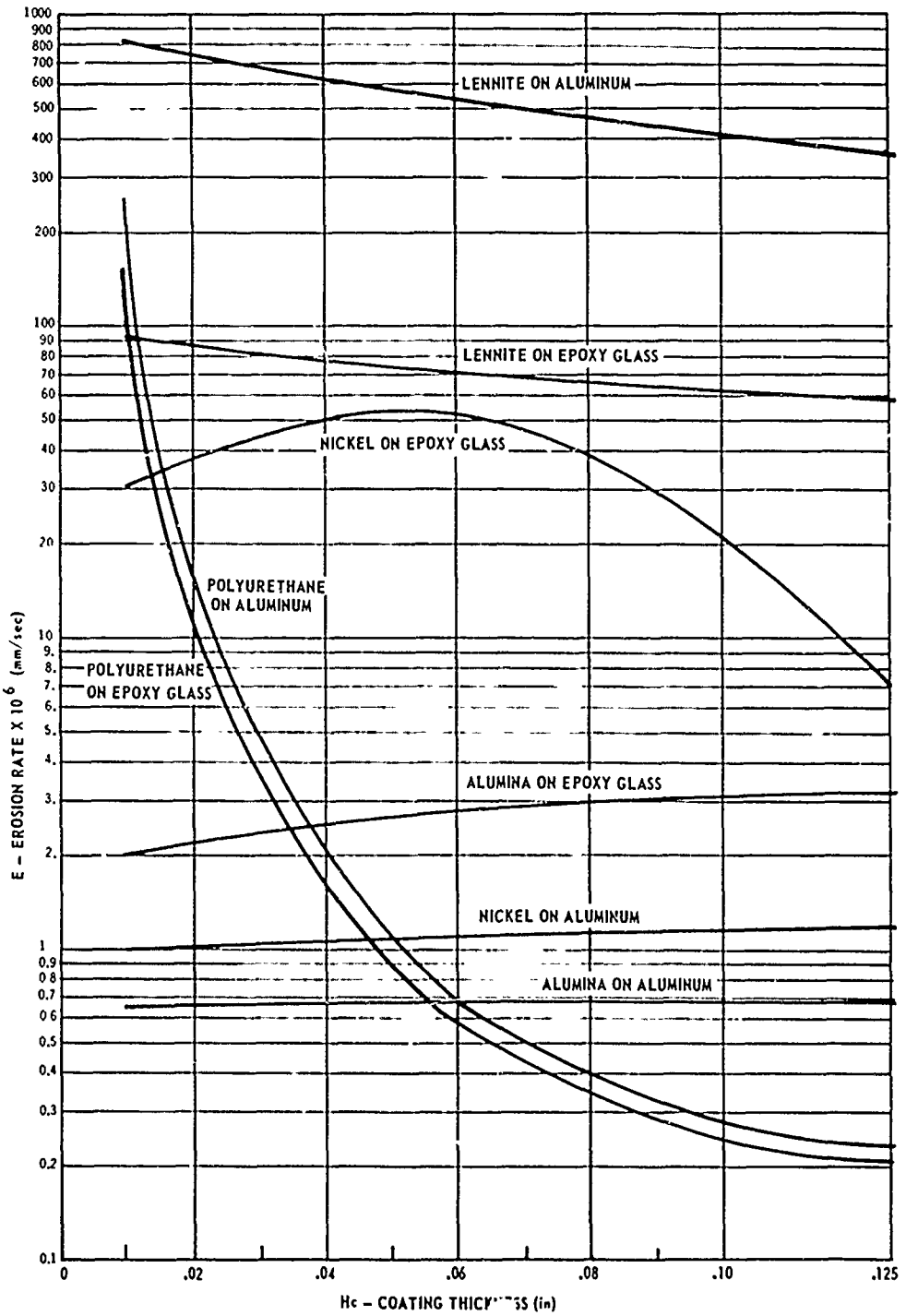

Figure 18. Erosion rates of coated materials

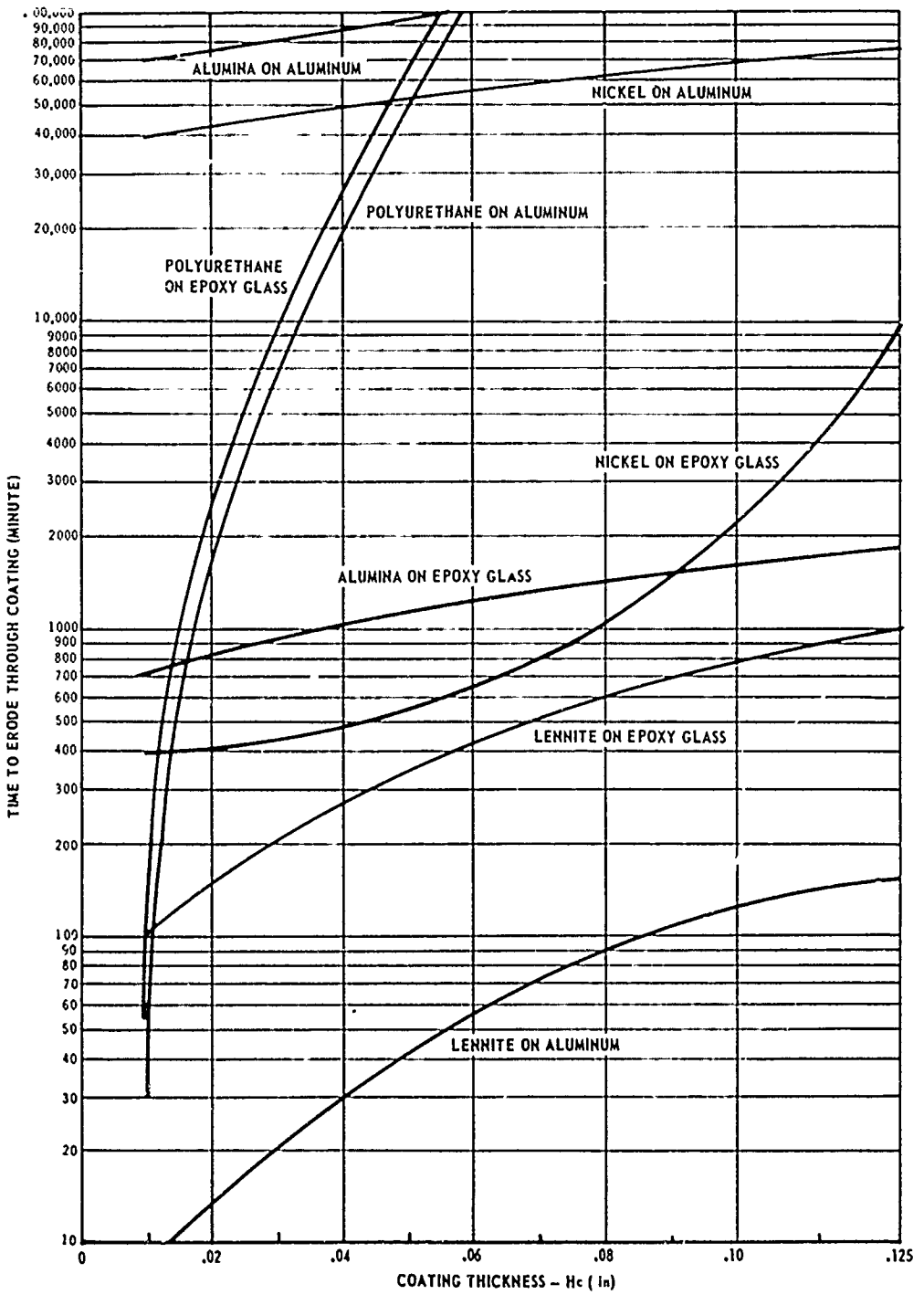

Figure 19. Total erosion times

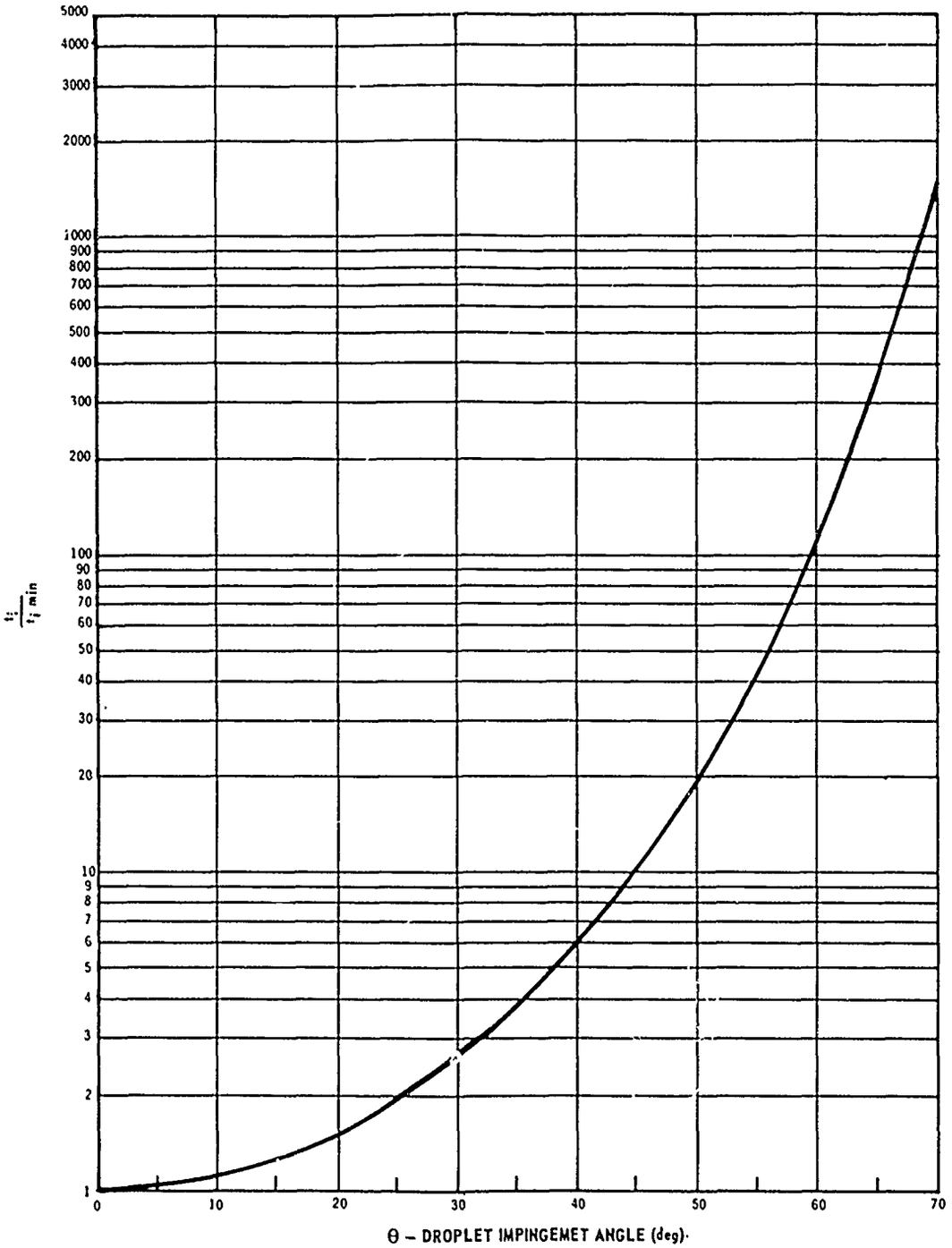

Figure 20. Increase in incubation time over minimum value at normal impingement

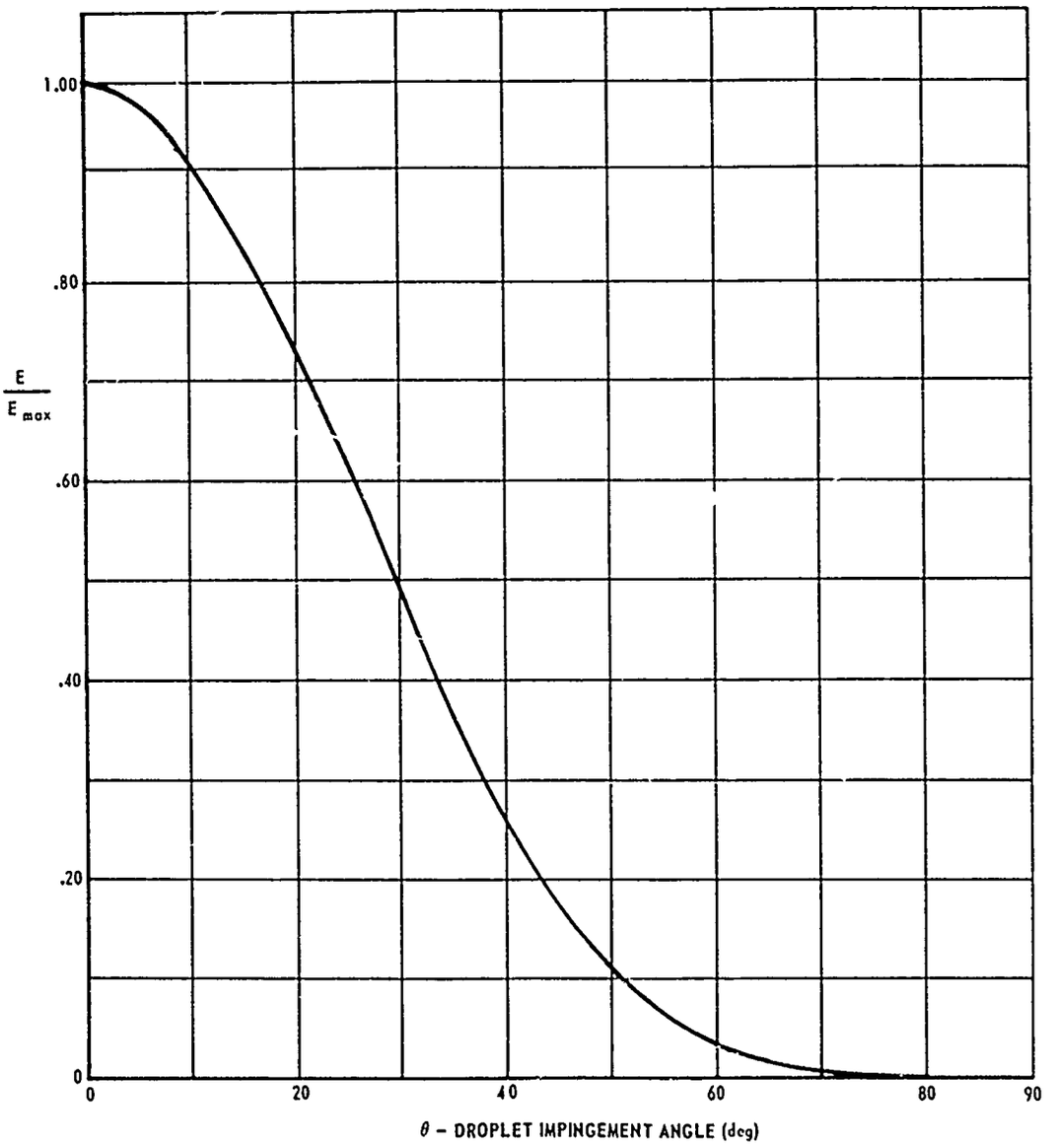

Figure 21. Erosion rate versus droplet impingement angle

Because the angle of attack of the blade changes as it rotates through each revolution, droplets which impact normal to the coating surface will be spread over a narrow region of the blade instead of impacting at one point. This effect should also tend to increase the life of the coating.

Most coatings are tested and rated for erosion resistance over a single time period of impact. A helicopter blade is usually subjected to many time periods of relatively short duration. The cumulative incubation time for a number of short periods of erosion may be longer than one continuous period of erosion.

The results for rain erosion may differ from those for sand, dust or snow erosion. The behavior of brittle materials was studied by Adler, who found several mechanisms for erosion.[14] Some of these mechanisms may not be important for solid particle erosion of a material such as Lennite or polyurethane. Additional experiments are required to obtain the erosion rates of coatings subjected to solid particle impacts.

DIELECTRIC PROPERTIES OF ROTOR ICE FOR ENGINEERING PURPOSES (LITERATURE SEARCH)

The feasibility of a microwave deicer depends upon the dielectric constant and the loss tangent of the ice appearing on helicopter rotor blades. Our literature search has revealed that this specific information is not now directly available; however, based upon the published values of the dielectric properties of ice, water and the composition of "rotor ice", a reasonable hypothesis concerning the dielectric properties of "rotor ice" can be made. After studying the composition of rotor ice, we can also state with reasonable certainty that the loss tangent of "rotor ice" will differ significantly from statically grown, pure, single crystal ice used for scientific purposes and from naturally grown ice found in glaciers and soils, and on mountain tops.

The Composition of Rotor Ice

As mentioned above, rotor ice differs significantly from statically or naturally grown ice. Some of the significant differences are:

[14]Adler, et al. "Analytical Modeling of Subsonic Particle Erosion", AFML-TR-74-144 (July 1972).

1) Unfrozen water content (super-cooled water content)
2) Air content
3) Impurities
4) Rate of growth
5) Crystal structure

Unfrozen Water and Air Content

Rotor ice forms in the range between 0° to -40°C; below about -40°C no icing takes place. The deicer requirements call for consideration of rotor icing down to -20°C. In this temperature range it is well established that super-cooled water droplets do not all freeze instantaneously. It should therefore be expected that there will be a relatively high content of unfrozen water in the ice, depending upon ambient temperature and drop size. At surface temperatures near but below 0°C and with large water drops, since freezing is not instantaneous, the drops have an opportunity to spread over the surface before freezing to form a clear layer referred to as glaze ice. This ice will have a relatively low air content. When the temperature is lower and droplet size smaller, more water will freeze on impact. The ice will form in great numbers of discrete particles with air and some water entrapped between them to produce white crystalline deposits known as rime ice.

Rate of Growth

Rotor ice grows rapidly from impinging droplets on the blades. Layers up to .2 inch forming, in some cases, in less than three minutes. It is very likely that the composition of the ice will vary with time during this stage of development.

Crystal Structure

Impact ice formed rapidly on rotor blades is polycrystalline containing many impurities such as salt, sand, dust, carbon particles from exhaust fumes, etc.

Loss Tangent of Rotor Ice

The loss tangent of various forms of ice and water (including super-cooled water) uncovered in the literature search to date are plotted

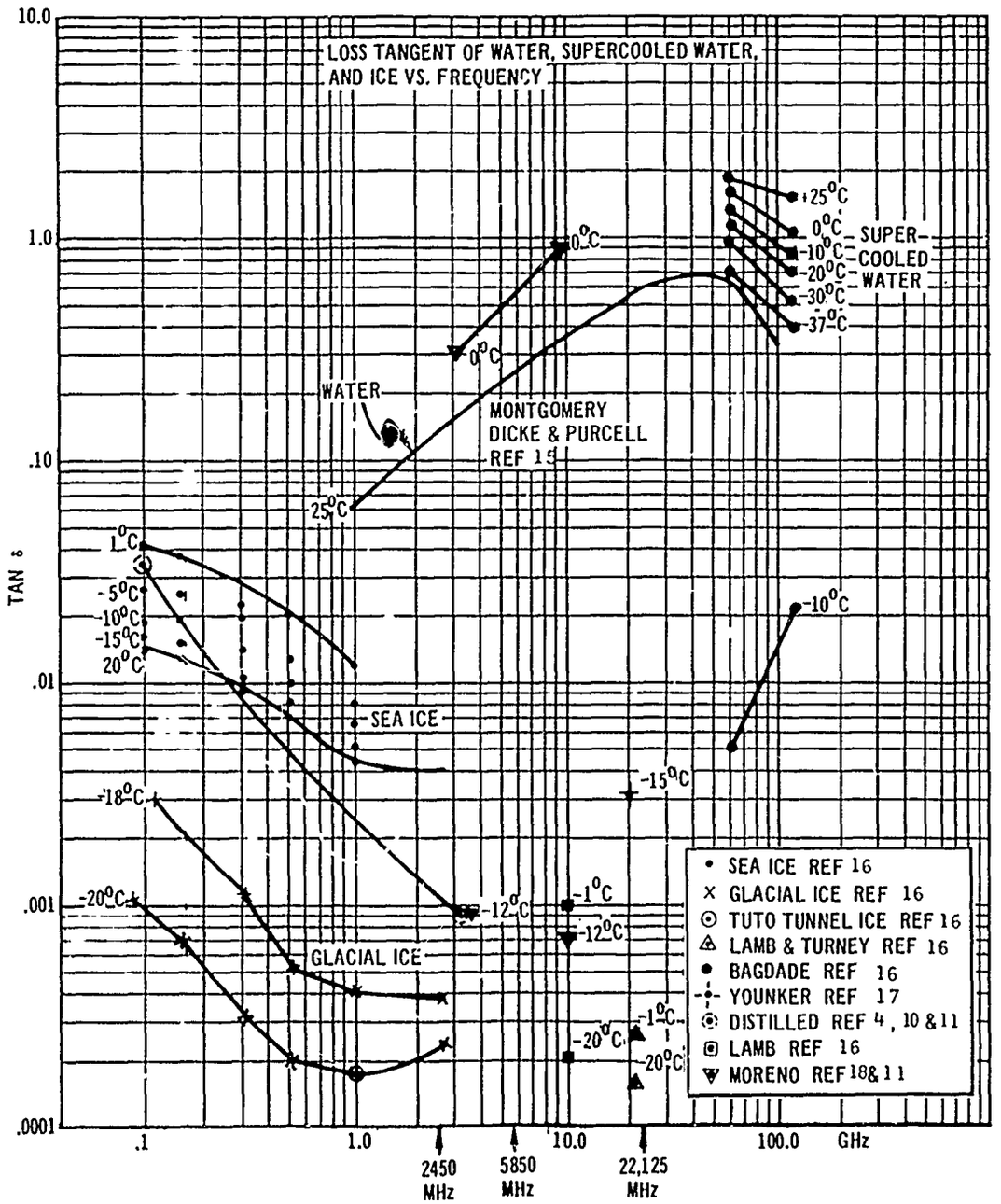

Figure 22. Loss tangent of water, supercooled water, and ice versus frequency

in Figure 22. This figure demonstrates the wide range of values that tan δ may take depending upon the impurities present in the ice. (The scatter in measured values of tan δ can only be accounted for by the presence of impurities.)

While dielectric or microwave heating can be significant even with low concentrations of impurities such as salt, sand, grease, exhaust carbon, etc., by and large the most significant parameter affecting the loss tangent is the percent unfrozen water content. Water molecules have such a large electric moment that even a small percentage of moisture is sufficient to cause considerable heating.

If the water content of rotor ice is large, it should be expected that a plot of tan δ vs. frequency will take on the shape of the upper curves in Figure 22 with reduced values of tan δ, depending upon other impurities present. It is expected that a certain percentage of unfrozen water will always be present in natural rotor ice and the lowest curves of Figure 22 will never be realized in practice.

This literature search was intended only to seek out published values of the dielectric constant and loss tangent of ice at microwave frequencies that may have been measured in the past. It is hoped that this information can be used to characterize the kind of ice encountered on rotor blades for engineering purposes. We were not interested in the general scientific study of the dielectric properties of ice, this being a very complex subject well beyond the scope of this program.

Dielectric Constant of Ice (Real Part)

A table of measured values of the dielectric constant of ice uncovered in our literature search is presented in Table 6. This data leaves little doubt that the dielectric constant for ice to be used for engineering purposes in the range of frequencies of interest to microwave deicing will lie in the vicinity of 2.8 to 3.2. If Arctic ice is neglected, the dielectric constnat of ice to be used for engineering purposes is 3.2.

TABLE 6. REAL PART DIELECTRIC CONSTANTS OF ICE (MEASURED)

APPROXIMATE FREQUENCY OF MEASUREMENT	T°C	~ 100 MHz	~ 1000 MHz	~ 3000 MHz	~ 10,000 MHz	~ 25,000 MHz	~ 60,000 MHz	~ 100,000 MHz	Reference
Ice (Pure Distilled Water)	-12	3.45		3.2	--	--	--	--	4
Freshly Fallen Snow	-20	1.2		1.2	--	--	--	--	4
Hard Packed Snow	- 6	1.55		1.5	--	--	--	--	4
Ice	-15	--			--	3.3	--	--	18
Ice (Lamb & Turney)	- 1 -10 -20				-- -- --	3.18 3.18 3.18	-- -- --	--	16
Dartmouth Firm Ice #12	- 1 -10 -20	3.21 3.19 3.18	3.20 3.19 3.18	3.201 3.188 3.175	-- -- --	-- -- --	-- -- --	--	16
Dartmouth Sea Ice #14	- 1 -10 -20	3.38 3.26 3.22	3.28 3.24 3.20	-- -- 3.197	-- -- --	-- -- --	-- -- --	--	16
Tuto Tunnel Ice	- 1 -10 -20	3.21 3.18 3.17	3.20 3.18 3.17	3.197 3.182 3.170	-- -- --	-- -- --	-- -- --	--	16
Little America (Ice)	- 1 -10 -20	3.08 3.05 3.04	3.07 3.05 3.04	3.065 3.050 3.038	-- -- --	-- -- --	-- -- --	--	16
Arctic (Ice)	- 1 -10 -20	-- -- --	-- -- --	2.880 2.870 2.861	-- -- --	-- -- --	-- -- --	--	
Ice (W. Bagdade)	-10	--	--	--	--		3.2	3.18	16

Definition of Experiments to Validate Surface Waveguide Theory

While surface waveguide theory is well established and treated comprehensively in References 1 and 2 and Appendix A, the same cannot be said of experimental techniques for measuring the performance of surface waveguides; these techniques can be found, for the most part, only in the periodical literature. The techniques described here are based upon a search of References 1, 2, 20, 21, 22, 23, 24, 25, 26, 27, 28. Excerpts of some of the more applicable experiments uncovered in the literature search are discussed in Appendix G. Required experiments are described as Tasks 1a and 1b in Appendix C.

---

[20]G.J. Rich, "The Launching of a Plane Surface Wave," Proceedings of the IEE, London, vol. 102, part B, pp. 237-246.

[21]Cohn, Cassedy and Kott, "TE Mode Excitation on Dielectric Loaded Parallel Plane and Trough Waveguides," IRE Transactions on Microwave Theory and Techniques, pp. 545-552, September 1960.

[22]E.L. Ginzton, Microwave Measurements, New York: McGraw-Hill, 1957

[23]J.W. Duncan, "The Efficiency of Excitation of a Surface Wave on a Dielectric Cylinder," IRE Transactions on Microwave Theory and Techniques, pp. 257-268, April 1959.

[24]R.H. DuHamel and J.W. Duncan, "Launching Efficiency of Wires and Slots for a Dielectric Rod Waveguide," IRE Transactions of Microwave Theory and Techniques, July 1958.

[25]A.D. Frost, C.R. McGeoch and C.R. Mingins, "The Excitation of Surface Waveguides and Radiating Slots by Strip-Circuit Transmission Lines," IRE Transactions on Microwave Theory and Techniques, October 1956.

[26]James C. Wiltse, "Some Characteristics of Dielectric Image Lines at Millimeter Wavelengths," IRE Transactions on Microwave Theory and Techniques, pp. 65-99, January 1959.

[27]D.D. King and S.P. Schlesinger, "Losses in Dielectric Image Lines," IRE Transactions on Microwave Theory and Techniques, January 1957.

[28]S.P. Schlesinger and D.D. King, "Dielectric Image Lines," IRE Transactions on Microwave Theory and Techniques, July 1958.

SECTION 3

PHASE II - DISSIPATION AND DISTRIBUTION OF MICROWAVE ENERGY

MICROWAVE POWER REQUIRED TO SHED ICE FROM ROTOR BLADES

The mechanism of injecting microwave energy into ice layers by means of dielectric surface waveguides has been described in Section 2. In this section the amount of power and energy required to shed the ice is computed. The results of computations made here are presented in Figures 23 and 24, where it is obvious that the power requirements of a microwave deicer are an order of magnitude less than that of a thermal deicer. The remainder of the section describes the underlying principles upon which the calculations are based. Detailed calculations are presented in Appendix B.

ESTIMATES OF MICROWAVE POWER REQUIRED TO SHED ICE ON UH-1 BLADES AT AMBIENT TEMPERATURES OF -15°C and -20.9°C

The microwave power required to shed the ice build-up on a helicopter blade is related to the magnitude of the area iced and the thickness of the ice layers; i.e., the volume and mass of the ice. Ideally, the computations should be based upon actual measured ice accumulations on the blade of a UH-1 helicopter. Such measurements are not available for a UH-1 but were found for a NACA 0012 blade at -15°C in Reference 29 and for a Bell 47-6 at -20.9°C in Reference 30. The ice accumulations for the UH-1 illustrated in Figure 25 were determined by scaling the iced area in proportion to the blade area from these two measurements. The resulting areas are given in Table B-5.

The microwave energy required to shed the ice is assumed to be the energy that must be injected into the ice to raise the temperature to the level at which shedding takes place. The microwave energy enters the

---

[29]J.B. Werner, "Ice Protection Investigation for Advanced Rotary-Wing Aircraft," USAAMRDL Technical Report 73-38, August 1973.

[30]J.R. Stallabrass, Flight Tests of an Experimental Helicopter Rotor Blade Electrical De-Icer, Ottawa, Canada: National Research Laboratories, November 1959.

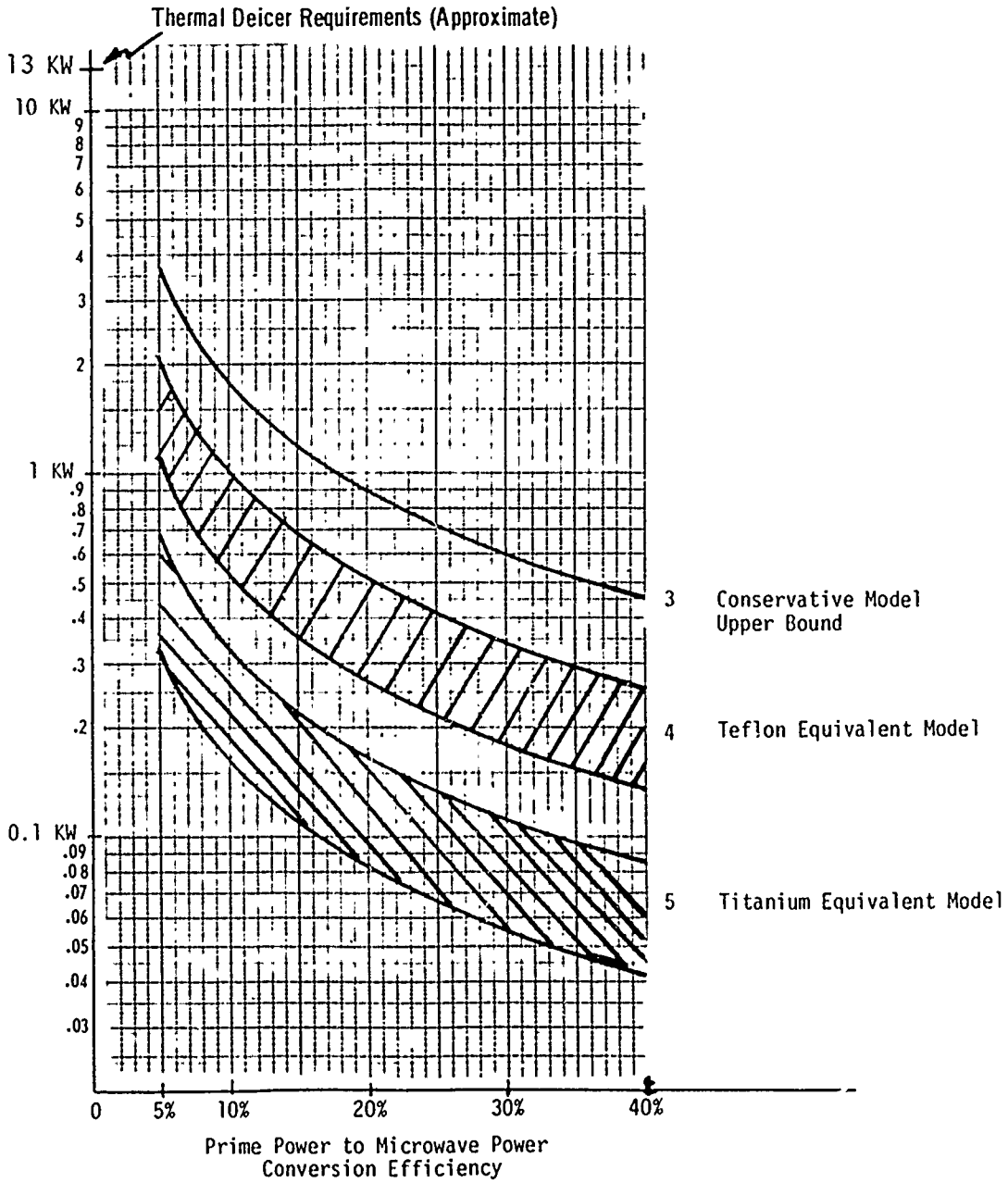

Figure 23. Estimated prime power required to shed ice on two UH-1 rotor blades $T_\infty = -15°C$

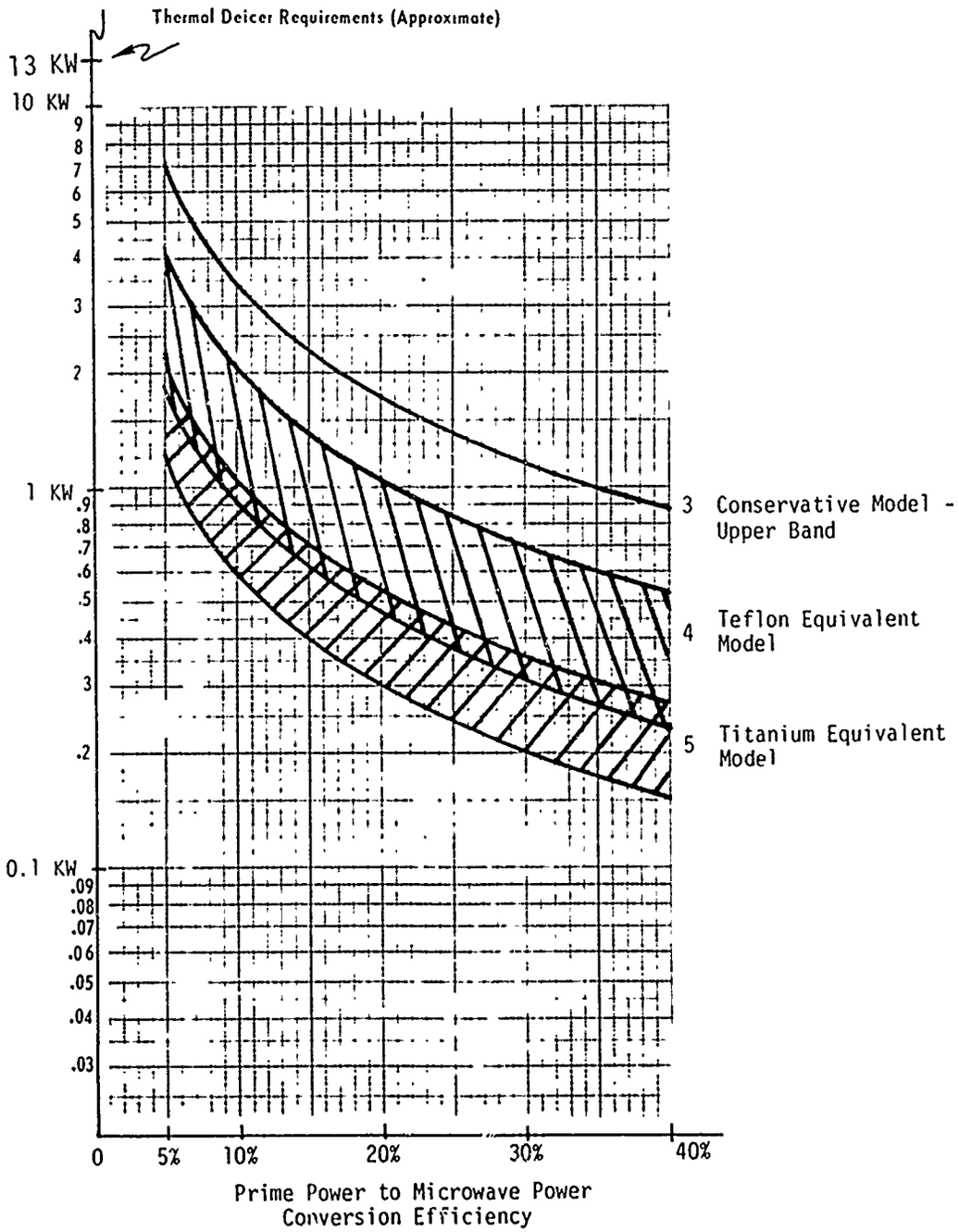

Figure 24. Estimated prime power required to shed ice on two UH-1 rotor blades T_{∞} = 20.9°C

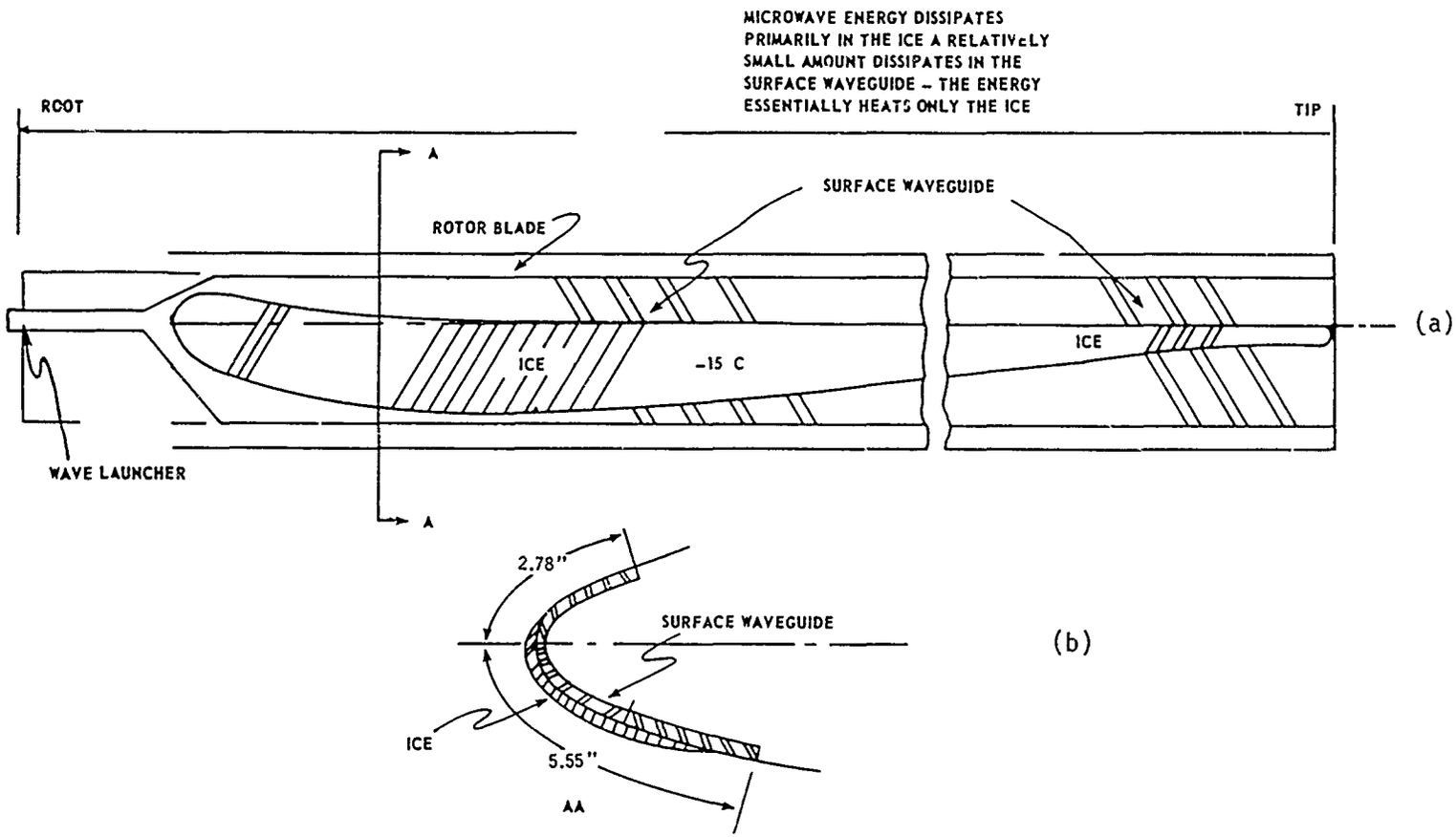

Figure 25. Typical ice buildup on UH-1 blade

ice by way of the surface waveguides located on the blade leading edges just under the ice, as illustrated in Figure 25 and discussed in Section 2. The surface waveguide, being relatively lossless and transparent to microwave energy, will experience only a minor elevation in temperature due to dissipation while the major dissipation takes place in the ice. No other heating occurs.

Stallabrass has shown that the ice does not need to be brought up to the melting point but merely to a shedding temperature, T_s, at which point the centrifugal force exerted on the ice mass is sufficient to break the ice adhesion bond.[31] He has shown that with decreasing temperature the force required to shed increases, the force is also a function of the adhesive properties of the material used in the leading edge. Because the centrifugal force increases with radius, the shed temperature required will decrease with radius. The shedding temperatures, as functions of blade radius, for the UH-1 helicopter have been computed in Appendix B for Teflon and Titanium and are illustrated by the upper curves in Figure 26.

Some rise in the temperature of the ice is also induced by aerodynamic heating; the more rapidly moving tip of the blade experiences greater heating. The equilibrium temperature thus depends upon the ambient temperature and the speed of the blade. The equilibrium temperatures for a UH-1 blade at ambient temperatures of -15°C and -20°C have been established in Appendix B and are plotted in Figure 26 where they can be compared to the shedding temperatures.

When the equilibrium temperature exceeds the shed temperature, natural shedding may take place, as is often experienced at the tip of the blade at higher ambient temperatures. This phenomenon is illustrated on the right in Figure 26, where the equilibrium temperature crosses the shed temperature. The equilibrium temperature is not in general sufficient to cause natural shedding of the entire blade.

---

[31] J.R. Stallabrass and R.D. Price, "On the Adhesion of Ice to Various Materials," National Research Laboratories, July 1962.

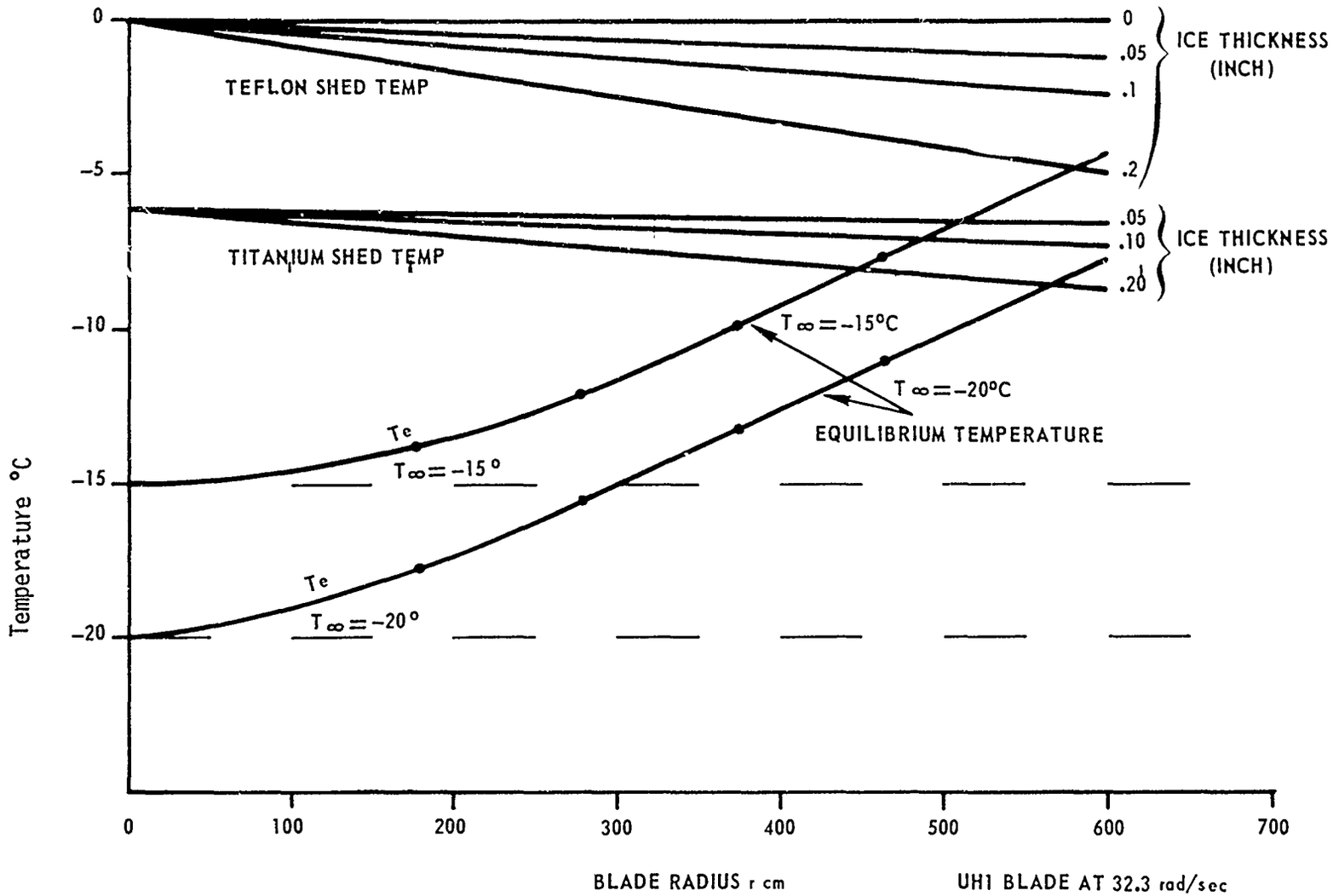

Figure 26 Shedding temperatures and equilibrium temperatures as functions of blade radius

The microwave energy that must be injected into the ice is that energy required to raise the ice from the equilibrium temperature, T_e, to the shed temperature, T_s. The energy required to do this is computed in Appendix B, the results of which are illustrated in Figures 23 and 24 for -20°C and -15°C ambient. Obviously, from Figure 24, more microwave energy will be required near the root of the blade where the difference between the shed temperature and the equilibrium temperature is greatest and the centrifugal force weakest.

Curve 3 of Figures 23 and 24 represents the average power that must be consumed to raise the ice from the ambient temperature to 0°C (but not melt the ice). Since 0°C is greater than the shedding temperature and T_∞ less than the equilibrium temperature (see Figure 26), Curve 3 represents a conservative model and represents an upper bound on power requirements. While Teflon is not mechanically suitable for the blade leading edge, it is electrically suitable and therefore Curve 4, performed for Teflon, should give a close indication of the real power requirements of other, similar dielectrics with more suitable mechanical properties. Curve 5 represents the power requirements assuming the dielectric coating has ice adhesive properties equivalent to that of titanium which, as measured by Stallabrass, showed the smallest ice adhesive properties of those materials he measured (aluminum, stainless steel, Teflon, titanium and Viton).[31] It probably represents a lower bound on power requirements. It is presently felt that actual requirements will fall somewhere between Curve 3 and Curve 5. In a sense, these curves may also be considered conservative, since the computations assumed that the entire layer of ice had to be raised to the shed temperature, whereas actually only a thin layer of ice in the neighborhood of the ice adhesion bond need be raised. Since the microwave power density can be engineered to reach a maximum at the adhesion layer, as illustrated in Figures 3 and 4, perhaps even less power than is indicated in Curve 5 may be required. Only experimentation can determine the true power requirements.

---

[31]J.R. Stallabrass and R.D. Price, "On the Adhesion of Ice to Various Materials," National Research Laboratories, July 1962.

The discussion up to this point assumed the microwave energy was to be applied continuously as long as ice existed on the blade. Actually, the computations of average power made in Appendix B assumed that the power was applied periodically in accordance with some duty cycle; the average power dissipated remaining unchanged, independent of the peak power. This implies higher peak powers for shorter duty cycles. In this model the ice is permitted to accrete only to a predetermined, tolerable thickeness before it is caused to shed by a long pulse of microwave energy. The power is applied for an "on period" long enough to shed the ice and then removed for an "off period", during which the ice is allowed to accumulate again (providing the icing condition persists). Typical "on times", "off times" and average power required for -15°C and -20°C have been computed in Appendix B and appear in Tables B-6, 7, 8 and B-12, B-13, and B-14 respectively. The peak power selected for the "on time" is determined by the time it is desired to take to shed the accumulated ice layer. To provide the on-off sequence, the power supply must include a simple periodic sequencer that periodically turns the power on and off in a predetermined sequence depending upon the severity of the icing condition.

DIELECTRIC HEATING OF THE ICE LAYER

In the previous section the amount of power required to shed the ice layer was computed independently of how the ice was heated. It was assumed that microwave energy injected into the ice layer was converted to heat. In this section we examine quantitatively the dielectric heating of the ice layer by the microwaves propagating within them.

The dielectric heating* of any material is given by:

$$W_d = \sigma \frac{E^2}{2} \quad \frac{\text{Watts}}{\text{Unit Volume}} \tag{1}$$

$$\sigma = \omega\varepsilon'' = \omega\varepsilon' \tan\delta$$

*A brief discussion of the physics of dielectric heating is given in Appendix H.

where:

E - electric field intensity
W_d = power converted to heat (power dissipated)
ω = frequency
ε' = real part of dielectric constant
ε'' = imaginary part of dielectric constant
$\tan\delta = \varepsilon''/\varepsilon'$ = loss tangent of material being heated
σ = conductivity

The typical amplitude distribution of the electric field, E or E^2, for surface waveguides has been studied in Section 2 and is illustrated in Figures 3 and 4 for varying thickness of ice. The surface waveguide is assumed to be composed of two dielectric layers: a stable, low-loss base layer and the transient, high-loss ice layer. A technique enabling the computation of the dielectric heating of both layers is developed in Appendix A utilizing Equation 1 and is presented in the form of attenuation constants, illustrated in Figures 27 through 33. The attenuation constant of the surface guide is a measure of the fraction of transmitted power that is lost per inch due to dielectric heating of the ice, expressed in decibels per inch. In Figures 27 through 33, d represents the sum of the base dielectric plus the ice.

$$d = d_1 + t_2$$

where

d_1 = thickness of the base dielectric
t_2 = thickness of the ice
$\tan\delta_1$ = loss tangent of the base dielectric
$\tan\delta_2$ = loss tangent of the ice layer

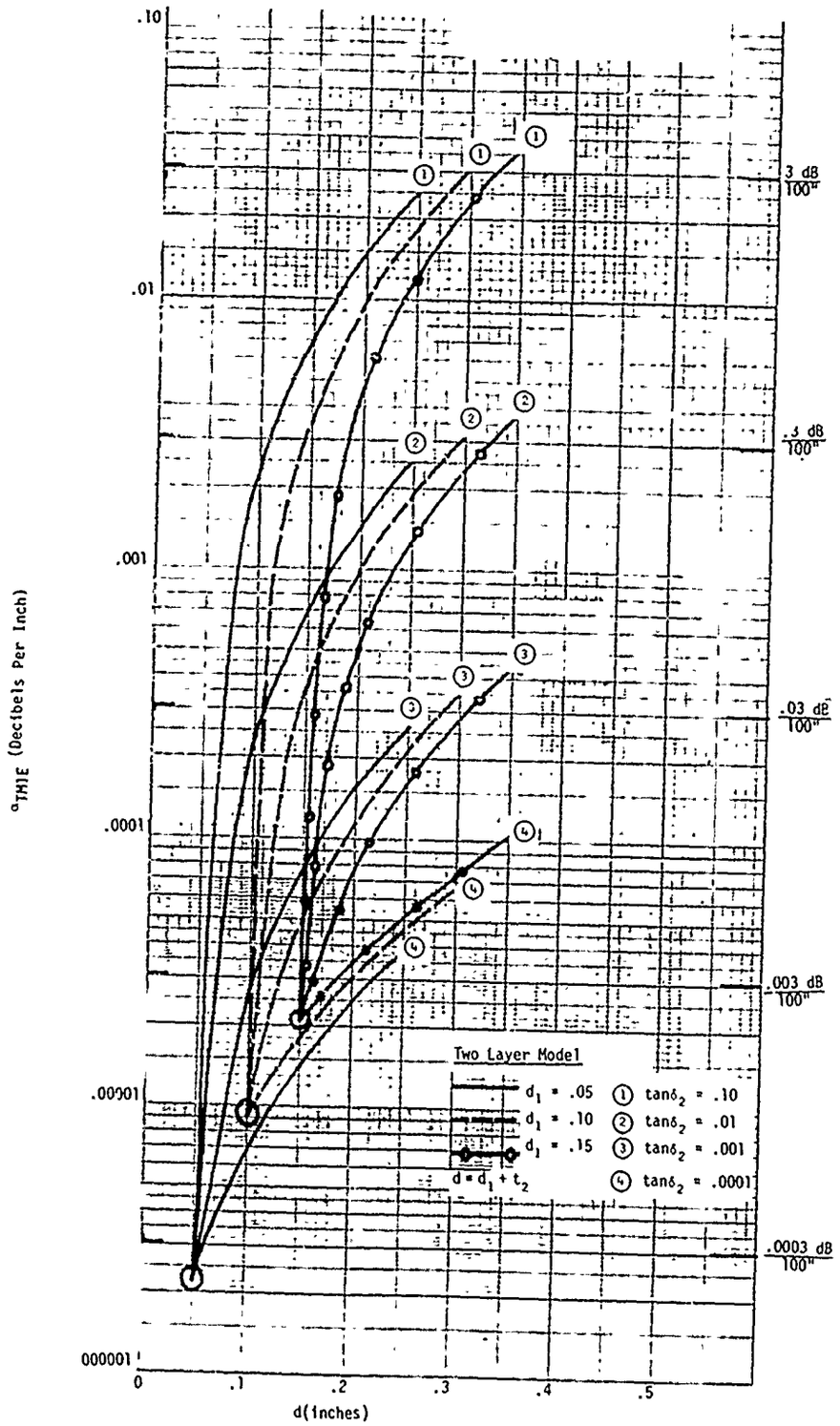

Figure 27. Attenuation versus thickness of dielectric for TM even mode f = 2,450 MHz, ε_1 = 2.8, $\tan\delta_1$ = .0002, ε_2 = 1.0

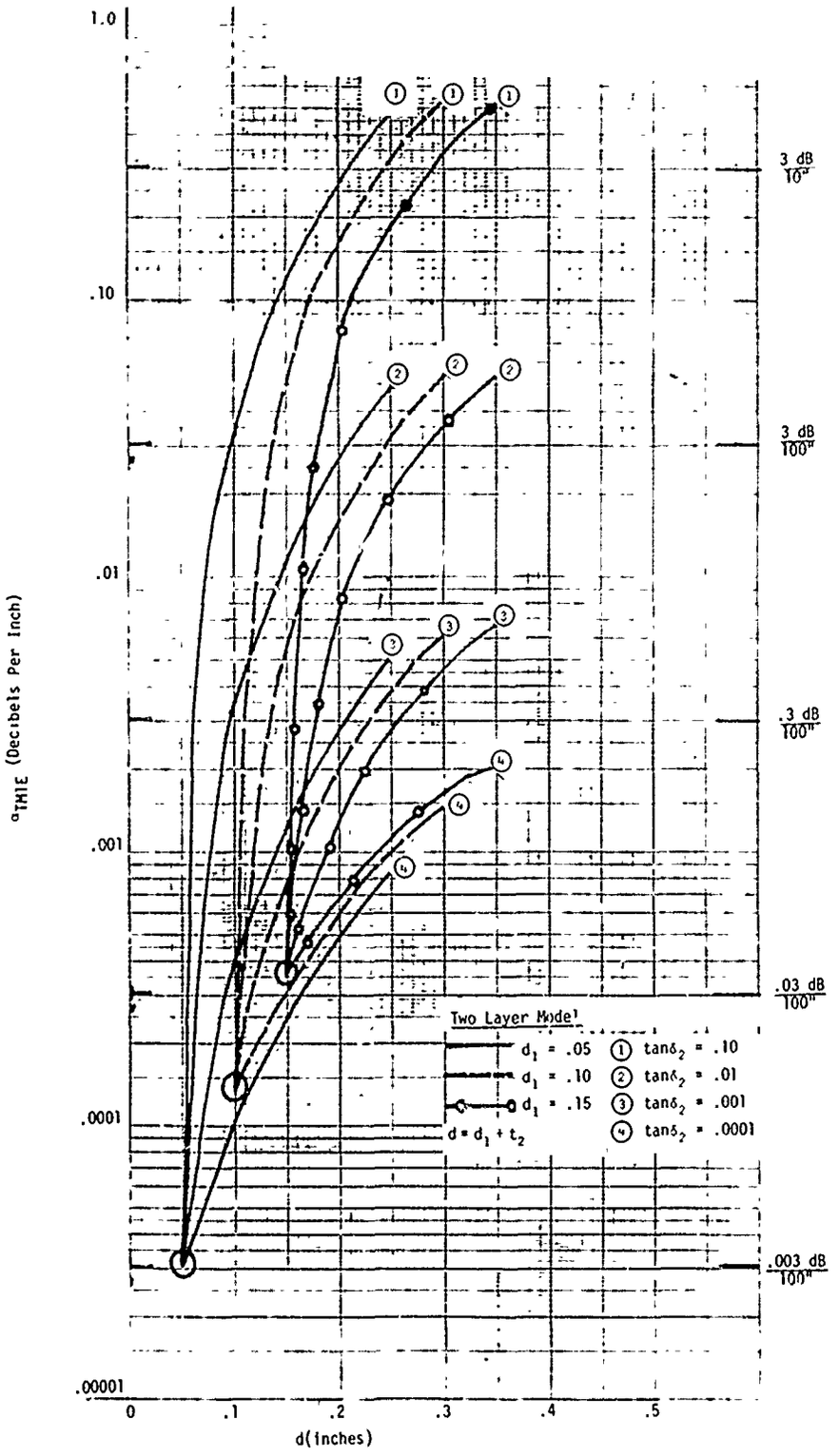

Figure 28. Attenuation versus thickness of dielectric for TM even mode
f = 5,850 MHz, ε_1 = 2.8, $\tan\delta_1$ = .0002, ε_2 = 1.0

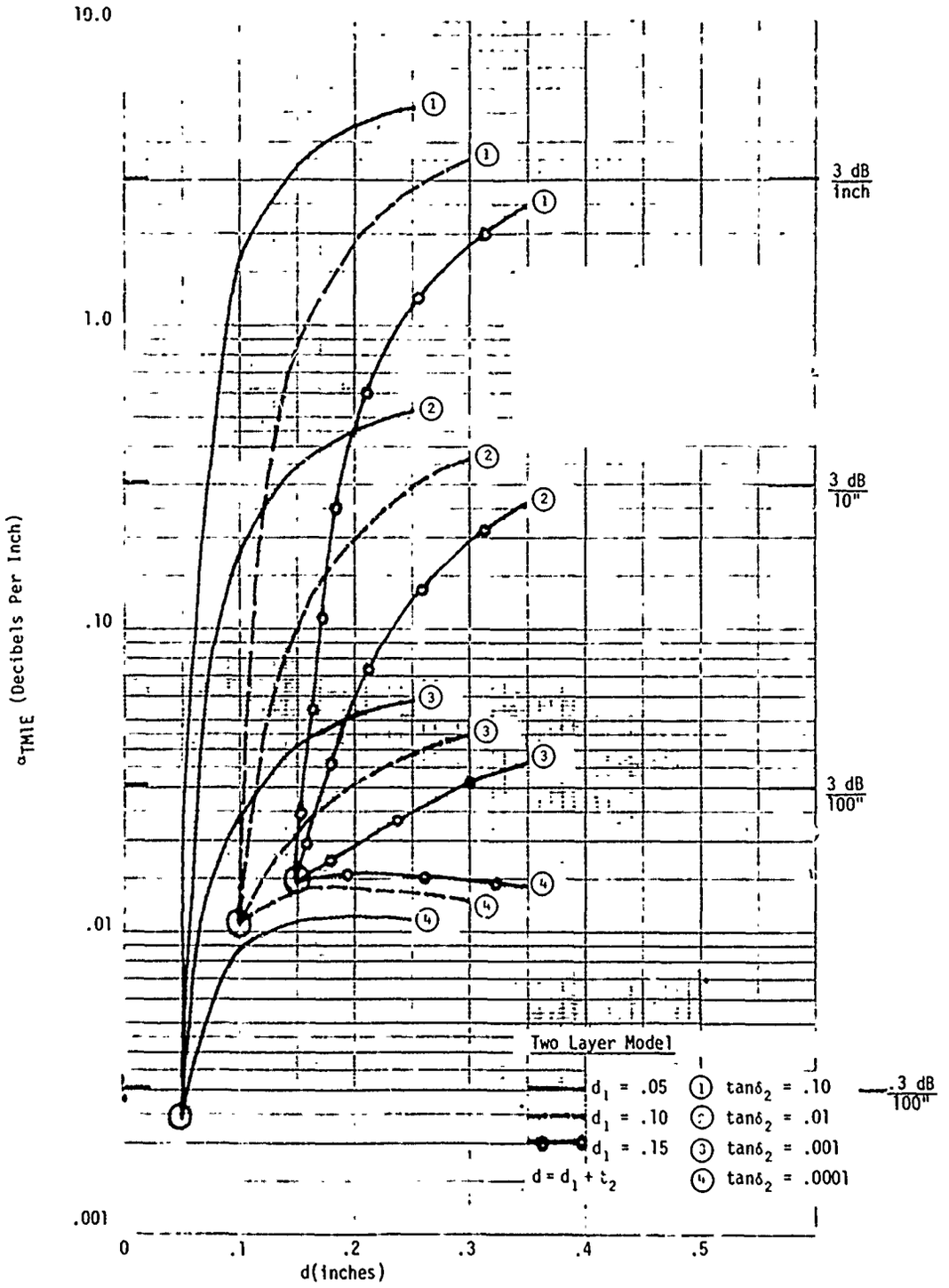

Figure 29. Attenuation versus thickness of dielectric for TM even mode
f = 22,125 MHz, ε_1 = 2.8, $\tan\delta_1$ = .0002, ε_2 = 1.0

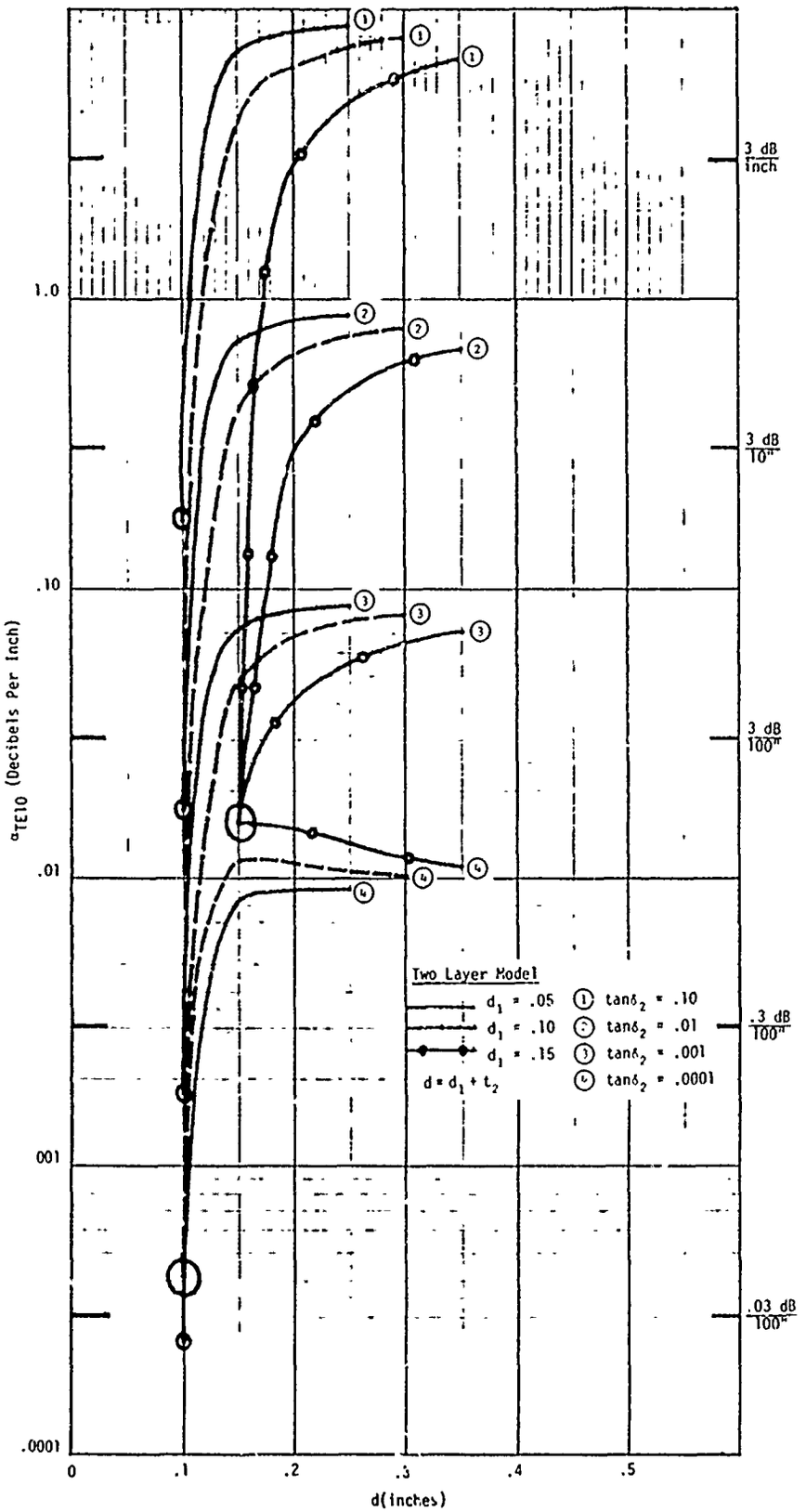

Figure 30. Attenuation versus thickness of dielectric for TE odd mode
$f = 22{,}125$ MHz, $\varepsilon_1 = 2.8$, $\tan\delta_1 = .0002$, $\varepsilon_1 = 1.0$

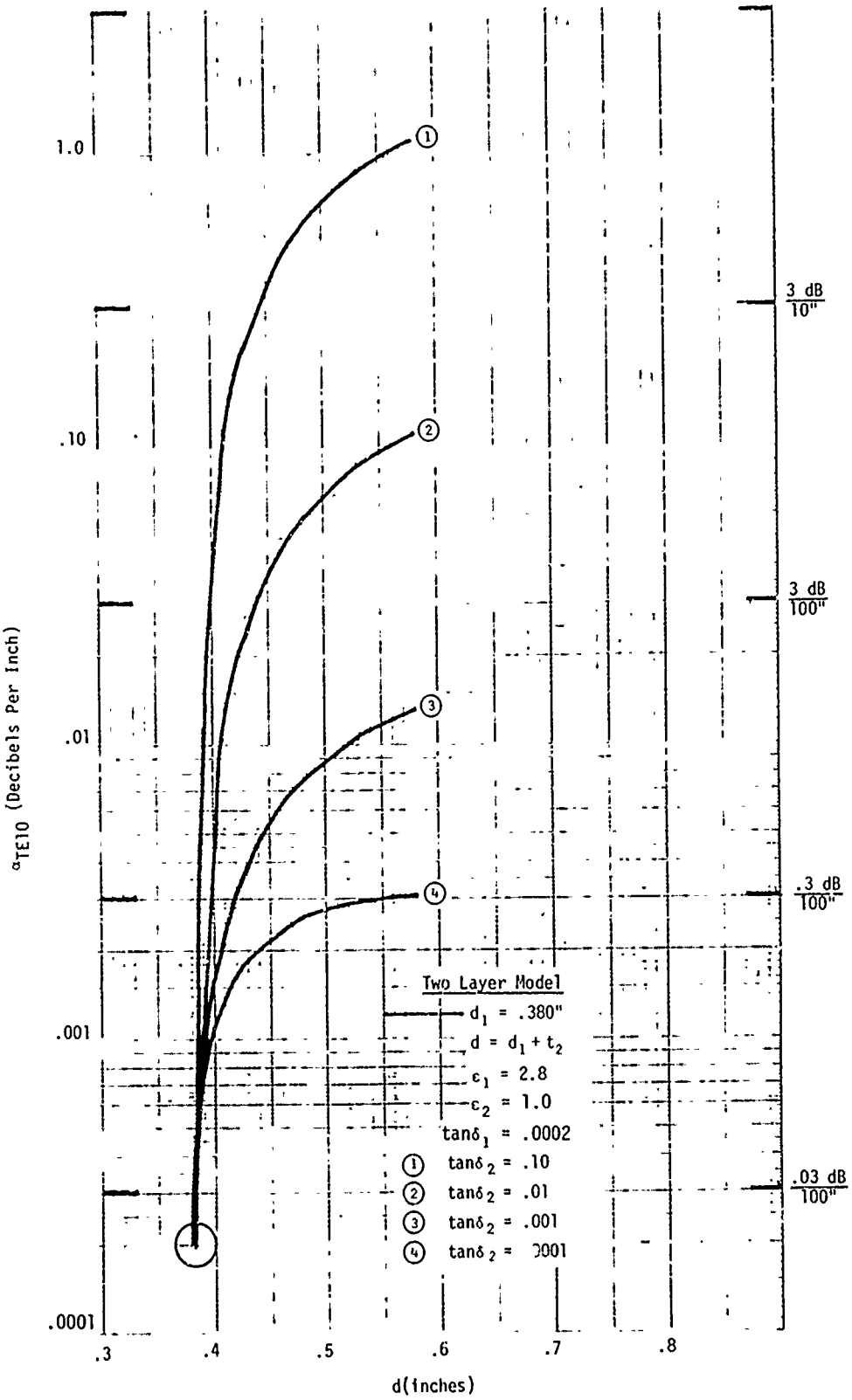

Figure 31. Attenuation versus thickness of dielectric for TE odd mode, f = 5,850 MHz

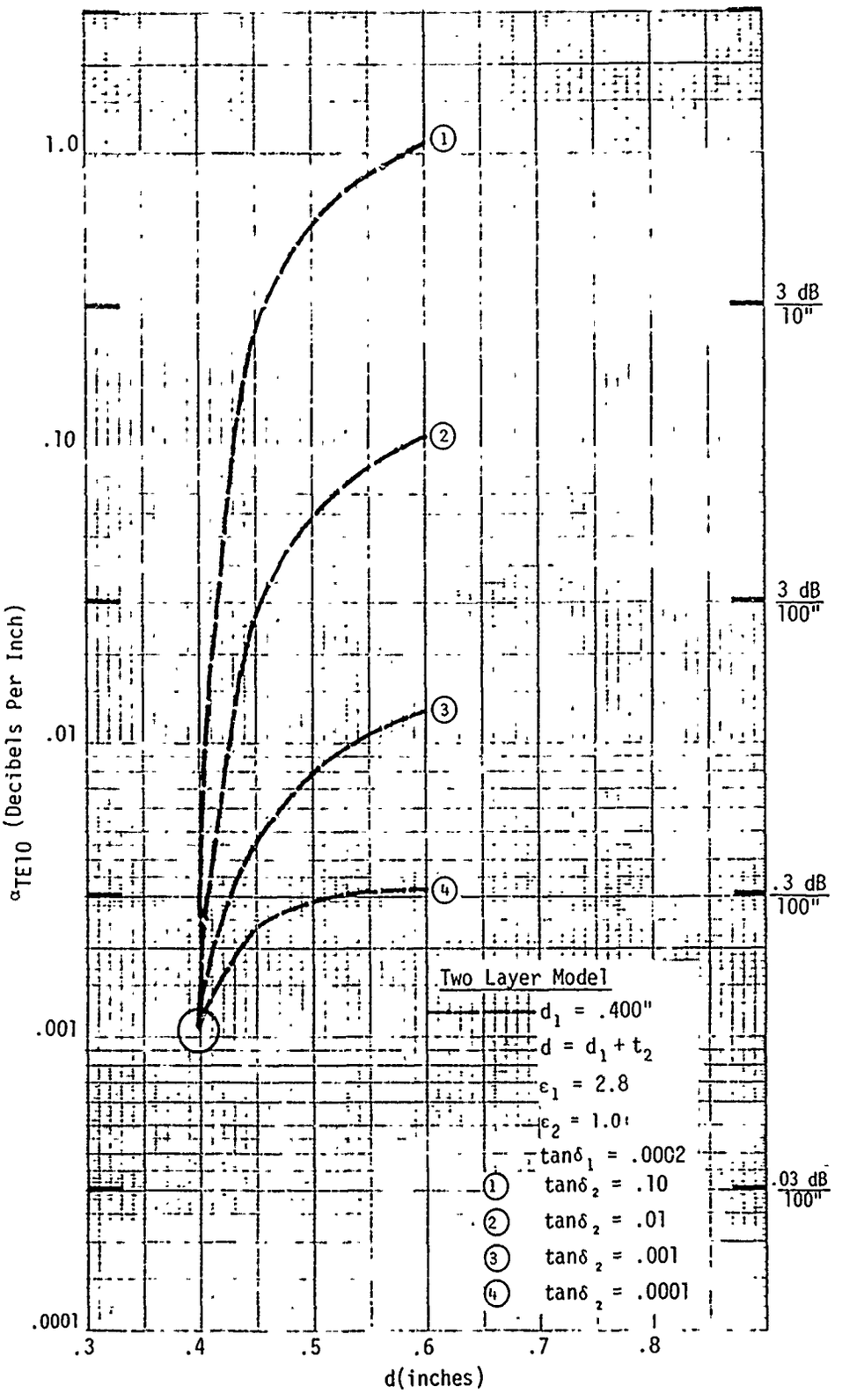

Figure 32. Attenuation versus thickness of dielectric for TE odd mode, f = 5,850 MHz

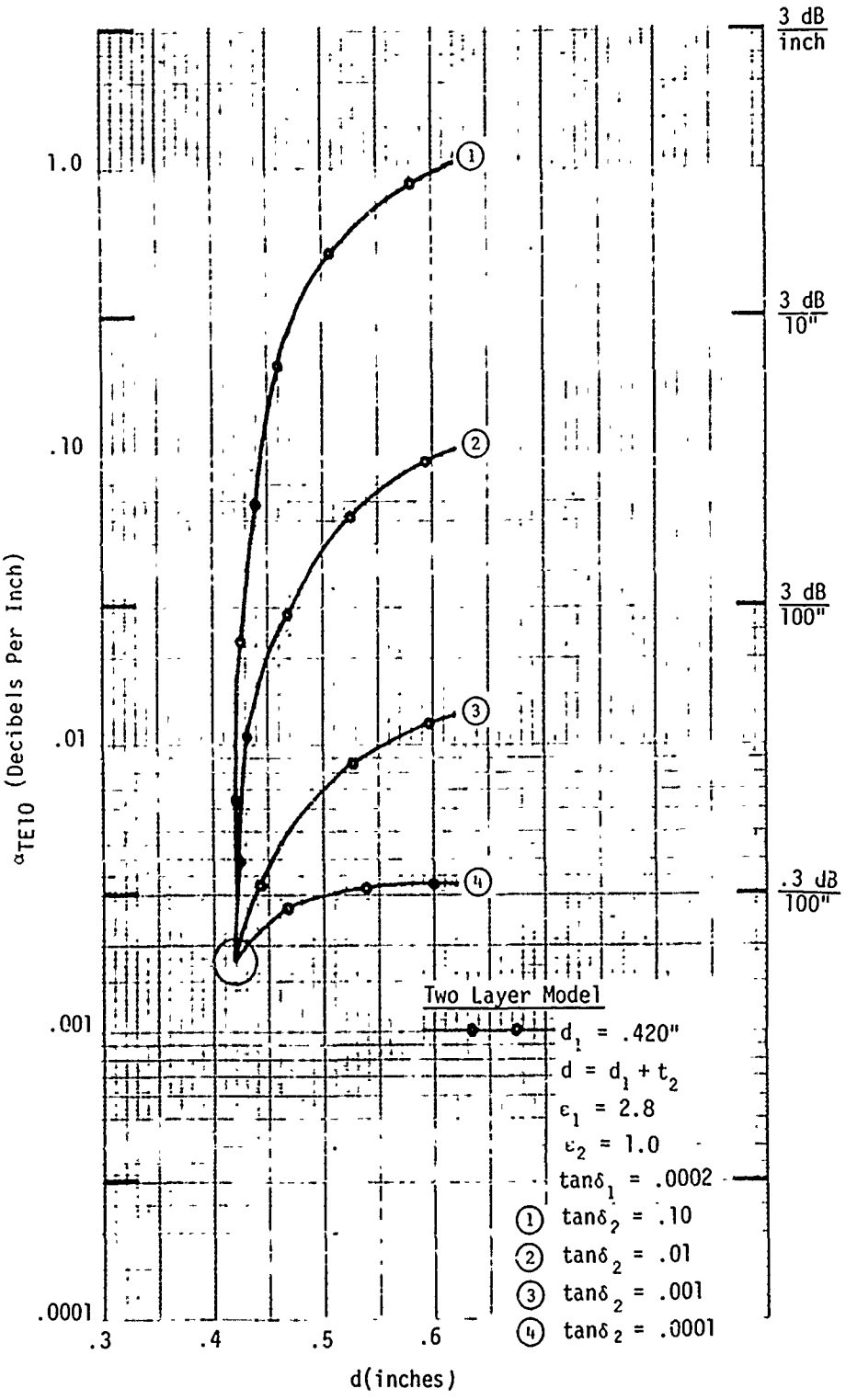

Figure 33. Attenuation versus thickness of dielectric for TE odd mode, f = 5,850 MHz

The thicknesses of the base dielectric, d_1, are indicated on each diagram. The attenuation, or power loss, in the base dielectric for each value is indicated by a circle at the lower-left extremity of each curve. As can be seen, these produce, in most cases, only minor losses and may be considered to be lossless for all practical purposes. The curves show that as the ice layers grow the attenuation rises rapidly. The rate of increase is dependent upon the loss tangent of the rotor ice.

Practical values of the loss tangent of rotor ice have been studied in the previous section and shown to fall in the range of .0001 to .1, in Figure 22, depending upon the impurities present in the ice. For this reason the attenuation constants of Figures 27 through 33 have been plotted parametrically over this range of $\tan\delta_2$. As concluded in the previous section, it is expected that rotor ice will contain many impurities, including a large fraction of unfrozen water, so that values of $\tan\delta_2$ below about .001 are not expected. Examination of Figures 27 through 33 reveal that workable deicers are realizable for values of $\tan\delta_2$ equal to or greater than .001.

The Effect of a Polyurethane Erosion Coat on Losses

Certain dielectric materials may require a polyurethane erosion coat. This coat has a loss tangent of .059 and will be subject to dielectric heating and losses. The techniques of Appendix A permit the evaluation of the effect of a thin, 12 mil, erosion coat. The polyurethane represents an additional layer of dielectric and is treated in the same manner as the base layer and the ice layer. This is the so-called 3-layer model of the surface waveguide. The attenuation constants for this model have been calculated and are presented in Figures 34 through 44. In these curves

$$d = d_1 + t_2 + t_3$$

where

d_1 = thickness of the base dielectric
t_2 = 0.012" = thickness of polyurethane
t_3 = thickness of the ice layer

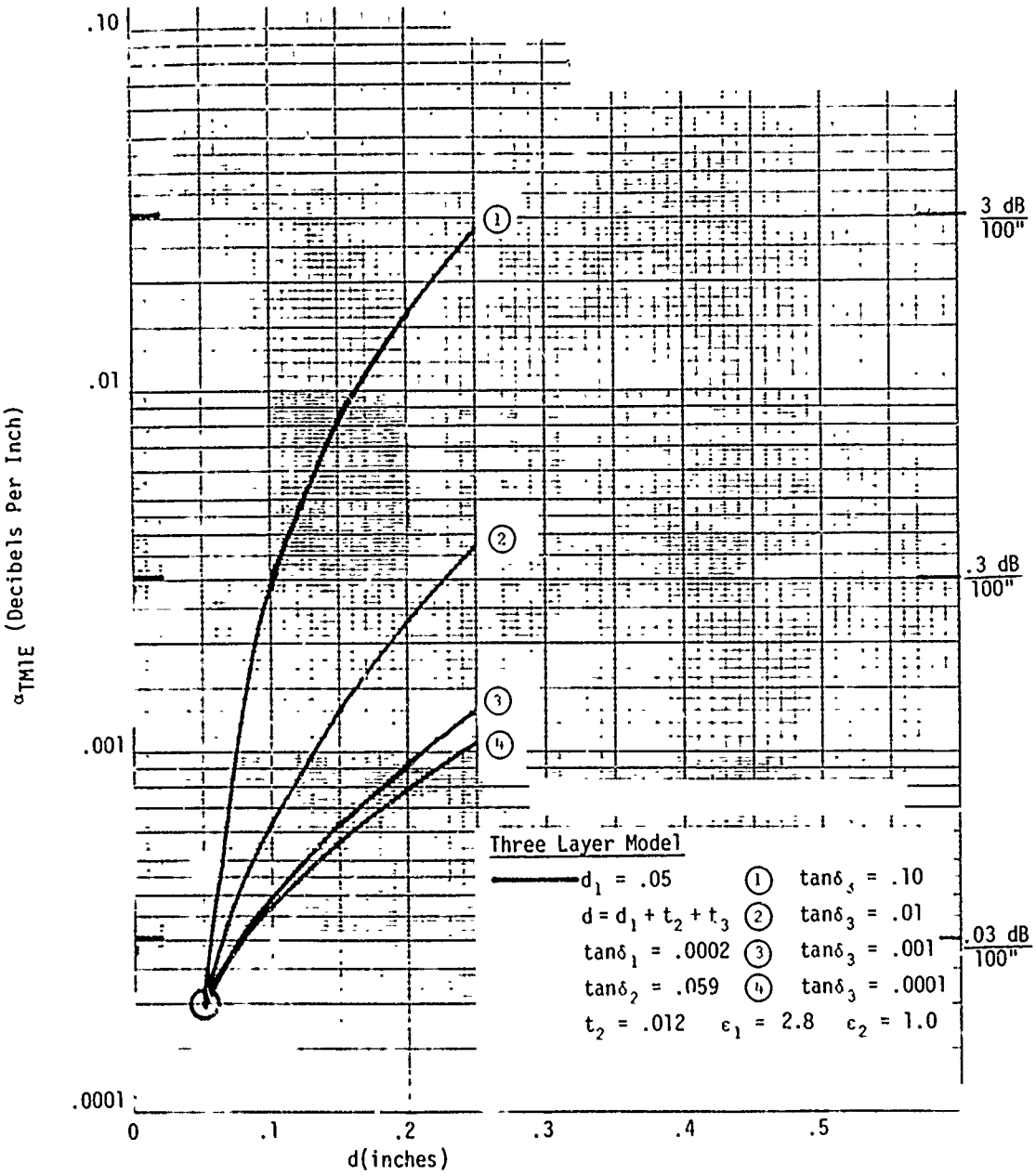

Figure 34. Attenuation versus thickness of dielectric for TM even mode
f = 2,450 MHz

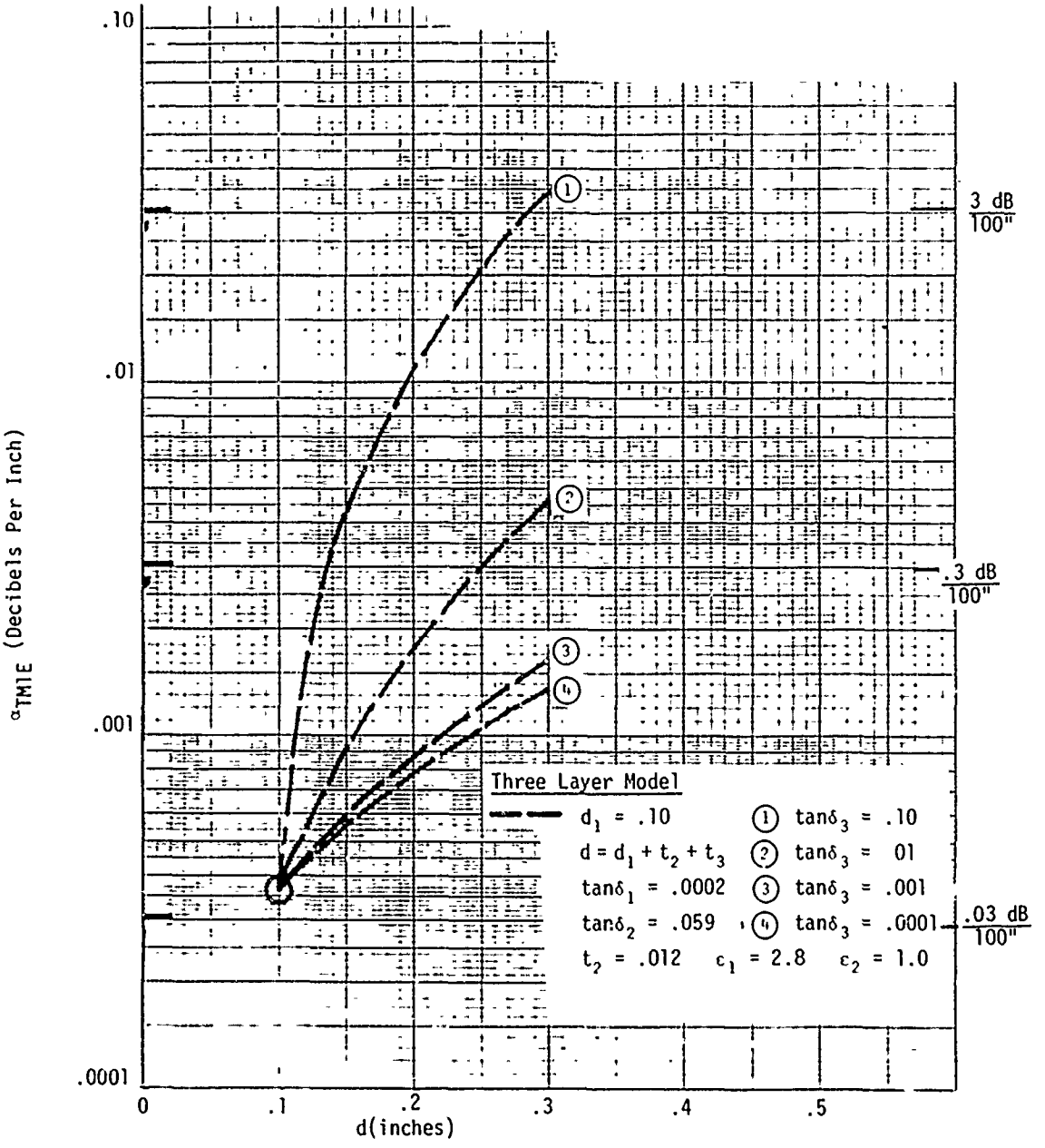

Figure 35. Attenuation versus thickness of dielectric for TM even mode
f = 2,450 MHz

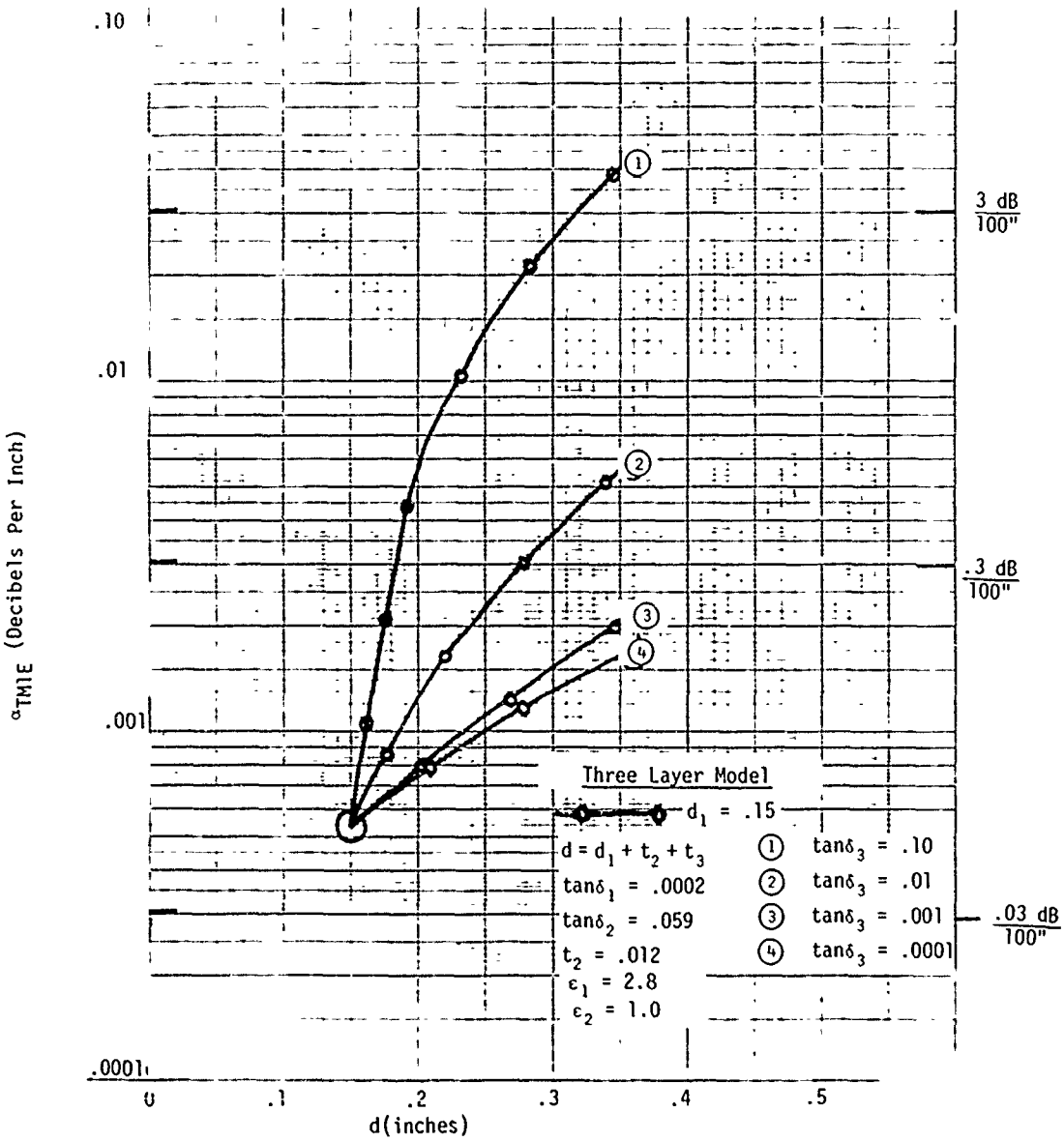

Figure 36. Attenuation versus thickness of dielectric for TM even mode
f = 2,450 MHz

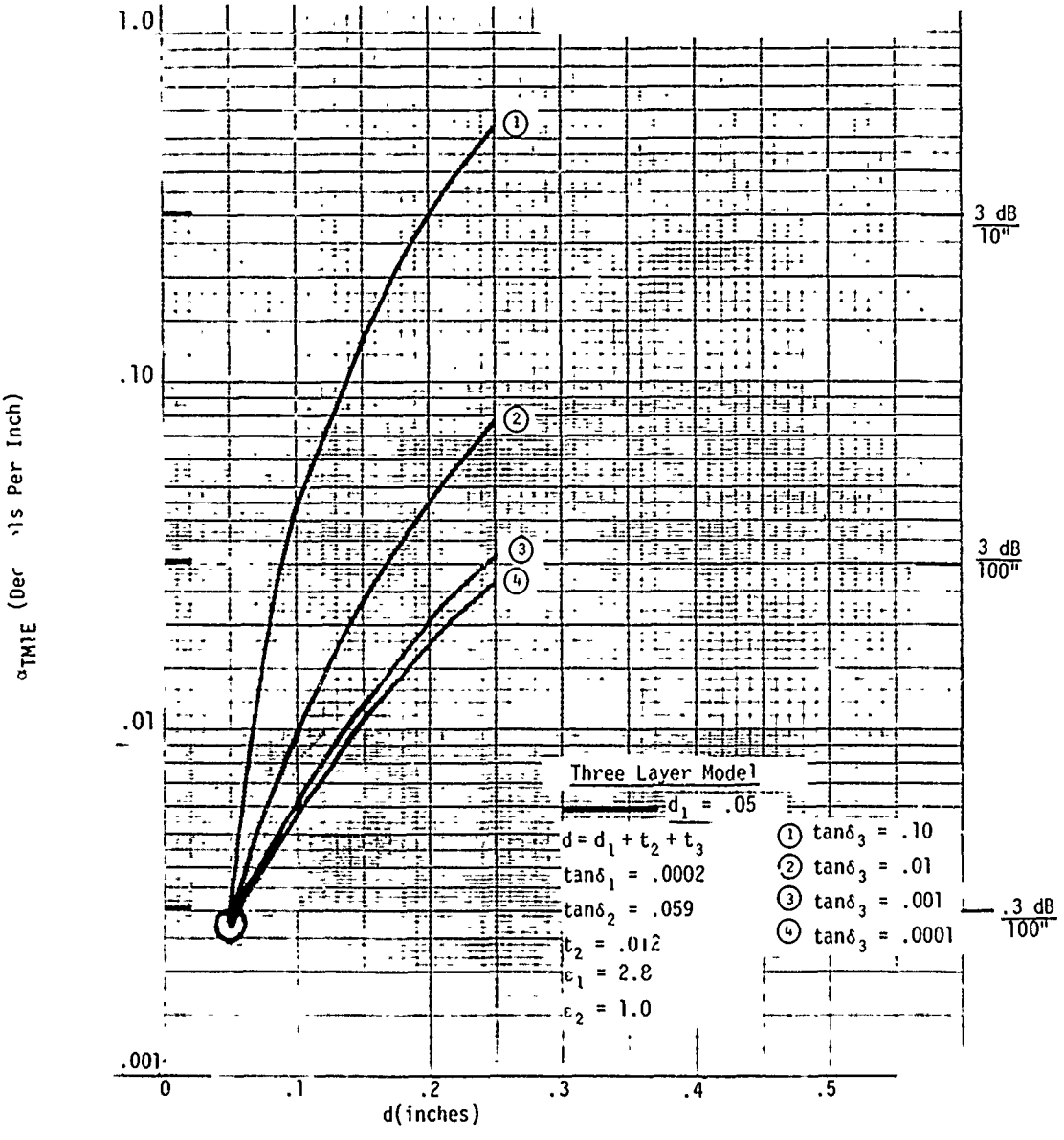

Figure 37. Attenuation versus thickness of dielectric for TM even mode
f = 5,850 MHz

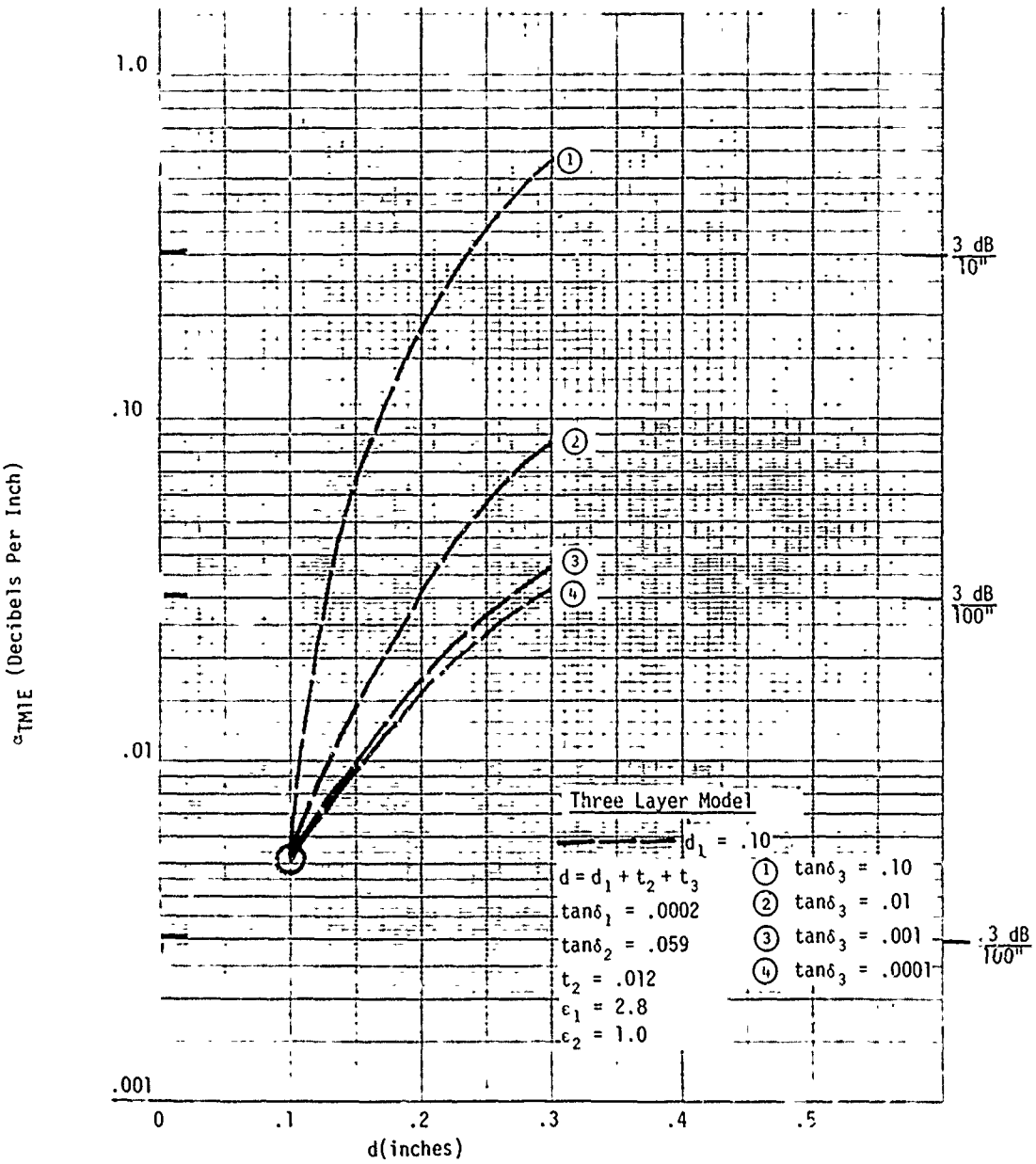

Figure 38. Attenuation versus thickness of dielectric for TM even mode
f = 5,850 MHz

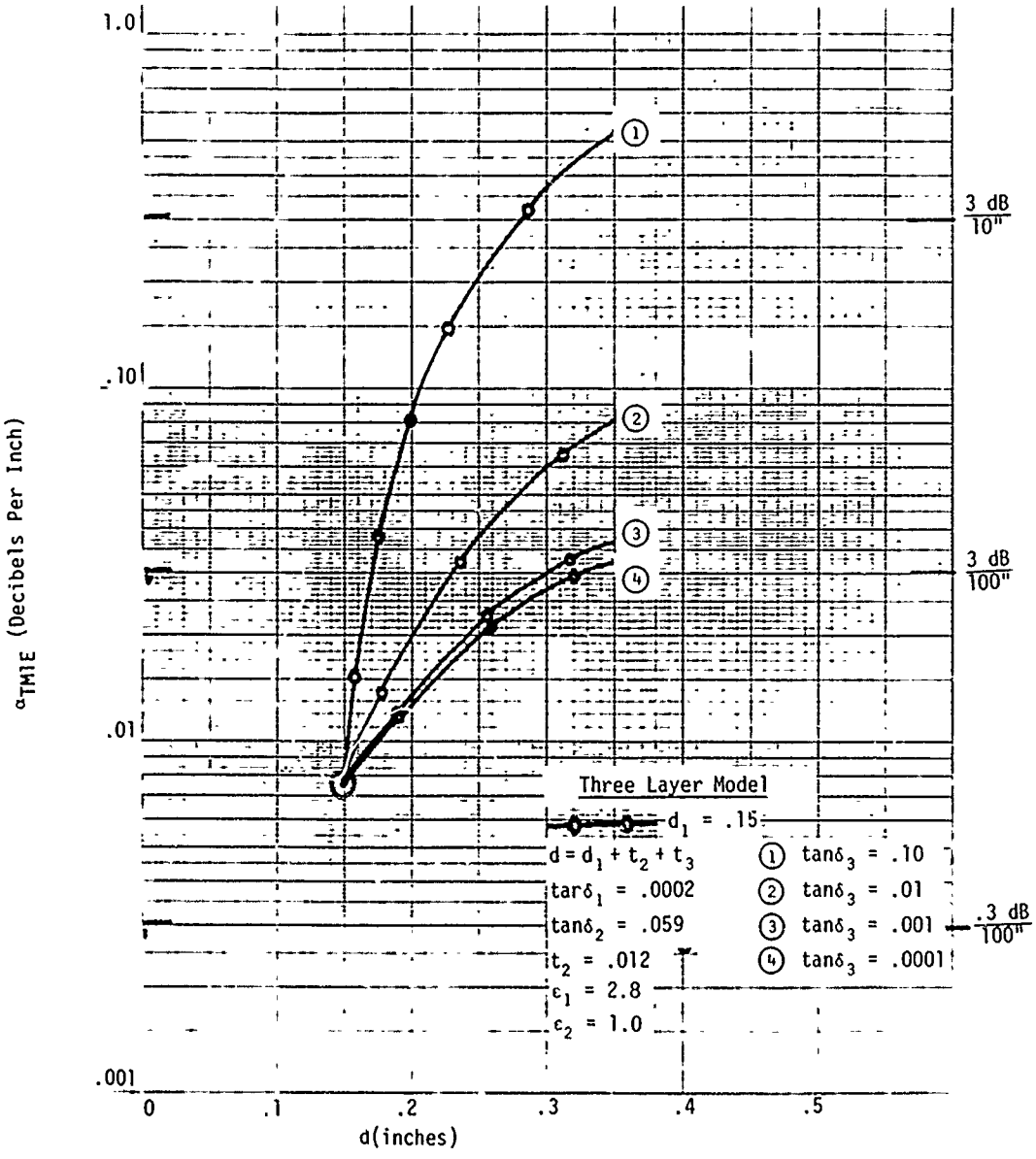

Figure 39. Attenuation versus thickness of dielectric for TM even mode
f = 5,850 MHz

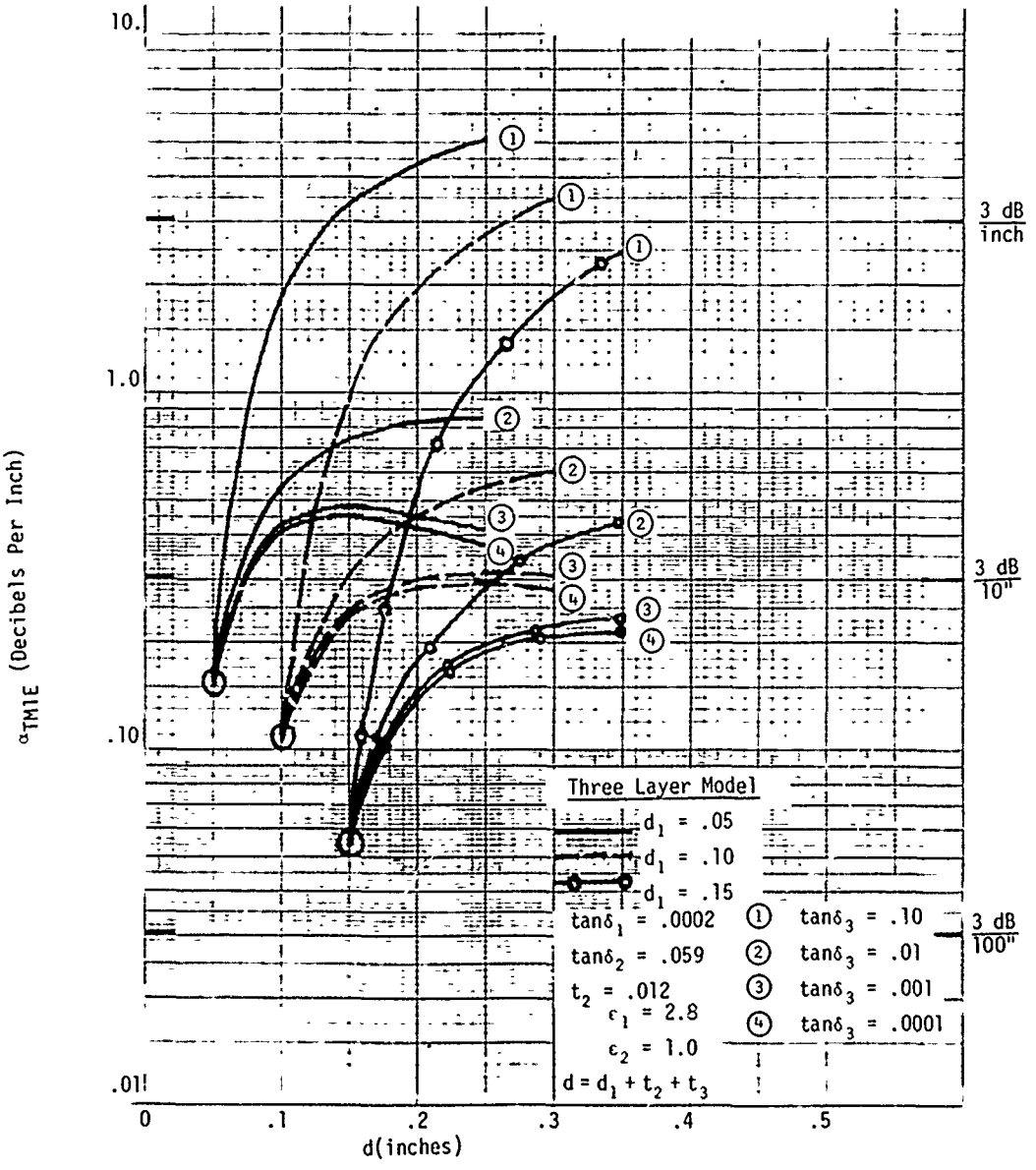

Figure 40. Attenuation versus thickness of dielectric for TM even mode
f = 22,125 MHz

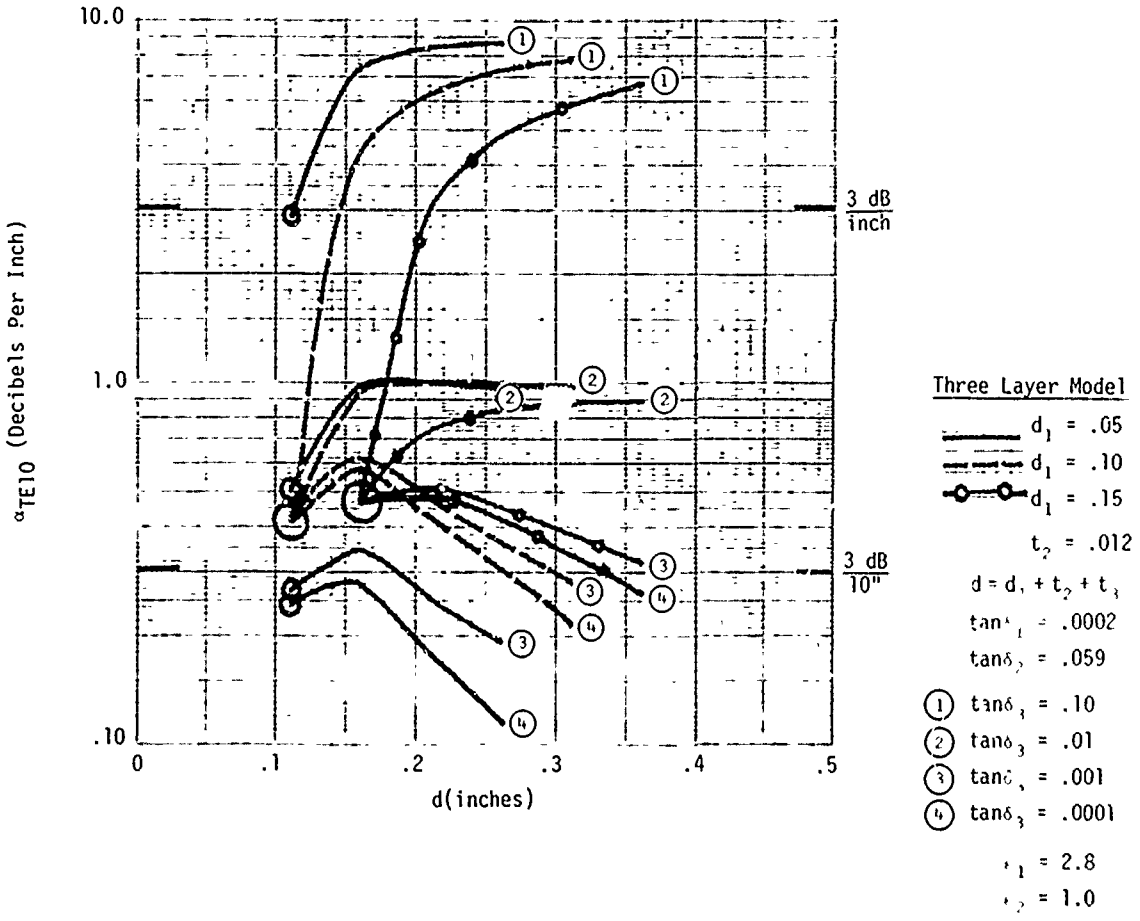

Figure 41. Attenuation versus thickness of dielectric for TE odd mode
f = 22,125 MHz

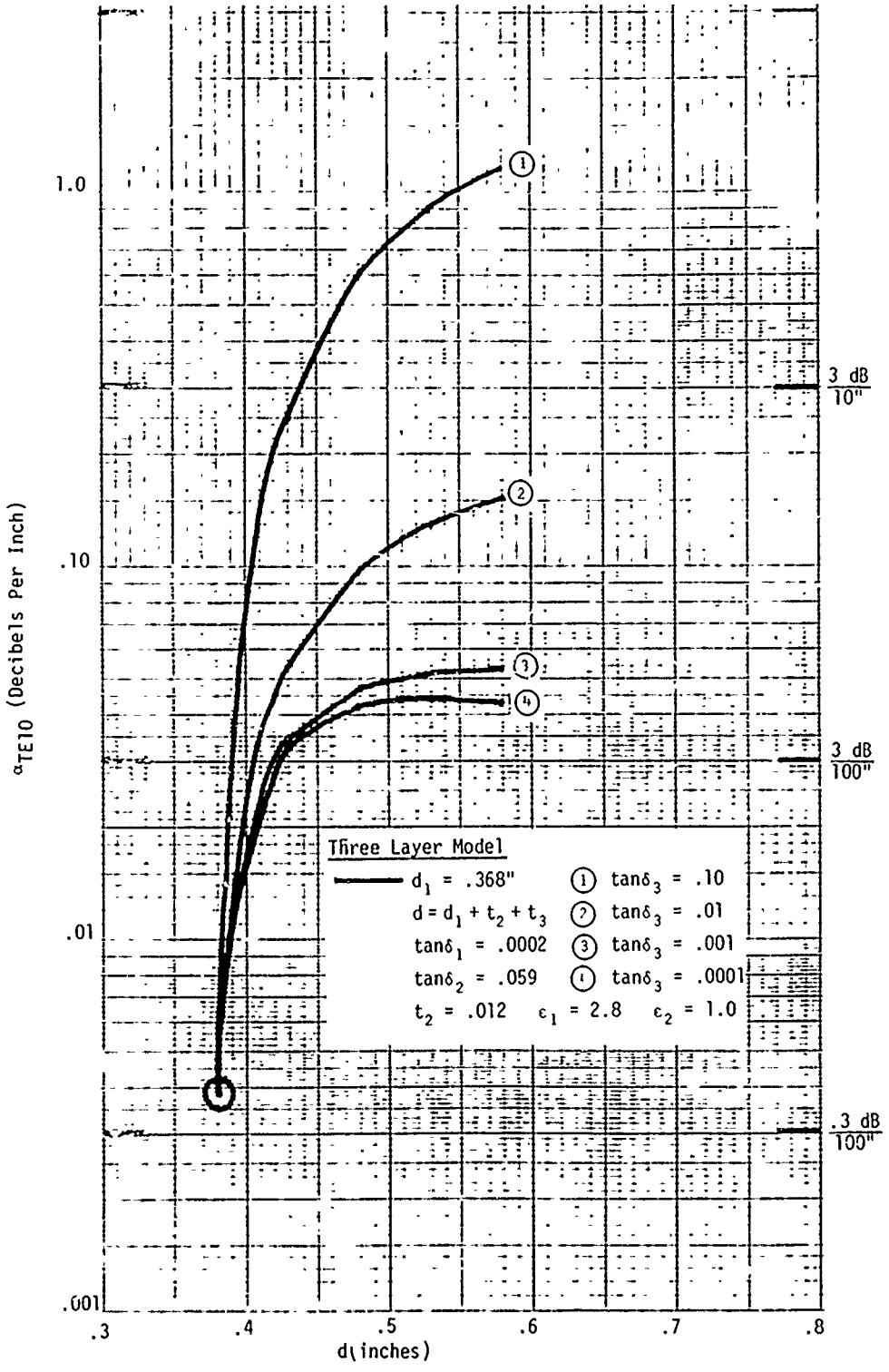

Figure 42. Attenuation versus thickness of dielectric for TE odd mode
f = 5,850 MHz

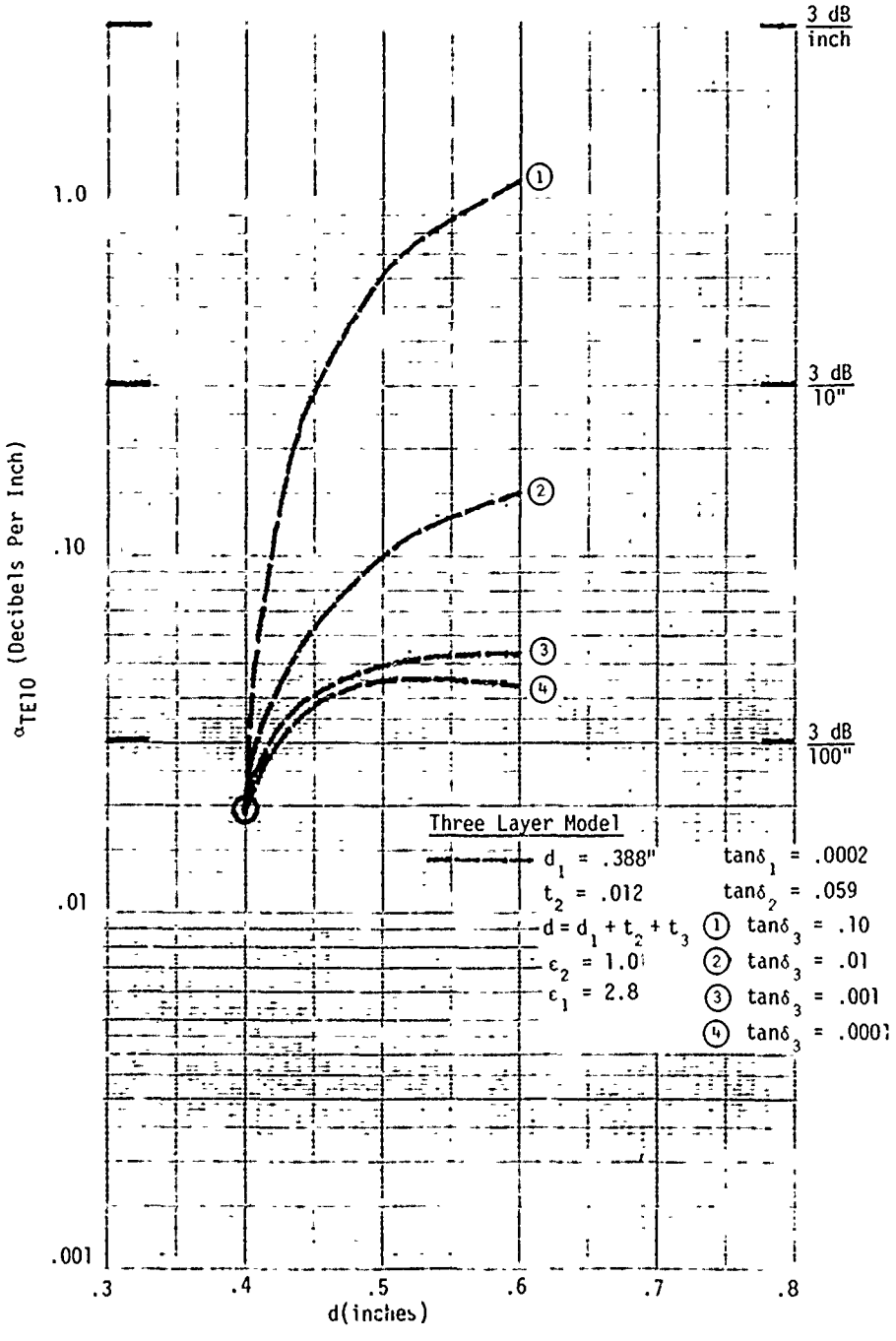

Figure 43. Attenuation versus thickness of dielectric for TE odd mode
f = 5,850 MHz

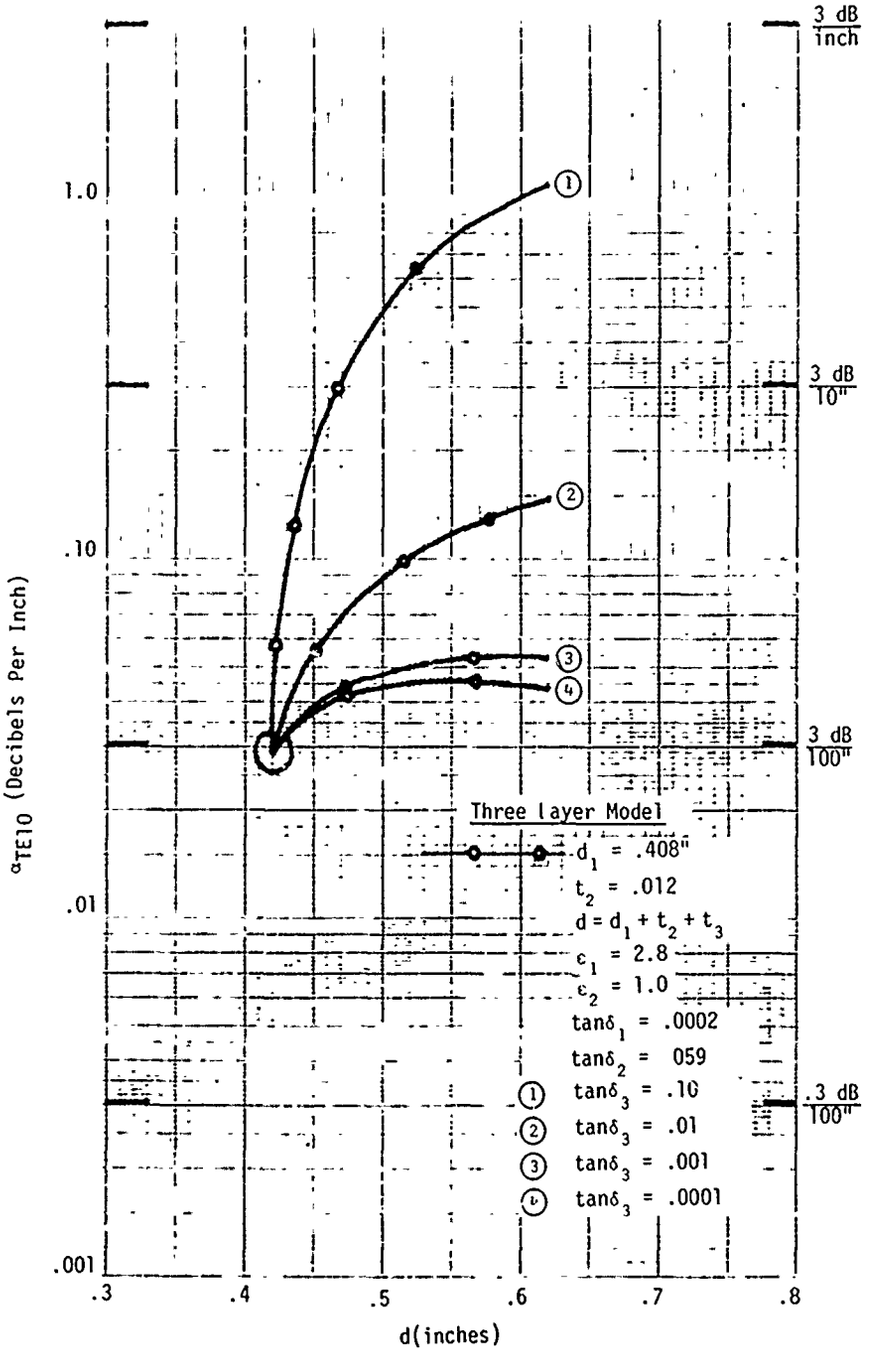

Figure 44. Attenuation versus thickness of dielectric for TE odd mode
f = 5,850 MHz

In these curves, the circled value at the lower-left extremity of each curve represents the attenuation constant of the base dielectric plus the polyurethane coat without any ice accretion. The effect of the growing layer of ice is the rapid increase in attenuation, with d illustrated in the diagrams.

MICROWAVE DEICER TRANSMISSION LINE EQUIVALENT CIRCUIT

It is convenient to represent the surface waveguide deicer by a transmission line equivalent circuit, as illustrated in Figure 45. In the ice-free condition, the transmission line is relatively lossless, represented by a low attenuation constant, α, and characteristic impedance Z_0. As ice accumulates, the characteristics of the line change drastically: α increases rapidly with ice thickness, as illustrated in Figures 27 through 44, and the characteristic impedance Z_0 changes.

The equivalent circuit of Figure 45 illustrates one rotor blade of length L with an accumulation of ice extending from r to the end of the blade. The portion between terminals 1 and 2 represents the ice-free portion (either at the tip or root) leading from the generator and has a characteristic impedance of Z_0 and a relatively low attenuation constant. The portion between terminals 2 and 3 represents the ice loaded section with a characteristic impedance of $Z_{oi}(d)$, which is dependent upon the thickness d of the ice layer plus the dielectric layer and a relatively high attenuation constant. The generator at terminal 1 represents the output of the feed system, injecting energy P_{in} into the surface waveguide. A matched load is shown terminating the transmission line at terminal 3 to assist in destroying any unwanted radiation. Power, P_{in}, injected into the line dissipates exponentially with distance r from the generator; the rate of dissipation is dependent upon the attenuation constant, illustrated by P_{ds} in Figure 45(b) and (c) for high- and low-loss lines respectively. The addition of an ice layer to the surface waveguide will tend to raise the attenuation constant, the effect being to increase the rate of power dissipation, as illustrated by P_{di} in Figure 45(b) and (c) for low- and high-ice attenuation constants respectively. Quantitative estimates of attenuation constants are given in Figures 27 through 44. Figure 45 serves to illustrate the hypothetical mechanism of rotor blade deicing.

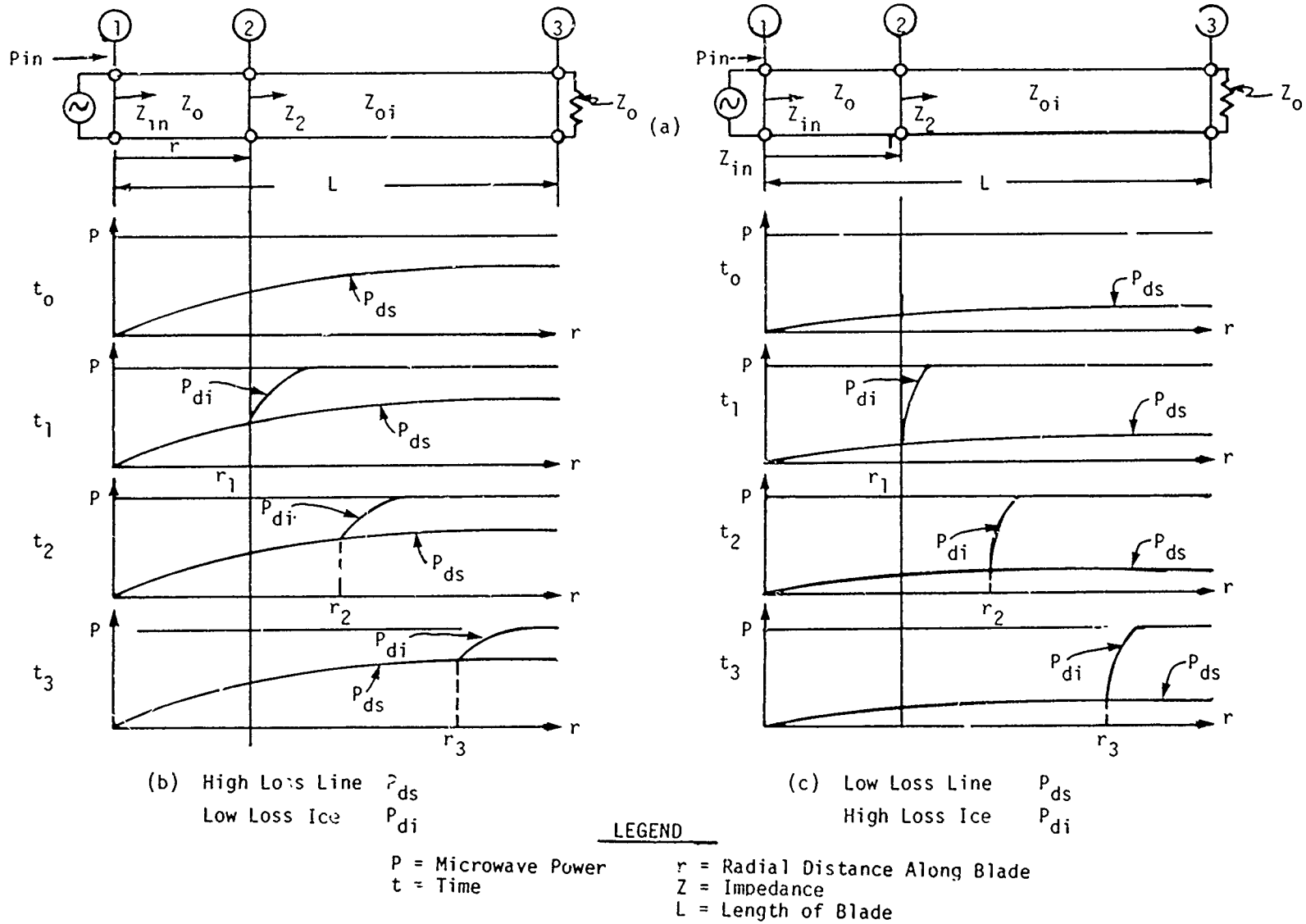

Figure 45. Equivalent circuit of microwave deicer tip-to-root or root-to-tip

In the ice-free condition, with a relatively low-loss surface waveguide, power injected into the line at terminal 1 will propagate down the line with only minor attenuation until it encounters the termination, where it will be absorbed (the deicer is normally off during this condition). In the iced condition, with a layer of ice extending from terminals 2 to 3, power injected at terminal 1 will propagate down the line with relatively low loss until it encounters the ice build-up at terminal 2; here the attenuation constant will undergo an increase, resulting in a larger exponential loss of power with distance. Power entering terminal 2 will be converted to heat and dissipated in the initial portions of the ice layer nearest the generator with very little, if any, power reaching terminal 3. The ice appears essentially as a matched load terminating the transmission line. The energy dissipated in the initial portions of the ice will elevate the temperature of these portions above the shed temperature, causing these portions to shed, thereby moving the location of terminal 2 down the line. The ice will shed progressively in the direction of propagation, in the manner illustrated in Figure 45(b) and (c) (t_1, t_2 and t_3), until all of the ice has shed and terminal 2 is coincident with terminal 3.

Figure 46 has been prepared to illustrate the exponential distribution of power on the UH-1 rotor blade as a function of the attenuation constant assuming ice accretions begin at station 50 and the attenuation constant remains the same throughout the length of the blade. The values of 3 dB/inch, 3 dB/10 inches, 3 dB/100 inches and 0.3 dB/100 in. have been used as convenient values for the attenuation constant, 3 dB representing 50% of the injected power. These values have also been flagged on Figures 27 through 44.

DESCRIPTIONS OF EXPERIMENTS TO BE PERFORMED TO VERIFY ESTIMATED POWER REQUIREMENTS

Experiments proposed for verifying the estimated power requirements for shedding ice are presented in Appendix C.

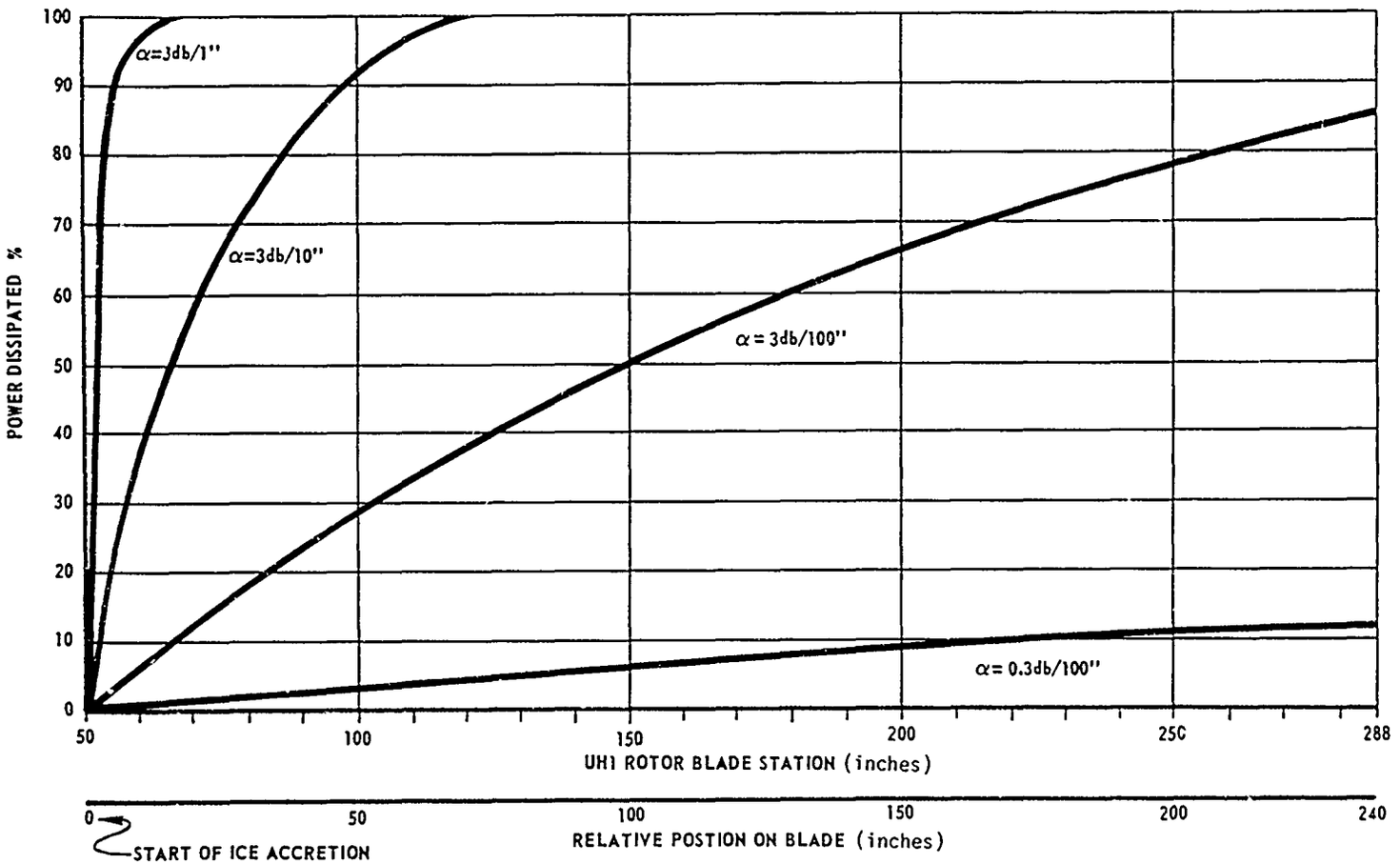

Figure 46. Exponential power dis bution on a UH-1 blade

SECTION 4
PHASE III - COUPLING TO SURFACE WAVEGUIDES

The problem of exciting surface waveguides differs somewhat from exciting rectangular or coaxial waveguides in that in surface waveguides the opportunity exists for some of the power intended for the surface waveguide to radiate into space. The efficiency of coupling is thus defined as the ratio of "power coupled to the surface waveguide" to the "radiated power plus coupled power". It is a measure of power coupled to the guide as opposed to that radiated.

Extensive experimental investigations of this problem exist in the technical literature and were identified in this study and discussed in Appendix G and the letter progress reports. Investigators report coupling efficiencies of greater than 70% and approaching 100%. Attention is brought primarily to two coupling techniques identified in the study that are simple, that will not require extensive modification of the rotor blade and that show a high probability of success: a coupler studied by DuHammel suitable for the TM modes and the coupler studied by Cohn suitable for the TE modes.[21],[24] Physical implementations of these couplers are illustrated in Figures 47 and 48 respectively. These couplers are recommended for initial development. Other coupling techniques (Appendix G) should not be ignored; these may have applications in other specific deicer designs.

THE TM_0 MODE COUPLER

An experimental investigation of the coupling efficiency of a coupler similar to that illustrated in Figure 47 was carried out by R.H. DuHammel.[24] DuHammel derived a formula for predicting efficiency. This

[21] Cohn, Cassedy and Kott, "TE Mode Excitation on Dielectric Loaded Parallel Plane and Trough Waveguides," IRE Transactions of Microwave Theory and Techniques, pp. 545-552 (September 1960).

[24] R.H. DuHamel and J.W. Duncan, "Launching Efficiency of Wires and Slots for a Dielectric Rod Waveguide," IRE Transactions of Microwave Theory and Techniques, July 1958.

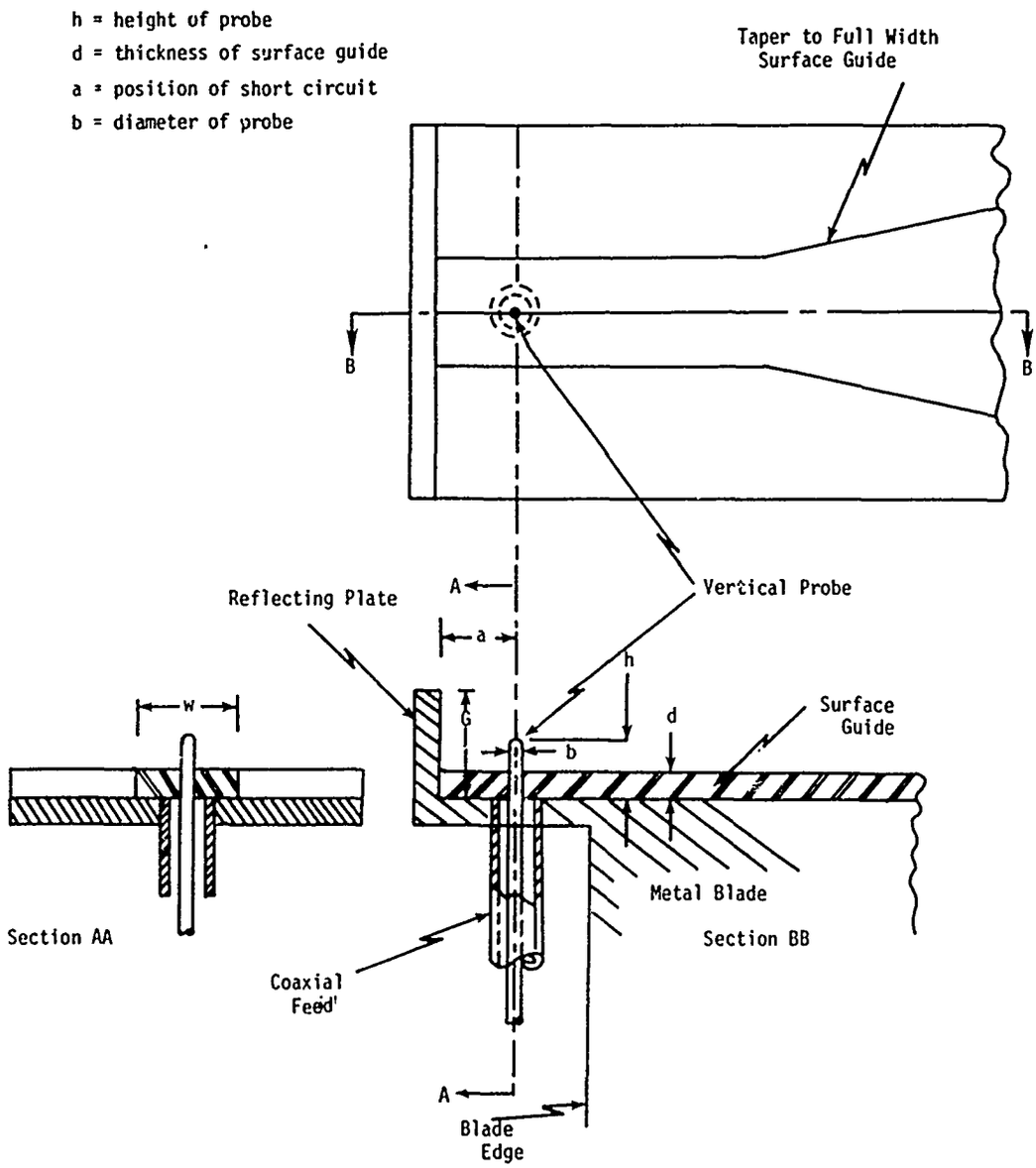

Figure 47. Experimental model - TM_0 mode coupler

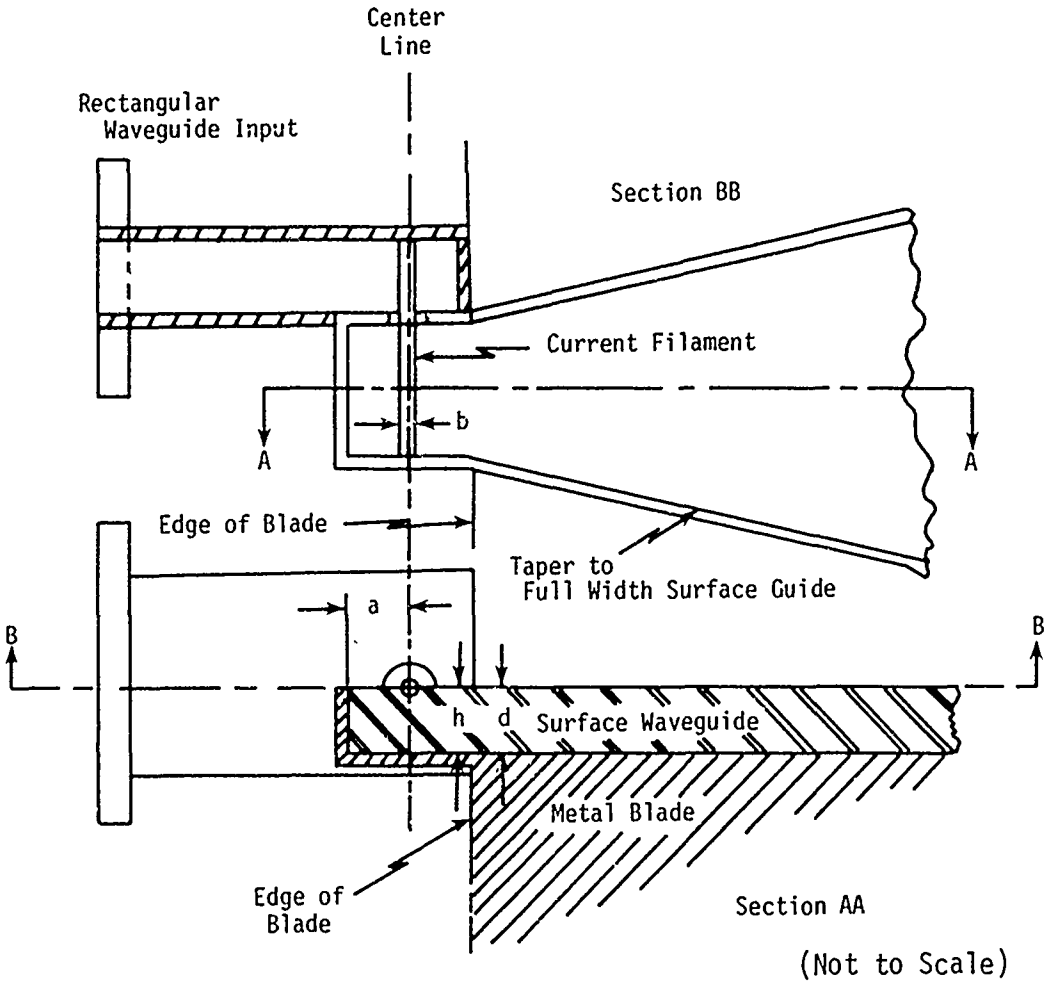

h = height of current filament above ground plane

d = thickness of dielectric

a = position of short circuit

b = diameter of current filament

Figure 48. Experimental model–TE_1 mode coupler

formula relates the efficiency of the launcher to its impedance as a scatterer on surface waveguides. Thus, by measuring the scatterer impedance, the efficiency may be calculated. Scatterer impedance was measured at six values of λ_g/λ, extending from 0.818 to 0.987. Two of the efficiency curves thus measured are illustrated in Figure 49 for λ_g/λ = 0.818 and 0.897, where efficiencies of 75% are indicated. Measurements were performed at 5,900 and 7,400 MHz. These measurements were checked by the Deschamps' method and show agreement to within 6% when the length of the wire was less than 0.35λ.

The work of DuHammel applies to the hybrid HE_{11} mode on dielectric rod image lines, as illustrated in Figure 7(e). This image line is similar to the rectangular image line illustrated in Figure 7(f) and used in the coupler (Figure 47). As the width of the dielectric image line is widened by tapering to full size surface guide, the HE_{11} mode will take on the characteristics of the TM_0 mode. Experimental investigations of rectangular image lines are reported on by Wiltse and Schlesinger.[26,28]

THE TE_1 MODE COUPLER

An experimental investigation of the coupling efficiency of a coupler similar to that illustrated in Figure 48 was carried out by Cohn in Reference 21. Cohn developed analytical and experimental tools to predict the bidirectional efficiency as a function of the dielectric thickness, the dielectric constant and the height of the probe above the dielectric. The unidirectional coupling achieved is twice the bidirectional coupling. Predicted and measured values of bidirectional coupling using Cohn's techniques are illustrated in Figure 50. The bidirectional coupling achieved

---

[21]Cohn, Cassedy and Kott, "TE Mode Excitation on Dielectric Loaded Parallel Plane and Trough Waveguides," IRE Transactions on Microwave Theory and Techniques, pp. 545-552, September 1960.

[26]James C. Wiltse, "Some Characteristics of Dielectric Image Lines at Millimeter Wavelengths," IRE Transactions on Microwave Theory and Techniques, pp. 65-69, January 1959.

[28]S.P. Schlesinger and D.D. King, "Dielectric Image Lines," IRE Transactions on Microwave Theory and Techniques, July 1958.

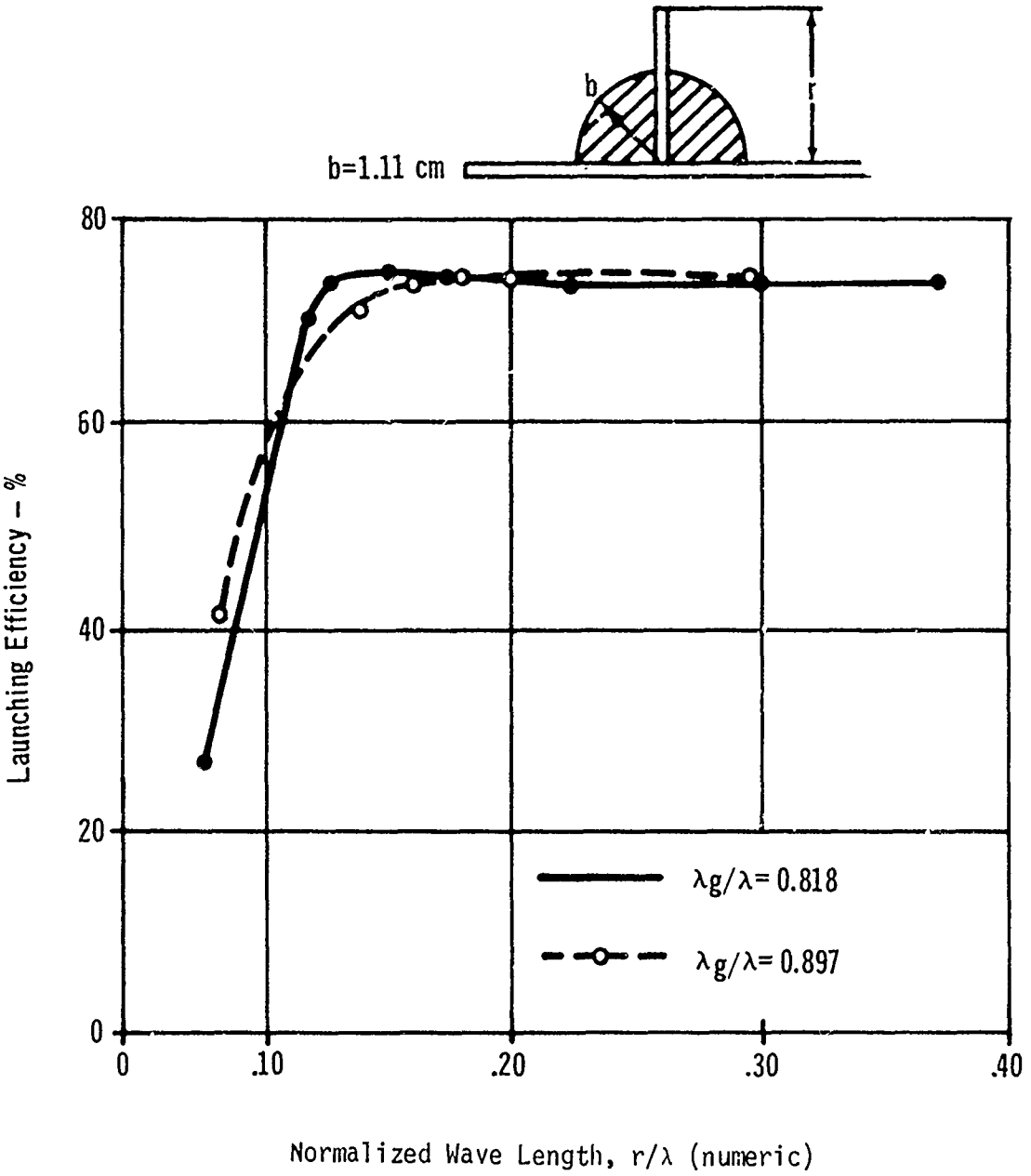

Figure 49. Launching efficiency of a vertical wire as a function of the normalized wire length (excerpted from DuHamel, Reference 24)

[24]R.H. DuHamel and J.W. Duncan, "Launching Efficiency of Wires and Slots for a Dielectric Rod Waveguide," IRE Transactions of Microwave Theory and Techniques, July 1958.

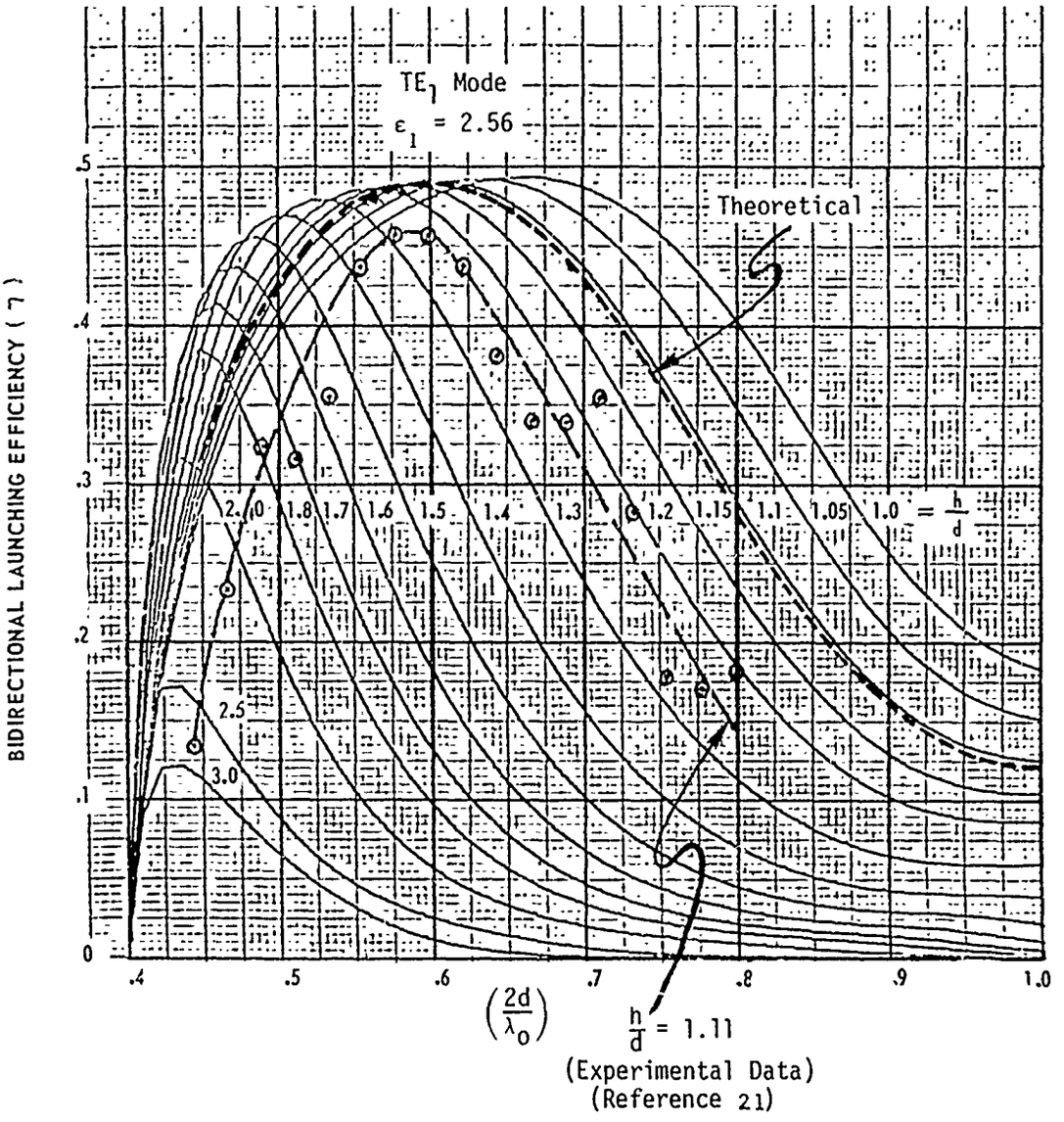

Figure 50. Computer-generated plot of bidirectional launching efficiency as a function of dielectric slab thickness for various values of current filament location and dielectric constant

[21] Cohn, Cassedy and Kott, "TE Mode Excitation on Dielectric Loaded Parallel Plane and Trough Waveguides," IRE Transactions of Microwave Theory and Techniques, pp. 545-552 (September 1960).

is 46%. The unidirectional coupling achieved by placing a short circuiting plate approximately a quarter wavelength from the probe is 92% (i.e., twice the bidirectional coupling). The results were measured for a dielectric constant of 2.56. Coupling curves for other dielectric constants computed with Cohn's technique are illustrated in Appendix G. Cohn's experiments were, strictly speaking, for trough lines. This would require the building up of side walls in the vicinity of the current filament. Ways will be sought to eliminate such walls.

LABORATORY DEMONSTRATION OF COUPLING THEORY

Experiments reported in the technical literature are sufficient to validate coupling theory.[19,20,21,23,24,25,32,33] We describe here experimental techniques that may be used to measure surface waveguide coupling. All of the microwave measurements required are performed with the apparatus illustrated in Figure C-1. Specific procedures required to measure couplings are grouped with other microwave measurements in Appendix D and are also described in Reference 21.

---

[19]A.L. Cullen, "The Excitation of Plane Surface Waves," Proceedings of the IEE, London, vol. 101, part IV, pp. 224-234, February 15, 1954.

[20]G.J. Rich, "The Launching of a Plane Surface Wave," Proceedings of the IEE, London, vol. 102, part B, pp. 237-246, March 1955.

[21]Cohn, Cassedy and Kott, "TE Mode Excitation on Dielectric Loaded Parallel Plane and Trough Waveguides," IRE Transactions on Microwave Theory and Techniques, pp. 545-552, September 1960.

[23]J.W. Duncan, "The Efficiency of Excitation of a Surface Wave on a Dielectric Cylinder," IRE Transactions on Microwave Theory and Techniques, pp. 257-268, April 1959.

[24]R.H. DuHamel and J.W. Duncan, "Launching Efficiency of Wires and Slots for a Dielectric Rod Waveguide," IRE Transactions of Microwave Theory and Techniques, July 1958.

[25]A.D. Frost, C.R. McGeoch and C.R. Mingins, "The Excitation of Surface Wave-Guides and Radiating Slots by Strip-Circuit Transmission Lines," IRE Transactions on Microwave Theory and Techniques, October 1956.

[32]M. Cohn, "Propagation in Dielectric-Loaded Parallel Plane Waveguide," IRE Transactions on Microwave Theory and Techniques, pp. 202-208, April 1959.

[33]M. Cohn, "TE Modes of Dielectric Loaded Trough Line," IRE Transactions on Microwave Theory and Techniques, pp. 449-454, July 1960.

SECTION 5

PHASE IV - MICROWAVE DEICER PRELIMINARY CONFIGURATION

A block diagram of a UH-1 rotor blade microwave deicer is illustrated in Figure 51. The following is a list of components, which will be described in this section:

Microwave Deicer Boot	Microwave Tube
Coupler	Power Supply
Distributor/Power Divider	Pilot's Control Panel
Feeder	Ice Detectors
Rotary Joint	Outside Temperature Detector

For the purposes of this initial feasibility analysis, all cost and weight estimates given in this section are based upon extrapolations from a) off the shelf components b) modified off the shelf components c) similar and comparable components previously manufactured.

MICROWAVE DEICER BOOT

Preliminary configurations of the microwave deicer boot are illustrated in Figures 52 through 56. The boot protects 10% of the top surface and 25% of the bottom chordwise. Spanwise it can be made to provide complete coverage from station 28 to the tip. The exact deicing coverage of the rotor blade required in the region of the doublers (Figure 52) between station 28 and 83 has not been defined in this preliminary feasibility study. This region is assumed to be a non-critical area and the possibility exists that only limited coverage need be provided here. If need be, the deicer boot can be tailored to provide limited coverage or complete coverage.

The preliminary boots illustrated in Figures 53 through 56 are suitable for the TM_0 mode and TE_1 mode of propagation. Figures 53 and 54 are suitable for both modes, whereas 55 and 56 will suppress the TM_0 mode. The extrusions illustrated in Figure 55 serve several purposes. They suppress the TM_0 mode, provide a polarization anchor for the TE_1 mode and provide a means of fastening the dielectric to the rotor blade.

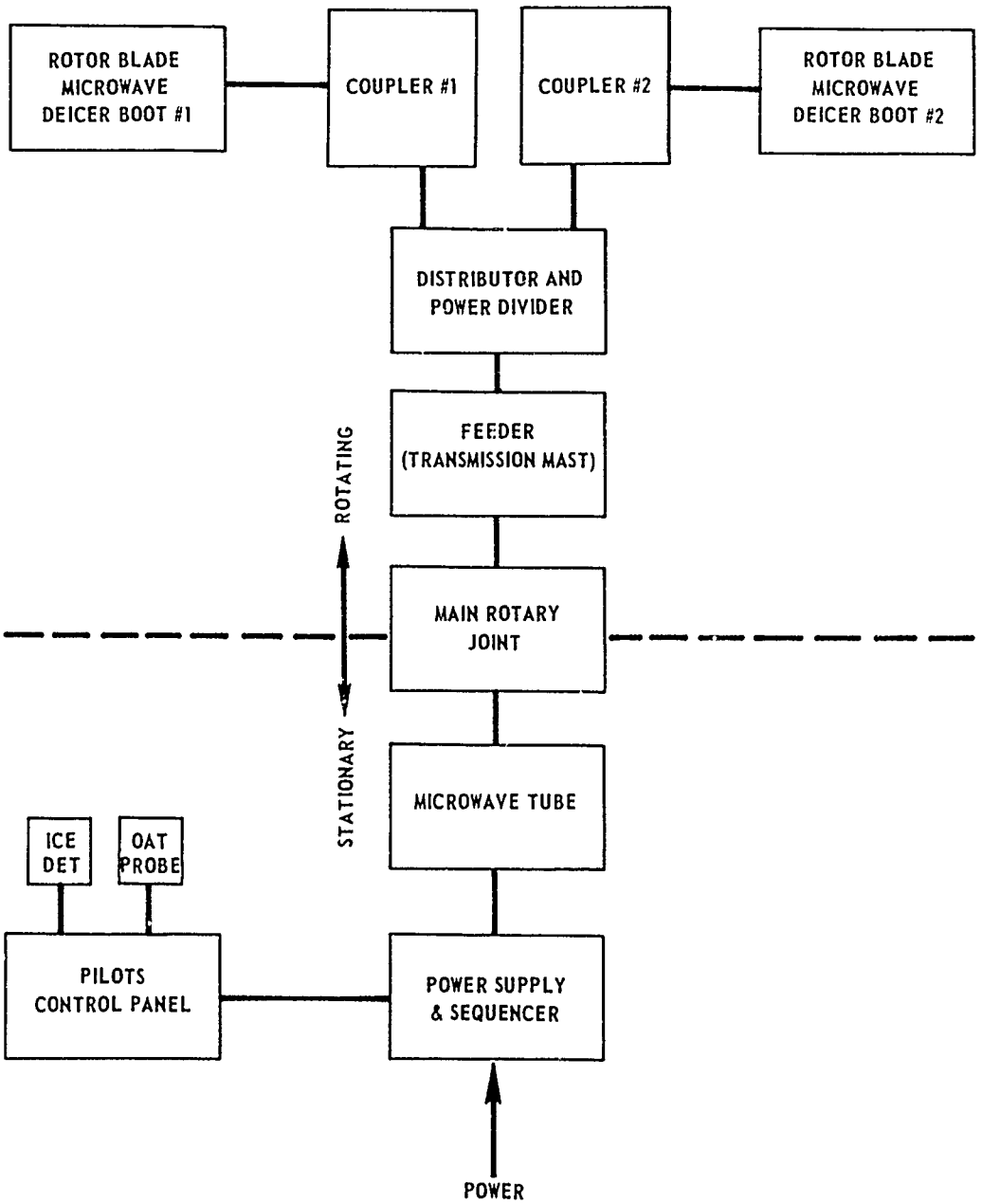

Figure 51. UH-1 rotor blade microwave deicer - block diagram

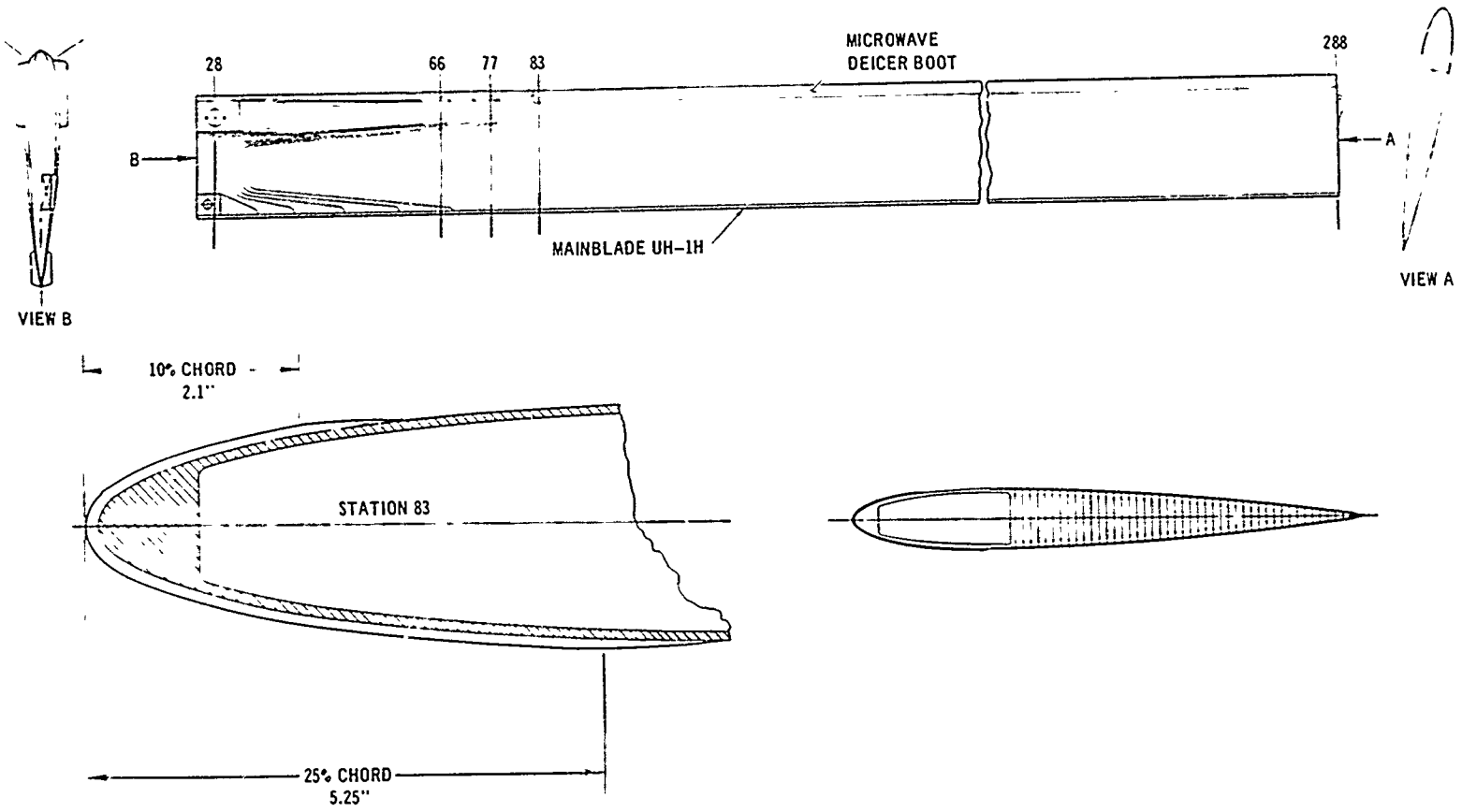

Figure 52. UH-1H blade with micr
runs full length

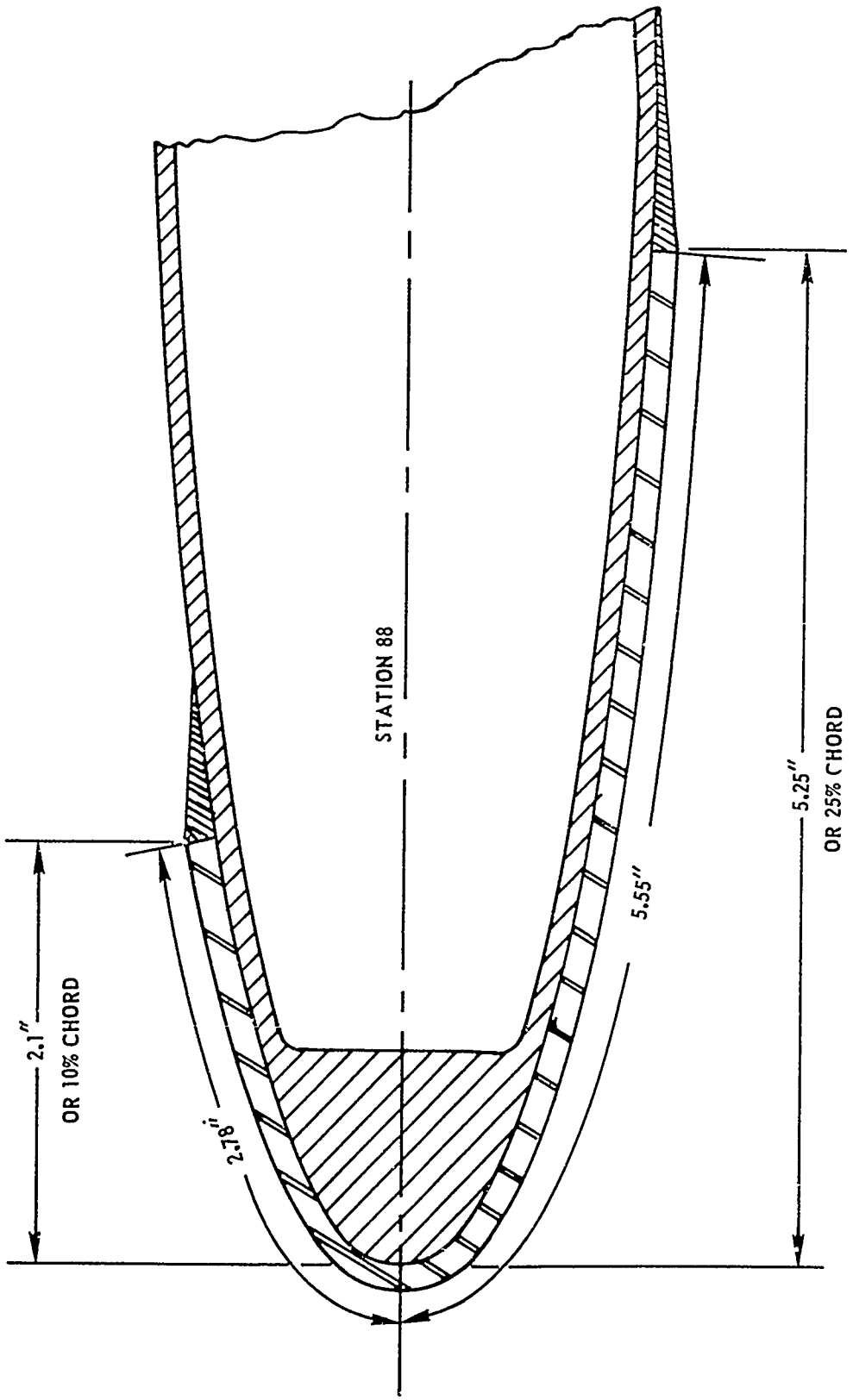

Figure 53. Preliminary cross section of TM_0 and TE_1 mode surface waveguide deicer station 33

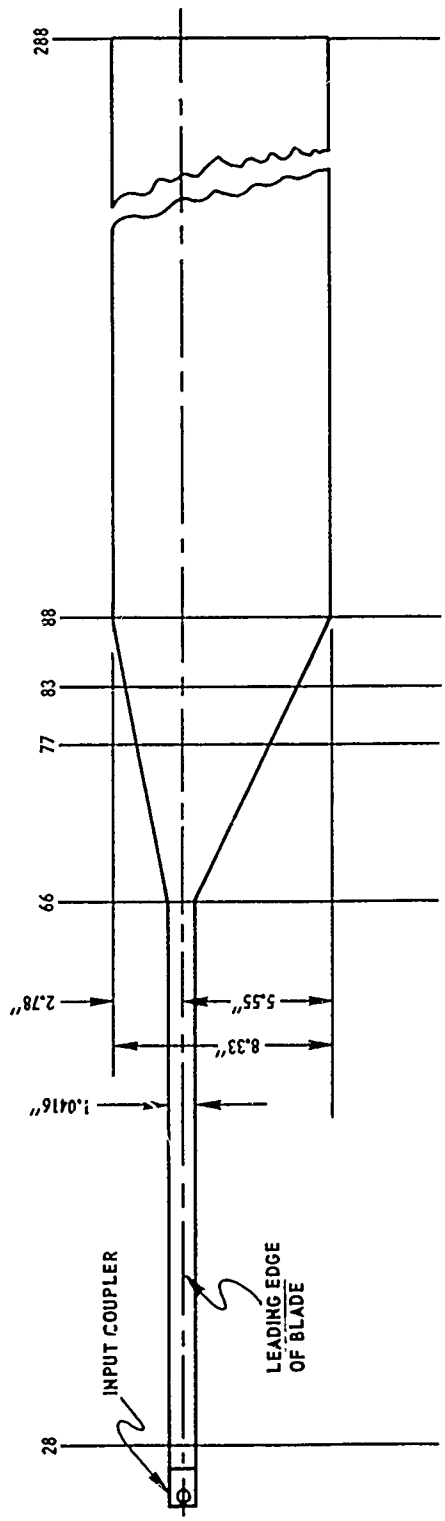

Figure 54. Preliminary design of root fed TM_0 and TE_1 mode surface waveguide deicers (waveguide laid out flat)

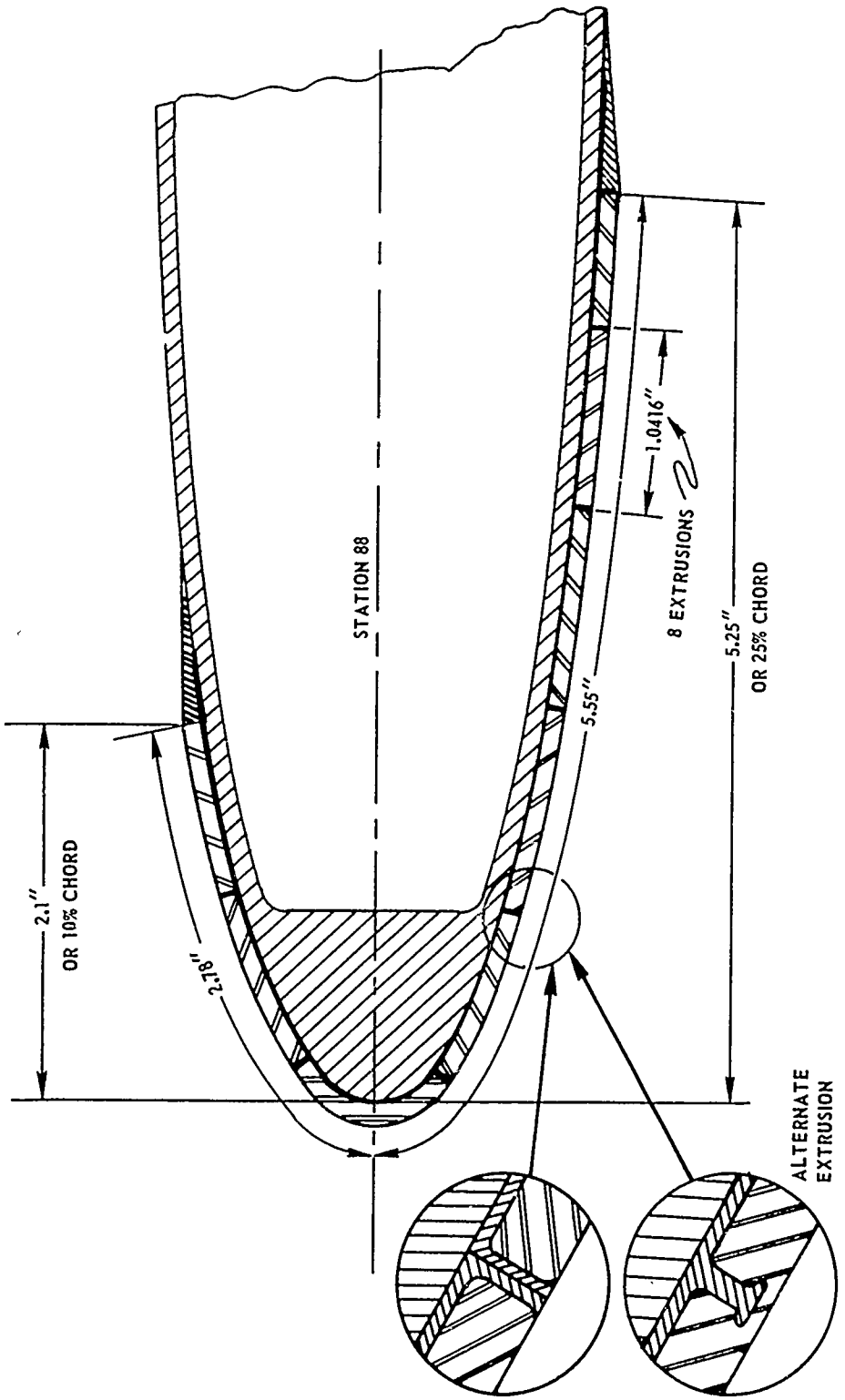

Figure 55. Preliminary cross section of the TE_1 mode surface waveguide, which runs the full length of blade, at deicer station 88

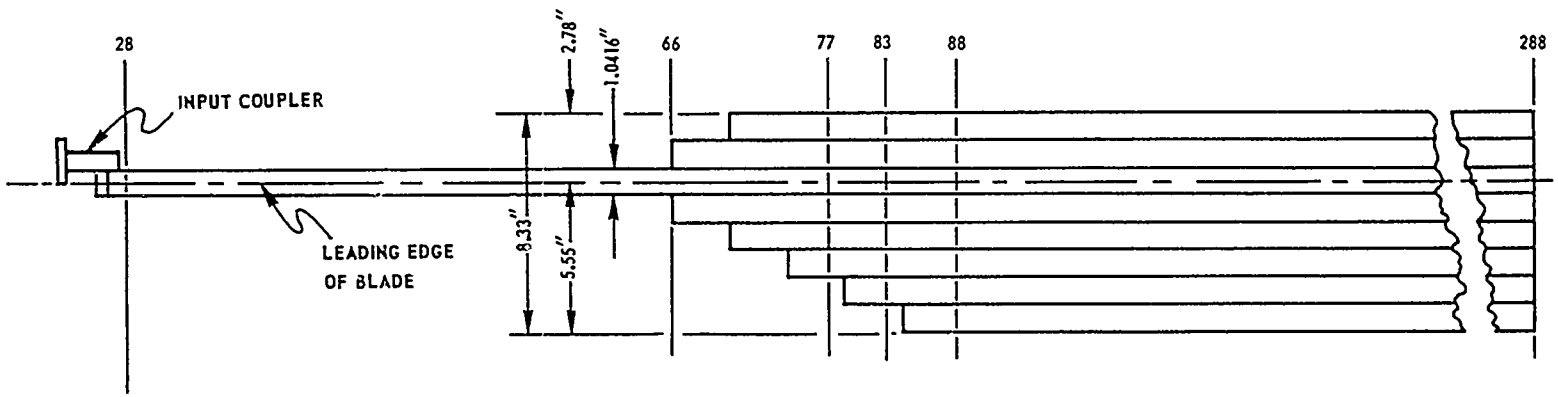

Figure 56. Preliminary design of the TE_1 mode surface waveguide deicer boot (developed) - root fed

Materials suitable for use on the blade are discussed in Section 2. The material used must be able to withstand the severe rain, sand and dust erosion environment encountered by rotor blades. Segments of the rotor blade near the tip, in the vicinity of the leading edge, will be subject to a more severe erosion environment due to higher speeds and higher angles ofimpingement than found on other portions of the blade. It is not unreasonable, therefore, to think of providing these regions with a dielectric material such as Alumina, which provides a high resistance to erosion. Remaining portions of the boot can be made from other materials of lower weight than nickel.

Estimated Weight of the Deicer Boot

The weight of the boot will depend upon its thickness and material. Weight computations for composite and metal blades, presented in Table 7, indicate a weight savings of approximately 10 pounds/blade for both composite and metal blades if the boot replaces the nickel erosion shield that protects approximately the same area.

Cost of the Blade

Installed, incremental costs of the blade are estimated to be $450 per blade, based on similar and comparable installations.

Microwave Coupler

The coupler is the subject of Section 4. Configurations of recommended couplers are illustrated in Figures 47 and 48. These couplers should weigh less than one pound each and cost no more than $250 each installed in production quantities. Couplers may be used at the root or tip end of the rotor.

Distributor and Power Divider

The power divider is required to divide the power from the microwave source into two equal parts for distribution to the two blades. Power dividers are relatively common microwave devices; their technology is very well developed. Power dividers may be obtained in either coaxial line or waveguide. Coaxial line dividers are suitable for the lower microwave frequencies (2,450 and 5,850 MHz), whereas waveguide dividers are required at

22,125 MHz. A typical coaxial line power divider is illustrated as the tee connector at the top of Figure 57, extending through the hub of the rotor.

TABLE 7. WEIGHT COMPUTATIONS OF MICROWAVE DEICER BOOT AND EROSION SHEILD

Significant Parameters

1)	Width of Deicer Boot	= 8.33 in
2)	Length of Deicer Boot	= 260 in
3)	Base Area of Deicer Boot	= 2,165.8 in^2
4)	Thickness of Nickel Erosion Shield	= .020 in
5)	Density of Nickel	= .3219 lb/in^3
6)	Weight of Nickel Erosion Shield	= 14.2 lb/blade
7)	Density of Polyethelene	= .0344 lb/in^3
8)	Density of Alumina	= .0980 lb/in^3

Assumed Deicer Boots for Weight Calculations

Composite Blades	Metal Blades
Alumina Coating .025 in Thick, Station 188 to 288 Polyethelene Coating .050 in Thick, Station 28 to 188 Weight of Alumina 2.04 lb Weight of Polyethelene 1.97 lb Total Weight of Boot ≅ 4.0 lb	Alumina Coating .025 in Thick, Station 91 to 288 (195.6 in long) Weight of Alumina Boot ≅ 4.0 lb

Net Savings over Nickel Erosion Shields

14.2 - 4.0 lb ≅ 10 lbs/blade
or 20 lb/two blades

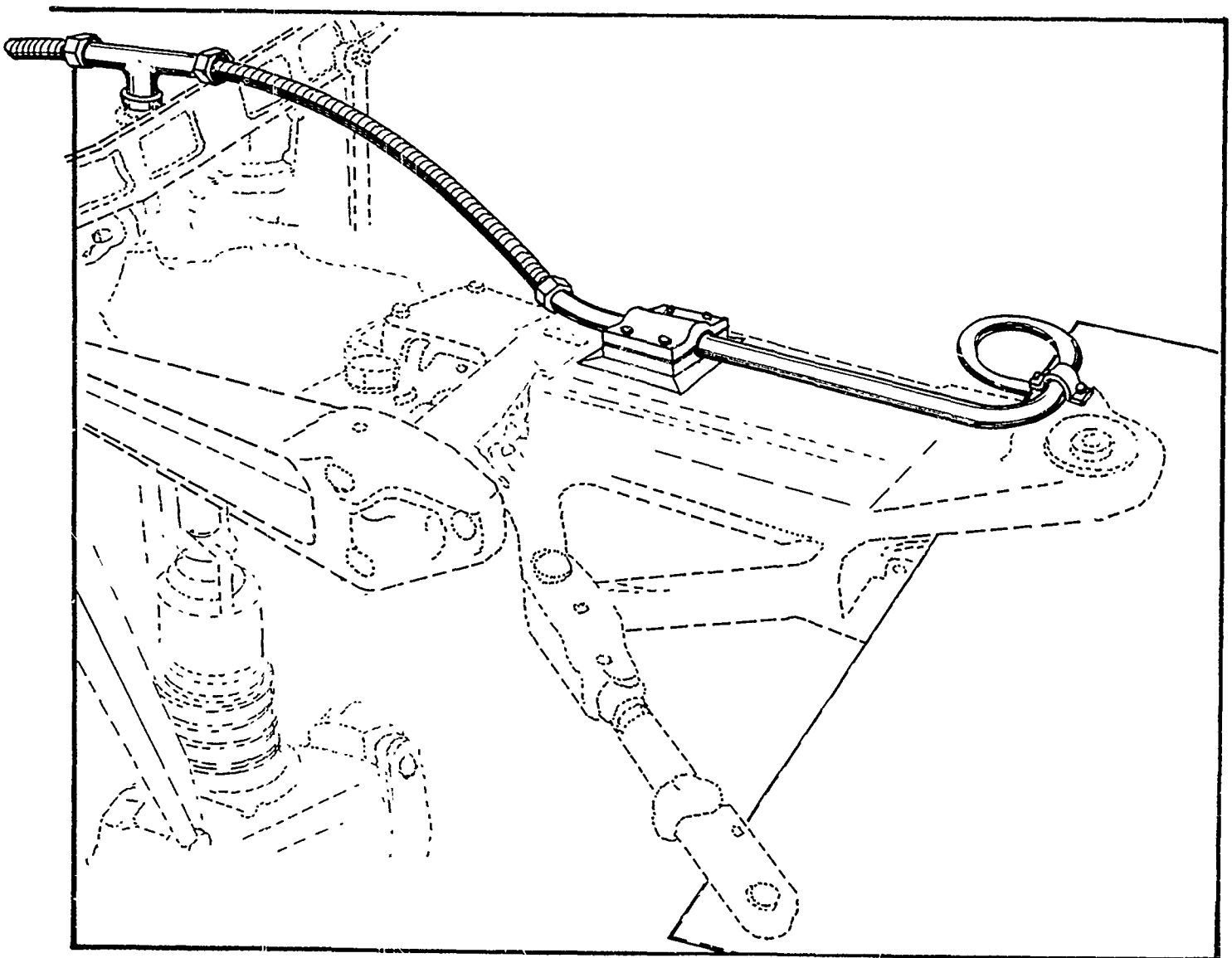

Figure 57. Coaxial line distributor applicable to 2,450 and 5,850 MHz

Power is carried to the deicer boot and coupler through the flexible, stainless steel coaxial lines illustrated in Figures 57 through 59. The flexible coaxial lines accommodate the rotor system motions for both dynamic and static conditions, as illustrated in Figure 58. These motions include hub flapping, blade feathering, stretching and bending.

It is believed that a similar system using flexible waveguide can be used for 22,125 MHz. A distributor for a radar system was developed for Bell Helicopter Company several years ago that could be adapted for distributor service. A photograph of this distributor is presented in Figure 60. It is presently believed that this distributor, intended for radar service, is over-designed, A photograph of a flexible waveguide distributor for use in the Bell Helicopter radar system is given in Figure 61.

Weight of Distributor Power Divider

The estimated weight of stainless steel power dividers and distributors, including fastening hardware, is less than 9 pounds.

Installed Cost of Power Divider and Distributor in Production Quantities

The estimated cost of a coaxial power divider and distributor is less than $850. The estimated cost of a waveguide power divider and distributor is less than $4,500.

FEEDER

The feeder is a long section of either coaxial line or waveguide that carries microwave energy up the rotor shaft. A photograph of a waveguide feeder for a radar system is shown in Figure 62. A 10-foot long, 1-inch-diameter coaxial feeder should weigh no more than 6 pounds and cost less than $850 installed in production quantities. A waveguide feeder is estimated to cost no more than $1,200 installed.

MAIN ROTARY JOINT

The main rotary joint provides the interface between the fuselage and the rotating rotor. One of the major benefits derived from the use of the rotary joint is that, unlike slip rings, it has no contacting parts and should provide a maintenance-free, highly reliable, long life. A photograph

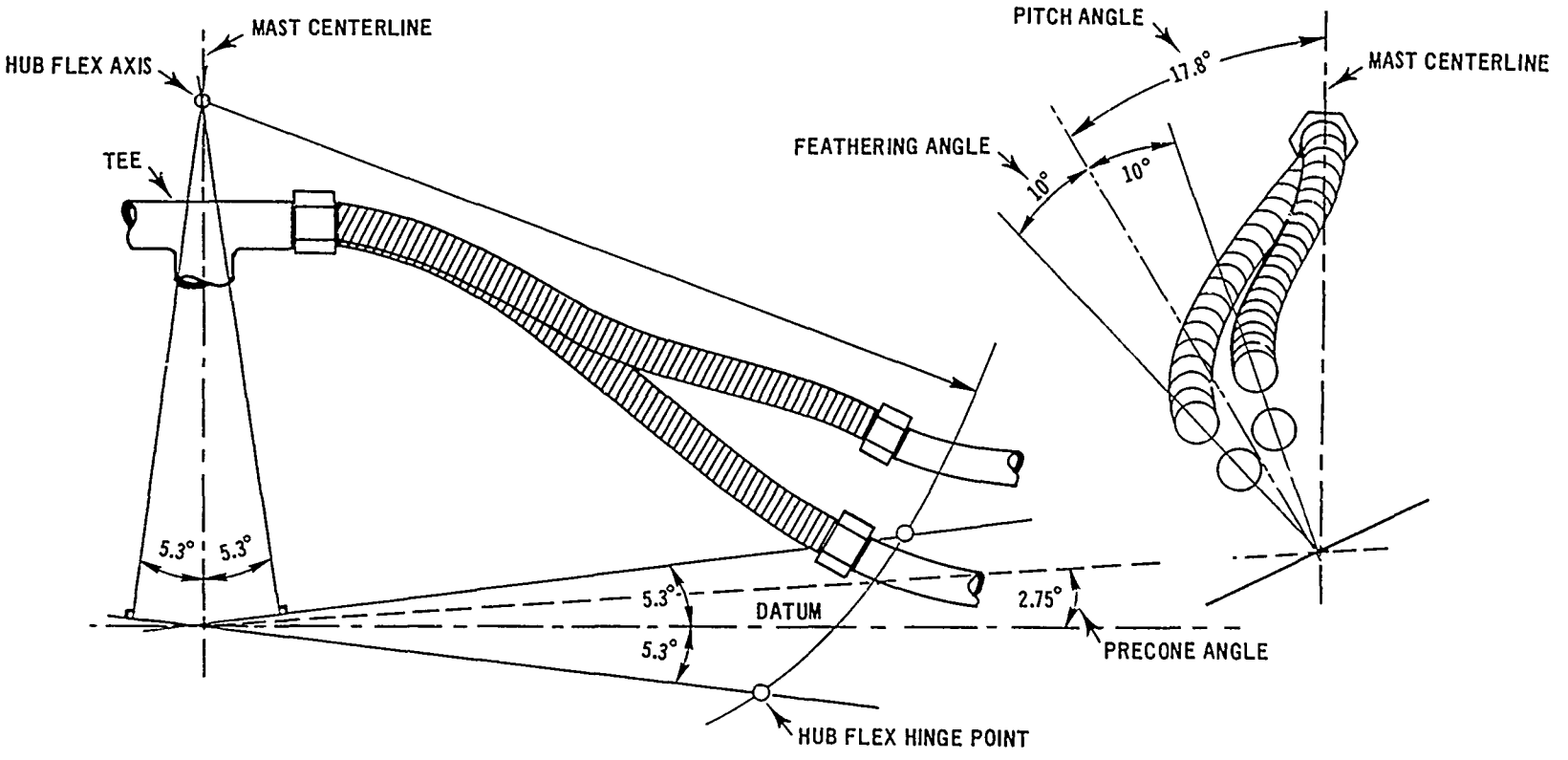

Figure 58. Coaxial line distributor

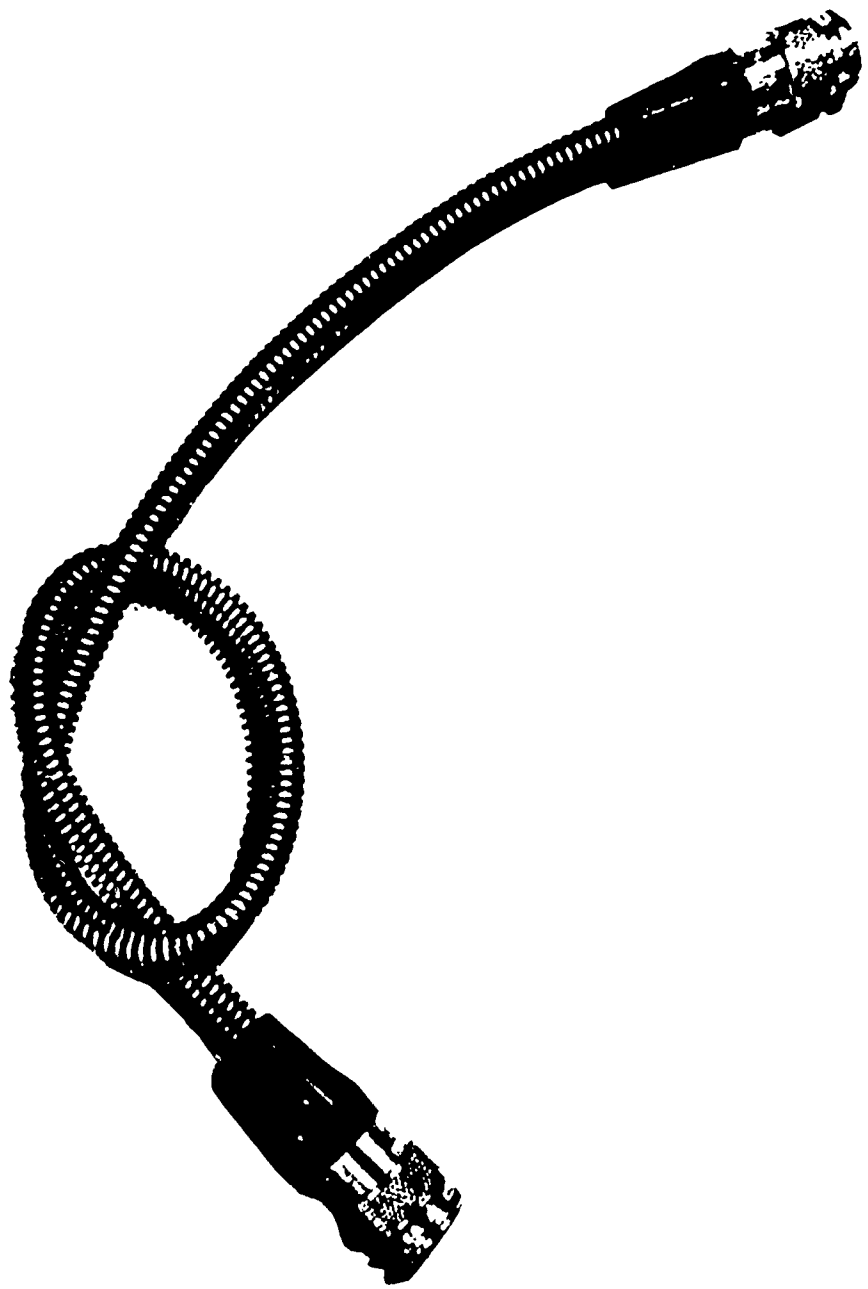

Figure 59. A typical stainless steel flexible coaxial line

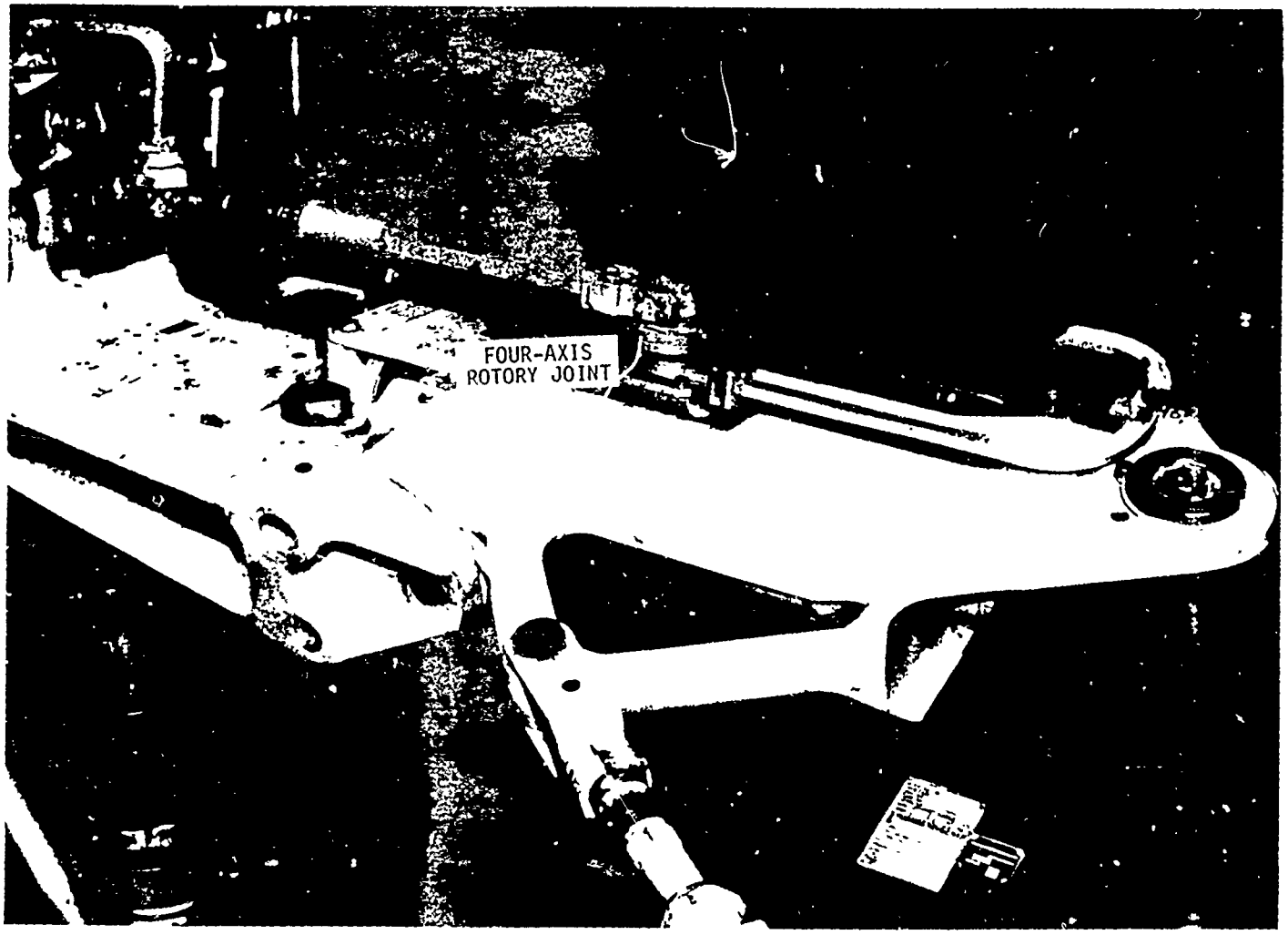

Figure 60. Radar system distributor adaptable for distributor service

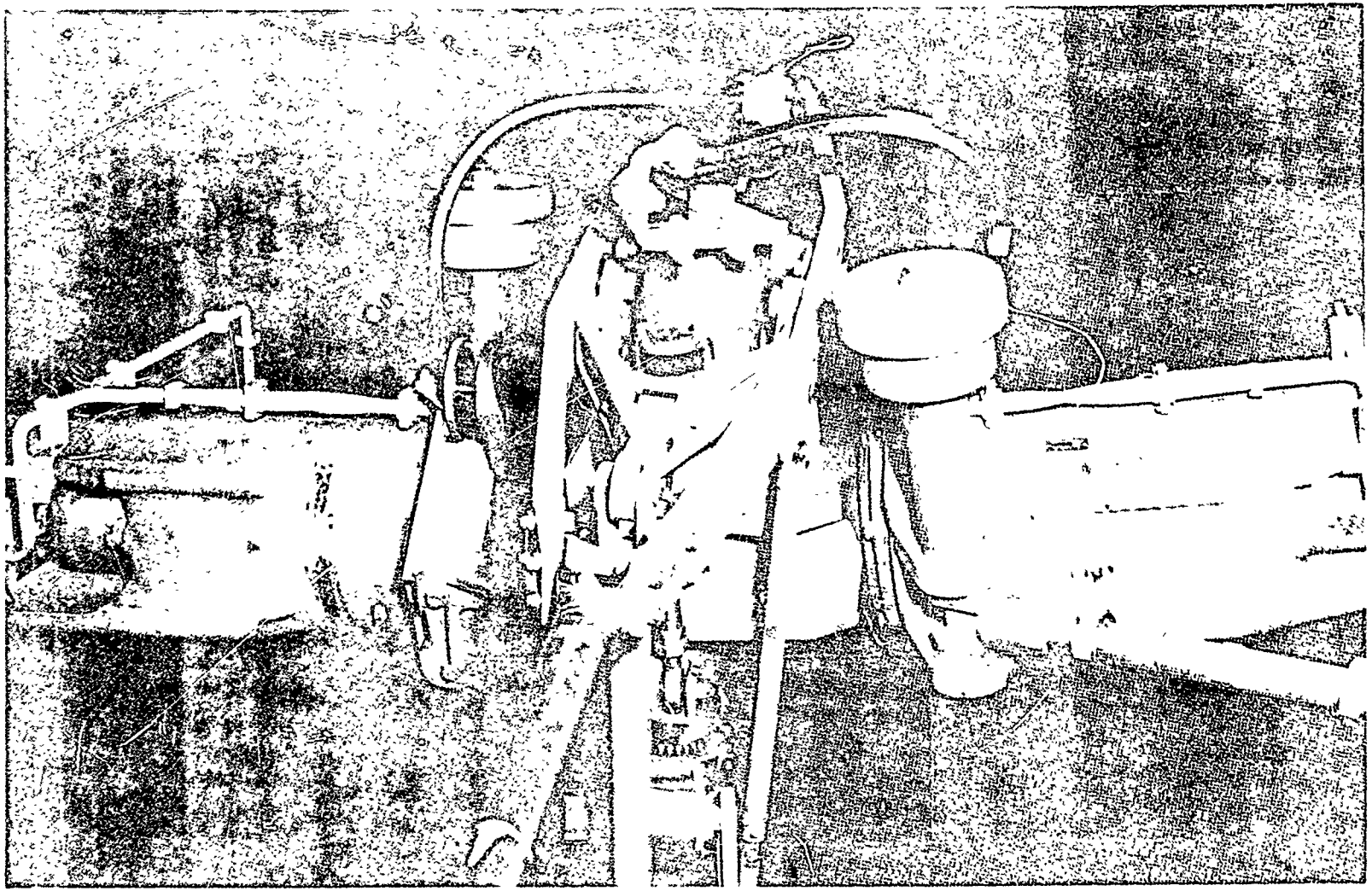

Figure 61. Flexible waveguide distributor for use in a Bell Helicopter radar system

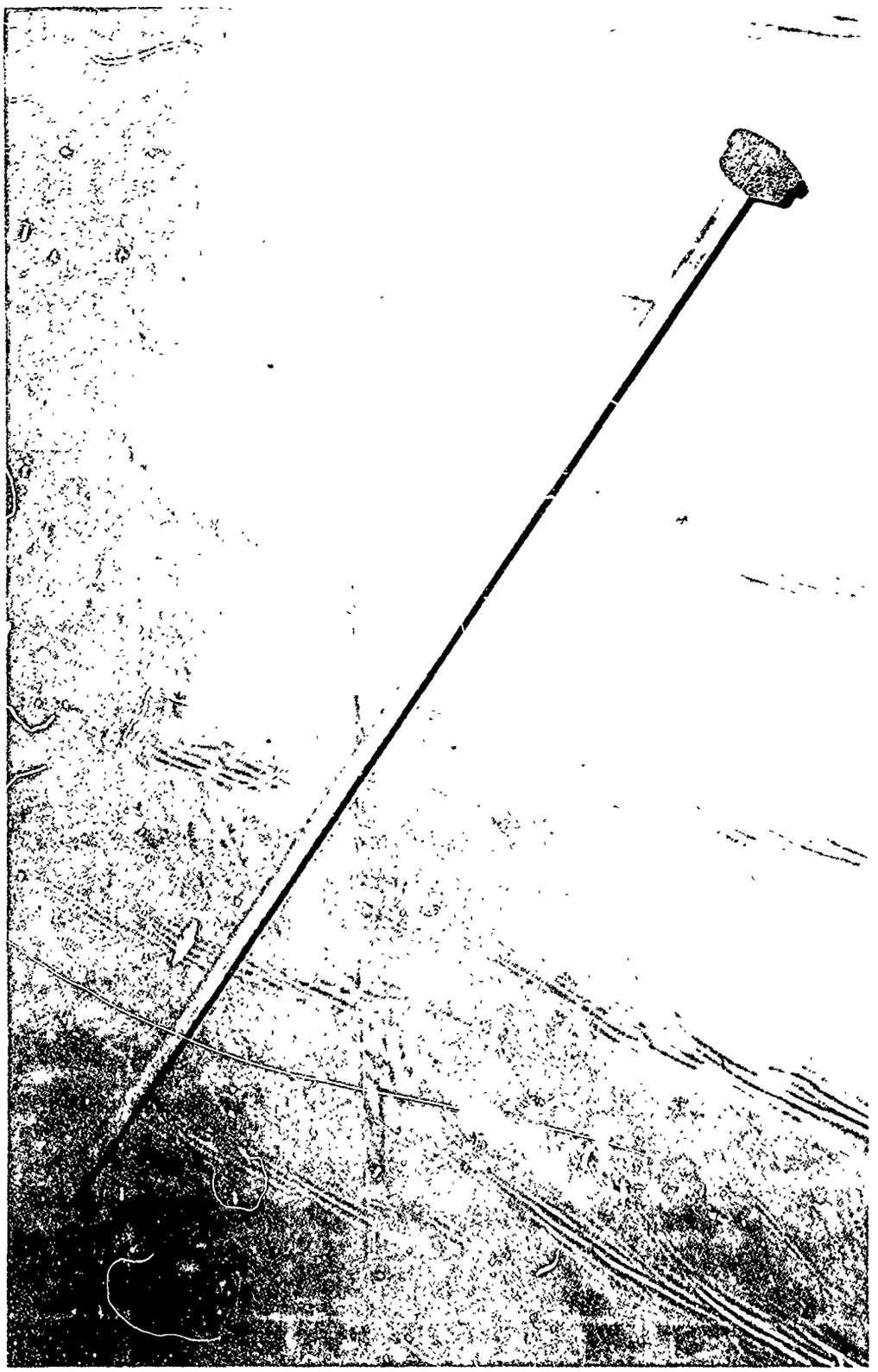

Figure 62. Waveguide feeder for a radar system

of a waveguide rotary joint developed for helicopter use is shown in Figure 63. This rotary joint should weigh no more than three pounds and cost less than $650 installed in production quantities.

MICROWAVE GENERATOR

A table of candidate tubes for a microwave deicer is presented in Table 8. An outline drawing of the most powerful tube on the list, the YJ1191A, 5 kw Magnetron, is presented in Figure 64. This is presented as an approximate upper bound of size and weight for all tubes in the 2,450 MHz band. Lower-power tubes are considerably smaller and weigh less. An outline and photograph of the Varian VKU-7791 Series is presented in Figures 65 and 66 to convey the same information for 22 GHz Klystrons.

An outline of a Varian extended interaction oscillator is presented in Figure 67 for use at 22 GHz.

Commercial heating tubes in the 2,450 MHz band are relatively inexpensive. It is unknown how these tubes will behave in a military environment, i.e., whether they meet the requirements in MIL-E-5400. One approach to gaining some statistical insight would be to submit a sufficient number of the commercial tubes to the required environment.

From the manufacturer's commercial catalog, 2,450 MHz Magnetron costs can range from $250 to $500, depending on power. We would assume from this that a ruggedized tube guaranteed to meet MIL-E-5400 would be estimated at less than $1,500 per tube in production quantities.

An Extended Interaction Oscillator for use at 22,125 MHz has been quoted as $3,000 to $4,000 per tube in production quantities. The EIO will require a heat exchanger estimated to be an additional $500. We estimate, therefore, that the tube and heat exchanger will cost less than $4,500 installed in production quantities.

POWER SUPPLY

A schematic of a power supply for the YJ1480 Magnetron used in commercial applications is presented in Figure 68. A photograph and typical dimensions for a power supply for the Varian VKU-7791 Series of Klystrons conforming to MIL-E-5400 prepared by Keltec, Florida, is

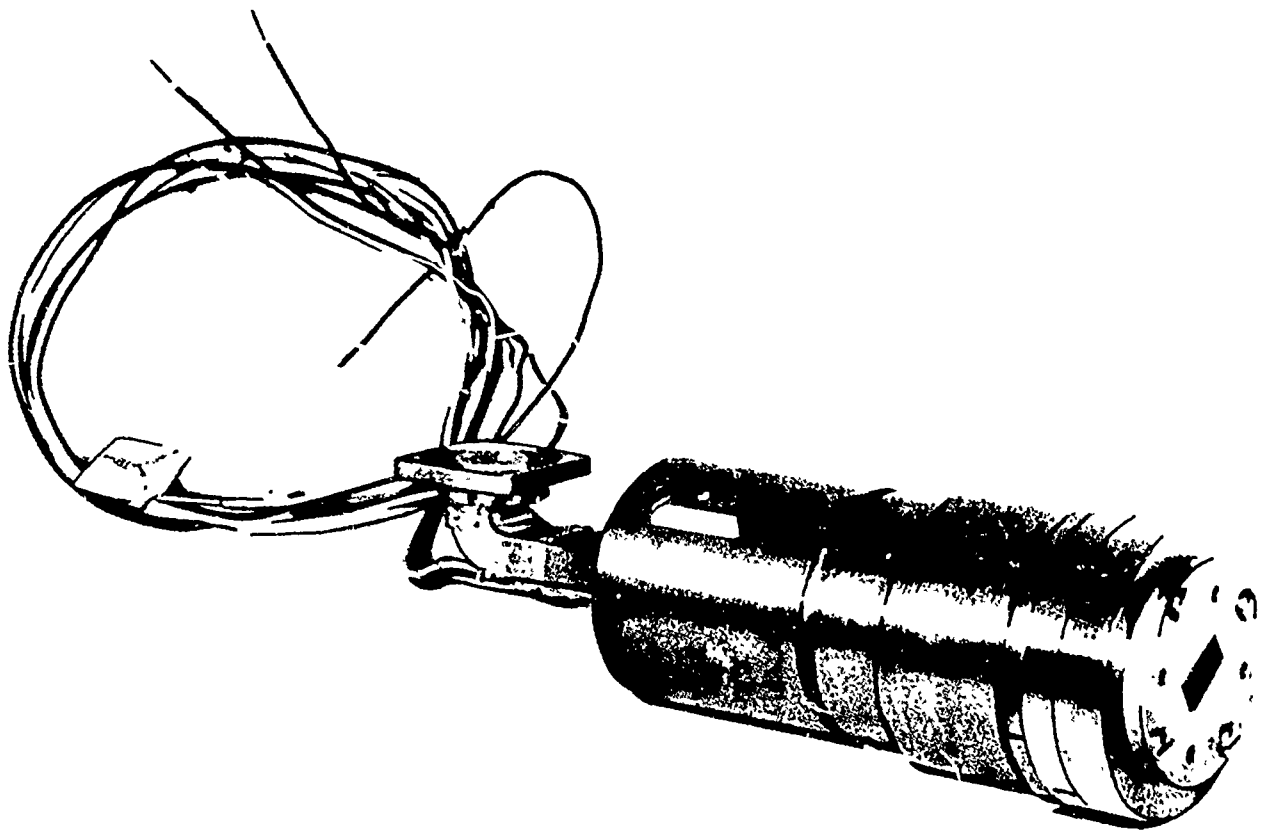

Figure 63. Waveguide rotary joint developed for helicopter use

TABLE 8. PARTIAL TABLE OF CANDIDATE TUBES FOR MICROWAVE DEICER

FREQUENCY GHz	TUBE TYPE	POWER OUTPUT kw (∿)	COOLING	EFFICIENCY n_t % (∿)	VOLTAGE TYP KV (∿)	CURRENT TYP ma (∿)	NOMENCLATURE	MFR	WEIGHT LBS.
2.45	MAG	0.75	Air	53	4.5	300	QKH1777	Ray	
12-18[2]	KLY	3.0	Liquid	35	9.0	1,000	VKU-7791A	Var	55
12-18[2]	KLY	1.2	Air	30	7.0	800	VKU-7791B	Var	55
12-18[2]	KLY	0.5	Air	25	5.0	500	VKU-7791C	Var	55
18-24	KLY	1.0	Liquid	11	8.0	---	VKK-7808A	Var	
22[1]	EIO	1.0	Liquid	20-30	≅10	≅ 500	VKQ-2435A	Var Can	15
2.45	MAG	0.2	Cond	60	1.65	200	7090	Amp	5
2.45	MAG	.8	Air	60	3.8	350	DX401	Amp	6.8
2.45	MAG	.8	Air	60	3.8	350	DX453	Amp	4.5
2.45	MAG	1.2	Air	56	5.6	380	DX206	Amp	9.0
2.45	MAG	1.5	Air	59	5.6	400	DX206F	Amp	9.0
2.45	MAG	2.5	Water	59	5.0	850	YJ1160	Amp	10.5
2.45	MAG	2.5	Air	59	5.0	850	YJ1162	Amp	16.5
2.45	MAG	5.0	Water	57	7.0	1,250	YJ1191A	Amp	12.5
2.45	MAG	2.5	Air	66	5.6	680	YJ1440	Amp	4.0
2.45	MAG	1.4	Air	64	5.9	370	YJ1480	Amp	4.0
2.45	MAG	1.2	Air	52	4.0	570	YJ1190	Amp	3.5
2.45	Triode	0.18	Air	40	1.4	.32	8940	EIM	2.0 Oz
2.45	Cross Field	2.5	Coolant	41	4.0	1,500	RW 619	Warn	17
5.850	Cross Field	2.5	Coolant	37	4.58	1,460	RW 620	Warn	17
2.45	MAG	1.6	Air	54	3.65	800	MCF1165	CSF	--
2.45	MAG	5.0	Water	60	5.2	1,600	MCF1327	CSF	--

[1] Efficiency improvement to 20-30% expected by collector depression techniques
[2] Requires a low power driver tube also

Ray - Raytheon
Var - Varian
Var Can - Varian Canada
Amp - Amperex
Warn - Warnecke
CSF - Thompson-CSF
EIM - EIMAC
MAG - Magnetron
KLY - Klystron
EIO - Extended Interaction Oscillator
Cross Field - Cross Field Oscillator

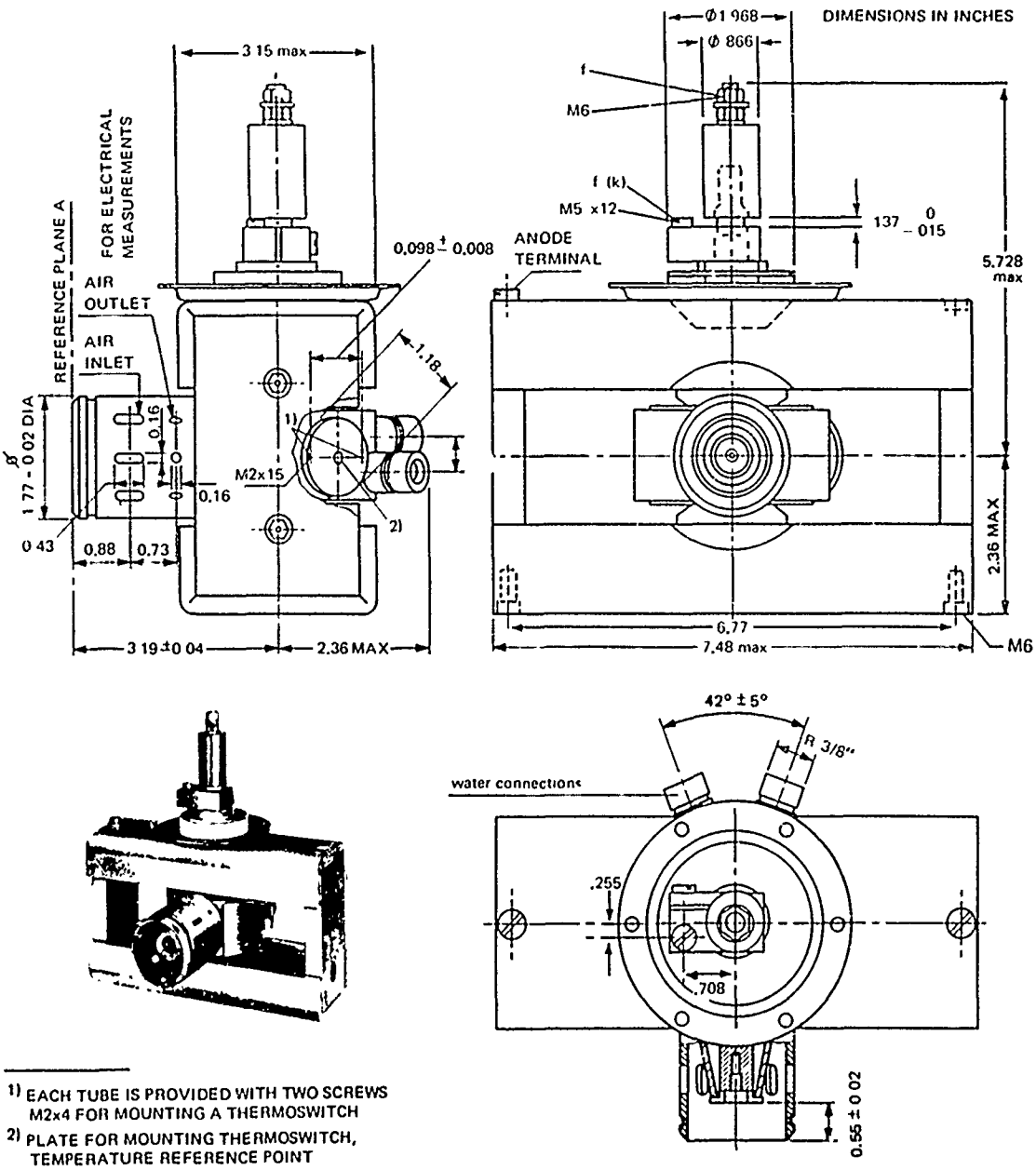

1) EACH TUBE IS PROVIDED WITH TWO SCREWS M2x4 FOR MOUNTING A THERMOSWITCH

2) PLATE FOR MOUNTING THERMOSWITCH, TEMPERATURE REFERENCE POINT

Figure 64. 2,450 MHz YJ1191-A Magnetron

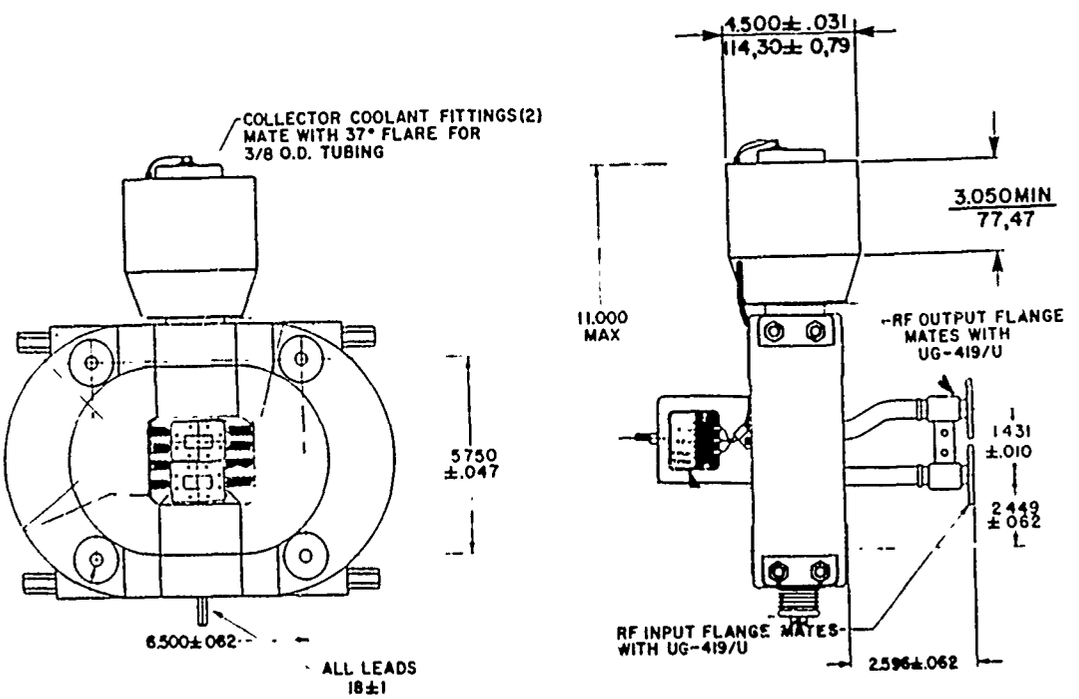

Figure 65. VKU-7791 outline drawing

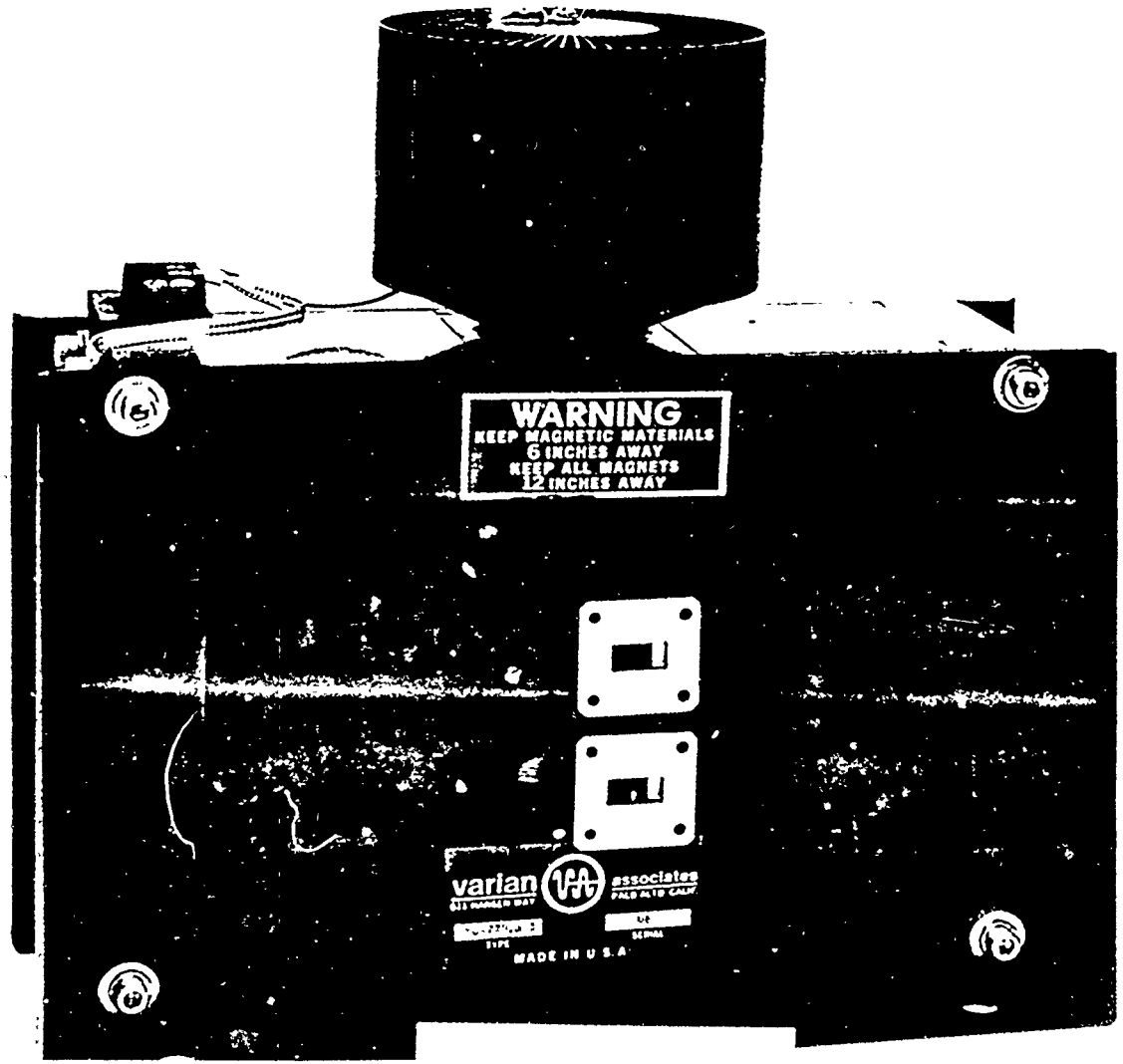

Figure 66. Photograph of VKU-7791N

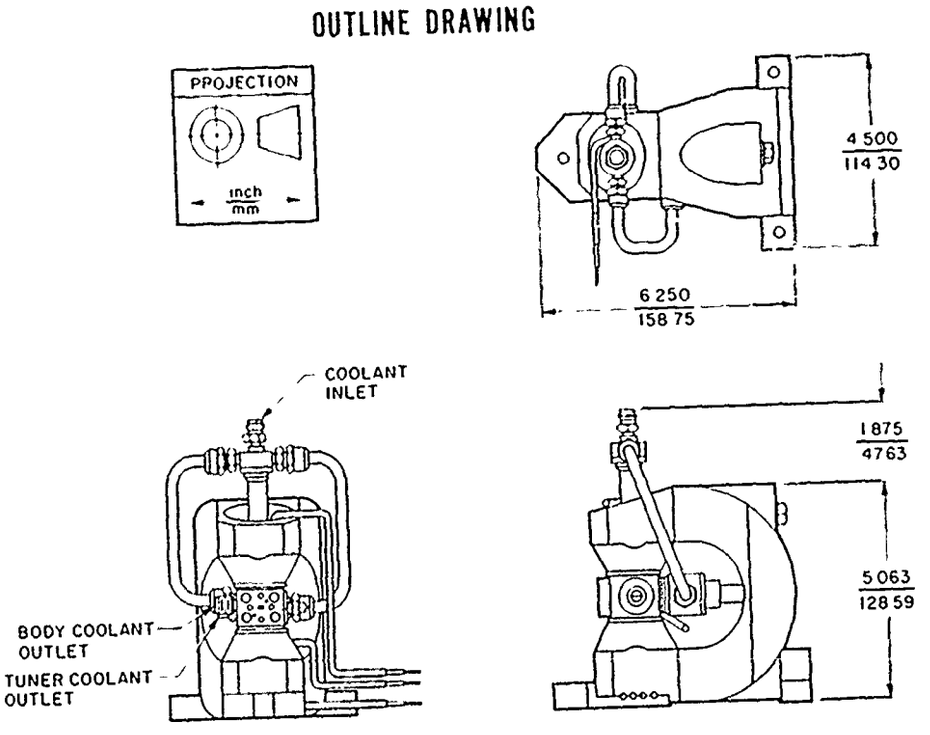

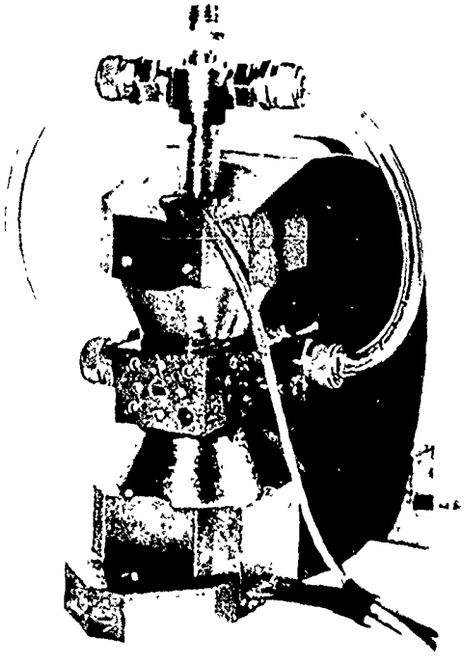

Figure 67. 22 GHz extended interaction oscillator

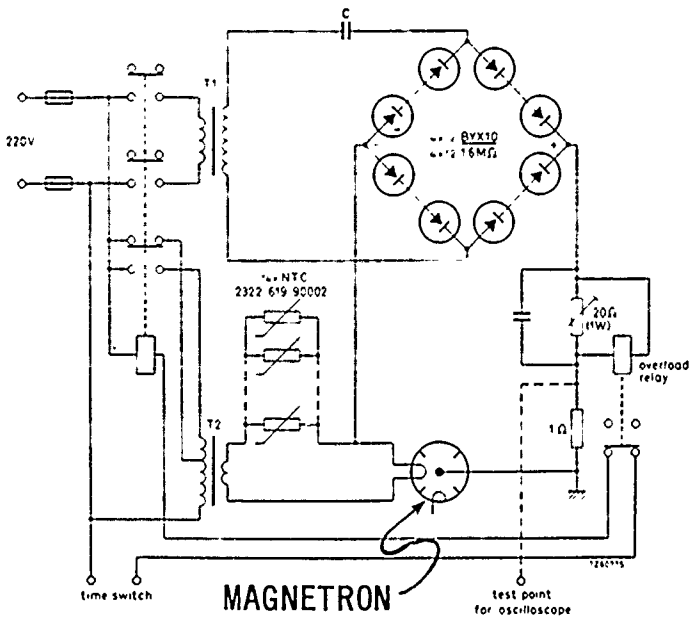

Figure 68. Circuit diagram of power supply unit for 1/1.5 kW Magnetron Type YJ1480 and 1481, typical

presented in Figure 69. This power supply may be considered typical for all tube types considered thus far. The power supply is estimated to measure less than 7 in x 4 in x 12 in, weigh less than 22 pounds and cost less than $1,300 each in production quantities. We estimate a cost of $1,800 per power supply installed.

COCKPIT CONTROL PANEL

The control panel, ice detectors and temperature sensors are estimated to weigh less than five pounds total and cost less than $1,000 installed.

COST, WEIGHT AND POWER REQUIREMENTS

A summary of the estimated costs, weights, and efficiencies of microwave deicers at three operating frequencies is presented in Table 9.

RADAR CROSS-SECTION CONSIDERATIONS

Only a cursory consideration was given to this topic.

After examination of various classified reports provided by the Army, it has been concluded that the microwave deicer boots are not fundamentally in conflict with radar cross-section reduction techniques presented in those reports but, in fact, may perhaps be used to enhance these techniques. The microwave deicer is made from materials that can be made to be essentially transparent to radar signals. A conceptual illustration of how the deicer boot can be made to be transparent is illustrated in Figure 70, sketches c and d. The use of lossy materials under the surface waveguide can be used to absorb radar signals. This technique may have distinct advantages in this respect over thermal deicers, which must use metallic components in their deicer boots.

DETECTABILITY

This topic was given only cursory consideration.

Figure 71 illustrates the atmospheric losses due to oxygen and water vapor that are available to reduce the detectability of the microwave deicer if 22 GHZ is chosen as the operating frequency.

Klystron Power Supply
Made by the Kelt c Florida Company,
a division of Aiken Industries, Inc.

115V, 3 Ø, 400 hz
Regulation: 2%
Airborne MIL-E-5400
Approx Size: 7" X 4" X 12"
Approx Weight: 22 lbs.

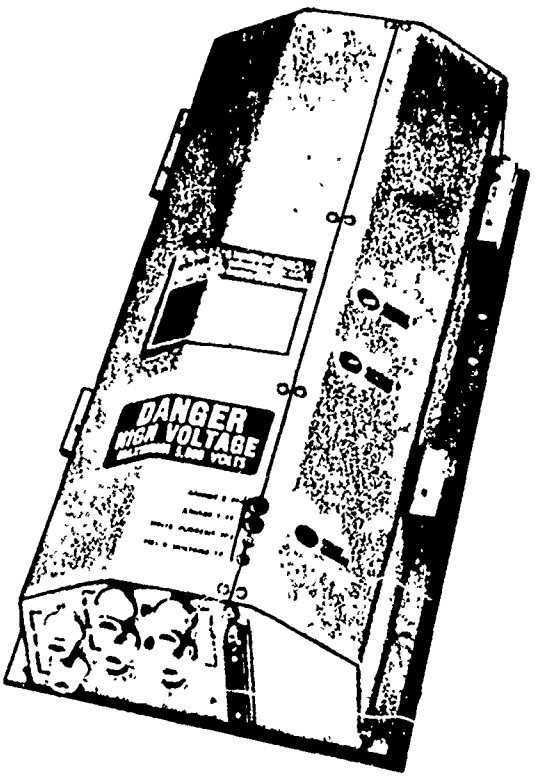

Typical
Shape

Figure 69. Power supply for Varian VKU-7791 series

TABLE 9. ESTIMATED WEIGHT, COST AND EFFICIENCY OF UH-1 HELICOPTER ROTOR BLADE MICROWAVE DEICERS FOR THREE DIFFERENT OPERATING FREQUENCIES

	Number Required	Operating Frequency											
		2,450 MHz				5,850 MHz				22,125 MHz			
		Estimated Cost Installed ($)	Estimated Weight Increment Installed (Lbs)	Estimated Efficiency, η		Estimated Cost Installed ($)	Estimated Weight Increment Installed (Lbs)	Estimated Efficiency, η		Estimated Cost Installed ($)	Estimated Weight Increment Installed (Lbs)	Estimated Efficiency, η	
				Min	Max			Min	Max			Min	Max
Microwave Deicer Boot (Two Blades)	2	900	(-20)[1]	.85	.9	900	(-20)[1]	.85	.9	900	(-20)[1]	.85	.9
Coupler	2	500	2	.75	.95	500	2	.75	.95	500	2	.75	.95
Power Divider Distributor	1	850	9	.9	.95	850	9	.85	.9	4,500	9	.85	.9
Feeder & Interconnects	1	850	10	.9	.95	850	10	.85	.9	1,200	10	.85	.9
Main Rotary Joint	1	650	3	.9	.95	650	3	.85	.9	650	3	.85	.9
Microwave Tube & Mount	1	1,500	4.5[2]	.55	.6	1,500	20[3]	.35	.4	4,500	18[4]	.2	.3[5]
Power Supply	1	1,800	22	.85	.9	1,800	22	.85	.9	1,800	22	.85	.9
Pilot's Control Panel	1	800	5			800	5			800	5		
TOTALS		7,850	35.5	.217	.395	7,850	51	.116	.224	15000	49	.060	.168
Titanium Equiv. Power Use (W)				280	150			500	275			900	300
Teflon Equiv. Power Use (W)				450	240			300	420			1400	570

[1] There is a net savings in weight since the dielectric deicer boot replaces the present nickel, stainless steel or other metallic erosion shield.

[2] Assumes a YJ1190 tube at 3.5 lbs.
[3] Assumes a cross field oscillator at 17 lbs.
[4] Assumes an EIO and coolant at 15 lbs.
[5] Assumes EIO oscillator utilizing collector depression technique to improve efficiency.

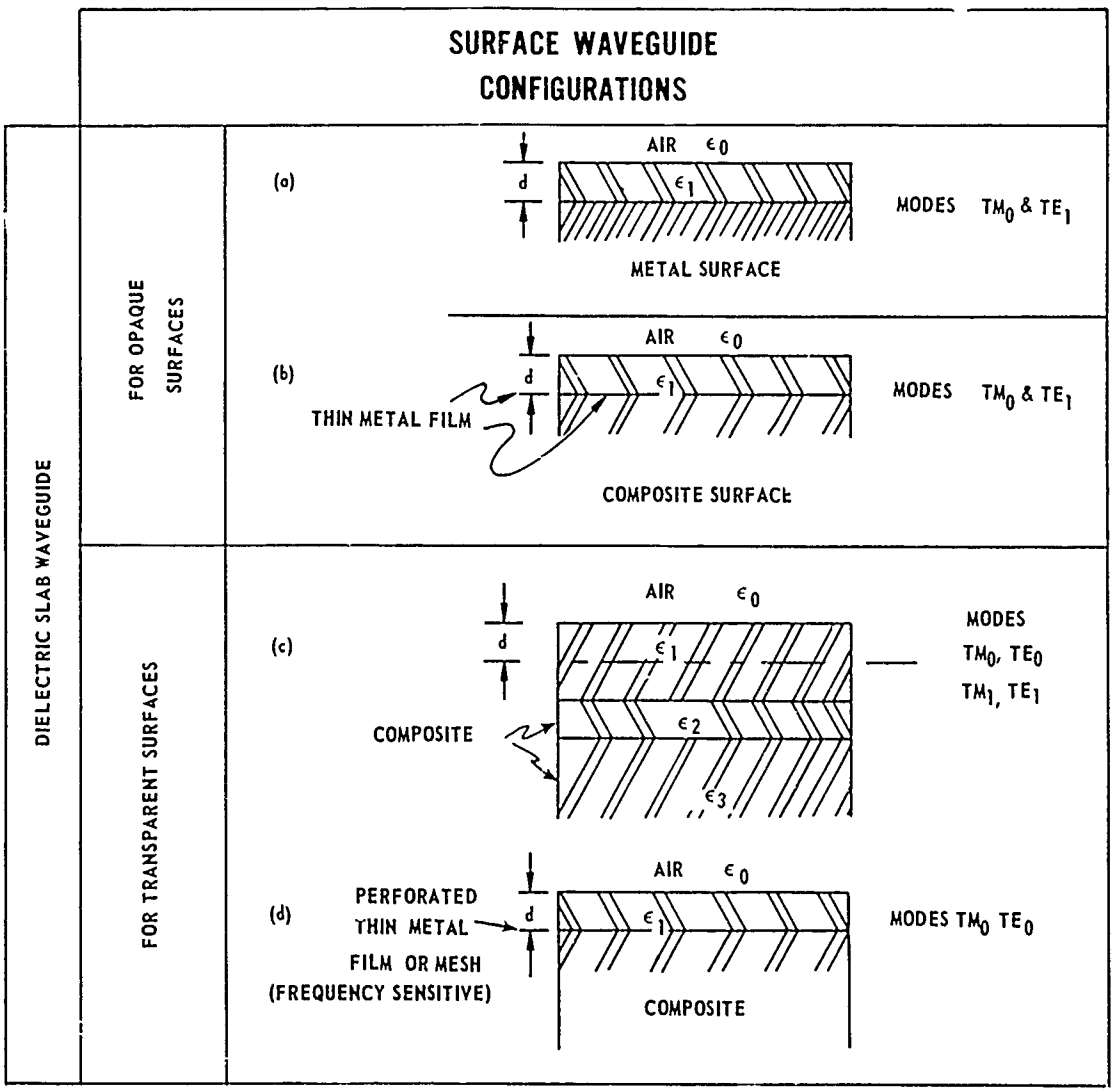

Figure 70. Surface waveguide configurations

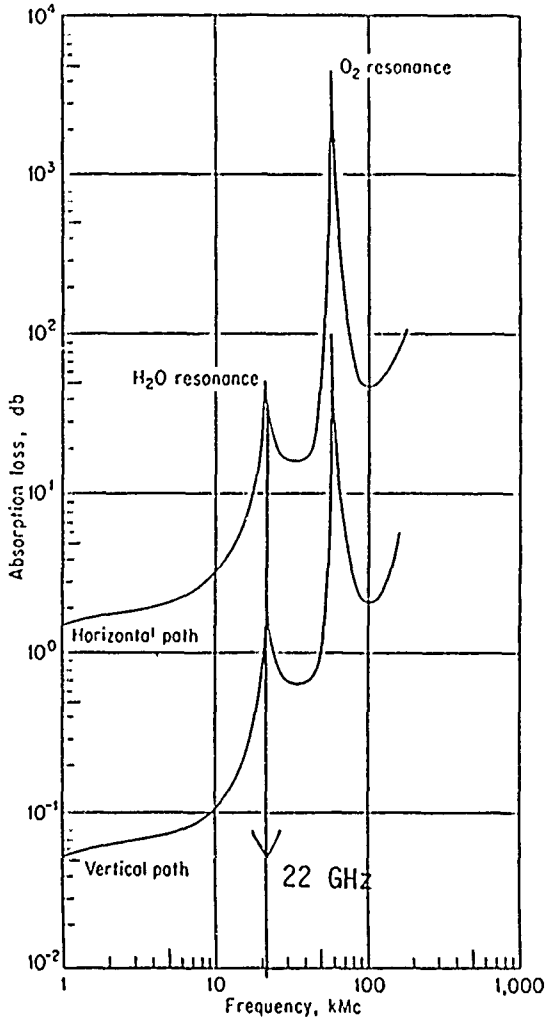

Figure 71. Composite oxygen and uncondensed water-vapor absorption at sea level (excerpt from Reference 34)

[34] George N. Krassner and Jackson V. Michaels. Introduction to Space Communication Systems, New York: McGraw-Hill Book Company.

Deicers in general are seldom on; they are turned on during icing conditions only and then only at the discretion of the pilot. Any radiation from the deicer will be unintentional: the design will be such as to eliminate or minimize radiation; all attempts will be made to insure that the rotor is not a good antenna. Such measures will combine to produce a low probability of being intercepted by a high-gain, scanning, enemy receiver.

Climate conditions that exist when icing occurs are the same as those that provide some attenuation of microwave signals. In addition, deicers that operate at 22,125 MHz fall in the oxygen water vapor absorption bands where any leakage signal will undergo heavy attenuation, practically eliminating the probability of intercept.

REFERENCES

1. R. Collin, Field Theory of Guided Waves, New York: McGraw-Hill, 1960.

2. Ramo, Whinnery and Van Duzer, Fields and Waves in Communications Electronics, New York: John Wiley & Sons, 1965.

3. Electronized Chemicals Corporation, Burlington, Massachusetts, Polyguide-Low-Loss Clad Laminates and Dielectrics for Microwave Stripline Applications.

4. Howard W. Sams & Co., Inc., Reference Data for Radio Engineers, 5th ed., Indianapolis/Kansas City/New York: Howard W. Sams & Co., Inc. (A Subsidiary of ITT), 1968.

5. Charles A. Harper (Editor), Handbook of Electronic Packaging, New York: McGraw-Hill Book Company, 1969.

6. Westlake Plastics Co. (Letter to B. Magenheim from Louis D'Orazio with attachment), "Lennite UHMW Polymer Engineering Data" (brochure).

7. Letter to B. Magenheim from Hugh I. Shulock with attachments of Alpha Associates, Inc., Commercial Brochures.

8. Olin Mathison Commercial Brochures on Astrocoat.

9. Owens/Corning Fiberglas Co. Commercial Brochures.

10. MIT Lab for Insulation Research, Tables of Dielectric Materials, Technical Report 119, vol. 5, April 1957.

11. MIT Lab for Insulation Research, Tables of Dielectric Materials, Technical Report 126, vol. 6, June 1958.

12. G.S. Springer, et al, "Analysis of Rain Erosion of Coated Materials," Technical Report AFML-TR-73-227, September 1973 (DDC No. AD 769448).

13. G.S. Springer, et al, "Analysis of Rain Erosion of Coated and Uncoated Fiber Reinforced Composite Materials," Technical Report AFML-TR-74-180, August 1974 (DDC No. ADA001086).

14. Adler, et al, "Analytical Modeling of Subsonic Particle Erosion," AFML-TR-72-144, July 1972.

15. Montgomery, C.G., R.H. Dicke and E.M. Purcell (Edited by), Principles of Microwave Circuits, New York: McGraw-Hill Book Company, Inc., 1948.

16. Letter from W.B. Westphal, MIT Lab for Insulation Research, Cambridge, Massachusetts, 8 September 1975.

REFERENCES
(Continued)

17. E.G. Younker, Dielectric Properties of Water and Ice at K-Band, Radiation Laboratory, Massachusetts Institute of Technology, Cambridge, Massachusetts, Report No. 644, December 4, 1944.

18. T. Moreno, Microwave Transmission Design Data, New York: Dover Publications, 1948.

19. A.L. Cullen, "The Excitation of Plane Surface Waves," Proceedings of the IEE, London, vol. 101, part IV, pp. 224-234, February 15, 1954.

20. G.J. Rich, "The Launching of a Plane Surface Wave," Proceedings of the IEE, London, vol. 102, part B, pp. 237-246, March 1955.

21. Cohn, Cassedy and Kott, "TE Mode Excitation on Dielectric Loaded Parallel Plane and Trough Waveguides," IRE Transactions on Microwave Theory and Techniques, pp. 545-552, September 1960.

22. E.L. Ginzton, Microwave Measurements, New York: McGraw-Hill, 1957.

23. J.W. Duncan, "The Efficiency of Excitation of a Surface Wave on a Dielectric Cylinder," IRE Transactions on Microwave Theory and Techniques, pp. 257-268, April 1959.

24. R.H. DuHamel and J.W. Duncan, "Launching Efficiency of Wires and Slots for a Dielectric Rod Waveguide," IRE Transactions of Microwave Theory and Techniques, July 1958.

25. A.D. Frost, C.R. McGeoch and C.R. Mingins, "The Excitation of Surface Waveguides and Radiating Slots by Strip-Circuit Transmission Lines," IRE Transactions on Microwave Theory and Techniques, October 1956.

26. James C. Wiltse, "Some Characteristics of Dielectric Image Lines at Millimeter Wavelengths," IRE Transactions on Microwave Theory and Techniques, pp. 65-99, January 1959.

27. D.D. King and S.P. Schlesinger, "Losses in Dielectric Image Lines," IRE Transactions on Microwave Theory and Techniques, January 1957.

28. S.P. Schlesinger and D.D. King, "Dielectric Image Lines," IRE Transactions on Microwave Theory and Techniques, July 1958.

REFERENCES
(Continued)

29. J.B. Werner, "Ice Protection Investigation for Advanced Rotary-Wing Aircraft," USAAMRDL Technical Report 73-38, August 1973.

30. J.R. Stallabrass, Flight Tests of an Experimental Helicopter Rotor Blade Electrical De-Icer, Ottawa, Canada: National Research Laboratories, November 1959.

31. J.R. Stallabrass and R.D. Price, "On the Adhesion of Ice to Various Materials," National Research Laboratories, July 1962.

32. M. Cohn, "Propagation in Dielectric-Loaded Parallel Plane Waveguide," IRE Transactions on Microwave Theory and Techniques, pp. 202-208, April 1959.

33. M. Cohn, "TE Modes of Dielectric Loaded Trough Line," IRE Transactions on Microwave Theory and Techniques, pp. 449-454, July 1960.

34. George N. Krassner and Jackson V. Michaels, Introduction to Space Communication Systems, New York: McGraw-Hill Book Company.

35. Department of the Army, Operator's Manual, Army Model UH-1D/H Helicopters, Technical Manual TM-55-1520-210-20, 24 August 1971.

36. Charles B. Sharpe, "A Graphical Method for Measuring Dielectric Constants at Microwave Frequencies," IRE Transactions on Microwave Theory and Techniques, pp. 155-159, March 1960.

37. G.S. Springer, Erosion by Liquid Impact, Manuscript for book to be published in 1976.

BIBLIOGRAPHY

Adler, "Analysis of Multiple Particle Impacts on Brittle Materials," AFML-TR-74-210.

Angelakos, D.J., "An Image Line Coupler," IRE Transactions on Microwave Theory and Techniques, pp. 391-392, July 1959.

Biernson, G. and D.J. Kinsley, "Generalized Plots of Mode Patterns in a Cylindrical Dielectric Waveguide Applied to Retinal Cones," IRE Transactions on Microwave Theory and Techniques, pp. 345-356, May 1965.

Birks and Hart, Progress in Dielectrics, "The Dielectric Properties of Ice," New York: John Wiley & Sons, 1961, Volume 13.

Bowie, D.M. and K.S. Kelleher, "Rapid Measurement of Dielectric Constant and Loss Tangent," IRE Transactions on Microwave Theory and Techniques, pp. 137-140, July 1956.

Brick, D.B., "The Radiation ofa Hertzian Dipole Over a Coated Conductor," Proceedings IEE (London), vol. 102, part C, pp. 104-121, December 1954.

Chappell, M.S., "A Resume of Simulation Techniques and Icing Activities at the Engine Laboratory of the National Research Council (Canada)," National Research Laboratories, May 1961.

Clemmow, P.C., "Some Extensions to the Method of Integration by Steepest Descents," Quarterly Journal of Mechanical and Applied Mathematics, vol. III, part 2, pp. 33-43, 1950.

Engel, Olive G., "Investigation of Energy-Absorbing Mechanisms in the Impact Behavior and Rain Erosion Resistance of Pure Nickel," Technical Report AFML-TR-73-206, August 1973 (DDC No. AD771027).

Envert, F., et al, "Parameters Governing the Erosion Resistance of Coating Substrate Systems," Catholic University of America, TR-74-1, July 1974.

Friedman, B. and Williams, W.E., "Excitation of Surface Waves," Proceedings of IEE (London), vol. 105, part C, pp. 252-258, March 1958.

Gabriel, W.F., "An Automatic Microwave Dielectrometer," IRE Transactions on Microwave Theory and Techniques, p. 481, October 1959.

Goubau, George, "Open Wire Lines," IRE Transactions on Microwave Theory and Techniques, pp. 197-200, October 1956.

Graham, T.L., "High Temperature Stable Subsonic Rain Erosion Resistant Fluoroelastomer Boot Material Development," Technical Report AFML-TR-74-9, May 1974.

BIBLIOGRAPHY
(Continued)

Hobbs, Peter V., Ice Physics, Oxford: Clarendon Press, 1974.

Hoekstra, P. and Delaney, A., "Dielectric Properties of Soils at VHF and Microwave Frequencies," Journal of Geophysical Research, vol. 79, no. 11, pp. 1699-1708, April 10, 1974.

Levi, L., and Aufdermaur, A.m., "Orientation of Ice Crystals Grown by Accretion of Supercooled Droplets," Physics of Ice, Riehl Bollemer Engelhardt, 1968.

Levy, Ralph, "Analysis and Synthesis of Waveguide Multiaperture Directional Couplers," IEEE Transactions on Microwave Theory and Techniques, vol. MTT-16, no. 12, December 1968.

Lockheed Missiles and Space Co., "The Development of an Advanced Anti-Deicing Capability for Army Helicopters," Contract DAAJ02-73-C-0107, L426375, 12 March 1974.

Marcuvitz, N. (Editor), Waveguide Handbook, First Edition, New York: McGraw-Hill Book Company, Inc., 1951.

Military Specification No. MIL-P-13949E, General Specification for Plastic Sheet, Laminated, Metal Clad (for Printed Wiring), 15 July 1971.

Moraveck, J.F. and Clarke, G.H., "Rain and Sand Erosion Resistant Polyurethane Protective Coatings," Technical Report AFML-TR-277, part II, July 1969 (DDC Number - Part I: AD831759, Part II: AD855544).

Owens/Corning Fiberglas Co., Letter to B. Magenheim from R. McElroy with Brochure Attachments: "Comparative Data-E, S, S-2 Glass". -- "FRP, An Introduction to Fiberglas-Reinforced Plastics/Composites". -- "Reinforced Plastics, Guide to Hand Lay-Up & Spray-Up Prototyping & Fabrication". -- "Introduction to Pultrusion". -- "Filament Winding with Type 30 Roving, A Practical Guide to Reinforcement Processing".

Polymer Technology Series, Handbook of Fiberglass and Advanced Plastics Composities, Edited by George Lubin, New York: VanNostrand Reinhold Co., n.d.

Rasool, S.I. (Editor), Chemistry of the Lower Atmosphere, New York, London: Plenum Press, 1973.

BIBLIOGRAPHY
(Continued)

Redheffer, R.M., "The Measurement of Dielectric Constants," Chapter 10, Technique of Microwave Measurements, New York: McGraw-Hill Book Company, Inc., 1948.

Richmond, J.H., "Surface Waves on Symmetrical Three-Layer Sandwiches," IRE Transactions on Microwave Theory and Techniques, September 1960.

Rush, C.K., "The Icing of Delta Wings of Unity Aspect Ratio Having Leading Edge Separation," National Research Laboratories, December 1959.

Rush, C.K., "Icing Tests of a 10-foot Delta Wing of Unity Aspect Ratio Having Leading Edge Separation," National Research Laboratories, January 1962.

Schmitt, George F., Jr., "Fluoroelastomer Coatings Resistant to Thermal Flash, High Temperature, and Subsonic Rain Erosion," Technical Report AFML-TR-74-25, April 1974 (DDC No. AD922438L).

Schmitt, George F., Jr., "Fluoroelastomer Coatings Resistant to Thermal Flash, High Temperature, and Subsonic Rain Erosion," Technical Report AFML-TR-74-23, April 1974.

Skolnik, Merrill I. (Editor), Radar Handbook, New York: McGraw-Hill Book Company, 1970.

Smyth, Charles P., Dielectric Behavior and Structure, New York: McGraw-Hill Book Company, Inc., 1955.

Sobel, F., F.L. Wentworth and J.C. Wiltse, "Quasi-Optical Surface Waveguide and Other Components for the 100- to 300-Gc Region," IRE Transactions on Microwave Theory and Techniques, pp. 512-518, November 1961.

Stallabrass, J.R. and G.A. Gibbard, "A Comparison Between the Spanwise and Chordwise Shedding Methods of Helicopter Rotor Blade De-Icing," National Research Laboratories, January 1960.

Stallabrass, J.R., and R.D. Price, "The Effect of Icing During Helicopter Ground Run-up," National Research Council of Canada, April 1967.

Stallabrass, J.R. and P.F. Hearty, "The Icing of Cylinders in Conditions of Simulated Freezing Sea Spray," National Research Council of Canada, July 1967.

BIBLIOGRAPHY
(Continued)

Stallabrass, J.R., "Review of Icing Detection for Helicopters," National Research Laboratories, March 1962.

Tai, C.T., "The Effect of a Grounded Slab on the Radiation from a Line Source," Journal of Applied Physics, vol 22, pp. 405-414, April 1951.

Textron's Bell Aerospace Company, "Characterization of Transparent Materials for Erosion Resistance," Quarterly Progress Report No. 1, August 1974, Contract No. F33615-73-C-5057.

Textron's Bell Aerospace Company, "Characterization of Transparent Materials for Erosion Resistance," Quarterly Progress Report No. 2, November 1974, Contract No. F33615-73-C-5057.

Textron's Bell Aerospace Company, Characterization of Transparent Materials for Erosion Resistance," Quarterly Progress Report No. 3, February 1975, Contract No. F33615-73-C-5057.

Ulrich, Noone and others, "Electrically Conductive Coating Materials," Technical Report AFML-TR-73-207, part I, August 1973.

U.S. Army, Organizational Maintenance Manual - Army Model UH1D/H Helicopters, Department of the Army Technical Manual, TM55-1520-210-20P, 10 September 1971.

U.S. Army, Organizational Maintenance - Repair Parts and Special Tool Lists, Department of the Army Technical Manual, TM55-1520-210-20P-1&2, April 1974.

U.S. Army, Proceedings of the United States Army Aviation Center "Staying Power Symposium", Ft. Rucker, 8-10 July 1975.

Visger, R.L., "High Temperature Subsonic Rain Erosion Resistant Flouroelastomer Coatings," Technical Report AFML-TR-73-237, November 1973, (DDC No. AD916594L).

Van Der Waerden, B.L., "On the Method of Saddle Points," Applied Science Research, vol. B2, pp. 33-43, 1950.

Von Hippel, A., Dielectric Materials and Applications, New York: John Wiley & Sons, Inc., 1954.

Von Hippel, A., Dielectrics and Waves, John Wiley & Sons, Inc., and MIT Press of MIT, 1954.

BIBLIOGRAPHY
(Continued)

Von Hippel, A., "Molecular Understanding of Electrochemical Process by Ice Research," Journal of the Electrochemical Society, vol. 119, no. 2, February 1972.

Wahl, Norman E., "Development and Characterization of Materials Resistant to Supersonic Erosion," Technical Report AFML-TR-74-139, May 1974 (DDC No. ADB000124L).

Weaver, J.H., "Electrodeposited Nickel Coatings for Erosion Protection," Technical Report AFML-TR-70-111, July 1970 (DDC No. AD874765).

Whitmer, Robert M., "Fields in Nonmetallic Waveguides," Proceedings of the Institute of Radio Engineers, pp. 1105-1109, September 1948.

APPENDIX A
SURFACE WAVEGUIDE THEORY

The wave solutions to Maxwell's equations in the semi-infinite dielectric slab of Figure A-1 may be divided into transverse magnetic (TM) modes and transverse electric (TE) modes with even and odd symmetry of the transverse components about the x = 0 plane. The field equations for the TM and TE modes are given in Equations A-1 through A-18.[2]

Tangential fields at x = d are equated, resulting in the continuity relations:

$$\text{TM:}\quad \left.\frac{E_{z1}}{H_{y1}}\right|_{x=d} = \left.\frac{E_{z2}}{H_{y2}}\right|_{x=d}, \qquad \text{TE:}\quad \left.\frac{H_{z1}}{E_{y1}}\right|_{x=d} = \left.\frac{E_{z2}}{H_{y2}}\right|_{x=d}$$

TM Modes

The relations for TM modes with even symmetry of transverse magnetic components are:

TM Even

$$E_{z1} = A \sin k_x x \tag{A-1}$$

$$H_{y1} = \frac{\omega\varepsilon_1}{\beta} E_{x1} = \frac{-j\omega\varepsilon_1 A}{k_x} \cos k_x x \tag{A-2}$$

$$E_{z2} = Ce^{-K_x(x-d)} \tag{A-3}$$

$$H_{y2} = \frac{\omega\varepsilon_2}{\beta} E_{x2} = \frac{-j\omega\varepsilon_2 C}{K_x} e^{-K_x(x-d)} \tag{A-4}$$

$$K_x = \frac{\varepsilon_2}{\varepsilon_1} k_x \tan k_x d \tag{A-5}$$

[2]Ramo, Whinnery and Van Duzer, Fields and Waves in Communication Electronics, New York: John Wiley & Sons, 1965.

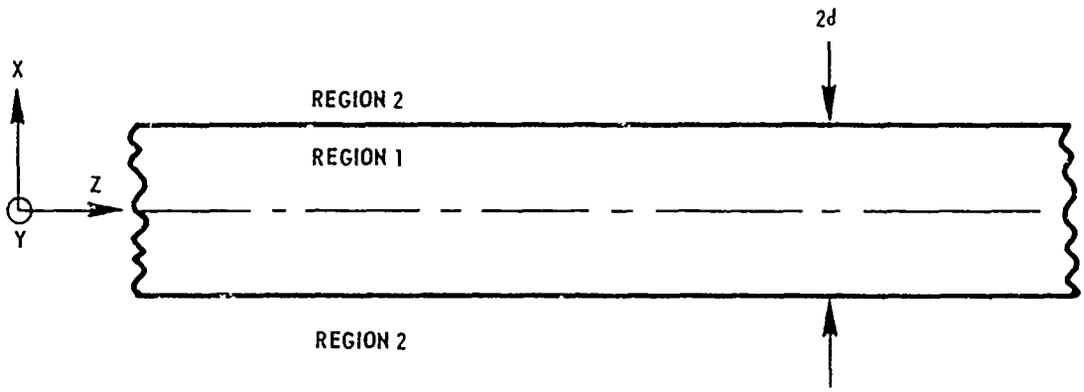

Z is the direction of propagation

Figure A-1. Dielectric slab waveguide

The relations for TM modes with odd symmetry of transverse magnetic components are:

TM Odd

$$E_{z1} = B \cos k_x x \tag{A-6}$$

$$H_{y1} = \frac{\omega\varepsilon_1}{\beta} E_{x1} = \frac{j\omega\varepsilon_1 B}{k_x} \sin k_x x \tag{A-7}$$

Other components have the same form as A-3 and A-4 for region 2.

$$K_x = -\frac{\varepsilon_2}{\varepsilon_1} k_x \cot k_x d \tag{A-8}$$

TE Modes

The relations for TE modes with even symmetry of the transverse electric components are:

TE Even

$$H_{z1} = D \sin k_x x \tag{A-9}$$

$$E_{y1} = \frac{-\omega\mu_1}{\beta} H_{x1} = \frac{j\omega\mu_1 D}{k_x} \cos k_x x \tag{A-10}$$

$$H_{z2} = Fe^{-K_x(x-d)} \tag{A-11}$$

$$E_{y2} = -\frac{\omega\mu_2}{\beta} H_{x2} = \frac{j\omega\mu_2}{K_x} Fe^{-K_x(x-d)} \tag{A-12}$$

$$K_x = \frac{\mu_2}{\mu_1} k_x \tan k_x d \tag{A-13}$$

The relations for TE modes with odd symmetry of transverse electric components are:

TE Odd

$$H_{z1} = E \cos k_x x \tag{A-14}$$

$$E_{y1} = \frac{-\omega\mu_1}{\beta} H_{x1} = \frac{-j\omega\mu_1 E}{k_x} \sin k_x x \tag{A-15}$$

Other components have the same form as A-11 and A-13 for region 2

$$K_x = \frac{-\mu_2}{\mu_1} k_x \cot k_x d \tag{A-16}$$

In these relations,

$$k_x^2 = k_1^2 - \beta^2 > 0 \tag{A-17}$$

$$K_x^2 = \beta^2 - k_2^2 > 0 \tag{A-18}$$

where

$$\beta = \frac{2\pi}{\lambda_g}; \quad k_1 = \frac{2\pi}{\lambda_1}; \quad k_2 = \frac{2\pi}{\lambda_2}$$

Determination of Eigenvalues

From A-17 and A-18 we may write

$$(k_x d)^2 = (k_1 d)^2 - (\beta d)^2 \tag{A-19}$$

$$(K_x d)^2 = (\beta d)^2 - (k_2 d)^2 \tag{A-20}$$

Adding (A-19) and A-20 gives

$$(k_x d)^2 + (K_x d)^2 = (k_1 d)^2 - (k_2 d)^2 \tag{A-21}$$

This is the equation of a circle of radius equal to

$$\sqrt{(k_1 d)^2 - (k_2 d)^2}$$

in the $k_x d$, $K_x d$ plane.

For the:

TM Even mode Eq. A-5 ; $(K_x d)^2 = \left(\frac{\varepsilon_2}{\varepsilon_1} k_x d \tan k_x d\right)^2$ (A-22a)

TM Odd mode Eq. A-8 ; $(K_x d)^2 = \left(-\frac{\varepsilon_2}{\varepsilon_1} k_x d \cot k_x d\right)^2$ (A-22b)

TE Even mode Eq. A-13; $(K_x d)^2 = (k_x d \tan k_x d)^2$ (A-22c)

TE Odd mode Eq. A-16; $(K_x d)^2 = (-k_x d \cot k_x d)^2$ (A-22d)

Substituting (22a,b,c,d) into (21) gives

For TM Even

$$(k_x d)^2 + \left(\frac{\varepsilon_2}{\varepsilon_1} k_x d \tan k_x d\right)^2 = (k_1 d)^2 - (k_2 d)^2 \quad \text{(A-23a)}$$

For TM Odd

$$(k_x d)^2 + \left(-\frac{\varepsilon_2}{\varepsilon_1} k_x d \cot k_x d\right)^2 = (k_1 d)^2 - (k_2 d)^2 \quad \text{(A-23b)}$$

For TE Even

$$(k_x d)^2 + (k_x d \tan k_x d)^2 = (k_1 d)^2 - (k_2 d)^2 \quad \text{(A-23c)}$$

For TE Odd

$$(k_x d)^2 + (-k_x d \cot k_x d)^2 = (k_1 d)^2 - (k_2 d)^2 \quad \text{(A-23d)}$$

k_x can now be solved for by successive approximations. Let

$$B \equiv (k_1 d)^2 - (k_2 d)^2 \quad \text{(A-24)}$$

Let AA, AB, AC and AD be defined as follows:

TM Even: $AA \equiv (k_x d)^2 + \left(\frac{\varepsilon_2}{\varepsilon_1} k_x d \tan k_x d\right)^2$ (A-25a)

TM Odd : $AB \equiv (k_x d)^2 + \left(-\frac{\varepsilon_2}{\varepsilon_1} k_x d \cot k_x d\right)^2$ (A-25b)

TE Even: $AC \equiv (k_x d)^2 + (k_x d \tan k_x d)^2$ (A-25c)

TE Odd : $AD \equiv (k_x d)^2 + (-k_x d \cot k_x d)^2$ (A-25d)

Having solved for k_x we can solve for K_x from equations A-22 a,b,c,d, solve for β from equation A-17 using the value of k_x satisfying equations A-23 a,b,c,d.

Cut-Off Frequencies

Cut-off occurs whenever $K_x = 0$ since this is the condition of intersection of the curves A and B on the $K_x d = 0$ axis (see Reference 1, page 472) and from equations A-5, A-8, A-13 and A-16.

TM Even: $\tan(k_x d) = 0;\ k_x d = n\pi$ (A-26a)

TM Odd : $\cot(k_x d) = 0;\ k_x d = (2n + 1)\frac{\pi}{2}$ (A-26b)

TE Even: $\tan(k_x d) = 0;\ k_x d = n\pi$ (A-26c)

TE Odd : $\cot(k_x d) = 0;\ k_x d = (2n + 1)\frac{\pi}{2}$ (A-26d)

where $n = 0,1,2,3,$etc., from which the cut-off frequency for each mode type is (see Section 1):

TM Even: $f_c = \dfrac{nc}{2d\sqrt{\varepsilon_1 - \varepsilon_2}}$; $n = 0,1,2,3,$etc (A-27a)

TM Odd : $f_c = \dfrac{\left(\frac{2n + 1}{2}\right)c}{2d\sqrt{\varepsilon_1 - \varepsilon_2}}$; $n = 0,1,2,3,$etc (A-27b)

TE Even: $f_c = \dfrac{nc}{2d\sqrt{\varepsilon_1 - \varepsilon_2}}$; $n = 0,1,2,3,$etc (A-27c)

TE Odd : $f_c = \dfrac{\left(\frac{2n + 1}{2}\right)c}{2d\sqrt{\varepsilon_1 - \varepsilon_2}}$; $n = 0,1,2,3,$etc (A-27d)

[1]R. Collin, Field Theory of Guided Waves, New York: McGraw-Hill, 1960.

Or equations A-27 may be combined as follows:

$$f_c = \frac{Nc}{2(2d)\sqrt{\epsilon_1 - \epsilon_2}} \qquad \text{(A-28)}$$

where

N = 0,2,4,6,... for Even modes

N = 1,3,5,7,... for Odd modes

POWER TRANSFER

Power Transfer for TM Even Modes

For TM even modes from Equations A-2 and A-4,

$$\frac{E_{x1}}{H_{y1}} = \frac{\beta}{\omega\varepsilon_1} = z_{TM1} \; ; \; \frac{E_{x2}}{H_{y2}} = \frac{\beta}{\omega\varepsilon_2} = z_{TM2} \tag{A-29}$$

Power Transfer Inside Dielectric

The axial component of the average Poynting vector is one-half the product of the transverse field magnitudes.

$$W_T = \int_{cs} \frac{1}{2} \mathrm{Re}[\bar{E} \times \bar{H}^*]_z \, ds \tag{A-30}$$

$$= \frac{1}{2} \int_{cs} |E_t| \, |H_t| \, ds \tag{A-31}$$

$$= \frac{z_{TM1}}{2} \int_{cs} |H_t|^2 \, ds \tag{A-32}$$

The power transfer inside the dielectric from Equation A-2 for $H_{y1} = H_t$ is

$$W_{TM1E} = \frac{z_{TM1}}{2} \int_{cs1} \left| \frac{-j\omega\varepsilon_1 A}{k_x} \cos k_x x \right|^2 ds \tag{A-33}$$

$$= \frac{z_{TM1}}{2} \left(\frac{\omega\varepsilon_1 A}{k_x} \right)^2 \int_{cs1} \cos^2 k_x x \ell dx \tag{A-34}$$

where $\ell dx = ds$,

Explanation of subscripts: TM = Transverse Magnetic
1 = Dielectric 1
E = Even

$$W_{TM1E} = \frac{z_{TM1}}{2}\left(\frac{\omega\varepsilon_1 A}{k_x}\right)^2 \ell \left[\frac{x}{2} + \frac{\sin 2k_x x}{4k_x}\right]_{x=0}^{x=d} \qquad (A\text{-}35)$$

(or x=-d to +d for a slab of thickness 2d)

$$W_{TM1E} = \frac{z_{TM1}}{2}\left(\frac{\omega\varepsilon_1 A}{k_x}\right)^2 \ell \left[\frac{d}{2} + \frac{\sin 2dk_x}{4k_x}\right] \qquad (A\text{-}36)$$

From Equation A-34 the power density, ρ, as a function of x is

$$\rho_1 = \frac{z_{TM1}}{2}\left(\frac{\omega\varepsilon_1 A}{k_x}\right)^2 \cos^2 k_x x \qquad (A\text{-}37)$$

Similarly the power transfer outside the dielectric from Equation A-5 is

$$W_{TM2E} = \frac{z_{TM2}}{2}\int_{cs} \left|H_{y2}\right|^2 ds \qquad (A\text{-}38)$$

From Equation A-5,

$$W_{TM2E} = \frac{z_{TM2}}{2}\int_{cs} \left|\frac{-j\omega\varepsilon_2 C}{K_x} e^{-K_x(x-d)}\right|^2 \ell dx \qquad (A\text{-}39)$$

$$W_{TM2E} = \frac{z_{TM2}}{2}\left(\frac{\omega\varepsilon_2 C}{K_x}\right)^2 \ell \int_{cs} e^{-2K_x(x-d)}\, dx \qquad (A\text{-}40)$$

Let $y = -2K_x(x-d)$, then $dx = dy/(-2K_x)$,

$$W_{TM2E} = \frac{z_{TM2}}{2}\left(\frac{\omega\varepsilon_2 C}{K_x}\right)^2 \ell \int_{cs} e^{+y}\, \frac{dy}{(-2K_x)} \qquad (A\text{-}41)$$

$$W_{TM2E} = \frac{z_{TM2}}{2}\left(\frac{\omega\varepsilon_2 C}{K_x}\right)^2 \ell \cdot \frac{1}{(-2K_x)} \int e^{+y}\, dy \qquad \text{(A-42)}$$

$$W_{TM2E} = \frac{z_{TM2}}{2}\left(\frac{\omega\varepsilon_2 C}{K_x}\right)^2 \frac{\ell}{(-2K_x)}\left[e^{y}\right]_{y_1=0}^{y_2=\infty} \qquad \text{(A-42a)}$$

$$W_{TM2E} = \frac{z_{TM2}}{2}\left(\frac{\omega\varepsilon_2 C}{K_x}\right)^2 \frac{\ell}{(-2K_x)}\left[e^{-2K_x(x-d)}\right]_{x=d}^{x=\infty} \qquad \text{(A-43)}$$

$$W_{TM2E} = \frac{z_{TM2}}{2}\left(\frac{\omega\varepsilon_2 C}{K_x}\right)^2 \frac{\ell}{(-2K_x)}\,[-1] \qquad \text{(A-44)}$$

$$W_{TM2E} = \frac{z_{TM2}}{2}\left(\frac{\omega\varepsilon_2 C}{K_x}\right)^2 \frac{\ell}{2K_x} \qquad \text{(A-45)}$$

The power density as a function of x outside the dielectric is from Equation A-40

$$\rho_2 = \frac{W_{TM2E}}{\ell dx} = \frac{z_{TM2}}{2}\left(\frac{\omega\varepsilon_2 C}{K_x}\right)^2 e^{-2K_x(x-d)} \qquad \text{(A-45)}$$

Total Power Transfer is

$$W_{TM} = W_{TM1E} + W_{TM2E}$$

The ratio of power in dielectric 1 to that in dielectric 2 is

$$\frac{W_{TM1E}}{W_{TM2E}}$$

The ratio of power transferred in dielectric 1 to power transferred in dielectric 2 is

$$\frac{W_{TM1E}}{W_{TM2E}} = \frac{\frac{z_{TM1}}{2}\left(\frac{\omega\varepsilon_1 A}{k_x}\right)^2 \ell\left[\frac{d}{2} + \frac{\sin 2dk_x}{4k_x}\right]}{\frac{z_{TM2}}{2}\left(\frac{\omega\varepsilon_2 C}{K_x}\right)^2 \ell/2K_x} \qquad \text{(A-45a)}$$

$$\frac{W_{TM1E}}{W_{TM2E}} = \frac{\varepsilon_1}{\varepsilon_2} \frac{\left(\frac{A}{k_x}\right)^2 \left[\frac{d}{2} + \frac{\sin 2dk_x}{4k_x}\right]}{\left(\frac{C}{K_x}\right)^2 / 2K_x} \qquad \text{(A-45b)}$$

From Equations A-1 and A-3 when x = d,

$$E_{z1} = E_{z2}$$

$$A \sin k_x d = C$$

$$\frac{W_{TM1E}}{W_{TM2E}} = \frac{\varepsilon_1}{\varepsilon_2} \frac{\left(\frac{1}{k_x}\right)^2 \left[\frac{d}{2} + \frac{\sin 2dk_x}{4k_x}\right]}{\left(\frac{\sin k_x}{K_x}\right)^2 / 2K_x} \qquad \text{(A-45c)}$$

Power Transfer for the TM Odd Modes

$$z_{TM1} = \frac{\beta}{\omega\varepsilon_1} \; ; \quad z_{TM2} = \frac{\beta}{\omega\varepsilon_2} \qquad \text{(A-46)}$$

Inside the Dielectric :

$$W_{TM10} = \frac{z_{TM1}}{2} \int_{cs} |H_t|^2 \, ds \qquad \text{(A-46)}$$

$H_t = H_{y1}$ from Equation A-7

$$= \frac{z_{TM1}}{2} \int_{cs} \left| \frac{j\omega\varepsilon_1 B}{k_x} \sin k_x x \right|^2 \ell dx \qquad \text{(A-48)}$$

$$= \frac{z_{TM1}}{2} \left(\frac{\omega\varepsilon_1 B}{k_x}\right)^2 \ell \int_{cs} \sin^2 k_x x \, dx \qquad \text{(A-49)}$$

$$= \frac{z_{TM1}}{2}\left(\frac{\omega\varepsilon_1 B}{k_x}\right)^2 \ell\left[\frac{x}{2} - \frac{\sin 2k_x x}{4k_x}\right]_{x=0}^{x=d} \qquad \text{(A-50)}$$

$$W_{TM10} = \frac{z_{TM1}}{2}\left(\frac{\omega\varepsilon_1 B}{k_x}\right)^2 \ell\left[\frac{d}{2} - \frac{\sin 2k_x d}{4k_x}\right] \qquad \text{(A-51)}$$

The power density from Equation A-49 is

$$\rho_1 = \frac{W_{TM10}}{\ell dx} = \frac{z_{TM1}}{2}\left(\frac{\omega\varepsilon_1 B}{k_x}\right)^2 \sin^2 k_x x \qquad \text{(A-52)}$$

Outside the Dielectric:

$$W_{TM20} = \frac{z_{TM2}}{2}\int_{cs} \left|H_t\right|^2 ds \qquad \text{(A-53)}$$

$H_t = H_{y2}$, from Equation A-4, integration was already performed in Equation A-42a.

$$W_{TM20} = \frac{z_{TM2}}{2}\left(\frac{\omega\varepsilon_2 C}{K_x}\right)^2 \frac{\ell}{2K_x}$$

The power density as a function of x outside the dielectric is

$$\rho_2 = \frac{W_{TM20}}{\ell dx} = \frac{z_{TM2}}{2}\left(\frac{\omega\varepsilon_2 C}{K_x}\right)^2 e^{-2K_x(x-d)}$$

Power Transfer for TE Even Mode

From Equation A-10,

$$Y_{TE1} = \frac{\beta}{-\omega\mu_1} \quad ; \quad Y_{TE2} = \frac{\beta}{-\omega\mu_2}$$

Inside the Dielectric:

$$W_{TE1E} = \frac{Y_{TE1}}{2} \int_{cs} \left|E_t\right|^2 ds \qquad \text{(A-57)}$$

From Equation A-10,

$$E_{t1} = E_{y1}$$

$$W_{TE1E} = \frac{Y_{TE1}}{2} \int_{cs} \left|\frac{j\omega\mu_1 D}{k_x} \cos k_x x\right|^2 ds \qquad \text{(A-58)}$$

$$W_{TE1E} = \frac{Y_{TE1}}{2} \left(\frac{\omega\mu_1 D}{k_x}\right)^2 \ell \left[\frac{d}{2} + \frac{\sin 2dk_x}{4k_x}\right] \qquad \text{(A-59)}$$

The power density is

$$\rho_1 = \frac{W_{TE1E}}{\ell dx} = \frac{Y_{TE1}}{2} \left(\frac{\omega\mu_1 D}{k_x}\right)^2 \cos^2 k_x x \ ; \qquad \text{(A-60)}$$

Outside the Dielectric:

$$W_{TE2E} = \frac{Y_{TE2}}{2} \left(\frac{\omega\mu_2 F}{K_x}\right)^2 \frac{\ell}{2K_x} \qquad \text{(A-61)}$$

The power density outside the dielectric is

$$\rho_2 = \frac{W_{TE2E}}{\ell dx} = \frac{Y_{TE2}}{2} \left(\frac{\omega\mu_2 F}{K_x}\right)^2 e^{-2K_x(x-d)} \qquad \text{(A-62)}$$

Power Transfer for TE Odd Mode

Inside the Dielectric (from Equation 15):

$$Y_{TE1} = \frac{\beta}{-\omega\mu_1} \quad ; \quad Y_{TE2} = \frac{\beta}{-\omega\mu_2} \tag{A-63}$$

$$W_{TE10} = \frac{Y_{TE1}}{2} \int_{cs} |E_t|^2 \, ds \tag{A-64}$$

From Equation A-16,

$$E_{t1} = E_{y1}$$

$$ds = \ell dx$$

$$W_{TE10} = \frac{Y_{TE1}}{2} \int_{cs} \left| \frac{-j\omega\mu_1 E}{k_x} \sin k_x x \right|^2 \ell dx \tag{A-65}$$

$$W_{TE10} = \frac{Y_{TE1}}{2} \left(\frac{\omega\mu_1 E}{k_x} \right)^2 \ell \left[\frac{d}{2} - \frac{\sin 2k_x d}{4k_x} \right] \tag{A-66}$$

The power density is

$$\rho_1 = \frac{W_{TE10}}{\ell dx} = \frac{Y_{TE1}}{2} \left(\frac{\omega\mu_1 E}{k_x} \right)^2 \sin^2 k_x x \tag{A-67}$$

Outside the Dielectric:

$$W_{TE20} = \frac{Y_{TE2}}{2} \left(\frac{\omega\mu_2 F}{K_x} \right)^2 \frac{\ell}{2K_x} \tag{A-68}$$

Power density as a function of x outside the dielectric is

$$\rho_2 = \frac{W_{TE20}}{\ell dx} = \frac{Y_{TE2}}{2} \left(\frac{\omega\mu_2 F}{K_x} \right)^2 e^{-2K_x(x-d)} \tag{A-69}$$

Summary of the Power Transfer Equations for the TM Even Modes

$$z_{TM1} = \frac{\beta}{\omega\varepsilon_1} \; ; \quad z_{TM2} = \frac{\beta}{\omega\varepsilon_2} \tag{A-70}$$

TM_{1E} Inside Dielectric:

$$W_{TM1E} = \frac{z_{TM1}}{2}\left(\frac{\omega\varepsilon_1 A}{k_x}\right)^2 \ell\left[\frac{d}{2} + \frac{\sin 2dk_x}{4k_x}\right] \tag{A-71}$$

$$\rho_{TM1E} = \frac{z_{TM1}}{2}\left(\frac{\omega\varepsilon_1 A}{k_x}\right)^2 \cos^2 k_x x \tag{A-72}$$

TM_{2E} Outside Dielectric:

$$W_{TM2E} = \frac{z_{TM2}}{2}\left(\frac{\omega\varepsilon_2 C}{K_x}\right)^2 \frac{\ell}{2K_x} \tag{A-73}$$

$$\rho_{TM2E} = \frac{z_{TM2}}{2}\left(\frac{\omega\varepsilon_2 C}{K_x}\right)^2 e^{-2K_x(x-d)} \tag{A-74}$$

Ratio of power transferred inside dielectric to power transferred outside dielectric:

$$\frac{W_{TM1E}}{W_{TM2E}} = \frac{\varepsilon_1}{\varepsilon_2} \cdot \frac{\left(\frac{1}{k_x}\right)^2\left[\frac{d}{2} + \frac{\sin 2dk_x}{4k_x}\right]}{\left(\frac{\sin k_x d}{K_x}\right)^2 / 2K_x} = R_{TM_E} \tag{A-75}$$

Summary of the Power Transfer Equations for the TM Odd Modes

Inside Dielectric:

$$W_{TM1O} = \frac{z_{TM1}}{2}\left(\frac{\omega\varepsilon_1 B}{k_x}\right)^2 \ell\left[\frac{d}{2} - \frac{\sin 2k_x d}{4k_x}\right] \tag{A-76}$$

$$\rho_{TM1O} = \frac{z_{TM1}}{2}\left(\frac{\omega\varepsilon_1 B}{k_x}\right)^2 \sin^2 k_x x \tag{A-77}$$

Outside Dielectric:

$$\begin{cases} W_{TM20} = \frac{z_{TM2}}{2}\left(\frac{\omega\epsilon_2 C}{K_x}\right)^2 \frac{\ell}{2K_x} & \text{(A-78)} \\ \rho_{TM20} = \frac{z_{TM2}}{2}\left(\frac{\omega\epsilon_2 C}{K_x}\right)^2 e^{-2K_x(x-d)} & \text{(A-79)} \end{cases}$$

The ratio of power transferred in dielectric 1 to dielectric 2 is

$$\frac{W_{TM10}}{W_{TM20}} = \frac{\epsilon_1}{\epsilon_2} \cdot \frac{\left(\frac{1}{k_x}\right)^2\left[\frac{d}{2} - \frac{\sin 2k_x d}{4k_x}\right]}{\left(\frac{\cos k_x d}{K_x}\right)^2 / 2K_x} = R_{TM_o} \qquad \text{(A-80)}$$

Summary of the Power Transfer Equations for the TE Even Modes

$$Y_{TE1} = \frac{\beta}{-\omega\mu_1} \quad ; \quad Y_{TE2} = \frac{\beta}{-\omega\mu_2} \qquad \text{(A-81)}$$

Inside Dielectric

$$\begin{cases} W_{TE1E} = \frac{Y_{TE1}}{2}\left(\frac{\omega\mu_1 D}{k_x}\right)^2 \ell\left[\frac{d}{2} + \frac{\sin 2dk_x}{4k_x}\right] & \text{(A-82)} \\ \rho_{TE1E} = \frac{Y_{TE1}}{2}\left(\frac{\omega\mu_1 D}{k_x}\right)^2 \cos^2 k_x x & \text{(A-83)} \end{cases}$$

Outside Dielectric

$$\begin{cases} W_{TE2E} = \frac{Y_{TE2}}{2}\left(\frac{\omega\mu_2 F}{K_x}\right)^2 \frac{\ell}{2K_x} & \text{(A-84)} \\ \rho_{TE2E} = \frac{Y_{TE2}}{2}\left(\frac{\omega\mu_2 F}{K_x}\right)^2 e^{-2K_x(x-d)} & \text{(A-85)} \end{cases}$$

$$\frac{W_{TE1E}}{W_{TE2E}} = \frac{\left(\frac{1}{k_x}\right)^2 \left[\frac{d}{2} + \frac{\sin 2dk_x}{4k_x}\right]}{\left(\frac{\sin k_x d}{K_x}\right)^2 / 2K_x} = R_{TE_E} \tag{A-86}$$

Summary of the Power Transfer Equations for the TE Odd Modes

Inside Dielectric:

$$\begin{cases} W_{TE1O} = \frac{Y_{TE1}}{2}\left(\frac{\omega\mu_1 E}{k_x}\right)^2 \ell \left[\frac{d}{2} - \frac{\sin 2k_x d}{4k_x}\right] & \text{(A-87)} \\ \rho_{TE1O} = \frac{Y_{TE1}}{2}\left(\frac{\omega\mu_1 E}{k_x}\right)^2 \sin^2 k_x x & \text{(A-88)} \end{cases}$$

Outside Dielectric:

$$\begin{cases} W_{TE2O} = \frac{Y_{TE2}}{2}\left(\frac{\omega\mu_2 F}{K_x}\right)^2 \frac{\ell}{2K_x} & \text{(A-89)} \\ \rho_{TE2O} = \frac{Y_{TE2}}{2}\left(\frac{\omega\mu_2 F}{K_x}\right)^2 e^{-2K_x(x-d)} & \text{(A-90)} \end{cases}$$

$$\frac{W_{TE1O}}{W_{TE2O}} = \frac{\left(\frac{1}{k_x}\right)^2 \left[\frac{d}{2} - \frac{\sin 2dk_x}{4k_x}\right]}{\left(\frac{\cos k_x d}{K_x}\right)^2 / 2K_x} = R_{TE_O} \tag{A-91}$$

LOSSES

Losses Due to Imperfectly Conducting Boundaries

(When boundaries exist - conducting boundaries do not exist in dielectric slab lines.)

$$W_{L1} = \frac{R_s}{2} \oint |H_t|^2 \, d\ell$$

For TM Even Modes,

$$|H_t|^2 = |H_{y1}|^2 = \left|\frac{-j\omega\varepsilon_1 A}{k_x} \cos k_x x\right|^2 = \left(\frac{\omega\varepsilon_1 A}{k_x}\right)^2 \cos^2 k_x x$$

For TM Odd Modes,

$$|H_t|^2 = |H_{y1}|^2 = \left|\frac{j\omega\varepsilon_1 B}{k_x} \sin k_x x\right|^2 = \left(\frac{\omega\varepsilon_1 B}{k_x}\right)^2 \sin^2 k_x x$$

For TE Even Modes,

$$|H_t|^2 = |H_{z1}|^2 = |D \sin k_x x|^2 = D^2 \sin^2 k_x x$$

For TE Odd Modes,

$$|H_t|^2 = |H_{z1}|^2 = |E \cos k_x x|^2 = E^2 \cos^2 k_x x$$

For the TM Even Mode,

$$\alpha_s = \frac{W_{L1}}{2W_{T1}} \qquad \text{(A-92)}$$

The surface current is computed from the tangential magnetic field at the surface; or when $x = 0$,

$$W_{L1} = \frac{1}{2} R_s \oint \left(\frac{\omega\varepsilon_1 A}{k_x}\right)^2 d\ell$$

$$W_{L1} = \frac{1}{2} R_s \left(\frac{\omega\varepsilon_1 A}{k_x}\right)^2 \ell$$

$$W_{T1} = W_{TM1E}$$

$$\alpha_s = \frac{\frac{1}{2} R_s \left(\frac{\omega\varepsilon_1 A}{k_x}\right)^2 \ell}{2z_{TM1}\left(\frac{\omega\varepsilon_1 A}{k_x}\right)^2 \ell \left[\frac{d}{2} + \frac{\sin 2dk_x}{4k_x}\right]}$$

$$\alpha_s = \frac{\frac{1}{2} R_s}{2z_{TM1}\left[\frac{d}{2} + \frac{\sin 2dk_x}{4k_x}\right]} \qquad \text{(A-93)}$$

where α_s is the ratio of power lost per unit length in the surface conductor to the power transferred in the dielectric slab.

For the TM odd mode and TE even mode since $\sin k_x x = 0$ when $x = 0$, $H_t = 0$ and the attenuation due to imperfect boundary conduction is zero.

For the TE Odd Mode,

$$\alpha_s = \frac{W_{L1}}{2W_{T1}}$$

when $x = 0$

$$W_{L1} = \frac{1}{2} R_s \oint E^2 \, d\ell = \frac{1}{2} R_s E^2 \ell$$

$$W_{T1} = W_{TE10}$$

$$\alpha_s = \frac{\frac{1}{2} R_s E^2 \ell}{2Y_{TE1}\left(\frac{\omega\mu_1 E}{k_x}\right)^2 \ell \left[\frac{d}{2} - \frac{\sin 2k_x d}{4k_x}\right]}$$

$$\alpha_s = \frac{R_s}{2Y_{TE1}\left(\frac{\omega\mu_1}{k_x}\right)^2 \left[\frac{d}{2} - \frac{\sin 2k_x d}{4k_x}\right]} \qquad \text{(A-94)}$$

where α_s is the ratio of the power lost per unit length in the surface conductor to the power transfer in the dielectric slab.

Note that when the conducting plane at x = 0 is removed in the TM even and TE odd modes, there is no loss due to an imperfect conductor. Loss is due only to an imperfect dielectric, which is treated elsewhere.

Attenuation in Lossy Dielectric

The attenuation constant of a wave traveling along a uniform system may be written as (Reference 2, page 42):

$$\alpha = \frac{W_D}{2W_T}$$

where W_T is the average power transfer and W_D is the average power loss in the line per unit length due to dielectric heating.

The dielectric loss per unit length in the z direction for the TM even modes is:

$$W_{DTM1E} = \frac{\sigma_d}{2} \cdot \int |E_{x1}|^2 \, ds$$

Since ds = ℓdx here,

$$W_{DTM1E} = \frac{\sigma_d \ell}{2} \cdot \int_0^d |E_{x1}|^2 \, dx$$

From Equation A-3,

$$|E_{x1}| = z_{TM1} \cdot \frac{\omega \varepsilon_1 A}{k_x} \cdot \cos k_x x$$

so

$$W_{DTM1E} = \frac{\sigma_d \ell}{2} \cdot z_{TM1}^2 \cdot \left(\frac{\omega \varepsilon_1 A}{k_x}\right)^2 \cdot \int_0^d \cos^2 k_x x \, dx$$

[2]Ramo, Whinnery and Van Duzer, Fields and Waves in Communication Electronics, New York: John Wiley & Sons, 1965.

$$W_{DTM1E} = \frac{\sigma_d \ell}{2} \cdot z_{TM1}^2 \cdot \left(\frac{\omega\varepsilon_1 A}{k_x}\right)^2 \cdot \left(\frac{d}{2} + \frac{\sin 2k_x x}{4k_x}\right) \qquad \text{(A-95)}$$

Now let $\alpha_{TM1} = \dfrac{W_{DTM1E}}{2W_{TM1E}}$

From Equation (71) for W_{TM1E},

$$\alpha_{TM1} = \frac{\dfrac{\sigma_d \ell}{2} \cdot z_{TM1}^2 \cdot \left(\dfrac{\omega\varepsilon_1 A}{k_x}\right)^2 \left(\dfrac{d}{2} + \dfrac{\sin 2k_x d}{4k_x}\right)}{2 \cdot \ell \cdot \dfrac{z_{TM1}}{2} \cdot \left(\dfrac{\omega\varepsilon_1 A}{k_x}\right)^2 \left(\dfrac{d}{2} + \dfrac{\sin 2k_x d}{4k_x}\right)}$$

$$\alpha_{TM1} = \frac{\sigma_d z_{TM1}}{2}$$

and since $\sigma_d = \omega\varepsilon_1 \tan\delta$ and $z_{TM1} = \dfrac{\beta}{\omega\varepsilon_1}$, this becomes

$$\alpha_{TM1} = \frac{1}{2}\omega\varepsilon_1 \tan\delta \cdot \frac{\beta}{\omega\varepsilon_1} = \frac{1}{2}\beta \tan\delta \qquad \text{(A-96)}$$

Now our attenuation constant α is defined by

$$\alpha_{TM1E} = \frac{W_{DTM1E}}{2(W_{TM1E} + W_{TM2E})} \qquad \text{in } \left(\frac{\text{nepers}}{\text{in}}\right)$$

$$= \frac{W_{DTM1E}}{2\left[W_{TM1E} + \left(\dfrac{W_{TM1E}}{R_{TME}}\right)\right]} \qquad \text{since } W_{TM2E} = \frac{W_{TM1E}}{R_{TME}} \quad \text{from A-75}$$

$$\alpha_{TM1E} = \frac{W_{DTM1E}}{2W_{TM1E}\left(1 + \dfrac{1}{R_{TME}}\right)}$$

$$\alpha_{TM1E} = \frac{\alpha_{TM1}}{\left(1 + \frac{1}{R_{TME}}\right)} \qquad \text{(A-97)}$$

(Note that when the power ratio R_{TME} is very large, $\alpha_{TM1E} \simeq \alpha_{TM1}$.)

Then the attenuation constant in $(\frac{db}{in})$ will be given by:

$$\alpha_{TM1E}\left(\frac{db}{in}\right) = 8.686\ \alpha_{TM1E}\left(\frac{nepers}{in}\right) \qquad \text{(A-98)}$$

For the TM odd mode:

$$W_{DTM10} = \frac{\sigma_d}{2}\int |E_{x1}|^2\ ds = \frac{\sigma_d \ell}{2}\int_0^d |E_{x1}|^2\ dx$$

$$= \frac{\sigma_d \ell}{2} \cdot z_{TM1}^2 \cdot \left(\frac{\omega\varepsilon_1 B}{k_x}\right)^2 \cdot \int_0^d \sin^2(k_x x)dx \qquad \text{from A-7}$$

$$= \frac{\sigma_d \ell}{2} \cdot z_{TM1}^2 \cdot \left(\frac{\omega\varepsilon_1 B}{k_x}\right)^2 \cdot \left(\frac{d}{2} - \frac{\sin 2k_x d}{4k_x}\right) \qquad \text{(A-99)}$$

$$\alpha_{TM1} = \frac{W_{DTM10}}{2W_{TM10}} = \frac{\frac{\sigma_d \ell}{2} \cdot z_{TM1}^2 \cdot \left(\frac{\omega\varepsilon_1 B}{k_x}\right)^2 \left(\frac{d}{2} - \frac{\sin 2k_x d}{4k_x}\right)}{2 \cdot \ell \cdot \left(\frac{z_{TM1}}{2}\right) \cdot \left(\frac{\omega\varepsilon_1 B}{k_x}\right)^2 \left(\frac{d}{2} - \frac{\sin 2k_x d}{4k_x}\right)} \qquad \text{from A-76}$$

$$\alpha_{TM1} = \frac{1}{2}\sigma_d\, z_{TM1} = \frac{1}{2}\omega\varepsilon_1 \tan\delta \cdot \frac{\beta}{\omega\varepsilon_1} = \frac{1}{2}\beta \tan\delta \qquad \text{(A-100)}$$

(Note that α_{TM1} is the same for both the TM even and odd modes.)

And, we will have the attenuation constant again, in nepers per inch:

$$\alpha_{TM10} = \frac{W_{DTM10}}{2(W_{TM10} + W_{TM20})} = \frac{\alpha_{TM1}}{\left(1 + \frac{1}{R_{TM0}}\right)} \qquad \text{(A-101)}$$

or converted to decibels per inch,

$$\alpha_{TM10}\left(\frac{db}{in}\right) = 8.686 \cdot \alpha_{TM10}\left(\frac{nepers}{in}\right) \tag{A-102}$$

For the TE even and odd modes, we will similarly have

$$W_{DTE1E} = \frac{\sigma_d \ell}{2} \cdot \left(\frac{\omega\mu_1 D}{k_x}\right)^2 \left(\frac{d}{2} + \frac{\sin 2k_x d}{4k_x}\right) \tag{A-103}$$

$$W_{DTE10} = \frac{\sigma_d \ell}{2} \cdot \left(\frac{\omega\mu_1 E}{k_x}\right)^2 \left(\frac{d}{2} - \frac{\sin 2k_x d}{4k_x}\right) \tag{A-104}$$

since $Y_{TE1} = \left|\frac{\beta}{\omega\mu_1}\right|$,

$$\alpha_{TE1} = \frac{W_{DTE1E}}{2W_{TE1E}} = \frac{\sigma_d}{2Y_{TE1}} = \frac{\omega^2\varepsilon_1\mu_1}{2\beta} \tan\delta = \frac{k_1^2}{2\beta} \tan\delta \tag{A-105}$$

$$\alpha_{TE1} = \frac{W_{DTE10}}{2W_{TE10}} = \frac{\sigma_d}{2Y_{TE1}} = \frac{\omega^2\varepsilon_1\mu_1}{2\beta} \tan\delta = \frac{k_1^2}{2\beta} \tan\delta \tag{A-106}$$

Once again, α_{TE1} is the same for both the TE even and odd modes and for the attenuation constants we will have:

$$\alpha_{TE1E} = \frac{W_{DTE1E}}{2(W_{TE1E} + W_{TE2E})} = \frac{\alpha_{TE1}}{\left(1 + \frac{1}{R_{TEE}}\right)} \quad \text{in } \frac{nepers}{in} \tag{A-107}$$

$$\alpha_{TE10} = \frac{W_{DTE10}}{2(W_{TE10} + W_{TE20})} = \frac{\alpha_{TE1}}{\left(1 + \frac{1}{R_{TE0}}\right)} \quad \text{in } \frac{nepers}{in} \tag{A-108}$$

and finally,

$$\alpha_{TE1E}\ \frac{db}{in} = 8.686 \cdot \alpha_{TE1E}\ \frac{nepers}{in} \qquad \text{(A-109)}$$

$$\alpha_{TE10}\ \frac{db}{in} = 8.686 \cdot \alpha_{TE10}\ \frac{nepers}{in} \qquad \text{(A-110)}$$

Cutoff Frequency Calculations

$$(n\pi)^2 = (k_1 d)^2 - (k_2 d)^2$$

$$\left(\frac{n\pi}{d}\right)^2 = k_1^2 - k_2^2$$

$$\left(\frac{n\pi}{d}\right)^2 = \left(\frac{2\pi}{\lambda_1}\right)^2 - \left(\frac{2\pi}{\lambda_2}\right)^2$$

$$\lambda_1 = \frac{c}{f_c\sqrt{\frac{\varepsilon_1}{\varepsilon_0}}} \quad ; \quad \lambda_2 = \frac{c}{f_c\sqrt{\frac{\varepsilon_2}{\varepsilon_0}}}$$

$$\left(\frac{n\pi}{d}\right)^2 = \left(\frac{2\pi\ f_c\sqrt{\frac{\varepsilon_1}{\varepsilon_0}}}{c}\right)^2 - \left(\frac{2\pi f_c}{c}\sqrt{\frac{\varepsilon_2}{\varepsilon_0}}\right)^2$$

$$\left(\frac{n\pi}{d}\right)^2 = \left(\frac{2\pi f_c}{c}\right)^2 \frac{\varepsilon_1}{\varepsilon_0} - \left(\frac{2\pi f_c}{c}\right)^2 \frac{\varepsilon_2}{\varepsilon_0}$$

$$\left(\frac{n\pi}{2d}\right)^2 = \left(\frac{\pi f_c}{c}\right)^2 \left(\frac{\varepsilon_1}{\varepsilon_0} - \frac{\varepsilon_2}{\varepsilon_0}\right)$$

$$\left(\frac{f_c}{c}\right)^2 = \frac{\left(\frac{n}{2d}\right)^2}{\left(\frac{\varepsilon_1}{\varepsilon_0} - \frac{\varepsilon_2}{\varepsilon_0}\right)}$$

$$\frac{f_c}{c} = \frac{\frac{n}{2d}}{\sqrt{\frac{\varepsilon_1}{\varepsilon_o} - \frac{\varepsilon_2}{\varepsilon_o}}}$$

$$f_c = \frac{nc}{2d\sqrt{\frac{\varepsilon_1}{\varepsilon_o} - \frac{\varepsilon_2}{\varepsilon_o}}}$$

$$f_c = \frac{nc}{2d\sqrt{\varepsilon_{r_1} - \varepsilon_{r_2}}} \qquad n=0,1,2,3,... \qquad \text{(A-111)}$$

Similarly for odd modes, n is replaced by

$$\frac{2n-1}{2}$$

or

$$f_c = \frac{\left(\frac{2n-1}{2}\right)c}{2d\sqrt{\varepsilon_{r_1} - \varepsilon_{r_2}}} \qquad n = 1,2,3,4,\text{etc.} \qquad \text{(A-112)}$$

Equations A-111 and A-112 may be rewritten as follows:

$$f_c = \frac{Nc}{2(2d)\sqrt{\varepsilon_{r_1} - \varepsilon_{r_2}}} \qquad \text{(A-113)}$$

where N = 0,2,4,6,...,etc, for even modes and N = 1,3,5,7,...,etc, for odd modes.

TABLE OF SYMBOLS FOR APPENDIX A

A,B,C,D,E	are arbitrary amplitude constants used in Equations A-1 through A-16
c	Velocity of light in free space
d	Thickness of dielectric slab as defined in Figure A-1
E_{ij}	Electric field intensity in direction i, in dielectric region j
E_t	Transverse electric field intensity
E_{ti}	Transverse electric field in region i
e	Base of common log
F	Arbitrary constant defined in Equation A-24 for convenience in successive approximations
FA,FB,FC,FD	Arbitrary constant used in Equations A-25a through A-25d for convenience in successive approximations
f	frequency
f_c	Cut-off frequency of surface guide
H_{ij}	Magnetic field intensity in direction i, in dielectric region j
H_t	Transverse magnetic field intensity
H_{ti}	Transverse magnetic field in region i
k_x	Eigenvalue for electric and magnetic fields inside the dielectric material
K_x	Eigenvalue for electric and magnetic field outside the dielectric (in air)
k_i	Phase constant of plane wave in dielectric i

TABLE OF SYMBOLS FOR APPENDIX A

(Continued)

n	Integer
N	Even integer for even modes -- odd integer for odd modes
R_{TMm}	Ratio of power transferred inside dielectric slab to power transferred outside of dielectric for the transverse magnetic mode (m = E for even and 0 for odd)
R_{TEm}	Ratio of power transferred inside dielectric to that transferred outside dielectric for the transverse electric mode (m = E for even and 0 for odd)
R_s	Surface resistivity of boundary conductor
W_T	Power
W_{TM1m}	Power transferred by the TM mode in region 1, m is E for even modes and 0 for odd modes
W_{TE1m}	Power transferred by the TE mode in region 1, m = E for even modes and 0 for odd modes
W_{Li}	Power loss in region i
W_D	Average power loss in line per unit length due to dielectric heating
W_{DTM1k}	Average power loss in line per unit length due to dielectric heating for the TM mode in region 1; k = E for even mode and 0 for odd mode
W_{DTE1k}	Average power loss in line per unit length due to dielectric heating for the TE mode in region 1; k = E for even mode and 0 for odd mode
x,y,z	Rectangular coordinates
Y_{TEk}	Admittance of TE modes in region k

TABLE OF SYMBOLS FOR APPENDIX A

(Continued)

Z_{TMk}	Impedance of transverse magnetic modes in dielectric region k
α	Attenuation constant
α_s	Attenuation constant due to imperfect conducting boundary
α_{TMi}	Attenuation constant of the TM mode in region i
α_{TEij}	Attenuation constant of the TE mode in region i; j = E for even mode and O for odd mode
β	Phase constant of surface wave
$\tan\delta$	loss tangent of dielectric
ε_i	Dielectric constant of region i. When noted, this term will be used interchangeably with the relative dielectric constant
ε_0	Dielectric constant of space
λ_i	Wavelength of plane wave in dielectric i
λ_g	Guide wavelength of surface wave
μ_i	Permeability of region i -- when noted, this term is used interchangeably with relative permeability
μ_0	Permeability of space
ρ_i	Power density in region i
σ_d	Conductivity of dielectric
ω	Radian frequency = $2\pi f$

APPENDIX B

MICROWAVE POWER REQUIRED TO SHED ICE

ENERGY REQUIRED TO SHED ICE

Referring to Figure B-1, the energy (in calories) required to heat the ice from the blade equilibrium temperature, T_e, to the shed temperature, T_s, at which the ice adhesion bond is broken, is given by:

$$dQ = (T_s - T_e)k_1 cd\ L\ dr \qquad \text{(B-1)}$$

where

c = specific heat of ice

T_e = equilibrium temperature of blade skin

T_s = temperature at which ice will shed

d, L and r are defined in Figure B-2

k_1 = density of ice

This actually is a conservative estimate of heat energy required since it assumes that the entire ice layer of thickness d must be elevated in temperature, whereas only the thin adhesion layer of ice adjacent to the blade skin must be elevated

ICE REMOVAL FORCE

The centrifugal ice removal force acting on the element of ice in Figure B-2 is:

$$f_s(r) = k_1 d\ L\ \Delta r\ \omega^2 r \qquad \left[\frac{\text{gm-cm}}{\text{sec}^2} \text{ or dynes}\right] \qquad \text{(B-2)}$$

where d L Δr, as defined in Figure B-2, is the volume of the ice element and k_1 is the density of the ice. ω is the angular velocity of the blade in rad/sec, and r is the radius of the ice element, as illustrated in Figure B-2, in cm.

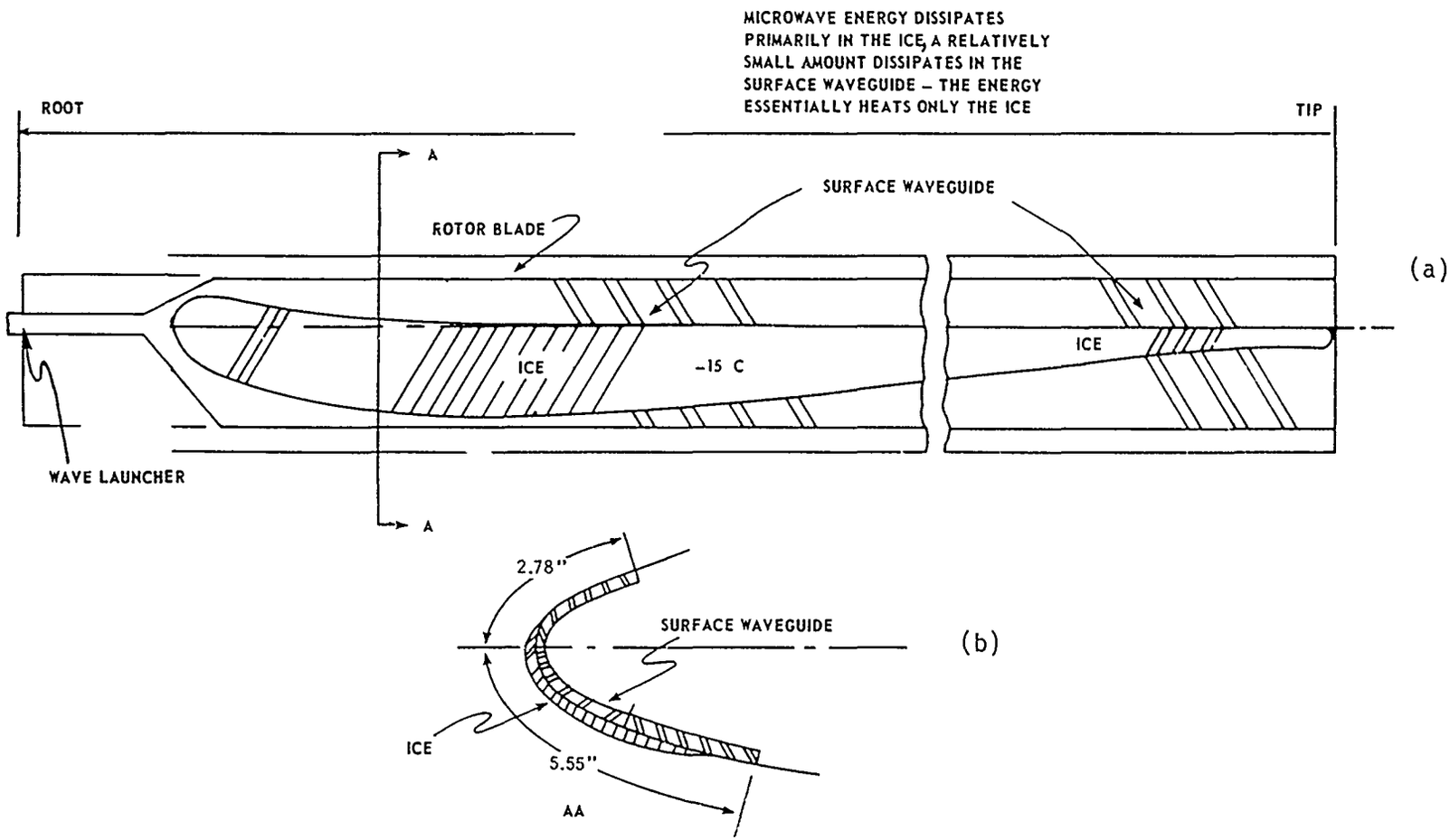

Figure B-1. Typical ice build-up on UH-1 blade

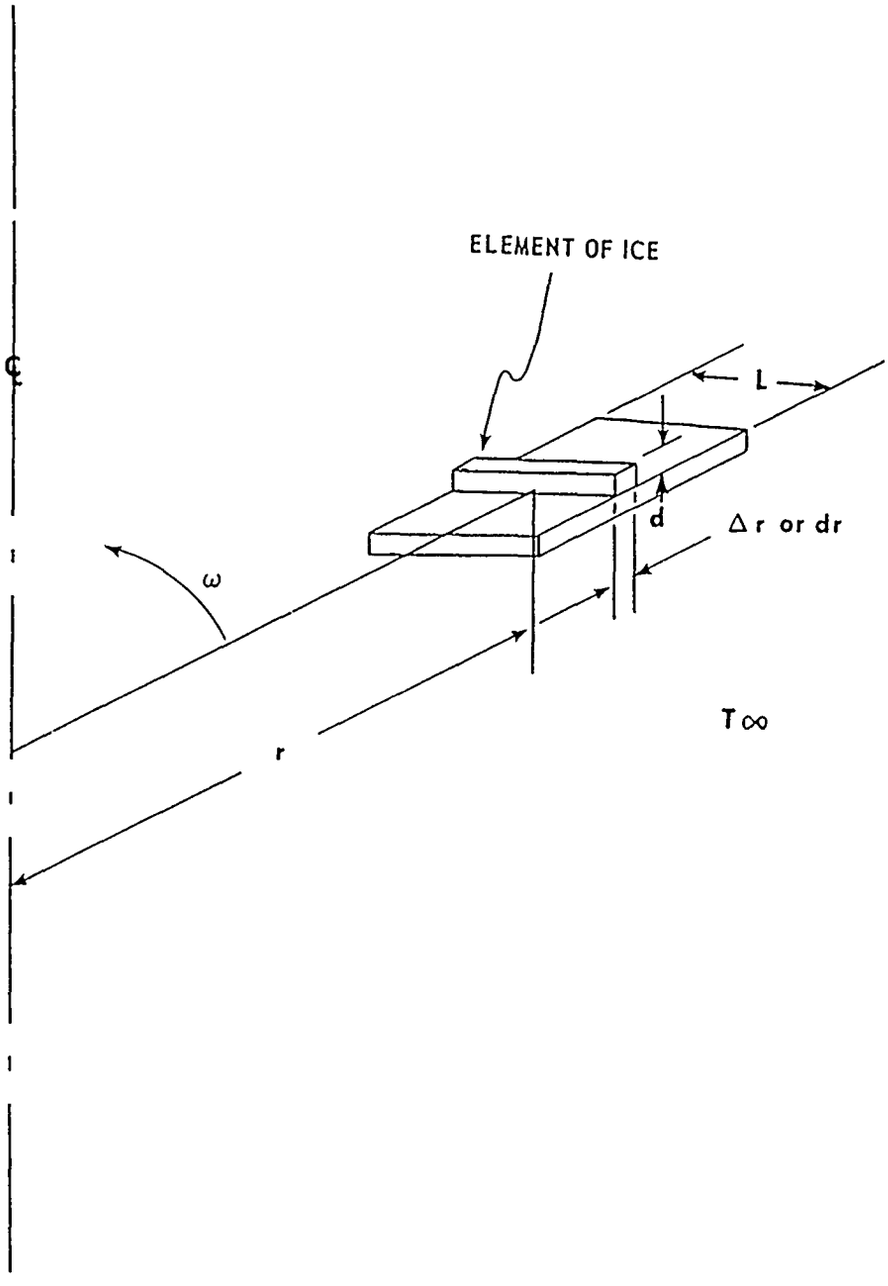

Figure B-2. Geometry of ice element on a rotor blade

FORCE REQUIRED TO BREAK THE ICE-TO-BLADE ADHESION BOND

From Stallabrass, the force required to break the ice adhesion bond is a function of the adhesion layer temperature, T_s; as the ice temperature increases, the ice removal force decreases.[31] If a linear approximation relating ice removal force with ice temperature is used, then the ice removal force in dynes/cm^2 for the element of ice is:

$$F_{sb} = pT_s(r) + s$$

$$f_{sb}(r) = F_{sb}L\Delta r \qquad \text{(B-3)}$$

$$f_{sb}(r) = (pT_s(r) + s)L\Delta r$$

where p and s are constants related to the material of the blade. Values of p and s established by making linear approximations to curves measured by Stallabrass (Reference 31, Figures 3-7) are given in Table B-1.

TABLE B-1. MATERIAL CONSTANTS

MATERIAL	p x10^4	s x10^4	s/p	K_1	K_2	K_3
65ST Aluminum	-15.6	- 75	4.81	-3,487	-14,901	- 6,285
Stainless Steel	- 6.96	- 30	4.31	-7,816	-15,633	- 7,017
Titanium	-11.43	- 69	6.036	-4,760	-13,109	- 4,493
Teflon	- 5.84	0	0	-9,315	-21,935	-13,319
Viton	-22.84	-165	7.224	-2,382	-11,341	- 2,755

[31]J.R. Stallabrass and R.D. Price. "On the Adhesion of Ice to Various Materials," National Research Laboratories, July 1962.

ICE TEMPERATURE THAT MUST BE OBTAINED TO SHED ICE

The ice adhesion bond will break when the centrifugal force $f_s(r)$, Equation B-2, is equal to the force required to break the bond, or:

$$k_1 dL\omega^2 r\Delta r = (pT_s(r) + s)L\Delta r \qquad \frac{gm\text{-}cm}{sec^2} \text{ or dynes} \tag{B-4}$$

Solving for $T_s(r)$:

$$T_s(r) = \frac{k_1 d\omega^2 r}{p} - \frac{s}{p} \tag{B-5}$$

An ideal situation, but one that may be impractical, is to design the deicer so that energy is distributed in such a way that $T_s(r)$ is reached simultaneously at all values of r. Ideally, when this is reached, all the ice will shed simultaneously.

ENERGY REQUIRED TO SHED THE ICE ASSUMING THAT THE SKIN TEMPERATURE OF THE BLADE IS AT AMBIENT

The blade temperature will normally assume an equilibrium temperature, due to aerodynamic heating, that is higher than the ambient temperature. This equilibrium temperature will reduce the temperature rise that need be imparted to the ice to reach T_s. For the present analysis, a conservative point of view is taken, and the equilibrium temperature is neglected. It is assumed that the blade surface assumes the ambient temperature only. Thus the heat required, from Equation B-1, is:

$$dQ = \left(\frac{k_1 d\omega^2 r}{p} - \frac{s}{p} - T_\infty\right) k_1 cdLdr \qquad \text{(B-6)}$$

$$dQ = \frac{k_1^2 d^2 \omega^2 cLr}{p}\, dr - \left(\frac{s}{p} + T_\infty\right) k_1 cdLdr$$

$$Q = \frac{k_1^2 d^2 \omega^2 cL}{p} \int_{r_1}^{r_2} rdr - \left(\frac{s}{p} + T_\infty\right) k_1 cdL \int_{r_1}^{r_2} dr$$

$$Q = \frac{k_1^2 d^2 \omega^2 cL(r_2 - r_1)(r_2 + r_1)}{2p} - \left(\frac{s}{p} + T_\infty\right) k_1 cdL(r_2 - r_1)$$

where r_1 is the point on the root end where icing starts, r_2 is the point on the tip end where it stops.

$$Q = \left[\frac{k_1^2 \omega^2 c}{p} L(r_2 - r_1)\left(\frac{r_2 + r_1}{2}\right)\right] d^2 - \left[\left(\frac{s}{p} + T_\infty\right) k_1 cL(r_2 - r_1)\right] d \qquad \text{(B-7)}$$

$$Q = K_1 d^2 - K_2 d \quad \text{calories} \qquad \text{(B-8)}$$

$$Q = (K_1 d^2 - K_2 d)/.2389 \quad \text{watt-sec or Joules} \qquad \text{(B-9)}$$

where

$$K_1 = \left[\frac{k_1^2 \omega^2 c}{p} \cdot L(r_2 - r_1) \cdot \frac{(r_2 + r_1)}{2}\right] \qquad \text{(B-10)}$$

$$K_2 = \left[\left(\frac{s}{p} + T_\infty\right) k_1 cL(r_2 - r_1)\right] \qquad \text{(B-11)}$$

The amounts of energy required for various thicknesses of ice accumulation, d, have been computed from Equation B-9 and are presented in Table B-2 for aluminum, stainless steel, titanium and teflon, in watt seconds. An even more conservative estimate of energy required to shed would be that energy required to raise the ice layer from ambient temperature, T_∞, to 0°C or from Equation B-1:

$$Q = (0 - T_\infty)k_1 cdL \frac{(r_2 - r_1)}{.2389} \text{ watt-sec} \qquad \text{(B-12)}$$

$$Q = K_4 d$$

where

$$K_4 = \frac{T_\infty k_1 cL(r_2 - r_1)}{.2389}$$

If d is in cm and T_∞ = -15°C:

$$K_{4_{cm}} = 91{,}819 \text{ (watt-sec)/cm}$$

If d is in inches and T_∞ = -15°C:

$$K_{4_{in}} = 233{,}219 \text{ (watt-sec)/in}$$

These estimates of energy have been computed and appear in Tables B-2 and B-3. Tables B-4 and B-5 give the constants used in these calculations.

TABLE B-2 ENERGY IN WATT-SEC PER UH-1 BLADE REQUIRED TO SHED ICE - BLADE ASSUMED TO BE AT AN AMBIENT TEMPERATURE OF (T_∞ =-15°C)

From Eq. 9 $Q = (K_1 d^2 - K_2 d)/.2389$					Eq. 12
THICKNESS	TEMPERATURE OF ICE RAISED FROM T_∞ TO T_s				TEMP. RAISED T_∞ TO 0°C
d Inches	65ST Aluminum (Watt-sec)	Stainless Steel (Watt-sec)	Titanium (Watt-sec)	Teflon (Watt-sec)	(Watt-sec)
0.05	7,686	7,783	6,647	11,032	11,661
0.10	14,901	14,507	12,653	20,806	23,322
0.20	28,025	24,794	22,733	36,583	46,643

TABLE B-3. ENERGY IN WATT-SEC PER UH-1 BLADE REQUIRED TO SHED ICE - BLADE ASSUMED TO BE AT AN EQUILIBRIUM TEMPERATURE OF (T_∞ = -15°C)

From Eq. 14 $Q = (K_1 d^2 - K_3 d)/.2389$					Eq. 12
THICKNESS	TEMPERATURE OF ICE RAISED FROM T_ϵ TO T_s				TEMP. RAISED T_∞ TO 0°C
d Inches	65ST Aluminum (Watt-sec)	Stainless Steel (Watt-sec)	Titanium (Watt-sec)	Teflon (Watt-sec)	(Watt-sec)
0.05	3,105	3,201	2,066	6,450	11,661
0.10	5,739	5,350	3,489	11,642	23,322
0.20	9,596	6,474	4,408	18,255	43,643

TABLE B-4. CONSTANTS USED IN CALCULATIONS

AREA OF BLADE ICED

T_∞ = -15°C $\quad L(r_2 - r_1) = 503.7 \text{ in}^2 = 3{,}249 \text{ cm}^2$

T_∞ = -20.9°C $\quad L(r_2 - r_1) = 765 \text{ in}^2 = 4{,}936 \text{ cm}^2$

AVERAGE WIDTH OF ICED AREA

T_∞ = -15°C $\quad L_{av} = (503.7)/(r_2 - r_1) = 2.376 \text{ in} = 6.035 \text{ cm}$

T_∞ = -20.9°C $\quad L_{av} = (765)/(r_2 - r_1) = 3.610 \text{ in} = 9.166 \text{ cm}$

$r_1 = 50 \text{ in}$

$r_2 = 262 \text{ in}$

$$\frac{r_2 + r_1}{2} = 156 \text{ in} = 396.2 \text{ cm}$$

Specific Heat of Ice	$c = 0.5$ cal/gm-°C
Density of Ice	$K_1 \tilde{=} 0.9$; $K_1^2 = 0.81$
Angular Velocity of UH-1 Main Rotor	$294 \leq \omega \leq 324$ rev/min $30.7 \leq \omega \leq 33.9$ rad/sec
Average Angular Velocity	$\omega_{av} = 32.3$ rad/sec $\omega_{av}^2 = 1043.29$ rad^2/sec^2

TABLE B-5. BLADE DIMENSIONS USED IN CALCULATIONS

Helicopter or Blade Type	NACA 0012 (Ref. 3)	UH-1 (Ref. 65)	BELL 47-G NACA 0011 TO NACA 0017 Ref. 31)
Chord Length (In.)			
Tip	28	21	10
Root	28	21	13.75
Blade Surface Area (2 Sides of Blade) $(In)^2$	17,472	11,004 (12,090)[1]	4,655
Relative Blade Area (Rel. to UH-1)	1.588 (1.445)[1]	1.0	0.423
Iced Area (In^2)			
-15°C	728	458.7 (503.7)[1]	---
-20.9°C	---	765	324

[1] Values in parentheses are slightly larger than actual values and were used in the calculations. These larger values come from Reference 35 where the UH-1 blade area is reported as 12,090 in^2. Later calculations based on blade dimensions yielded 11,004 in^2. Since the slightly larger values yield slightly greater power requirements, they were used. All iced areas are scaled values.

---

35 Department of the Army, Operator's Manual, Army Model UH-1D/H Helicopters, Technical Manual TM-55-1520-210-20, 24 August 1971.

ENERGY REQUIRED TO SHED ICE ASSUMING BLADE SKIN ASSUMES THE EQUILIBRIUM TEMPERATURE

If the aerodynamic heating of the blade is not neglected, less energy must be provided to shed the ice. A linear approximation of the equilibrium temperature assumed by the UH-1 blade at -15°C and -20°C ambient has been extracted from Figure 172 of Reference 29. It is (see Figure B-3):

$$T_e = mr + b \tag{B-13}$$

where at -15°C: $m = .0232°C/cm$ and $b = -18.3°C$

at -20°C: $m = .0250°C/cm$ and $b = 22.5°C$

If T_e is used in Equation (6) in place of T_∞, then

$$dQ = \left[\frac{k_1 d\omega^2 r}{p} - \frac{s}{p} - (mr + b)\right] k_1 cLd\, dr$$

$$Q = \left(\frac{k_1 d\omega^2}{p} - m\right) k_1\, cLd \int_{r_1}^{r_2} r\, dr - \left(\frac{s}{p} + b\right) k_1 cLd \int_{r_1}^{r_2} dr$$

$$Q = \left[\frac{k_1^2 \omega^2 cL(r_2 - r_1)}{p} \cdot \frac{(r_2 + r_1)}{2}\right] d^2$$

$$- \left[\frac{s}{p} + \frac{m(r_2 + r_1)}{2} + b\right] k_1 cL(r_2 - r_1)d$$

$$Q = K_1 d^2 - K_3 d \tag{B-14}$$

where

$$K_1 = \left[\frac{k_1^2 \omega^2 cL(r_2 - r_1)}{p} \cdot \frac{(r_2 + r_1)}{2}\right] \tag{B-15}$$

$$K_3 = \left[\frac{s}{p} + \frac{m(r_2 + r_1)}{2} + b\right] k_1 cL(r_2 - r_1) \tag{B-16}$$

29J.B. Werner, "Ice Protection Investigation for Advanced Rotary-Wing Aircraft." USAAMRDL Technical Report 73-38, August 1973.

Values of energy in watt-sec needed to raise the temperature of the ice from T_e to T_s have been computed in accordance with Equation B-14 and are presented in Table B-3; it will be noted that these values are smaller than those in Table B-2. It should also be noted that the values in Tables B-2 and B-3 are both smaller than those for the most conservative model, which requires that the temperature be raised from T_∞ to 0°C, also given in Tables B-2 and B-3 for comparison. A closer approximation to the real power required to shed the ice could be represented by empirical equations, rather than by a linear approximation, with the actual temperature in the ice layer taken into account. It is felt that such a fine model would be of academic interest only, since it must be bracketed between the most optimistic value (titanium) and the most conservative values, which have already been established and are relatively close to each other.

THE AVERAGE POWER REQUIRED PER BLADE

In this model of the microwave deicer it is assumed that ice will be permitted to accrete only to a predetermined, tolerable thickness, d_t, before it is caused to shed by the application of microwave power. This technique assumes that the power is applied for an "on period" long enough to shed the ice accumulation and then removed for an "off period" during which the ice is allowed to accumulate to d_t again. Therefore,

$$P_{av} = \frac{p_p T_{on}}{T_{on} + T_{off}} \qquad \text{(B-17)}$$

where

P_{av} = average power required per blade

p_p = peak power (power during "on time")

T_{on} = "on time" or time required to shed

T_{off} = "off time" or time during which a layer of ice d_t inches thick is allowed to accumulate where d_t is tolerable ice thickness

It will be noted that the numerator of Equation B-17, $p_p T_{on}$, is the energy required to shed the ice in watt-sec. Thus using the energy required to shed computed above (Tables B-2 and B-3), the value of T_{on} can be determined as a function of typical values of peak power, p_p, and ice thickness, d. The on times and average power injected into the ice have been computed for three models:

1) Conservative Model - ice temperature raised from T_∞ to 0°C

2) Teflon Equivalent Model - ice temperature raised from T_ϵ to T_S; surface assumed to have ice adhesive properties similar to Teflon.

3) Titanium Equivalent Model - ice temperature raised from T_ϵ to T_S; surface assumed to have ice adhesive properties similar to titanium.

These models are represented in Tables B-6, B-7 and B-8 respectively.

TABLE B-6. TIME TO SHED ICE (T_{on}) AS A FUNCTION OF ICE THICKNESS, d_t, AND PEAK POWER AVAILABLE, p_p, T_∞ = -15°C; CONSERVATIVE MODEL, EQUATION B-12

ICE THICKNESS d_t (Inches)	PEAK POWER AVAILABLE, p_p, FROM MICROWAVE DEICER - WATTS					TIME TO ACCUMULATE d_t
	100 W	200 W	400 W	800W	1600W	T_{off}
	(Sec)	(Sec)	(Sec)	(Sec)	(Sec)	(Sec)
0.05	116.5	58.2	29.12	14.5	7.28	120
0.10	233	116.5	58.2	29.12	14.5	240
0.20	466	233	116.5	58.2	29.2	480
Average Power Required P_{av}	49.2W	65.3W	78.01W	86.2W	91.5W	

where

$$P_{av} = \frac{p_p T_{on}}{T_{on} + T_{off}} = \frac{1}{1/p_p + 1/aK_4}$$

Average Accretion Rate = $a \cong 4.16 \times 10^{-4}$ in/sec
(extracted from Ref. 3, Figures 100-102)

$$T_{on} = \frac{K_4 d}{p_p}$$

K_4 = 233,161 (Watt-sec)/inch

TABLE B-7. TIME TO SHED ICE (T_{on}) AND AVERAGE POWER REQUIRED AS A FUNCTION OF ICE THICKNESS AND PEAK POWER AVAILABLE; T_∞ = -15°C, TITANIUM EQUIVALENT MODEL, ONE BLADE

ICE THICKNESS (Inches)	PEAK POWER, p_p, AVAILABLE FROM MICROWAVE DEICER - WATTS					TIME TO ACCUMULATE d_t
	100 W	200 W	400 W	800 W	1600W	T_{off}
0.05	$\frac{20.66}{14.6}$	$\frac{10.33}{15.8}$	$\frac{5.162}{16.4}$	$\frac{2.58}{16.83}$	$\frac{1.29}{17.0}$	120
0.10	$\frac{34.88}{12.68}$	$\frac{17.4}{13.51}$	$\frac{8.7}{13.99}$	$\frac{4.36}{14.27}$	$\frac{2.18}{14.4}$	240
0.20	$\frac{44.08}{8.4}$	$\frac{22.04}{8.78}$	$\frac{11.02}{8.97}$	$\frac{5.51}{9.07}$	$\frac{2.75}{9.12}$	480

$\frac{T_{on} \text{ - sec}}{P_{av} \text{ - Watts}}$

$$P_{av} = \frac{p_p \, T_{on}}{T_{on} + T_{off}}$$

a = Average Accretion Rate $\tilde{=} 4.16 \times 10^{-4}$ inches/second
(Extracted from Ref. 3, Figures 100-102)

$$T_{on} = \frac{(K_1 d^2 - K_3 d)/.2389}{p_p} = \frac{\text{Table B-3}}{p_p}$$

K_1 and K_3 from Table B-1

TABLE B-8. TIME TO SHED ICE (T_{on}) AND AVERAGE POWER REQUIRED AS A FUNCTION OF ICE THICKNESS AND PEAK POWER AVAILABLE; T_∞ = -15°C, TEFLON EQUIVALENT MODEL, ONE BLADE

ICE THICKNESS (Inches)	PEAK POWER, p_p, AVAILABLE FROM MICROWAVE DEICER - WATTS					TIME TO ACCUMULATE d_t
	100 W	200 W	400 W	800 W	1600W	T_{off} (sec)
0.05	64.5 / 34.95	32.25 / 42.6	16.12 / 47.36	8.06 / 50.37	4.03 / 51.98	120
0.10	116.42 / 32.6	58.21 / 39.	29.1 / 43.2	14.5 / 45.5	7.27 / 47.04	240
0.20	182.55 / 27.5	91.28 / 31.95	45.6 / 34.7	22.8 / 36.2	11.4 / 37.1	480

$\frac{T_{on} \text{ - sec}}{P_{av} \text{ - Watts}}$

$$P_{av} = \frac{p_p T_{on}}{T_{on} + T_{off}}$$

a = Average Accretion Rate $\tilde{=} 4.16 \times 10^{-4}$ inches/second
(Extracted from Ref. 3, Figures 100-102)

$$T_{on} = \frac{Q}{p_p} = \frac{(K_1 d^2 - K_3 d)/.2389}{p_p} = \frac{\text{Table B-3}}{p_p}$$

K_1 and K_3 from Table B-1

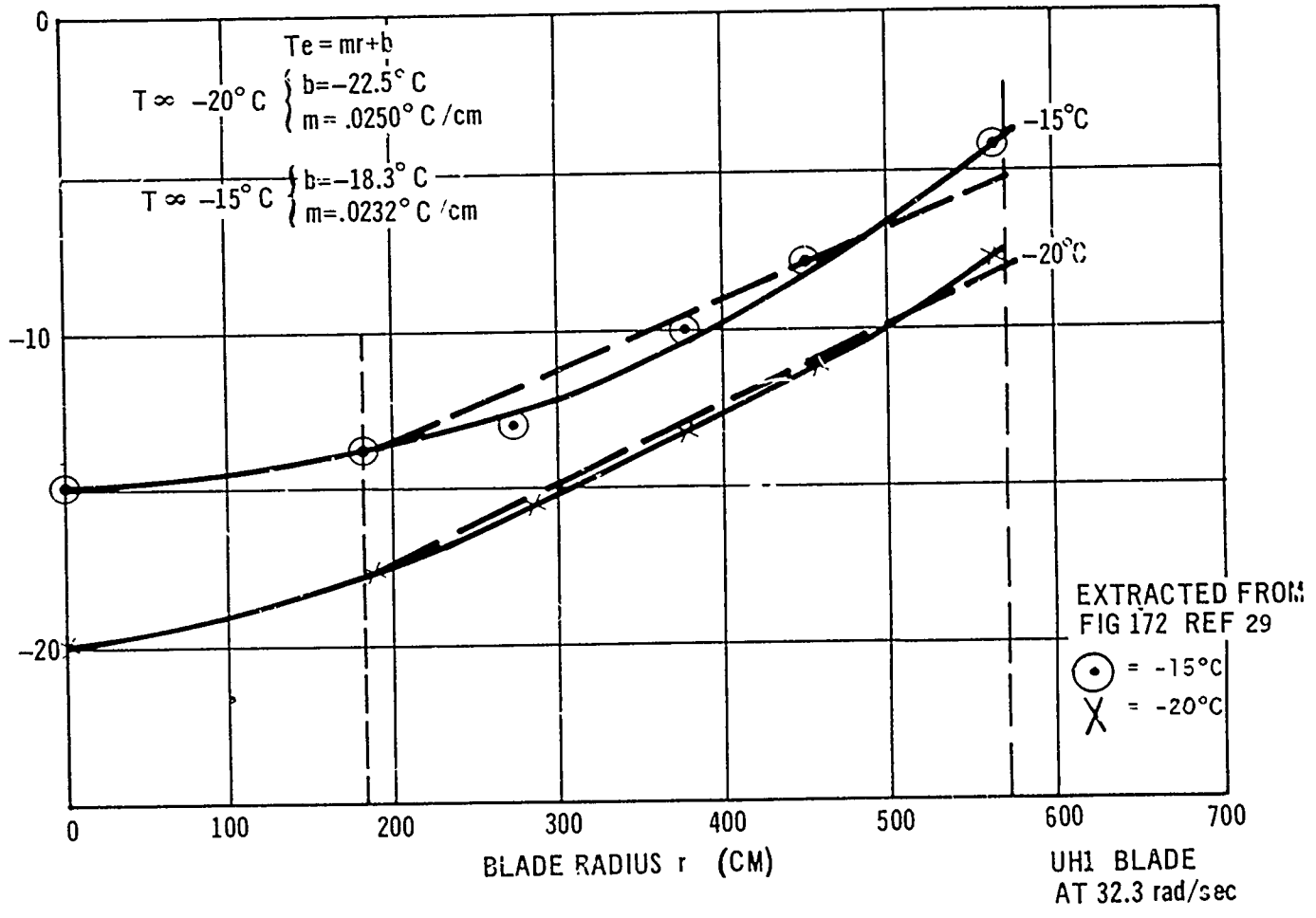

Figure B-3. Linear approximation of UH-1 blade equilibrium temperature

[29] J.B. Werner, "Ice Protection Investigation for Advanced Rotary-Wing Aircraft," USAAMRDL Technical Report 73-38 (August 1973).

ESTIMATES OF POWER REQUIRED TO SHED ICE FROM TWO UH-1 ROTOR BLADES WHEN AMBIENT TEMPERATURE IS AT -20.9°C

Tables B-1 through B-3 and B-6 through B-8 represent power estimates for when the ambient temperature is at -15°C. Computations were repeated for ambient temperatures of -20.9°C, and these appear in Tables B-9 through B-14.

TABLE B-9. MATERIAL CONSTANTS (T_∞ -20.9°C)

MATERIAL	$p \times 10^4$	$s \times 10^4$	s/p	K_1	K_2	K_3
65ST Aluminum	-15.6	- 75	4.81	- 5,296	-35,735	-15,321
Stainless Steel	- 6.96	- 30	4.31	-11,841	-36,846	-16,481
Titanium	-11.43	- 69	6.036	- 7,229	-33,013	-12,598
Teflon	- 5.84	0	0	-14,148	-16,418	-36,004
Viton	-22.84	-165	7.224	- 3,618	-30,344	- 9,959

TABLE B-10. ENERGY IN WATT-SEC PER UH-1 BLADE REQUIRED TO SHED ICE, BLADE ASSUMED TO BE AT AMBIENT TEMPERATURE (T_∞ = -20.9°C)

From Equation 9 $Q = (K_1 d^2 - K_2 d)/.2389$					Equation 12
THICKNESS	TEMPERATURE OF ICE RAISED FROM T_∞ TO T_s				TEMP. RAISED T_∞ TO 0°C
d Inches	65ST Aluminum (Watt-Sec)	Stainless Steel (Watt-Sec)	Titanium (Watt-Sec)	Teflon (Watt-Sec)	(Watt-Sec)
0.05	18,639	18,786	17,062	23,721	24,676
0.10	36,563	36,969	33,147	45,531	49,352
0.20	70,267	65,524	62,390	83,421	98,705

TABLE B-11. ENERGY IN WATT-SEC PER UH-1 BLADE REQUIRED TO SHED ICE, BLADE ASSUMED TO BE AT EQUILIBRIUM TEMPERATURE (T_∞ = -20.9°C

From Equation 14 $Q = (K_1 d^2 - K_3 d)/.2389$					Equation 12
THICKNESS	TEMPERATURE OF ICE RAISED FROM T_ε TO T_s				TEMP. RAISED T_∞ TO 0°C
d Inches	65ST Aluminum (Watt-Sec)	Stainless Steel (Watt-Sec)	Titanium (Watt-Sec)	Teflon (Watt-Sec)	(Watt-Sec)
0.05	7,787	7,933	6,209	12,869	24,676
0.10	14,859	14,264	11,442	23,827	49,352
0.20	26,858	22,116	18,980	40,012	98,705

TABLE B-12. TIME TO SHED ICE (T_{on}) AS A FUNCTION OF ICE THICKNESS, d_t, AND PEAK POWER AVAILABLE, p_p, T_∞ = -20.9°C; CONSERVATIVE MODEL, EQUATION B-12

ICE THICKNESS dt (Inches)	PEAK POWER AVAILABLE, Pp, FROM MICROWAVE DEICER - WATTS					TIME TO ACCUMULATE d_t
	100 w (Sec)	200 w (Sec)	400 w (Sec)	800 w (Sec)	1600w (Sec)	T_{off} (Sec)
0.05	247	123	62	31	15	114
0.10	494	247	123	62	31	227
0.20	987	494	247	123	62	455

where

$$P_{av} = \frac{p_p T_{on}}{T_{on} + T_{off}} = \frac{1}{1/p_p + 1/aK_4}$$

Average Accretion rate = $a \tilde{=} 4.4 \times 10^{-4}$ in/sec
(Extracted from Ref. 31. Figure 21)

$$T_{on} = \frac{K_4 d}{p_p}$$

K_4 = 233,161 (Watt-Sec)/Inch

ABLE B-13. TIME TO SHED ICE (T_{on}) AND AVERAGE POWER REQUIRED AS A FUNCTION OF ICE THICKNESS AND PEAK POWER AVAILABLE, T_∞ = -20.9°C; TITANIUM EQUIVALENT MODEL, ONE BLADE

ICE THICKNESS Inches	PEAK POWER, P_p, AVAILABLE FROM MICROWAVE DEICER - WATTS					TIME TO ACCUMULATE d_t
	100	200	400	800	1600	T_{off}(sec)
	(Sec)	(Sec)	(Sec)	(Sec)	(Sec)	
0.05	62.1 / 35.3	31.0 / 42.9	15.5 / 48.1	7.8 / 51.1	3.9 / 52.8	113.6
0.10	114.4 / 33.5	57.2 / 40.2	28.6 / 44.7	14.3 / 47.7	7.2 / 48.8	227.3
0.20	189.8 / 29.5	94.9 / 34.5	47.5 / 37.8	23.7 / 39.7	11.9 / 40.7	454.5

$\frac{T_{on} \text{ - Sec}}{P_{av} \text{ - Watts}}$

$$P_{av} = \frac{p_p \, T_{on}}{T_{on} + T_{off}}$$

a = Average Accretion Rate $\cong 4.4 \times 10^{-4}$ inches/second (Extracted from Reference 31, Figure 21)

$$T_{on} = \frac{Q}{p_p} = \frac{(K_1 d - K_3 d)/.2389}{p_p} = \frac{\text{Table B-3a}}{p_p}$$

K_1 and K_3 from Table B-1

TABLE B-14. TIME TO SHED ICE (T_{on}) AND AVERAGE POWER REQUIRED AS A FUNCTION OF ICE THICKNESS AND PEAK POWER AVAILABLE; T_∞ = -20.9°C TEFLON EQUIVALENT MODEL - ONE BLADE

ICE THICKNESS Inches	PEAK POWER, Pp, AVAILABLE FROM FROM MICROWAVE DEICER - WATTS					TIME TO ACCUMULATE d_t
	100 w	200 w	400 w	800 w	1600 w	
	(Sec)	(Sec)	(Sec)	(Sec)	(Sec)	T_{off}(sec)
0.05	128.7 / 53.1	64.3 / 72.3	32.2 / 88.3	16.1 / 99.2	8.0 / 105.8	113.6
0.10	238.3 / 51.2	119.1 / 58.8	59.6 / 83.0	29.8 / 92.7	14.9 / 98.4	227.3
0.20	400.1 / 46.8	200.1 / 61.1	100.0 / 72.2	50.0 / 79.3	25.0 / 83.4	454.5

$$\frac{T_{on} \text{ - Sec}}{P_{av} \text{ - Watts}}$$

$$P_{av} = \frac{p_p \, T_{on}}{T_{on} + T_{off}}$$

a = Average Accretion Rate $\tilde{=} 4.4 \times 10^{-4}$ inches/second (Extracted from Ref. 31, Figure 21)

$$T_{on} = \frac{Q}{p_p} = \frac{(K_1 d^2 - K_3 d)/.2389}{p_p} = \frac{\text{Table B-3a}}{p_p}$$

K_1 and K_3 from Table B-1

PRIME POWER TO MICROWAVE POWER CONVERSION EFFICIENCY

A block diagram of a possible microwave deicer system showing the efficiency of each component is illustrated in Figure B-4 where all parameters are defined, from which the "Prime Power to Microwave Conversion Efficiency" may be computed as follows:

$$P_{p1} = P_p/\eta_{d1}$$

$$P_{p2} = 2P_{p1} = 2P_p/\eta_{d1}$$

$$P_{p3} = P_{p2}/\eta_{d2} = 2P_p/\eta_{d2} \cdot \eta_{d1}$$

$$P_{p4} = P_{p3}/\eta_t = 2P_p/\eta_t \cdot \eta_{d2} \cdot \eta_{d1}$$

$$P_{av} = P_{p4}\rho/\eta_p = 2P_p\rho/\eta_p \cdot \eta_t \cdot \eta_{d2} \cdot \eta_{d1} = \frac{2P_{avI}}{\eta_s}$$

$$P_{avI} = P_p\rho$$

The "Prime Power to Microwave Power Conversion Efficiency" is:

$$\eta_s = \eta_p \cdot \eta_t \cdot \eta_{d1} \cdot \eta_{d2}$$

and

$$\rho = \text{duty cycle}$$

Plots of prime power required as a function of conversion efficiency are presented in Section 3 for ambient temperatures of -15°C and -20.9°C, respectively. These curves are derived from Tables B-6 through B-8 and B-12 through B-14. For the conservative model, Table B-6, only the maximum power requirement was used. For the teflon and titanium models, the maximum and minimum values of average power required from Tables B-7, B-8, B-13 and B-14 were used. These correspond to .050 inches and .200 inch of ice accumulation.

Since the powers indicated in all tables are for single blades, they must be doubled and divided by the assumed conversion efficiency to find the prime powers required from the helicopter.

Note: DIST = DISTRIBUTION

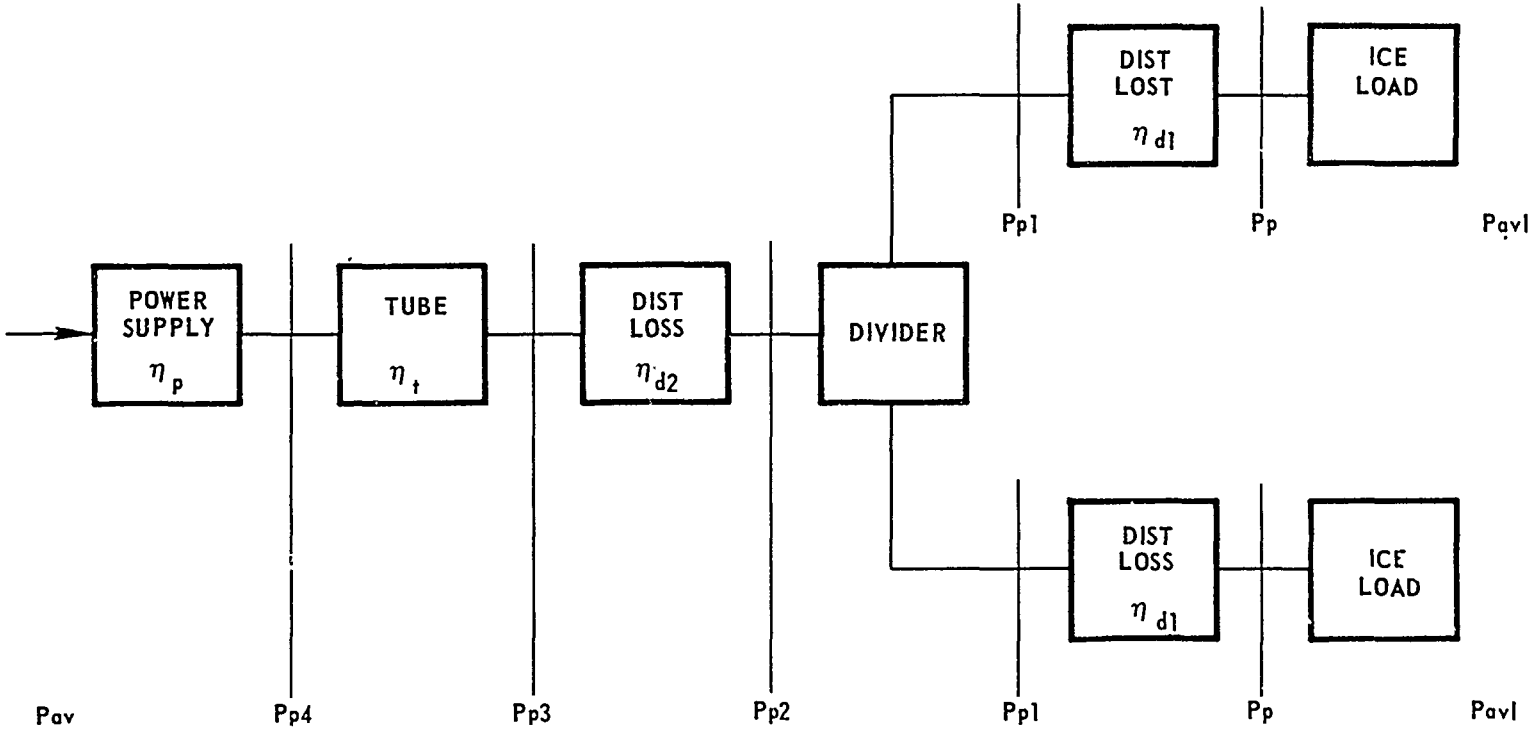

Figure B-4. Microwave deicer system loss schematic for UH-1

The curves also assume that practical power supplies can be built that can provide the peak powers required in Tables B-12 and B-14 while drawing only average power from the helicopter. Various power supply manufacturers have been consulted on this matter, and all believe that this can be done. A complete design of the deicer will require careful attention to the power supply to yield the maximum benefit of the techniques outlined here.

Zone cycling of the microwave generator is another means of averaging out the power demands on the helicopter. It would require a lower power microwave generator that is on continuously during icing conditions but which is switch-shared between zones on the blade in a manner similar to that used in the thermal cyclic deicer.

TABLE OF SYMBOLS FOR APPENDIX B

a	Ice accretion rate in/sec
b	y axis intercept of straight line approximation of blade equilibrium temperature °C (Figure B-3)
c	Specific heat of ice
d	Thickness of ice (Figure B-2)
d_r	Width of ice element (Figure B-2)
dt	Tolerable thickness of ice
f_s	Centrifugal ice removal force
F_{sb}	Force required to remove the ice element
k_1	Density of ice
K_1	A constant defined for mathematical convenience in Equations A-10 and A-15
K_2	A constant defined for mathematical convenience in Equation A-11
K_3	A constant defined for mathematical convenience in Equation A-16
K_4	A constant defined for mathematical convenience in equation following Equation A-12
L	Width of ice (Figure B-2)
m	Slope of straight line approximation of blade equilibrium temperature °C/cm (Figure B-3)
p	Material constant of blade derived from Stallabrass curves (Reference 31) $\frac{\text{dynes}}{\text{cm}^2 - °C}$

[31] J.R. Stallabrass and R.D. Price, "On the Adhesion of Ice to Various Materials," National Research Laboratories, July 1962.

TABLE OF SYMBOLS FOR APPENDIX B

(Continued)

P_{av}	Average microwave power required per blade dissipated in ice
P_{avs}	Average power required by system (prime power required) (DC power drawn from helicopter)
P_p	Peak power delivered to the ice load
P_{p1}	Peak power inserted into surface waveguide couplers
P_{p2}	Peak power inserted into dividers
P_{p3}	Power injected into transmission system (power output of tube)
P_{p4}	Peak power input to tube
Q	Heat energy
r	radius of ice element from center of rotation
r_1	Radius nearest root end of blade where icing starts
r_2	Radius nearest tip end at blade where icing ends
s	Material constant of blade derived from Stallabrass curves $\frac{\text{dynes}}{\text{cm}^2}$
T_e	Equilibrium temperature
T_∞	Ambient temperature
T_{off}	Time duration between microwave bursts during which ice has the opportunity to reform to a thickness d_t
T_{on}	Time duration of microwave burst of P_p

TABLE OF SYMBOLS FOR APPENDIX B

(Continued)

T_s	Shed temperature
Δr	Width of ice element (Figure B-2)
η_{d1}	Efficiency of surface waveguide couplers (includes loss in surface waveguides). The efficiency quantifies the coupler-surface guide distribution loss.
η_{d2}	Efficiency of transmission line up mast includes dissipative losses in power divider (which are very small) and transmission line connected to tube
η_p	Efficiency of power supply
η_t	Efficiency of tube
ρ	Duty cycle of deicer
ω	radian frequency of rotation

APPENDIX C

DESCRIPTIONS OF PROPOSED EXPERIMENTS FOR VERIFYING SURFACE WAVEGUIDE THEORY POWER-TO-SHED REQUIREMENTS AND SURFACE WAVEGUIDE COUPLING SYSTEMS

INTRODUCTION

This appendix contains outlines of procedures proposed for verifying the suitability of using surface waveguides for shedding rotor ice, for determining the power needed to shed ice, and for investigating surface waveguide couplings.

TASK 1

Task 1a - Laboratory Demonstration of Surface Waveguide Performance

This task will demonstrate in the laboratory the performance predictions of surface waveguide theory established in Phase I of the statement of work. The demonstration includes the measurement of the following parameters as functions of frequency, dielectric thickness, dielectric constant, loss tangent and mode:

- Guide Wavelength λ_g
- Phase Constant β
- Attenuation Constant α
- External Eigenvalue K_x
- Internal Eigenvalue k_x
- Power Ratio P_r
- Injected Power P_{in}
- Complex Dielectric Constant of Materials ε_1

As a practical means of varying the dielectric constant and loss tangent, measurements may be performed on the candidate dielectric materials tabulated in Table C-1. This table provides at least five variations in dielectric constant and loss tangent in any operating frequency. The measurements can be performed with the test apparatus illustrated in Figure C-1. The major pieces of test equipment needed for these measurements are a pin-leveled R.F. plug-in; sweeper main frame; network analyzer main frame; frequency converter; polar display; reflection, transmission unit; and spectrum analyzer. A description of how each of the parameters above are measured is given in Appendix D.

TABLE C-1. CANDIDATE MATERIALS WITH AND WITHOUT EROSION COATS

	(a)	(b)	(c)
1	Ultra-High Molecular Weight Polyethelene Erosion Coat	With 12 Mil Polyurethane Erosion Coat	With Alumina Erosion Coat
2	Irradiated, High-Density Polyolefin Laminate Polyguide	With 12 Mil Polyurethane Erosion Coat	With Alumina Erosion Coat
3	High Quartz Fiber Silicone Resin Laminate - Alphaquartz	With 12 Mil Polyurethane Erosion Coat	With Alumina Erosion Coat
4	Glass Laminate Silicone Resin Fiberglass	With 12 Mil Polyurethane Erosion Coat	With Alumina Erosion Coat
5	Alumina Aluminum Oxide	----	----

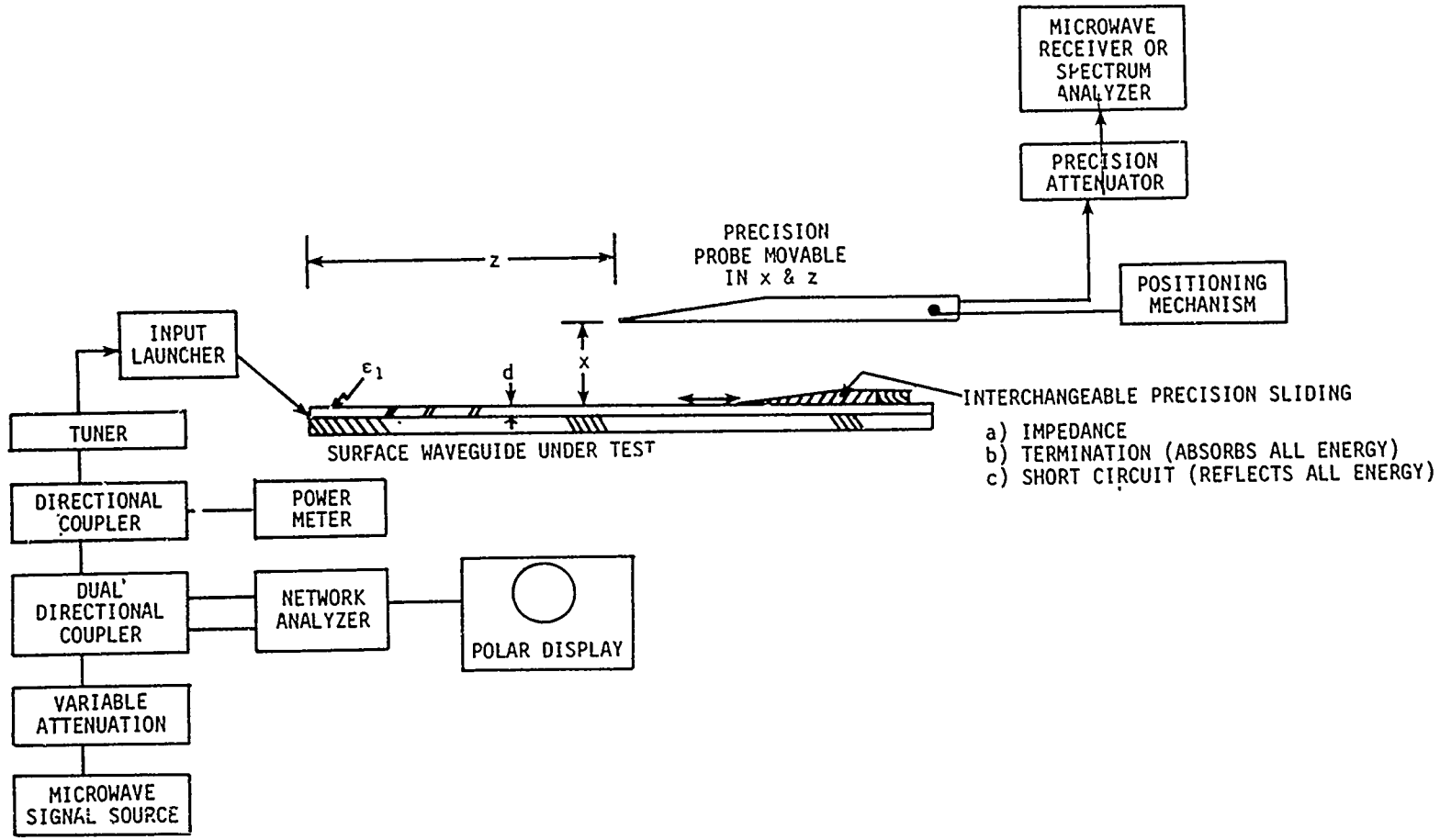

Figure C-1. Test equipment for measuring performance of surface waveguides

Task 1b - Measurement of the Complex Dielectric Constant of Ice

This task will measure the complex dielectric constant of ice grown in the laboratory. The complex dielectric constant will be measured at three frequencies of interest to microwave deicing and at several ambient temperatures between 0°C and -20°C. Tests are performed by the techniques described in Appendix D. The major pieces of test equipment required are listed under Task 1a.

TASK 2

Task 2a - Laboratory Demonstration of the Power Required to Shed Ice (Static Tests - Gravity Load-Statically Grown Ice)

This will be the first laboratory demonstration of the feasibility of shedding ice by means of microwaves. This task will demonstrate in the laboratory the shedding of ice and the accuracy of the predictions of the power required to shed established in Phase II of the statement of work. It will also demonstrate how microwave power distributes itself in the ice layer by the measurement of the following parameters on an ice-loaded surface guide as functions of mode, frequency, dielectric thickness, ice thickness, dielectric constant and loss tangent:

- Guide Wavelength λ_g
- Phase Constant β
- Attenuation Constant α
- External Eigenvalue K_x
- Internal Eigenvalue k_x
- Power Ratio P^r
- Injected Power P^{in}
- Power Required to Shed (Energy Required to Shed) E_s

The above parameters are measured using the same test equipment and measurement procedures described in Task 1 and Figure C-1 with the exception that tests are performed in a cold box in which the ambient temperature may be controlled. Surface waveguide test fixtures that would be fabricated and tested in Task 1 would be used here without modification. The surface waveguide test fixtures would be mounted on a tilting table that permits tests to be performed and an ice layer grown while the test

fixture was horizontal. To determine ~~the~~ energy required to shed the ice when acted on by the force of gravity, the table was tilted to the vertical position and microwave power applied until the ice sheds under the force of gravity.

Task 2b - Demonstration of the Power Advantage of Microwave Deicing

In this task the model microwave deicer, which is illustrated in Figure C-2 and which will have been constructed in Task 1, will be used to prove that the power requirement of a microwave deicer is an order of magnitude less than that of an equivalent thermal deicer. This will be done by constructing an equivalent thermal deicer, as shown in Figure C-3, having the same surface dimensions as the microwave deicer and mounting each deicer on an arm of a whirling-arm test fixture, as illustrated in Figure C-4. Identical ice accumulations will be statically grown on each deicer while the arms are at rest. The power and time required to shed the ice accumulations on both deicers while the arms are whirled, will then be measured and compared. The power and time to shed will be measured as functions of the following parameters:

- Ice Thickness, t $.05 \leq t \leq .250$
- Centrifugal Force or Angular Velocity
- Ambient Temperature, T $-20° \leq T \leq 0°C$
- Microwave Frequency $f = 5{,}850$ MHz, $f = 2{,}450$ MHz, $f = 22$ GHz

A camera, a strobe light and a clock arranged as in Figure C-4 will be used to determine the instant of shed and to record the shedding process.

Task 2c - Laboratory Demonstration of the Power Required to Shed Droplet-Impact Ice when Loaded by Centrifugal Force

This task will demonstrate the feasibility of shedding rotor ice with microwave energy when the ice is acted upon by centrifugal force, and verify the power requirement estimates of Phase II of the statement of work.

This experiment is essentially a modification of the whirling arm tests performed by Stallabrass, who measured "the adhesion of ice to various materials."[31] The modification is the use of test surfaces made of sections

[31] J.R. Stallabrass and R.D. Price, "On the Adhesion of Ice to Various Materials," National Research Laboratories, July 1962.

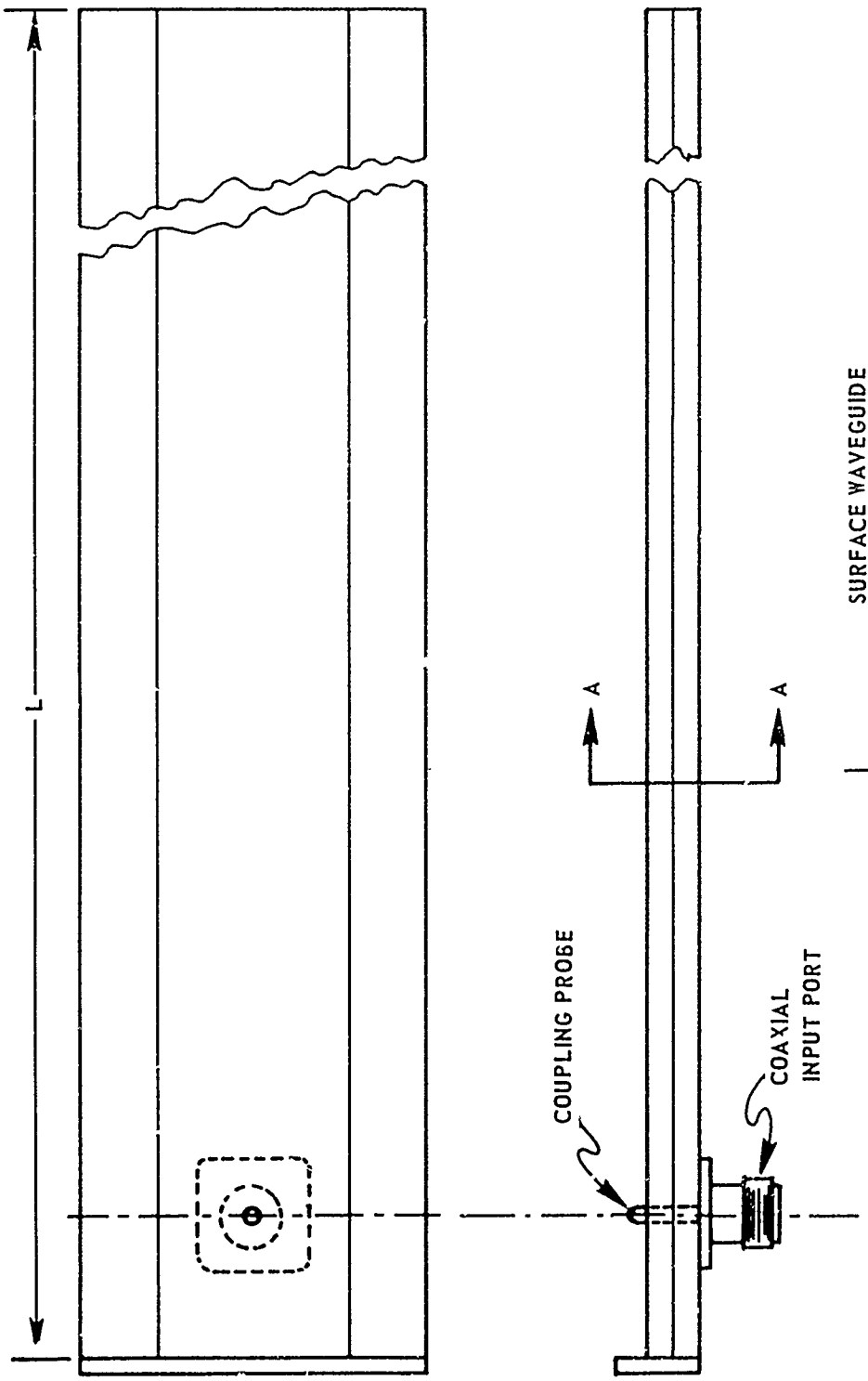

Figure C-2. Model microwave deicer used in feasibility study

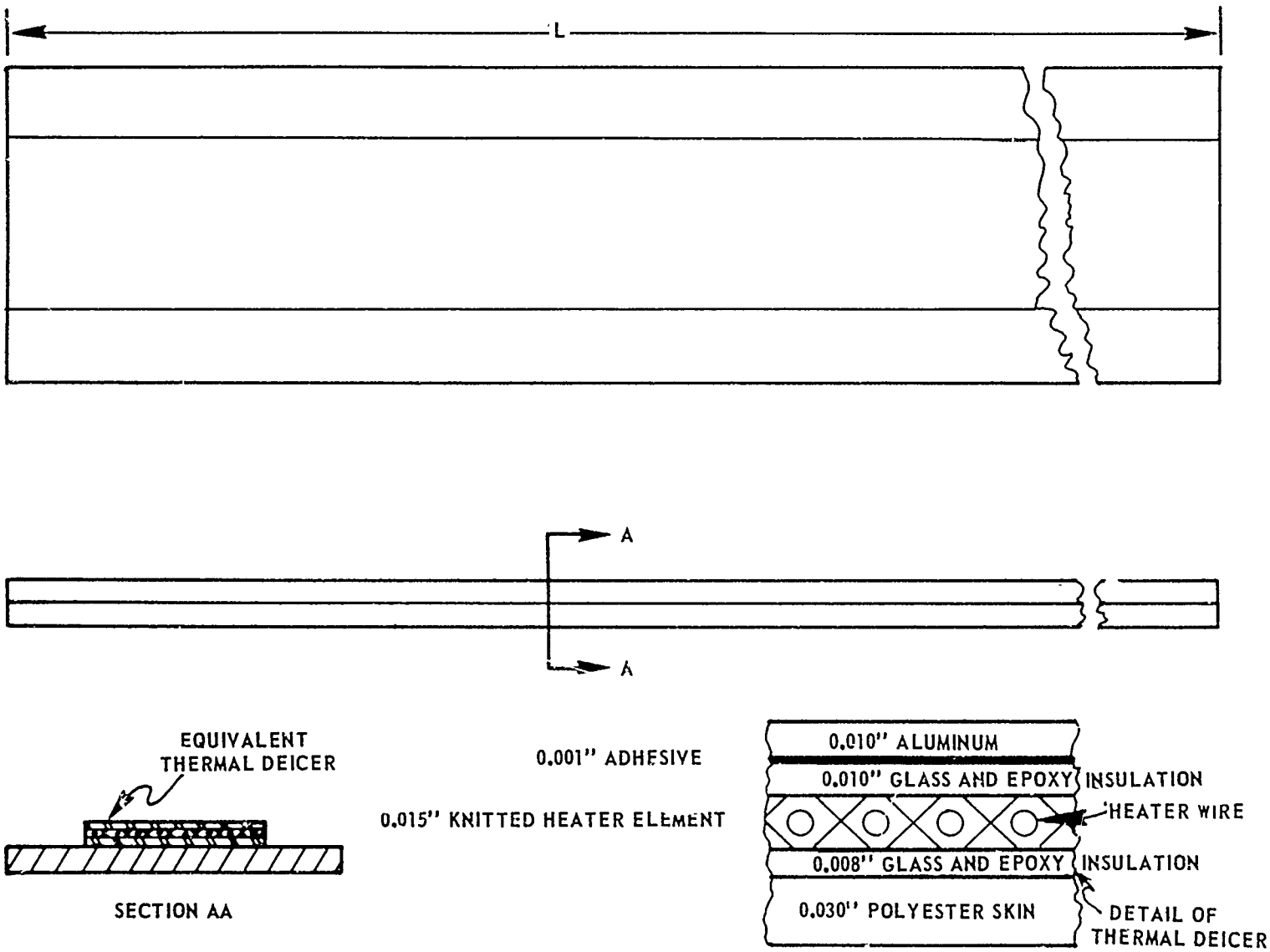

Figure C-3. Thermal deicer

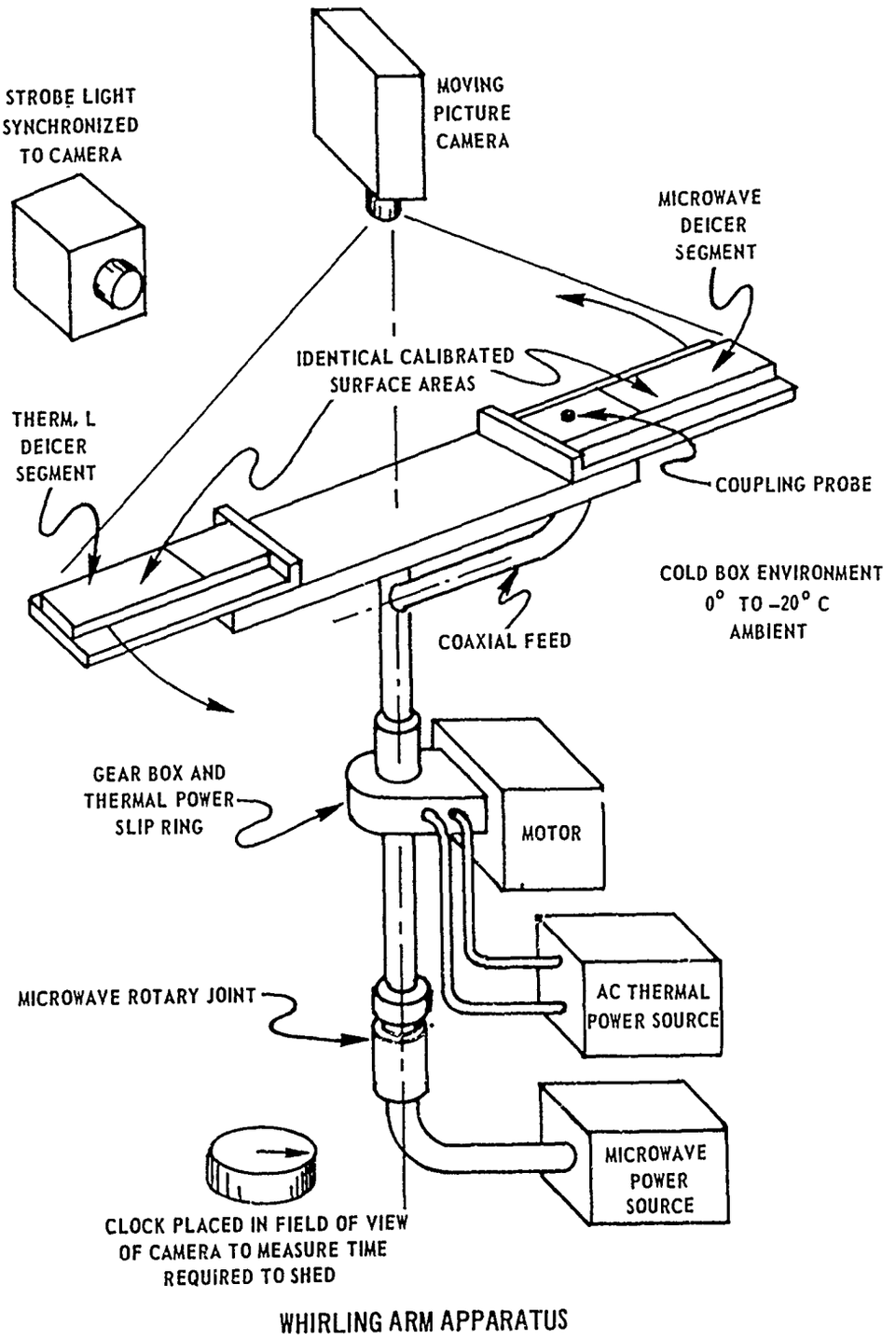

Figure C-4. Equipment used for the demonstration of the power advantage of microwave deicing over thermal deicing

of surface waveguides, constructed from the materials in Table 1, into which measured quantities of microwave energy will be injected. Droplet impact ice will be permitted to accrete as the arms whirl, and then the microwave energy required to shed the ice will be measured as a function of centrifugal shear force and other parameters described below.

Verification of Microwave Power Requirements. To verify the analytically estimated power requirements, the microwave energy required to shed ice accretions on the calibrated test surface will be measured as a function of:

- Ambient Temperature $-20° \leq T \leq 0°$
- Ice Thickness
- Droplet Size
- Shear Force on Ice Adhesion Layer
- Microwave Frequency
- Surface Guide Material
- Surface Guide Thickness
- Surface Waveguide Mode (TM_0 or TE_1)

Whirling Arm Apparatus. The whirling arm apparatus will be similar to that used by Stallabrass.[36] The apparatus will consist of a two-bladed, 9-foot diameter rotor situated in a 10-foot by 10-foot cold chamber.* A cloud of supercooled water droplets will be produced in the cold chamber by atomizing nozzles capable of varying droplet size. The nozzles will be located close to the floor of the chamber and sprayed upwards. The test surface waveguide, mounted on the rotor blade, will intercept the stream of droplets on each revolution. Undesired ice buildups on structure surrounding the test surfaces that might interfere with measurements will be inhibited by electrical heater pads. A stroboscopic light and moving picture camera will be used to observe and record progress of the tests.

*Size of rotor and cold box are tentative depending on whirling arm facility available.

[36] J.R. Stallabrass and R.D. Price, "On the Adhesion of Ice to Various Materials," National Research Laboratories, July 1962.

Test Surface Waveguide Deicers. The test specimens will be sections of surface waveguide fabricrated and tested in the laboratory as described in Task 1a and made from dielectric materials listed in Table 1. The supports for the test specimens will be cylinders about a foot in length and milled on the top and the bottom. The test specimens will be fastened to the leading edges. In this way, ice will be confined only to the calibrated leading edge surface area of the test surface guide. Microwave energy will be inserted by means of calibrated test couplers (to be designed in Task 3). Microwave power will be obtained from a laboratory microwave signal source outside the cold box and fed to the whirling arm fixture through a commercially available rotary joint. Power will be measured with precision directional couplers and power meters.

Measurement of Shed Force. Shed force will be measured by methods similar to those used by Stallabrass.[31] The shed force is the centrifugal force exerted by the ice at the moment the adhesion bond breaks down. Thus, the difference between the radial load of the test specimen immediately before and immediately after the ice sheds is the desired shed force.

The centrifugal load of the surface guide (and ice) will be measured by strain gauges. The surface waveguide will be allowed to slide freely along a radial support rod and bear upon a spring plate on each side of which strain gauges will be mounted. The two gauges will be connected through slip rings to form a bridge circuit with two resistors outside the chamber. The bridge will be driven by a dc voltage. The output will be fed to a multi-channel recorder.

Calibration of Strain Gauges. With the rotor turning at 500 rpm, the recorder will be set for zero pen deflection. The rotor will then be stopped and static radial loads will be applied to the surface waveguide until the pen again registers zero. Further load increments will then be applied and the position of the pen versus the applied load increment

[31] J.R. Stallabrass and R.D. Price, "On the Adhesion of Ice to Various Materials," National Research Laboratories, July 1962.

will be repated until the pen has traversed the full width of the recording paper.

Icing Procedure. With the temperature set to one of the desired values and the rotor turning at 500 rpm, the recorder will be set to zero deflection. The nozzle producing the spray of droplets of desired diameter will then be turned on. When an ice buildup of thickness d has been reached, heat will be applied to the heater pads to remove all unwanted ice that might interfere with the measurements.

As ice accretes on the surface waveguide, its centrifugal force will be registered by an increase in the deflection of the pen recorder.

Microwave power at frequency f will then be injected into the surface waveguide and turned off at the instant of ice shed. The microwave energy required to shed is the product of the injected power and the time applied.

As the adhesion bond fails and the ice sheds, the pen recorder will drop sharply to near zero. This change in pen deflection can be considered the adhesive shear force (shed force) of the bond.

Range of Tests. The test procedures above will be repeated so that the microwave energy required and the force required to shed can be measured as functions of:

T	Chamber Temperature $0° \leq T \leq -20°C$
d_i	Ice Thickness $.050" \leq d \leq .250"$
a	Droplet Size $10\mu \leq a \leq 45\mu$
f	Operating Microwave Frequency
S	Surface Guide Material (Table 1)
d	Thickness of Surface Guide
M	Mode Type, TM_0 or TE_1

TASK 3

Task 3a - Laboratory Demonstration of the Application of Coupling Theory to TE_1 Modes

This task will demonstrate experimentally TE_1 mode coupling theory described by Cohn and will result in experimental TE_1 mode couplers for use in the experiments of Tasks 1, 2 and 3.[21] The empirical data thus accumulated will represent design information for use in prototype design.

An experimental TE_1 mode coupler designed in accordance with Reference 21 is illustrated in Figure C-5. Critical dimensions for the coupler are also defined in Figure C-5. The theoretical relationship between bidirectional efficiency and these critical dimensions is illustrated in Figure C-6. From Figure C-6 it is seen that, theoretically, the bidirectional coupling efficiency approaches broad maximums as d, (the thickness of the slab) increases for a fixed h/d radio and frequency. The coupling efficiency, n, can then be measured as described in Appendix D using the apparatus of Figure C-1, while the dimensions h, d, a and b (Figure C-5) are varied. From these measurements, an empirical curve of efficiency as a function of h and d at desired frequencies is obtained that can be used to design prototype couplers. It should be kept in mind that bidirectional coupling efficiency is one-half the unidirectional efficiency. The unidirectional coupler is achieved by placing a reflecting metal plate at the proper distance, a (Figure C-5), from the current filament. After dimensions h and a are determined for the optimum bidirectional coupler, "a" is varied experimentally to obtain the maximum unidirectional coupling.

[21] Cohn, Cassedy and Kott, "TE Mode Excitation on Dielectric Loaded Parallel Plane and Trough Waveguides," IRE Transactions on Microwave Theory and Techniques, pp. 545-552 (September 1960).

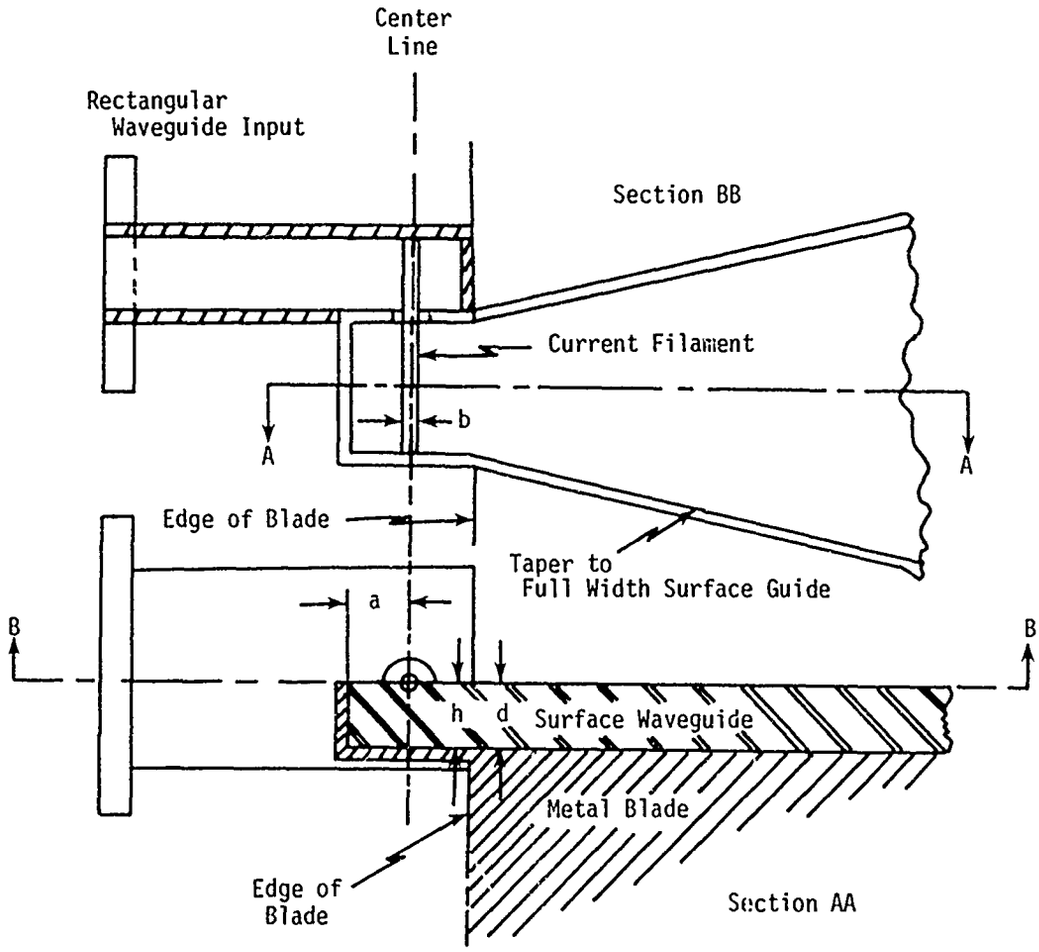

h = height of current filament above ground plane

d = thickness of dielectric

a = position of short circuit

b = diameter of current filament

Figure C-5. Experimental model TE_1 mode coupler

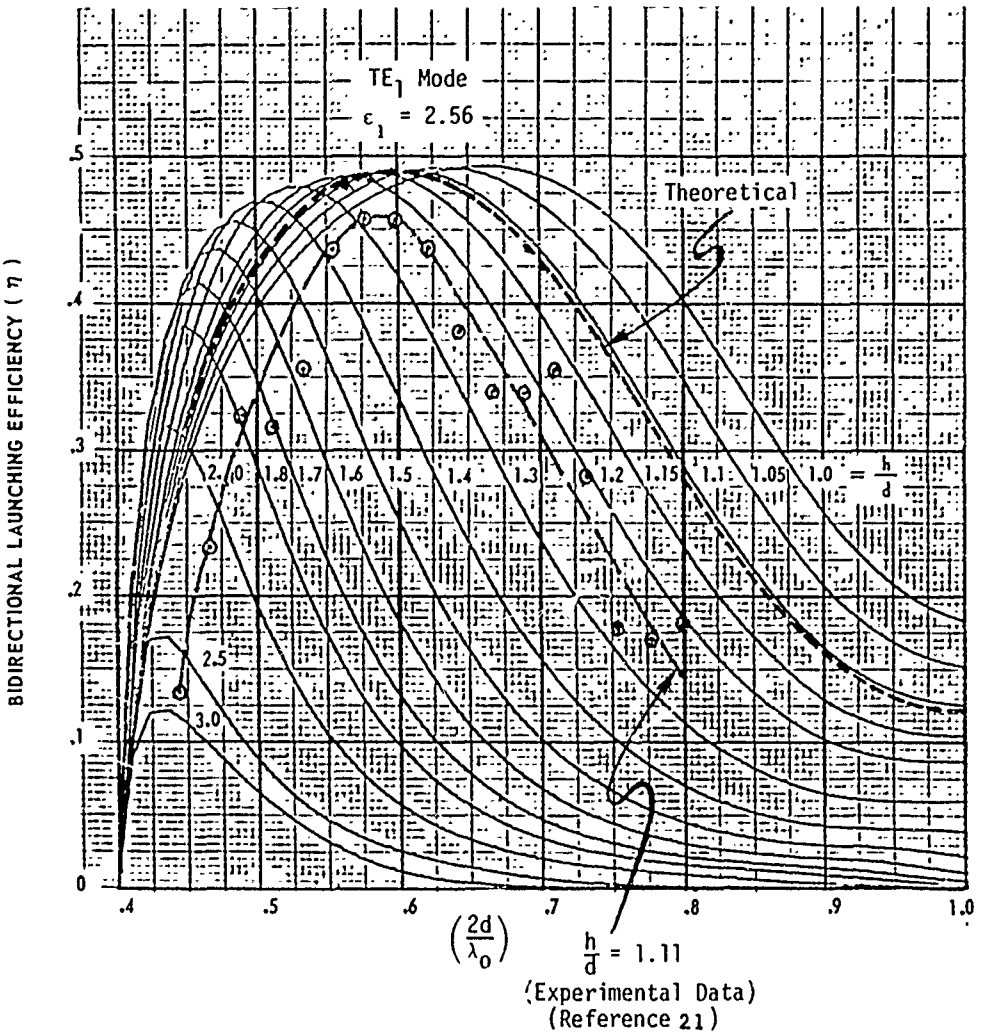

Figure C-6. Computer-generated plot of bidirectional launching efficiency as a function of dielectric slab thickness for various current filament locations and dielectric constants

---

21 Cohn, Cassedy and Kott, "TE Mode Excitation on Dielectric Loaded Parallel Plane and Trough Waveguides," IRE Transactions on Microwave Theory and Techniques, pp. 545-552 (September 1960).

Task 3b - Laboratory Demonstration of the Application of Coupling Theory to TM_0 Modes

This task will demonstrate experimentally TM_0 mode coupling theory, similar to that used by DuHamel and Duncan and will also result in experimental TM_0 mode couplers for use in Tasks 1, 2 and 3.[24] This task will also result in the evolution of the TM_0 mode coupler design technology.

A proposed breadboard TM_0 mode coupler is illustrated in Figure C-7. This coupler is designed in accordance with the principles of DuHamel and Duncan. It differs in that it uses a rectangular image line rather than a semicircular image line. These two lines being roughly equivalent, equivalent results are expected. The coupling efficiency will be measured as described in Appendix D using the apparatus of Figure C-1 while the dimensions h, d, a, b and w are varied. Efficiency will then be plotted as a function of h/d for various values of w at experimental frequencies. The empirical data thus accumulated will be used to design the experimental and prototype couplers. Experimental values of efficiency obtained by DuHamel for a semicircular image line are illustrated in Figure C-8.

[24] R.H. DuHamel and J.W. Duncan, "Launching Efficiency of Wires and Slots for a Dielectric Rod Waveguide," IRE Transactions of Microwave Theory and Techniques, July 1958.

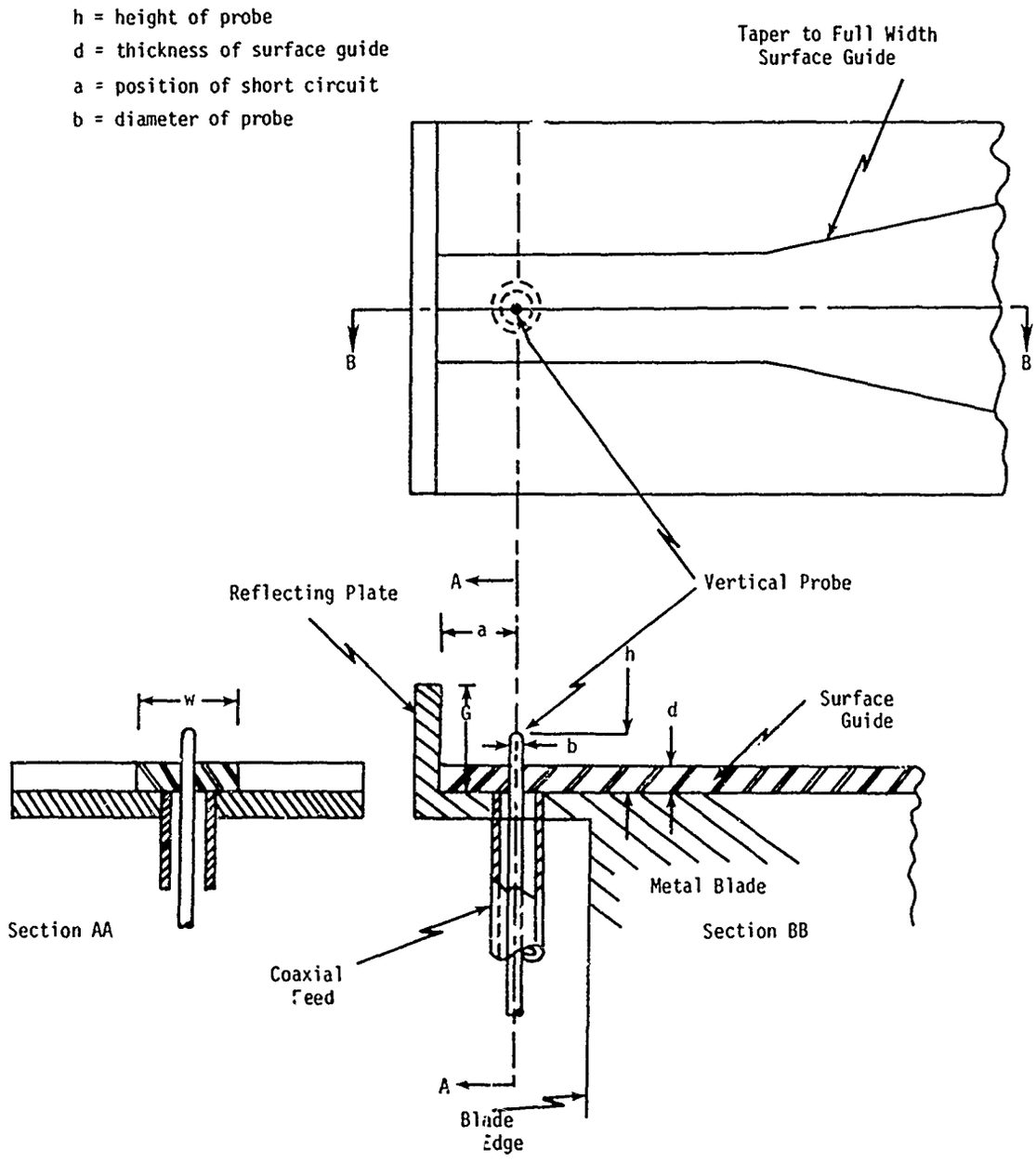

Figure C-7. Experimental model TM_0 mode coupler

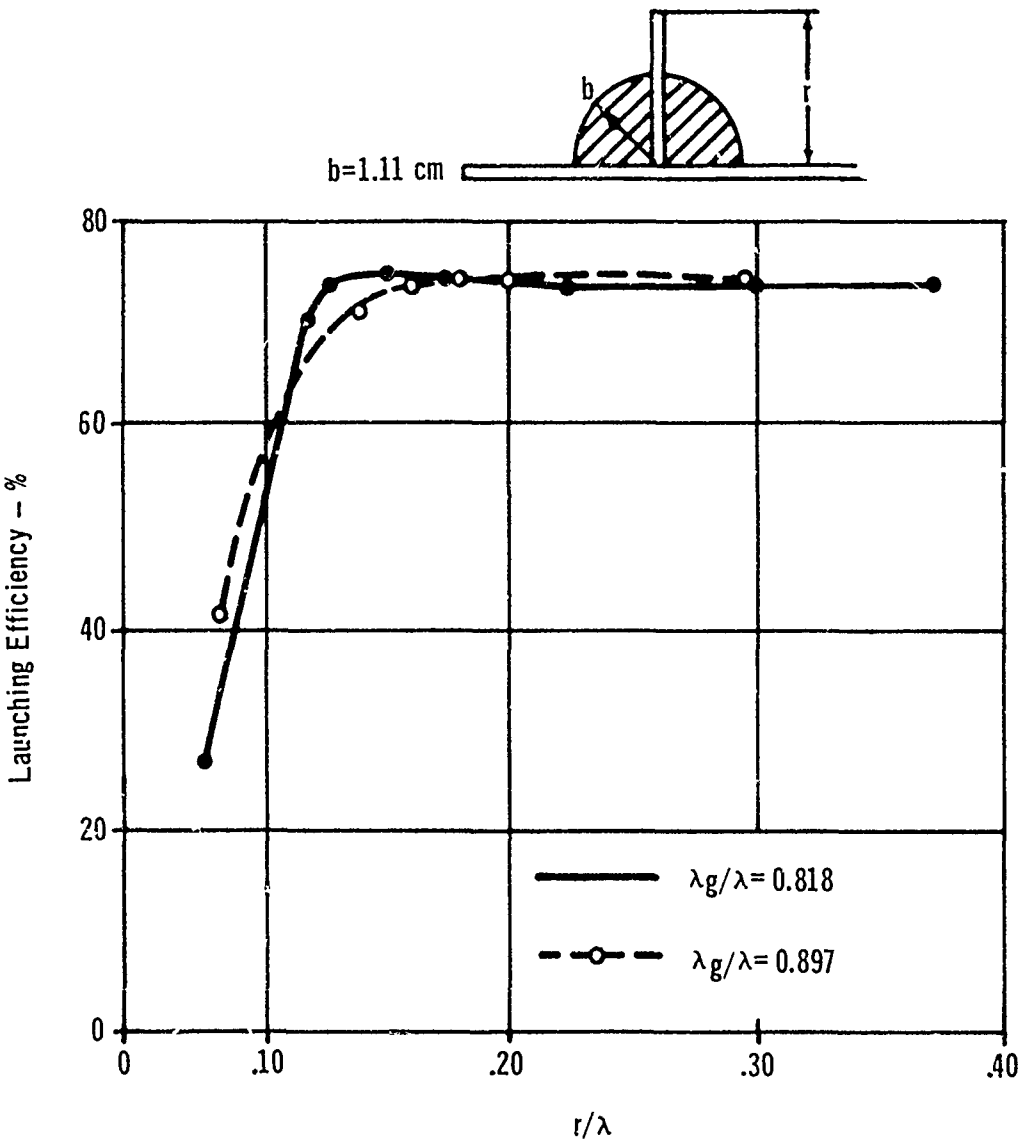

(Excerpted from DuHamel, Reference 24)

Figure C-8. Launching efficiency of a vertical wire as a function of the normalized wire length

[24] R.H. DuHamel and J.W. Duncan, "Launching Efficiency of Wires and Slots for a Dielectric Rod Waveguide," IRE Transactions of Microwave Theory and Techniques, July 1958.

APPENDIX D

SURFACE WAVEGUIDE MEASUREMENT METHODS

VALIDATION OF SURFACE WAVEGUIDE PERFORMANCE

To validate the theoretical predictions of surface waveguide theory, the following parameters will be measured as functions of frequency f, slab thickness d, dielectric constant ε_1, and loss tangent tanδ:

- Guide Wavelength λ_g
- Phase Constant β
- Attenuation Constant α
- Internal Eigenvalue k_x
- External Eigenvalue K_x
- Power Ratio P_r^x
- Injected Power P_{in}

Measurements will be performed on surface waveguides fabricated from the materials listed in Table D-1.

TEST APPARATUS AND DESCRIPTION OF EXPERIMENTS

All of the above parameters c. . be measured with the test apparatus illustrated in Figure D-1.

Measurement of Guide Wavelength, λ_g

The guide wavelength, λ_g, is measured in the following manner for different values of slab thickness, source frequency and material.

a) The precision probe (Figure D-1) is elevated above the surface waveguide so that it has a negligible effect on the surface wave.

b) A sliding short circuit, or any large slideable reflection, is placed at the end of the surface guide.

c) The sliding short is moved until minimum power is received by the probe as indicated on the receiver; the position of the short is measured and then moved until another minimum is observed. The difference between the two positions of the short circuit represents one-half the guide wavelength.

TABLE D-1. CANDIDATE MATERIALS WITH AND WITHOUT AN ASTROCOAT EROSION COAT

	(a)	(b)	(c)
1	Ultra-High Molecular Weight Polyethelene Erosion Coat	With 12 Mil Polyurethane Erosion Coat	With Alumina Erosion Coat
2	Irradiated, High-Density Polyolefin Laminate Polyguide	With 12 Mil Polyurethane Erosion Coat	With Alumina Erosion Coat
3	High Quartz Fiber Silicone Resin Laminate - Alphaquartz	With 12 Mil Polyurethane Erosion Coat	With Alumina Erosion Coat
4	Glass Laminate Silicone Resin Fiberglass	With 12 Mil Polyurethane Erosion Coat	With Alumina Erosion Coat
5	Alumina Aluminum Oxide	----	----

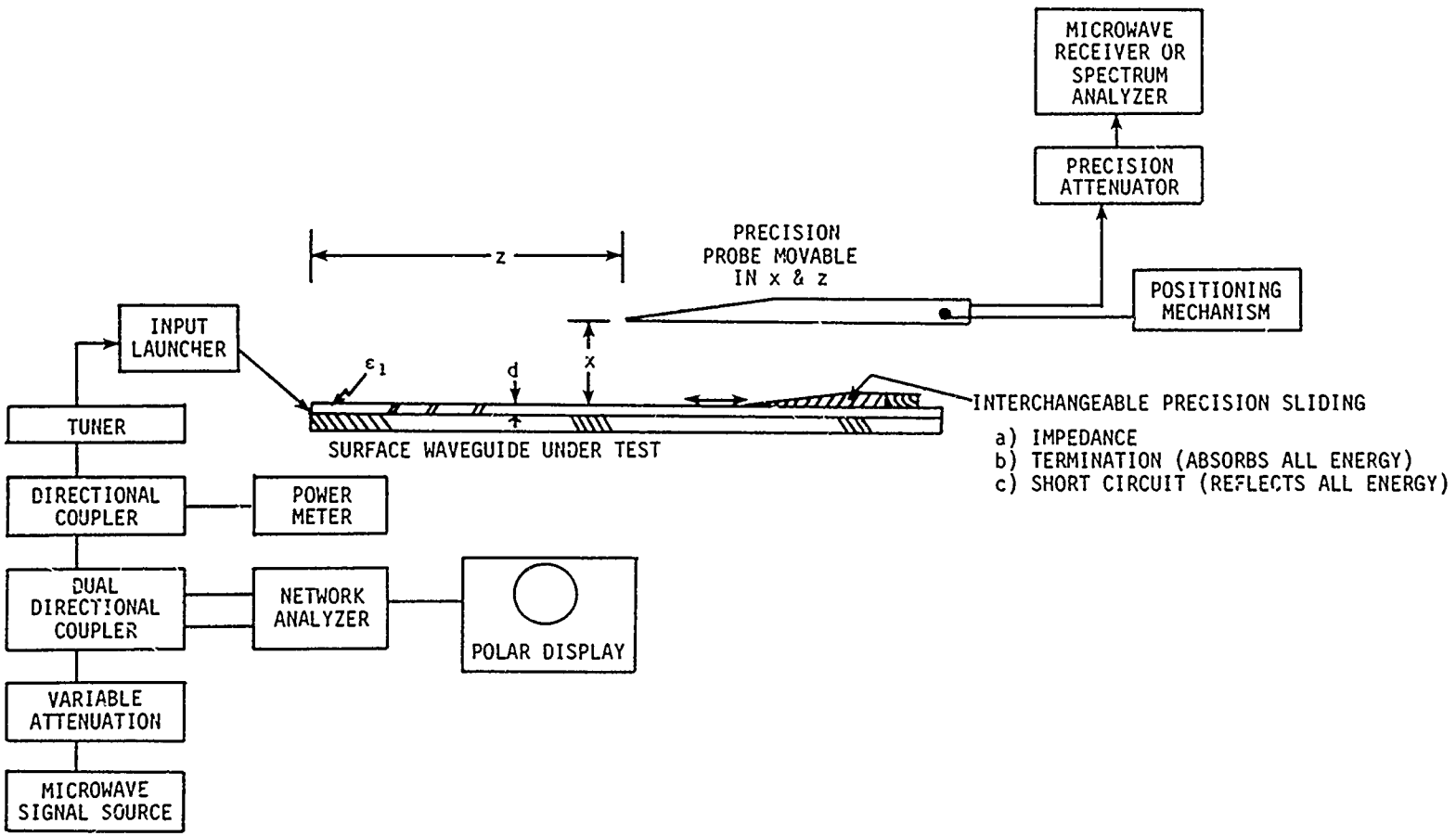

Figure D-1. Test equipment for measuring performance of surface waveguides

d) As a check, the short can remain stationary and the probe moved to measure the difference between two minimums.

$$\frac{\lambda_g}{2} = \text{difference between two minimums}$$

Phase Constant, β

Using the value of λ_g found above,

$$\beta = \frac{2\pi}{\lambda_g}$$

Measurement of External Eigenvalue, K_x (Decay of Field with x)

A termination is placed at the end of the surface waveguide. The precision probe is moved in the x direction (Figure D-1) keeping the power received by the microwave receiver at a constant level by removing attenuation in the precision attenuator as x is increased. A plot of attenuator reading as a function of x is then made, is illustrated in Figure D-2. As shown below, this should be a straight line, the slope of which is the external eigenvalue K_x. This is shown as follows: From the surface mode field equations A-1 to A-18, the electric field intensity external to the dielectric decays exponentially with distance x above the surface. The attenuation in the x direction is thus

$$(A_2 - A_1) = 20 \log_{10} e^{-K_x(x_2 - x_1)} \qquad \text{(D-1)}$$

where $A_2 - A_1$ is the difference in the attenuator readings and $x_2 - x_1$ is the difference in elevation of the probe, or

$$A_2 - A_1 = 8.686\, K_x(x_2 - x_1)$$

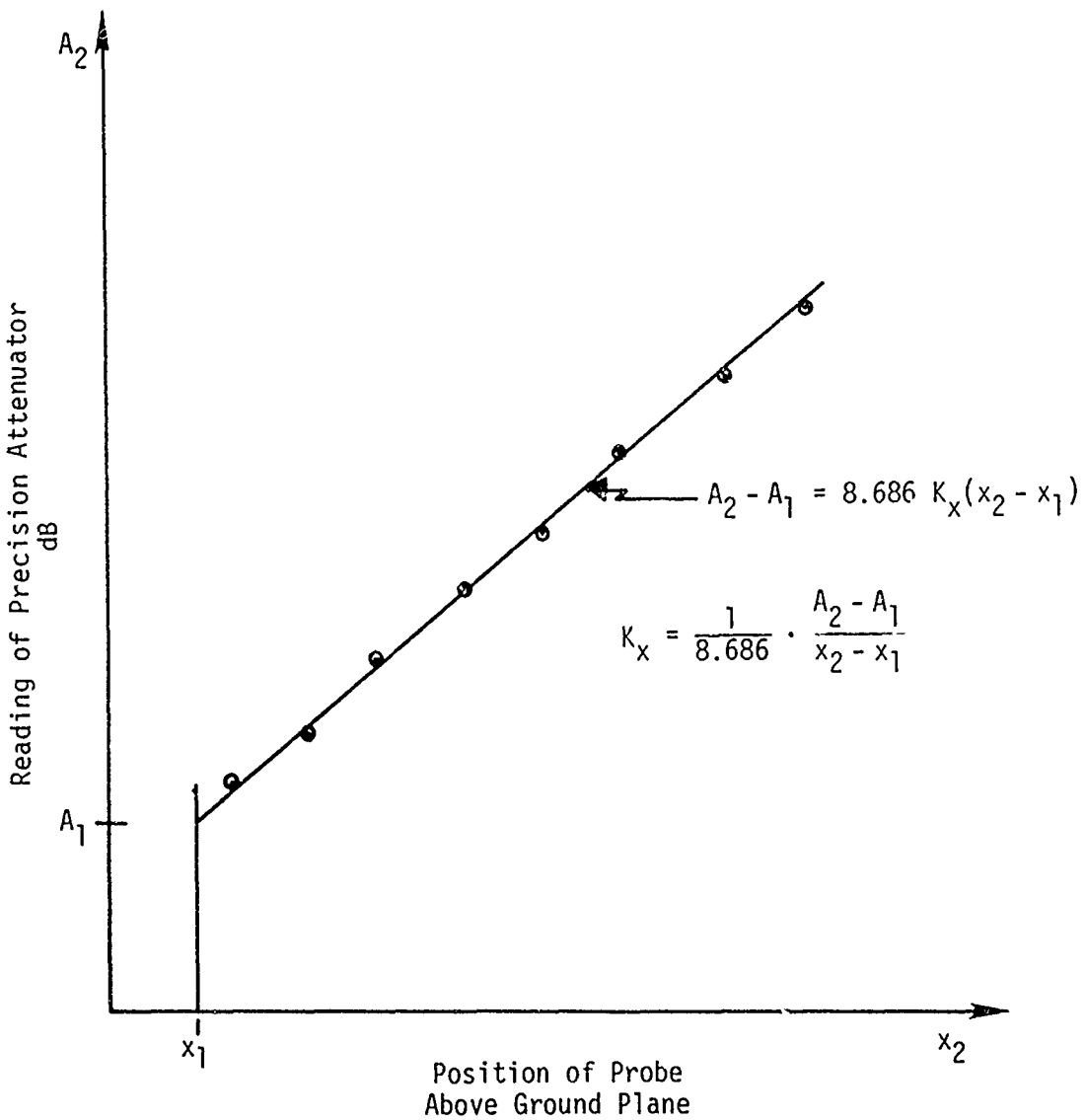

Figure D-2. Determining the external transverse eigenvalue K_x

$$K_x = -\frac{1}{8.686} \cdot \frac{A_2 - A_1}{x_2 - x_1}$$

where

$$\frac{A_2 - A_1}{x_2 - x_1}$$

is the slope of the straight line. This technique will render accurate measurements of K_x since it depends upon several or many measurements.

The value of K_x is also obtainable indirectly from Equation A-18 as

$$K_x = \sqrt{\beta^2 - k_2^2}$$

where

$$\beta = \frac{2\pi}{\lambda_g} \qquad \lambda_g = \text{guide wavelength}$$

$$k_2 = \frac{2\pi}{\lambda_o} \qquad \lambda_o = \frac{c}{f} = \text{free space wavelength}$$

This method of determining K_x is simple, but not as accurate as the above method. It should be used only as a check.

k_2 is accurately determined since it is, in this case, the phase constant of a plane wave in free space.

Measurement of Internal Eigenvalue, k_x

A direct measurement of this value would be very difficult since it would require probing the dielectric. It can be measured indirectly from measurement of the external Eigenvalue, K_x, and a measurement of the dielectric constant of the dielectric slab, ε_1, using Equations A-17 and A-18.

$$k_x = \sqrt{k_1^2 - \beta^2}$$

$$k_1 = \frac{2\pi}{\lambda_1} = \frac{2\pi\sqrt{\varepsilon_1}}{\lambda_o}$$

where: ε_1 = relative dielectric constant of the dielectric, measured elsewhere

$\lambda_o = \frac{c}{f}$ = free space wavelength

$\beta = \sqrt{K_x^2 - k_2^2}$

K_x is measured directly according to instructions above.

$k_2 = \frac{2\pi}{\lambda_o}$

Measurement of the Attenuation Constant

Two independent techniques are contemplated for measuring the attenuation characteristics of the surface waveguide.

The first method (Ginzton, Reference 22, Page 469, and Cohn, Reference 21), well suited to attenuation measurements on surface waveguide, is "the variable length transmission cavity technique". The cavity is formed by two noncontacting short circuits placed on the surface of the guide. The short nearest the generator is maintained at a fixed position and the short on the probe side adjusted to a resonant position, as indicated by a rise in the output of the probe detector on the load side of the cavity. The microwave source is then swept in frequency, and the output waveform is displayed on an oscilloscope. The Q of the cavity is determined from the 3 dB bandwidth. The output short is then moved to another position where the output is again maximized and the Q measured again at the new frequency. This procedure can be repeated as many times as desired. A plot is then made of 1/Q versus 1/L, which should result in a straight line. Extrapolating the straight line to the point 1/L = 0 produces an intercept on the 1/Q axis, whose value is given by:

$$\frac{1}{Q_i} = \left(\frac{\lambda_1}{\lambda_g}\right)^2 \frac{\alpha\lambda_g}{\pi}$$

[22] E.L. Ginzton, Microwave Measurements, New York: McGraw-Hill, 1957.

[21] Cohn, Cassedy and Kott, "TE Mode Excitation on Dielectric Loaded Parallel Plane and Trough Waveguides," IRE Transactions on Microwave Theory and Techniques, pp. 545-552 (Septeberm 1960).

Solving for α yields

$$\alpha = \left(\frac{\lambda_g}{\lambda_1}\right)^2 \frac{\pi}{\lambda_g Q_i}$$

where

λ_g = surface guide wavelength (measured above)

λ_1 = plane wavelength in dielectric medium

$$\lambda_1 = \frac{\lambda_0}{\sqrt{\varepsilon_1}} = \frac{c}{f\sqrt{\varepsilon_1}}$$

ε_1 = dielectric constant of slab

$1/Q_i$ = value of $1/Q$ at intercept

α = attenuation constant

Alternate Method for the Measurement of Attenuation Constant

In this method, the surface guide is terminated in a short circuit and the input vswr, r, is measured with the probe. The attenuation, A, between the point of measurement and the short circuit terminating the line is given by the following equations.

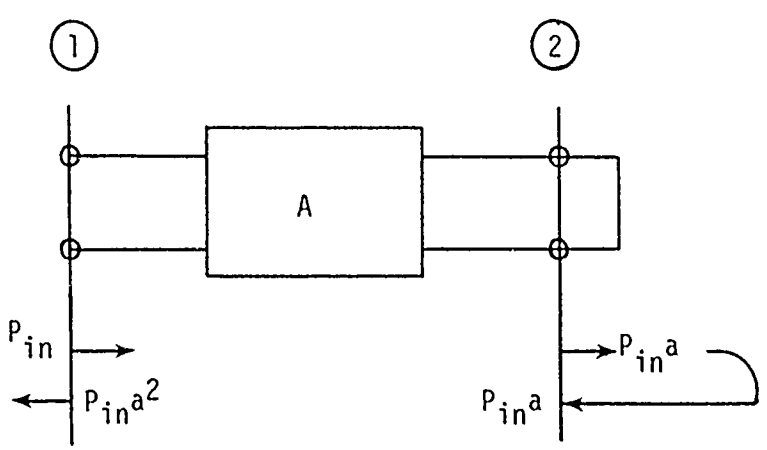

For

Γ = voltage reflection coefficient

r = standing wave ratio

A = attenuation between 1 and 2 in dB

D = distance between 1 and 2 in inches

α = attenuation constant dB/inch

$$|\Gamma| = \frac{r - 1}{r + 1}$$

The equation for the return loss, L_r, is

$$L_r = 10 \log r^2 = 2A$$

$$L_r = 10 \log\left(\frac{r - 1}{r + 1}\right)^2 = 2A$$

or, for attenuation,

$$A = 10 \log \left(\frac{r - 1}{r + 1}\right)$$

The attenuation constant is

$$\alpha = \frac{A}{D} \text{ dB/inch}$$

where D is the distance between the point of measurement of the vswr and the short circuit.

Measurement of Complex Dielectric Constant $\varepsilon = \varepsilon' + j\varepsilon''$ by the Network Approach

The dielectric material, e.g., ice or other material, is made to completely fill a section of waveguide as illustrated in Figure D-3a and b. The equipment required is illustrated in Figure D-4a and b.

Measurement of the Real Part of the Complex Dielectric Constant.

The waveguide containing the dielectric sample is terminated in a matched load. The procedure is as follows: The polar display (Figure D-4) is calibrated by placing a short circuit on terminal 1 (Figure D-4a) and adjusting the dot or the cluster appearing on the polar display to $\Gamma = -1e^{-j\,\pi/2}$. The short circuit is then removed and replaced by the terminated dielectric sample. The value of the reflection coefficient Γ or vswr, r, is then read directly from the display.

The real part of the complex dielectric constant is

$$\varepsilon_1' = r^2$$

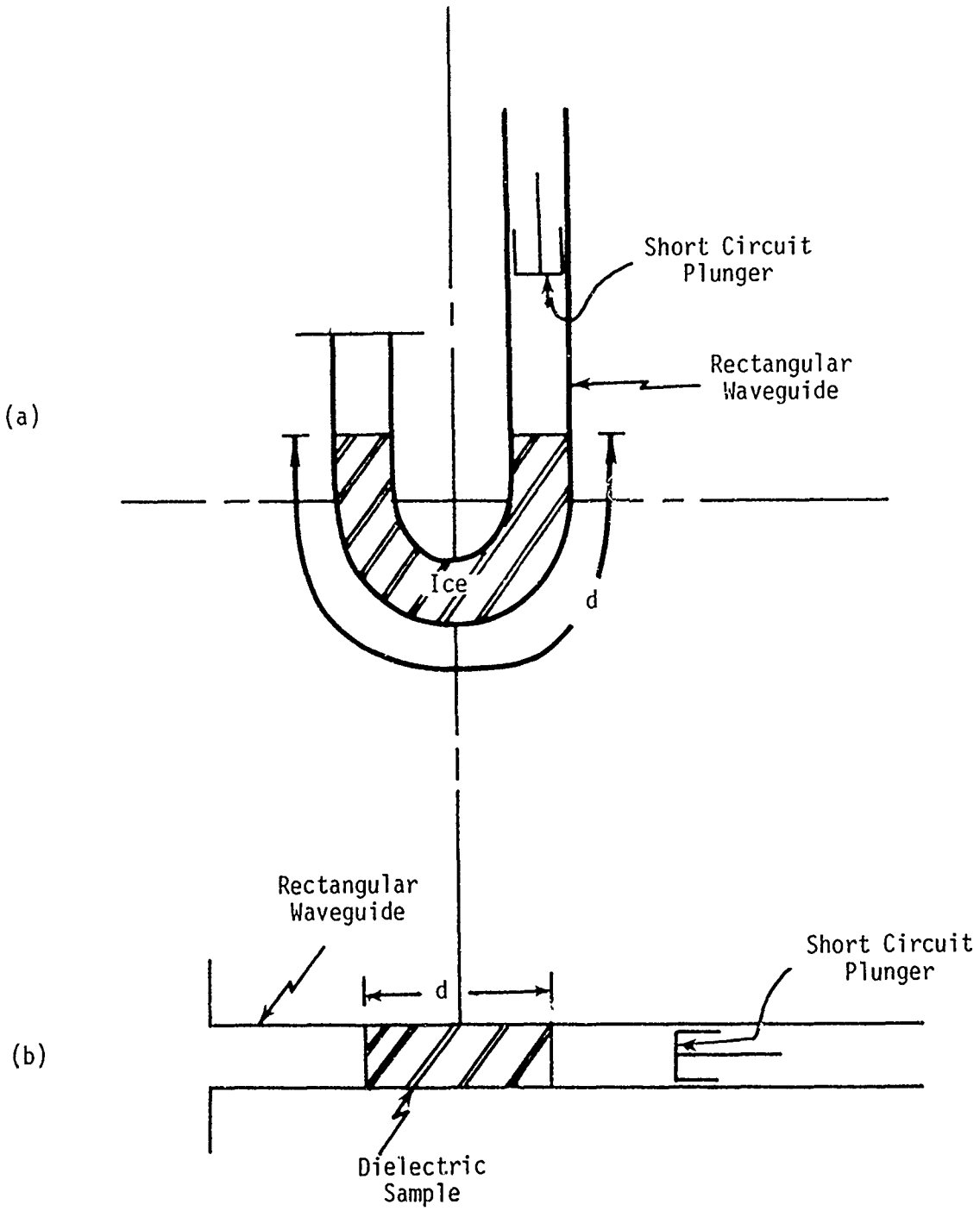

Figure D-3. Sample mounts for dielectric constant measurements

(a)

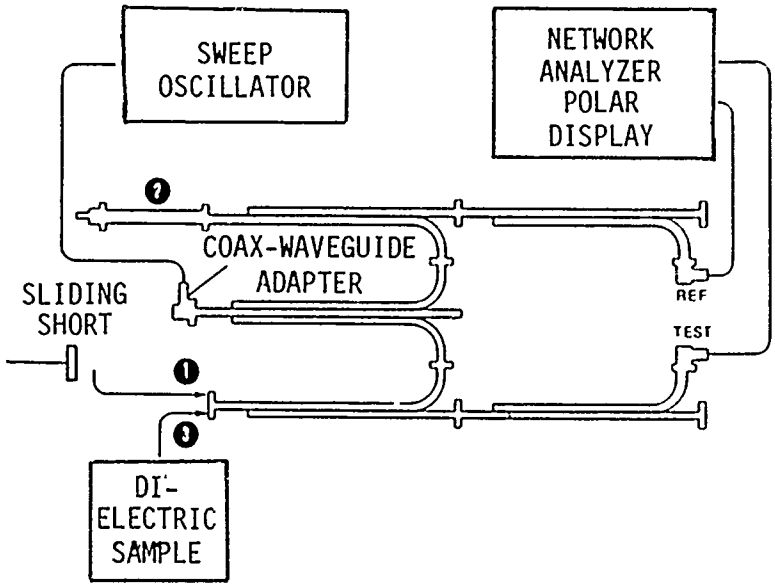

(b)

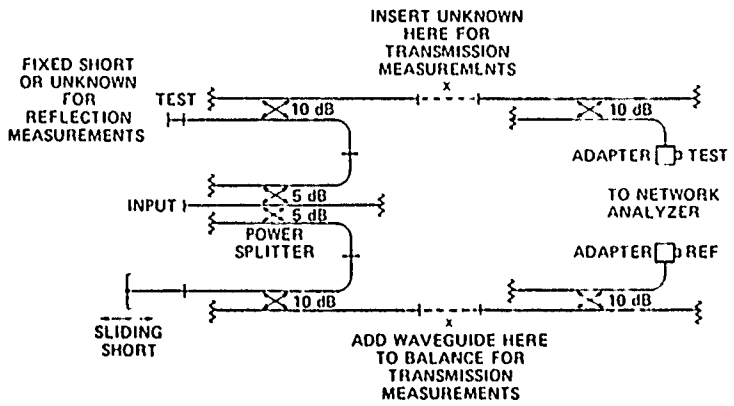

Figure D-4. Apparatus for measuring the complex dielectric constant

Measurement of Imaginary Part of Complex Dielectric Constant[36]

In this technique the waveguide containing the sample is terminated in a precision sliding short circuit. The short circuit is moved through a series of points separated by some fraction of a guided wavelength. The trace on the polar display (Figure D-4) will describe a circle, the radius "R" of which is measured. The distance of the center of the circle from the center of the polar display, p, is also measured; then ε'' is calculated as follows: (d is defined in Figure D-4)

$$2\alpha d = \ln \frac{\sqrt{(1+R)^2 - p^2} + \sqrt{(1-R)^2 - p^2}}{\sqrt{(1+R)^2 - p^2} - \sqrt{(1-R)^2 - p^2}}$$

Knowing ε', the desired ε'' is then obtained from either

$$\varepsilon'' \cong 2 \left(\frac{\alpha\lambda}{2\pi}\right)^2 \sqrt{1 + \left(\frac{2\pi}{\alpha\lambda}\right)^2 \varepsilon'} \qquad \text{(TEM modes)},$$

where λ is the free-space wavelength or

$$\varepsilon'' \cong \frac{\alpha\lambda_{og}}{\pi} \frac{\sqrt{\left[1 + (\lambda_{og}/\lambda_c)^2\right]\varepsilon' - (\lambda_{og}/\lambda_c)^2}}{1 + (\lambda_{og}/\lambda_c)^2} \qquad \text{(H modes)}$$

Measurement of Injected Microwave Power

Measurement of microwave power injected into the surface waveguide requires a knowledge of the coupling efficiency of the surface waveguide coupler used. The design of optimum couplers is the subject of Phase III, so that couplers of optimum design may not be available for feasibility experiments. While couplers used in feasibility experiments may be less than optimum, they will, in the worst case, always be better than 50% efficient. The exact coupling of any coupler used in feasibility experiments

[36] Charles B. Sharpe, "A Graphical Method for Measuring Dielectric Constants at Microwave Frequencies," IRE Transactions on Microwave Theory and Techniques, pp. 155-159 (March 1960).

will be measured (calibrated) using the technique described by Cohn (see Reference 21). The power injected into the surface guide is then:

$$P_{in} = P_a \eta$$

where

P_{in} = power injected into surface wave

P_a = available power at input to coupler

η = coupling efficiency

Measurement of Coupling Efficiency:[21] Referring to Figure D-1, a matched load (termination) is placed on the surface waveguide. The tuner at the input to the input launcher is adjusted for a match, which would be indicated on the polar display. The termination is then replaced by a sliding short circuit which produces a standing wave on the input line to the launcher, the magnitude of which is displayed on the polar display. As the short is moved in the z direction, the standing wave will go through successive maximums and minimums. The coupling efficiency is then calculated as follows:

$$\eta = \frac{(r_{max} - 1)(r_{min} - 1)}{(r_{max}\, r_{min} - 1)}$$

where

r_{max} = maximum standing wave ratio

r_{min} = minimum standing wave ratio

η = coupling efficiency

[21] Cohn, Cassedy and Kott, "TE Mode Excitation on Dielectric Loaded Parallel Plane and Trough Waveguides," IRE Transactions on Microwave Theory and Techniques, pp. 545-552.

Measurement of Power Injected into Surface Wave. Referring to Figure D-1 with a matched load (termination) placed on the surface waveguide, the power entering the launcher is measured with the power meter and precision directional coupler. The power injected into the surface guide is then computed as follows:

$$P_{in} = P_a \eta$$

where

P_{in} = power injected into surface wave

P_a = power measured entering launcher

η = measured coupling efficiency

APPENDIX E

THEORY OF RAIN EROSION OF HOMOGENEOUS AND COATED MATERIALS

In this section, a description of the analytic model of rain erosion developed by Springer is presented.[12,13,37] Included are the equations used to compute the incubation time, erosion rate, substrate stress, and total time required to erode through a coating of prescribed thickness. These expressons, which were designed to agree with existing experimental data, can be used to predict the erosion behaviors of various coating-substrate combinations under untested conditions.

When a surface is repeatedly bombarded by water droplets, the erosion process does not usually begin until a time interval called the incubation time has passed. Thereafter, mass loss proceeds at a nearly constant rate. By selecting a surface coating with the proper physical characteristics, one can reduce the stresses transmitted to the substrate and have a long incubation time and low erosion rate.

When a water droplet impinges on a surface (see Figure E-1), it immediately produces the water-hammer impact pressure

$$\sigma_1 = \frac{0.3047\, Z_c Z_L V \cos\theta}{Z_c + Z_L} \qquad N/m^2 \qquad \text{(E-1)}$$

where $V \cos\theta$ is the normal component of the impact velocity, and Z_c and Z_L are the impedances of the coating and the water, respectively. Impedance is defined as the product of the material's density and the speed of sound.

During the residence time of a droplet, the stress wave pattern shown in Figure E-2 is formed. The original impact pressure pulse, σ_1,

[12] G.S. Springer, et al., "Analysis of Rain Erosion of Coated Materials," Technical Report AFML-TR-73-227, September 1973 (DDC No. AD 769448).

[13] G.S. Springer, et al., "Analysis of Rain Erosion of Coated and Uncoated Fiber Reinforced Composite Materials," Technical Report AFML-TR-74-180, August 1974 (DDC No. ADA001086).

[37] G.S. Springer, Erosion by Liquid Impact, Manuscript for book to be published in 1976.

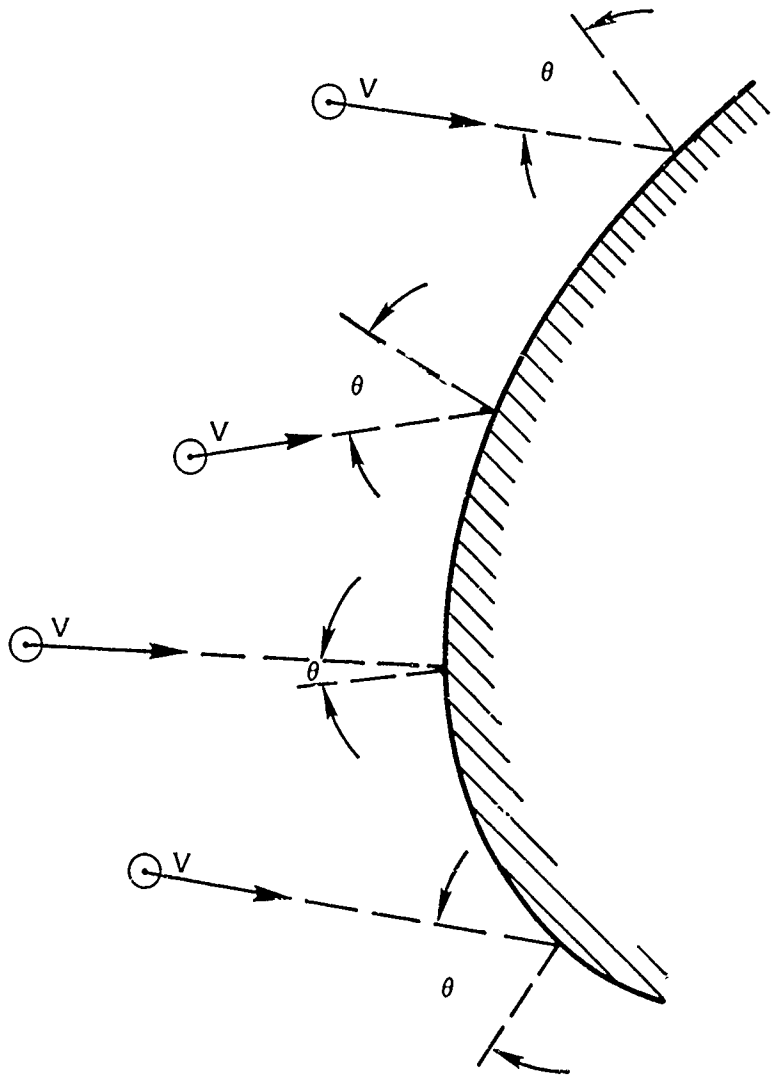

Figure E-1. Water droplets impinging on a surface

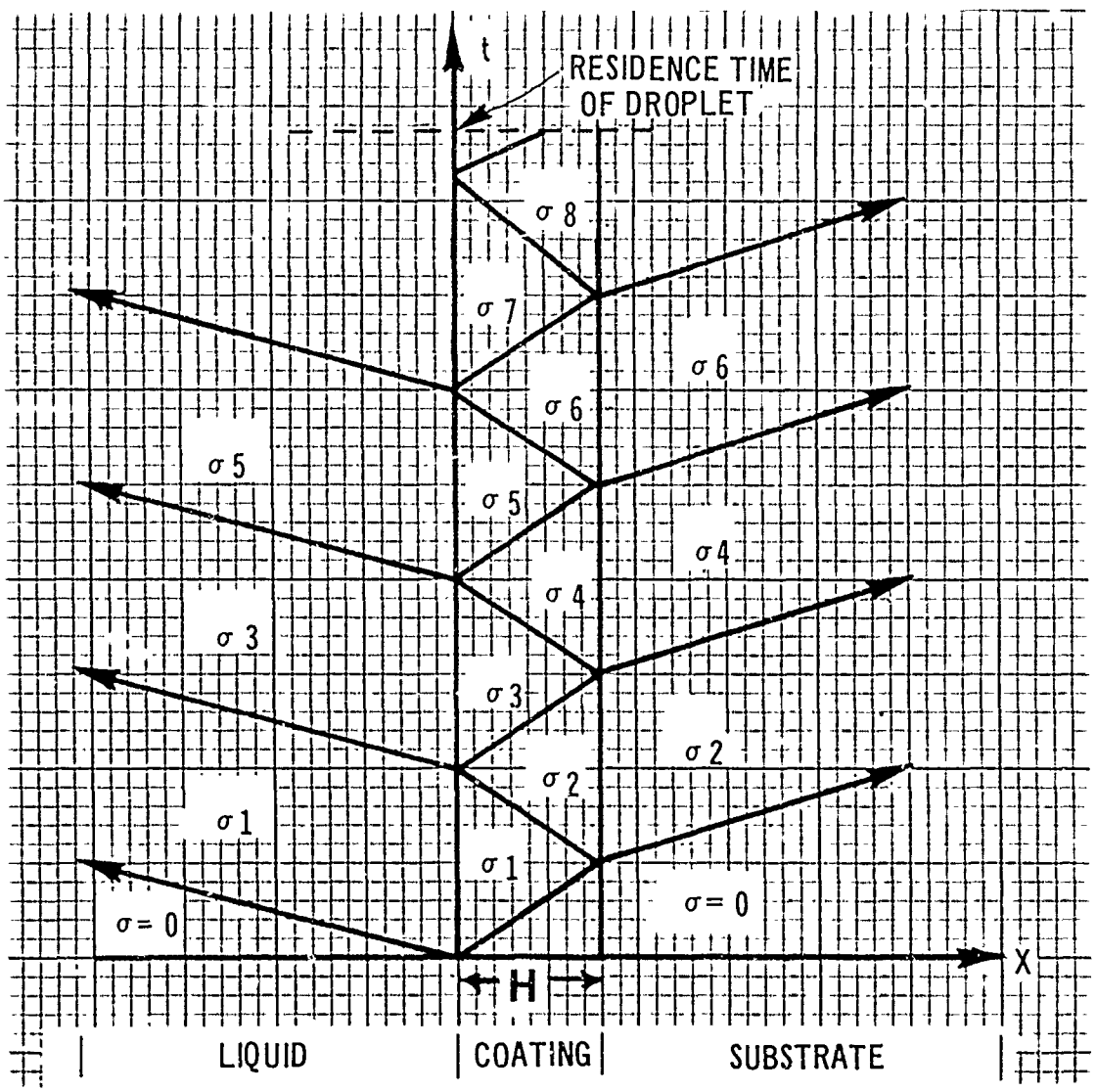

Figure E-2. Stress wave pattern

is transmitted as one wave into the coating and as another wave into the droplet. At the coating-substrate interface where there is a change in impedance, part of the advancing wave is transmitted and part is reflected. As the reflection process within the coating continues, the stress at the coating-substrate interface approaches σ_∞, the stress that would have been produced at the substrate surface by liquid impact in the absence of a protective coating. In most cases, however, the residence time of the droplet is sufficiently short to cut off the wave pattern before σ_∞ is reached.

The stress measured at the coating-substrate surface varies with time, and the particular distribution depends on the relative impedance of the coating and substrate in relation to that of water. Four cases are possible, as indicated in Figure E-3, where the variation of substrate surface stress with time is shown. In Cases I and II, the coating reduces the substrate stresses below σ_∞, but in Cases III and IV, the coating increases the stress at the substrate surface to values above σ_∞. In the selection of material for a coating, the impedance of the coating should place it in Case I or II for the effective protection of the substrate.

The impact pressure on the substrate without the coating is:

$$\sigma_\infty = \left[\frac{1 + \psi_{sc}}{1 - \psi_{sc}\psi_{Lc}}\right] \sigma_1 \qquad \text{(E-2)}$$

and the average stress at the coating surface is

$$\sigma_A = \frac{(1+\psi_{sc})\sigma_1}{1 - \psi_{sc}\psi_{Lc}} \left[1 - \psi_{sc}\left(\frac{1 + \psi_{Lc}}{1 + \psi_{sc}}\right)\left(\frac{1 - \exp(-\gamma)}{\gamma}\right)\right] \qquad \text{(E-3)}$$

where:

$$\gamma = \frac{C_c d}{C_L H}\left[\frac{z_s + z_L}{z_s + z_c}\right]\left[\frac{2z_c}{z_c + z_L}\right] \qquad \text{(E-4)}$$

$$\psi_{sc} = (z_s - z_c)/(z_s + z_c) \qquad \text{(E-5)}$$

$$\psi_{Lc} = (z_L - z_c)/(z_L + z_c) \qquad \text{(E-6)}$$

The quantity d is the droplet diameter, H is the coating thickness, and C_c and C_L are the sound speeds in the coating and liquid, respectively.

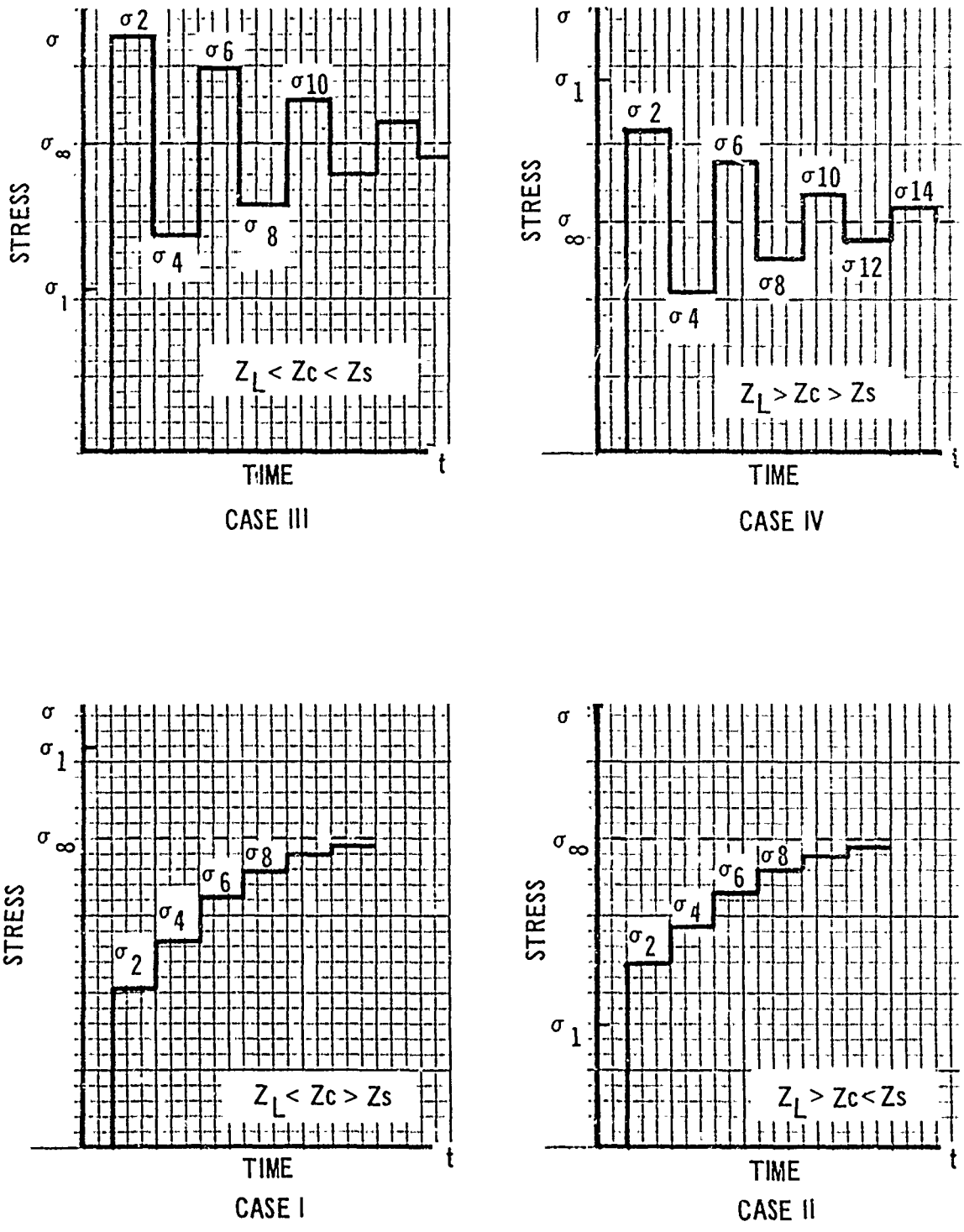

Figure E-3. The four cases of stress distribution on the substrate

TABLE OF SYMBOLS FOR APPENDIX E

A	Altitude (Km)
C_c	Coating speed of sound (m/sec)
C_s	Substrate speed of sound (m/sec)
E	Erosion rate (mm/sec)
E_{max}	Erosion rate with droplet impact normal to the surface (mm/sec)
H	Coating thickness (in)
R_i	Rainfall rate (mm/hr)
S_u	Ultimate tensile strength of coating (KN/m^2)
t_c	Time required to erode coating (min)
t_f	Total time to erode coating from initial droplet impact (min)
t_i	Incubation time (min)
V	Impingement velocity (ft/sec)
Z_c	Impedance of coating (Kg/m^2-sec)
Z_L	Impedance of water (Kg/m^2-sec)
θ	Impingement angle (deg)
ν	Poisson's ratio for coating

TABLE OF SYMBOLS FOR APPENDIX E
(continued)

ρ_c	Coating density (g/sec^2)
ρ_s	Substrate density (g/m^2)
σ_A	Average stress at coating surface (N/m^2)
σ_i	Water hammer impact pressure (N/m^2)
σ_∞	Substrate impact pressure without coating (N/m^2)

APPENDIX F

COMPUTER PLOTS OF NORMALIZED POWER DENSITY VERSUS POSITION NORMAL TO DIELECTRIC PLANE FOR DIFFERENT MODES

(All plots are labeled and appear in the following sequence)

Figure				GHz	GHz	GHz
F-1	TM Even	$\varepsilon_1 = 2.0$	$\varepsilon_2 = 1.0$	2.45	5.85	22.125
F-2	TM Even	$\varepsilon_1 = 2.0$	$\varepsilon_2 = 1.0$	2.45	5.85	22.125
F-3	TM Even	$\varepsilon_1 = 3.0$	$\varepsilon_2 = 1.0$	2.45	5.85	22.125
F-4	TM Even	$\varepsilon_1 = 3.0$	$\varepsilon_2 = 1.0$	2.45	5.85	22.125
F-5	TM Even	$\varepsilon_1 = 4.0$	$\varepsilon_2 = 1.0$	2.45	5.85	22.125
F-6	TM Odd	$\varepsilon_1 = 4.0$	$\varepsilon_2 = 1.0$	2.45	5.85	22.125
F-7	TM Odd	$\varepsilon_1 = 9.0$	$\varepsilon_2 = 1.0$	2.45	5.85	22.125
F-8	TM Odd	$\varepsilon_1 = 9.0$	$\varepsilon_2 = 1.0$	2.45	5.85	22.125
F-9	TM Odd	$\varepsilon_1 = 9.0$	$\varepsilon_2 = 3.0$	2.45	5.85	22.125
F-10	TM Odd	$\varepsilon_1 = 9.0$	$\varepsilon_2 = 3.0$	2.45	5.85	22.125
F-11	TE Even	$\varepsilon_1 = 2.0$	$\varepsilon_2 = 1.0$	2.45	5.85	22.125
F-12	TE Odd	$\varepsilon_1 = 3.0$	$\varepsilon_2 = 1.0$	2.4	5.85	22.125
F-13	TE Odd	$\varepsilon_1 = 3.0$	$\varepsilon_2 = 1.0$	2.4	5.85	22,125
F-14	TE Odd	$\varepsilon_1 = 4.0$	$\varepsilon_2 = 1.0$	2.4	5.80	22,125
F-15	TE Odd	$\varepsilon_1 = 4.0$	$\varepsilon_2 = 1.0$	2.4	5.85	22,125
F-16	TE Odd	$\varepsilon_1 = 9.0$	$\varepsilon_2 = 1.0$	2.4	5.85	22,125
F-17	TE Odd	$\varepsilon_1 = 9.0$	$\varepsilon_2 = 1.0$	2.4	5.85	22,125
F-18	TE Odd	$\varepsilon_1 = 9.0$	$\varepsilon_2 = 3.0$	2.4	5.80	22,125
F-19	TE Odd	$\varepsilon_1 = 9.0$	$\varepsilon_2 = 3.0$	2.4	5.85	22,125
F-20	TM Even	$\varepsilon_1 = 9.0$	$\varepsilon_2 = 1.0$	2.4	5.85	30,000
F-21	TM Even	$\varepsilon_1 = 9.0$	$\varepsilon_2 = 1.0$	2.45	5.85	30,000
F-22	TE Odd	$\varepsilon_1 = 9.0$	$\varepsilon_2 = 1.0$	2.45	5.85	30,000
F-23	TE Odd	$\varepsilon_1 = 9.0$	$\varepsilon_2 = 1.0$	2.45	5.85	30,000

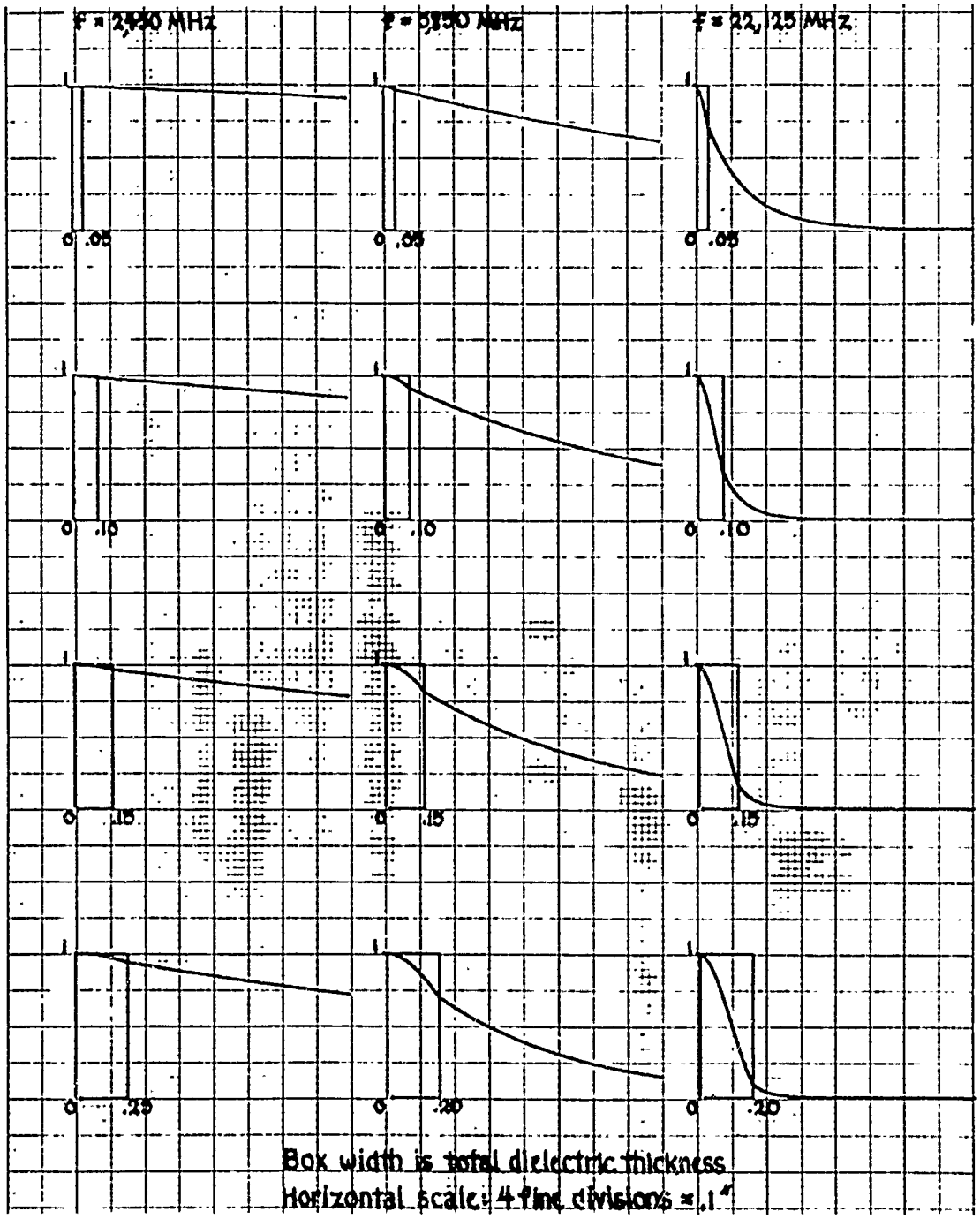

Figure F-1. Normalized power density (y-coordinate) versus vertical position (x-coordinate) for TM even mode, $\varepsilon_1 = 2.0$, $\varepsilon_2 = 1.0$

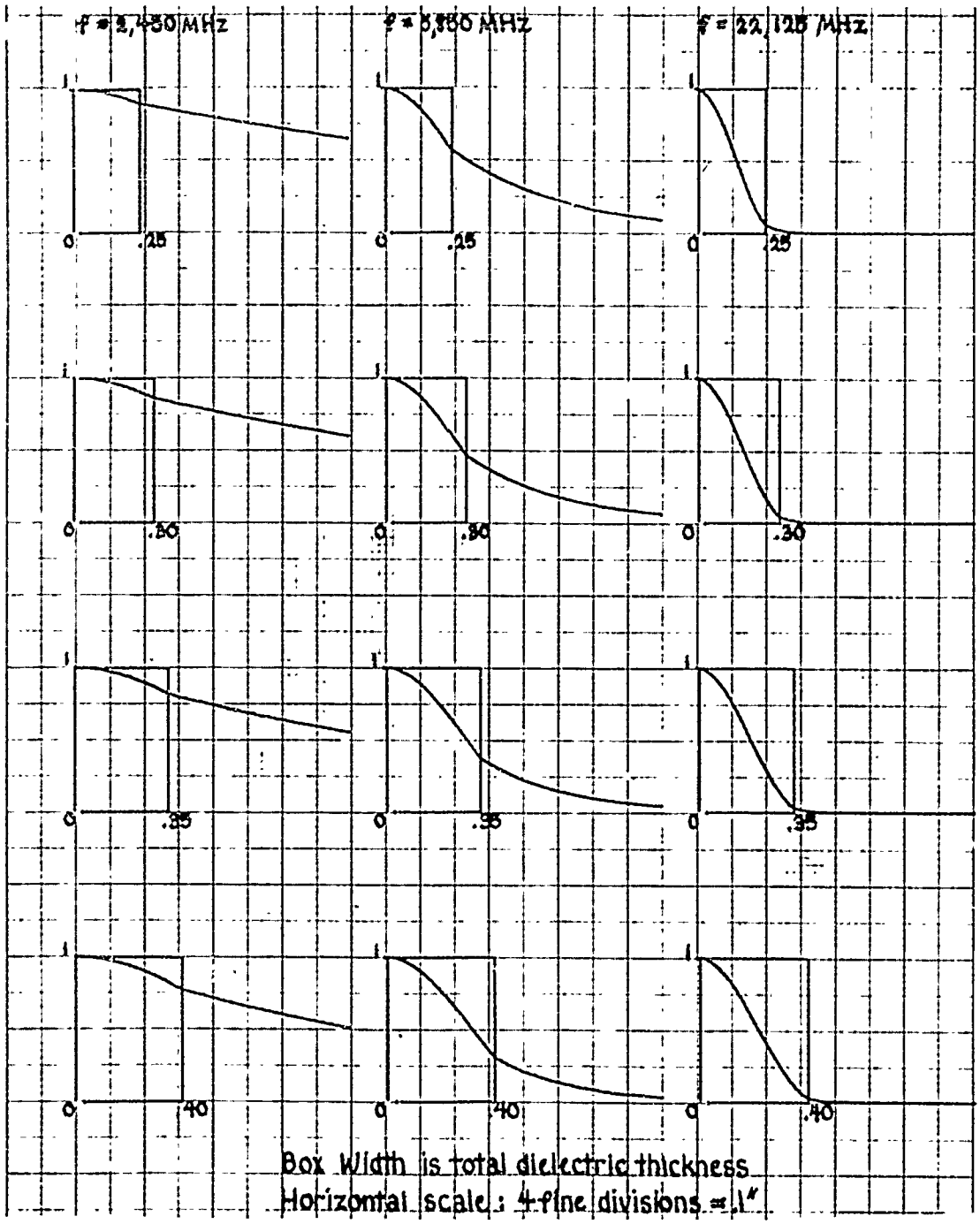

Figure F-2. Normalized power density (y-coordinate) versus vertical position (x-coordinate) for TM even mode, $\varepsilon_1 = 2.0$, $\varepsilon_2 = 1.0$

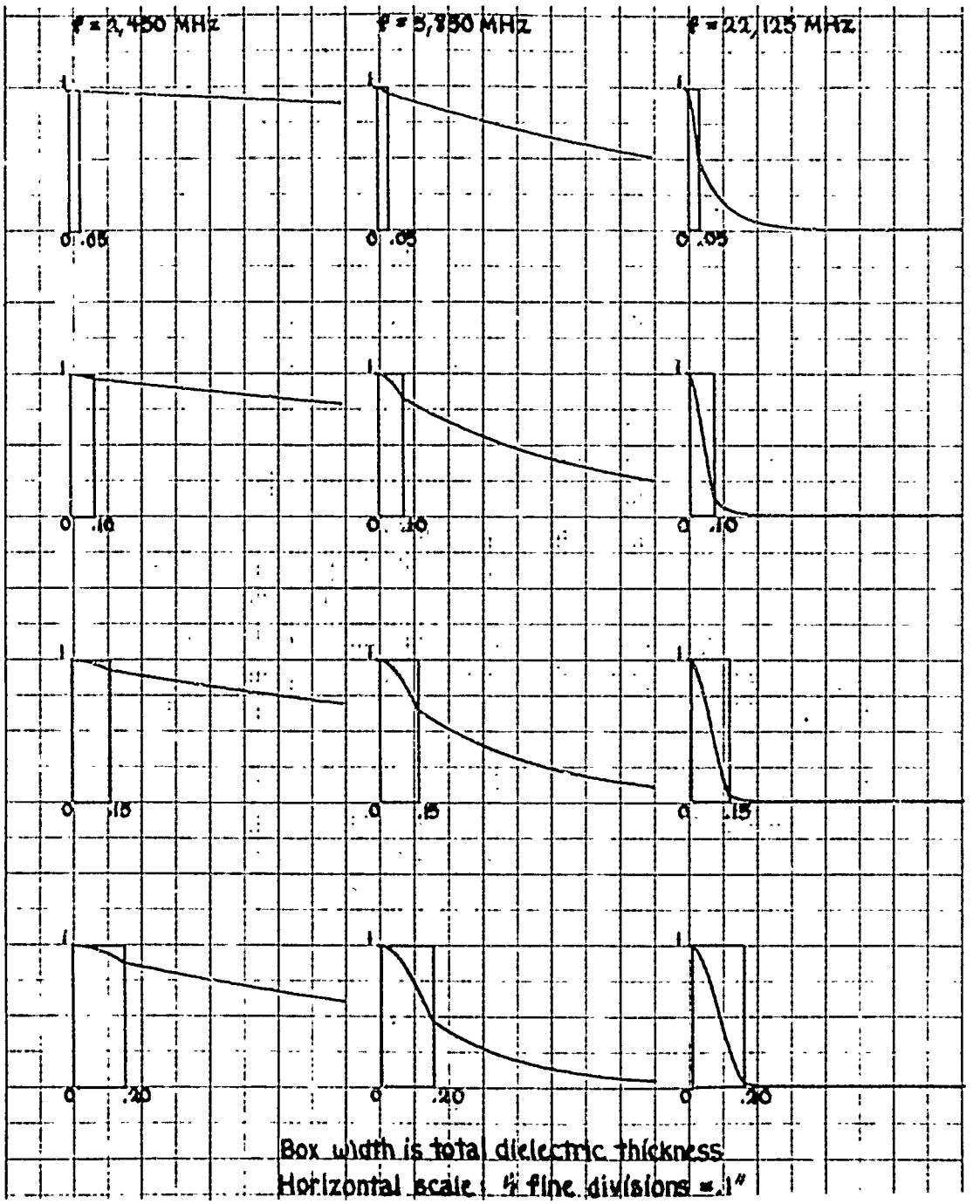

Figure F-3. Normalized power density (y-coordinate) versus vertical position (x-coordinate) for TM even mode, $\varepsilon_1 = 3.0$, $\varepsilon_2 = 1.0$

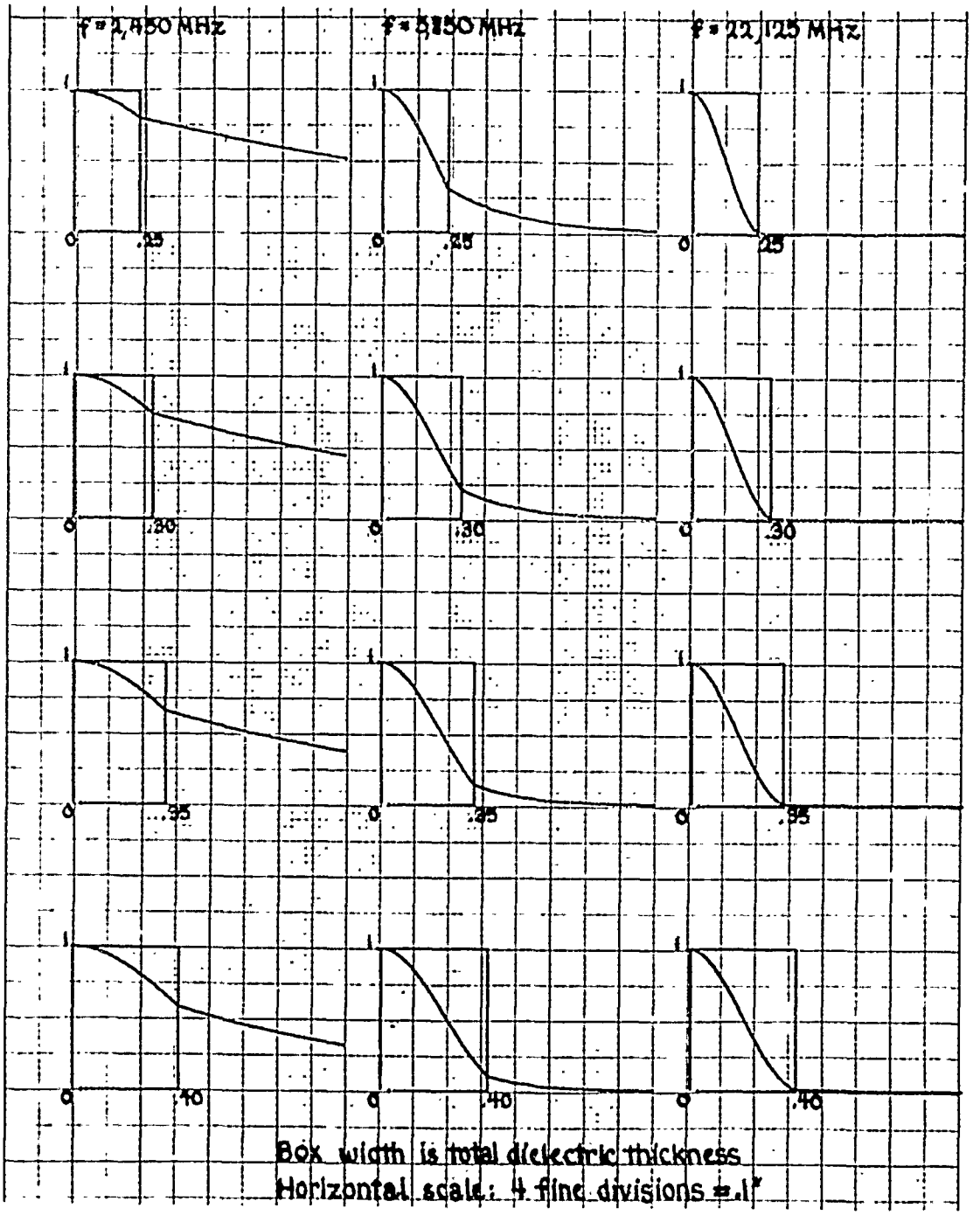

Figure F-4. Normalized power density (y-coordinate) versus vertical position (x-coordinate) for TM even mode, $\varepsilon_1 = 3.0$, $\varepsilon_2 = 1.0$

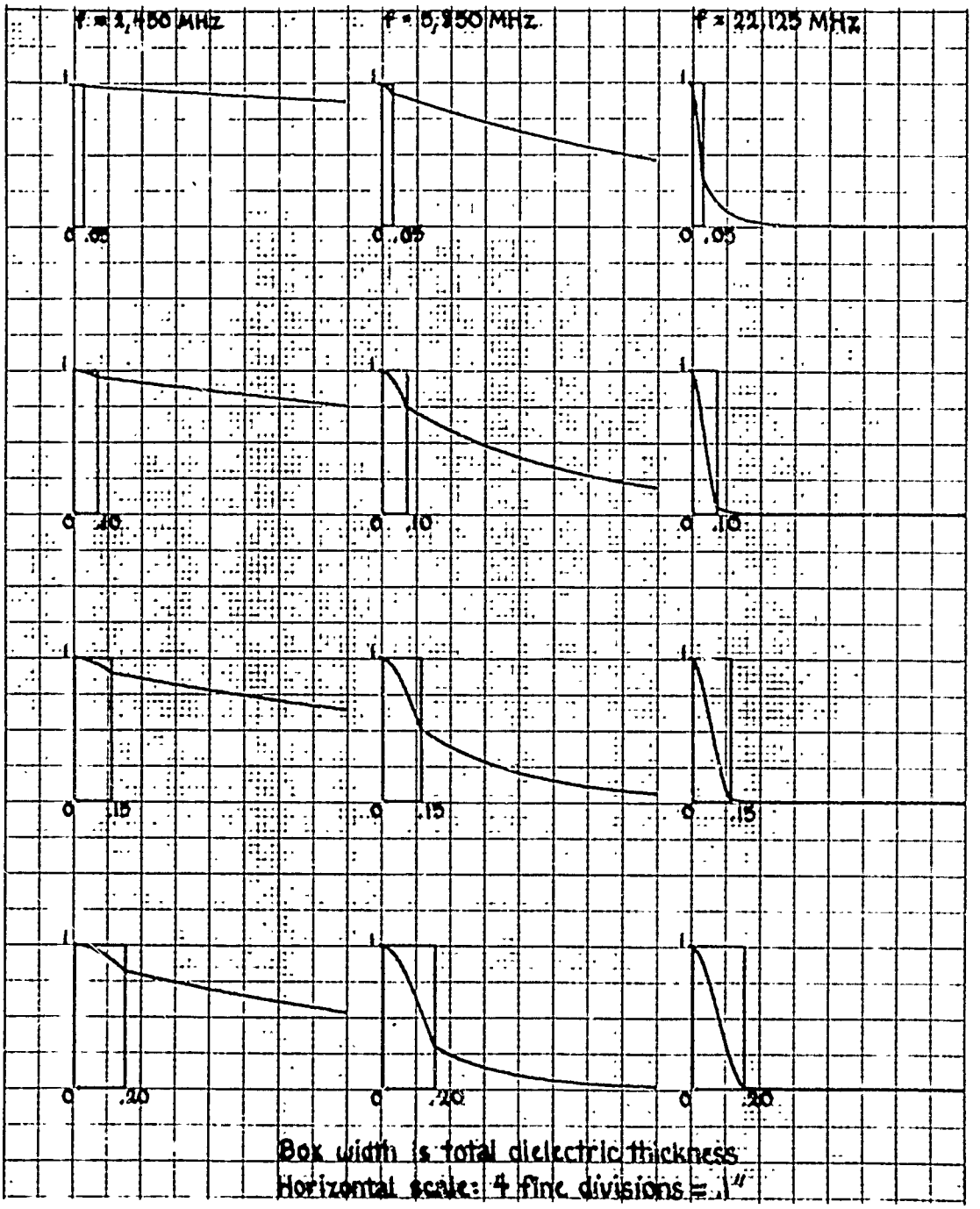

Figure F-5. Normalized power density (y-coordinate) versus vertical position (x-coordinate) for TM even mode, $\varepsilon_1 = 4.0$, $\varepsilon_2 = 1.0$

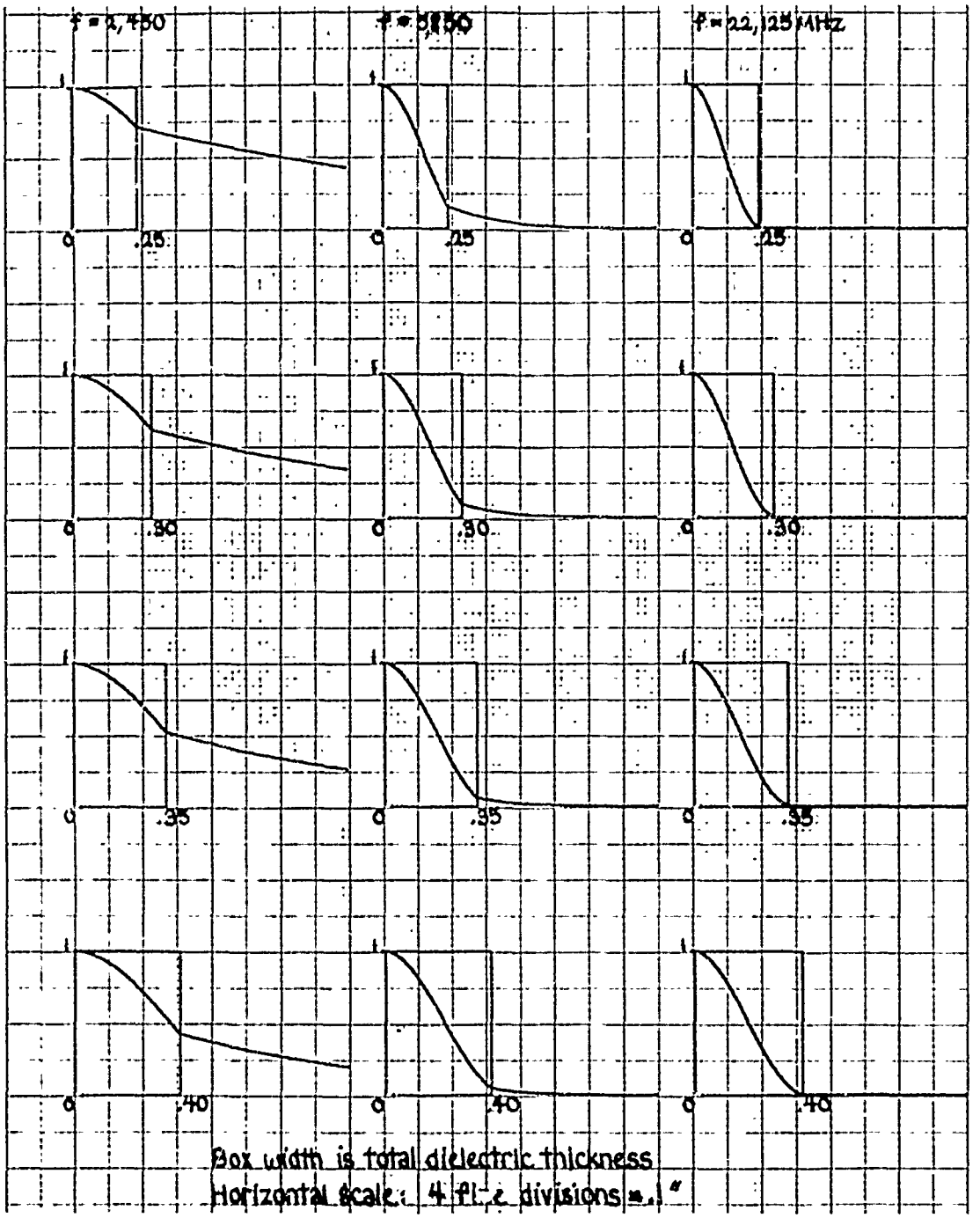

Figure F-6. Normalized power density (y-coordinate) versus vertical position (x-coordinate) for TM even mode, $\varepsilon_1 = 4.0$, $\varepsilon_2 = 1.0$

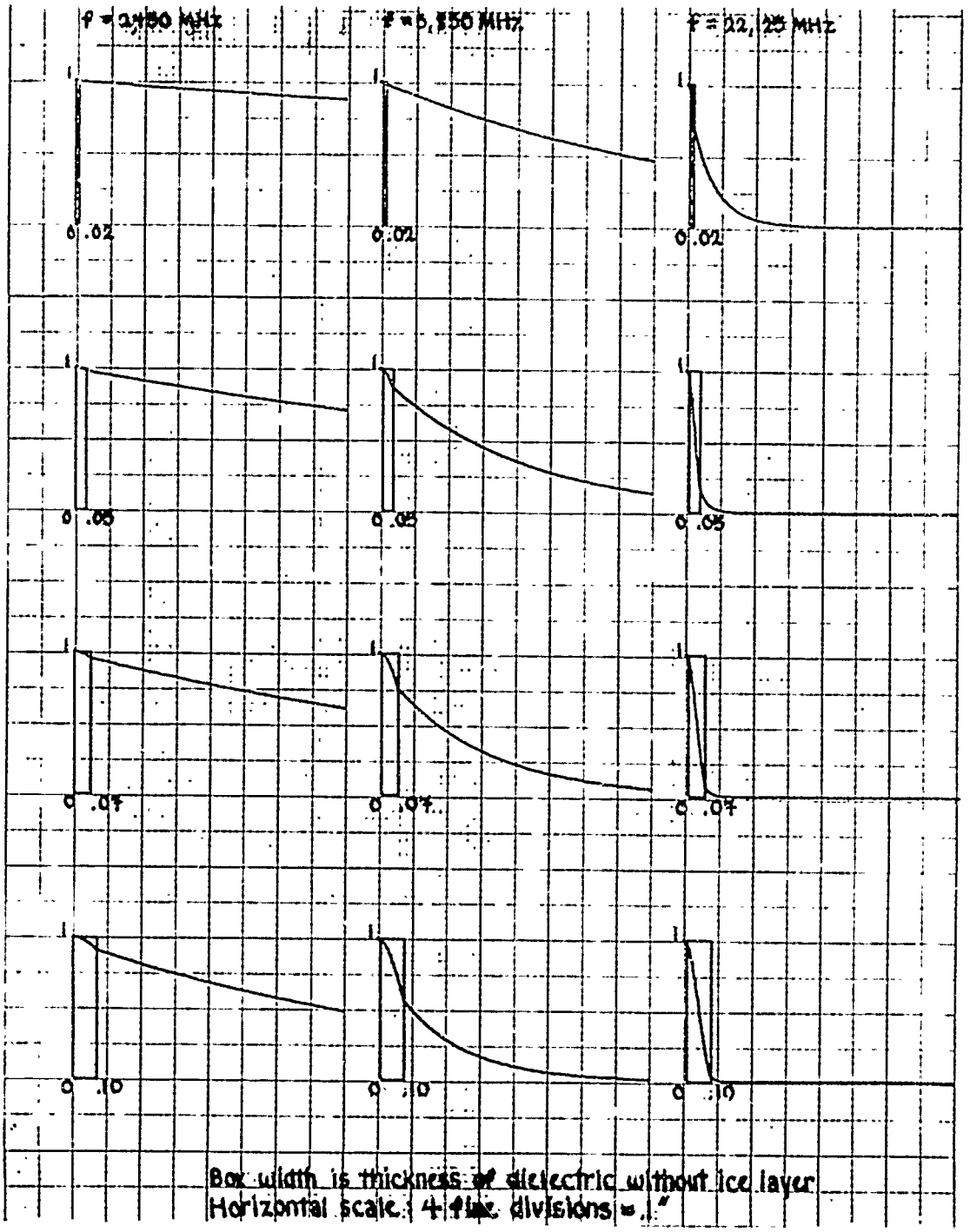

Figure F-7. Normalized power density (y-coordinate) versus vertical position (x-coordinate) for TM even mode, ε_1 = 9 0, ε_2 = 1.0

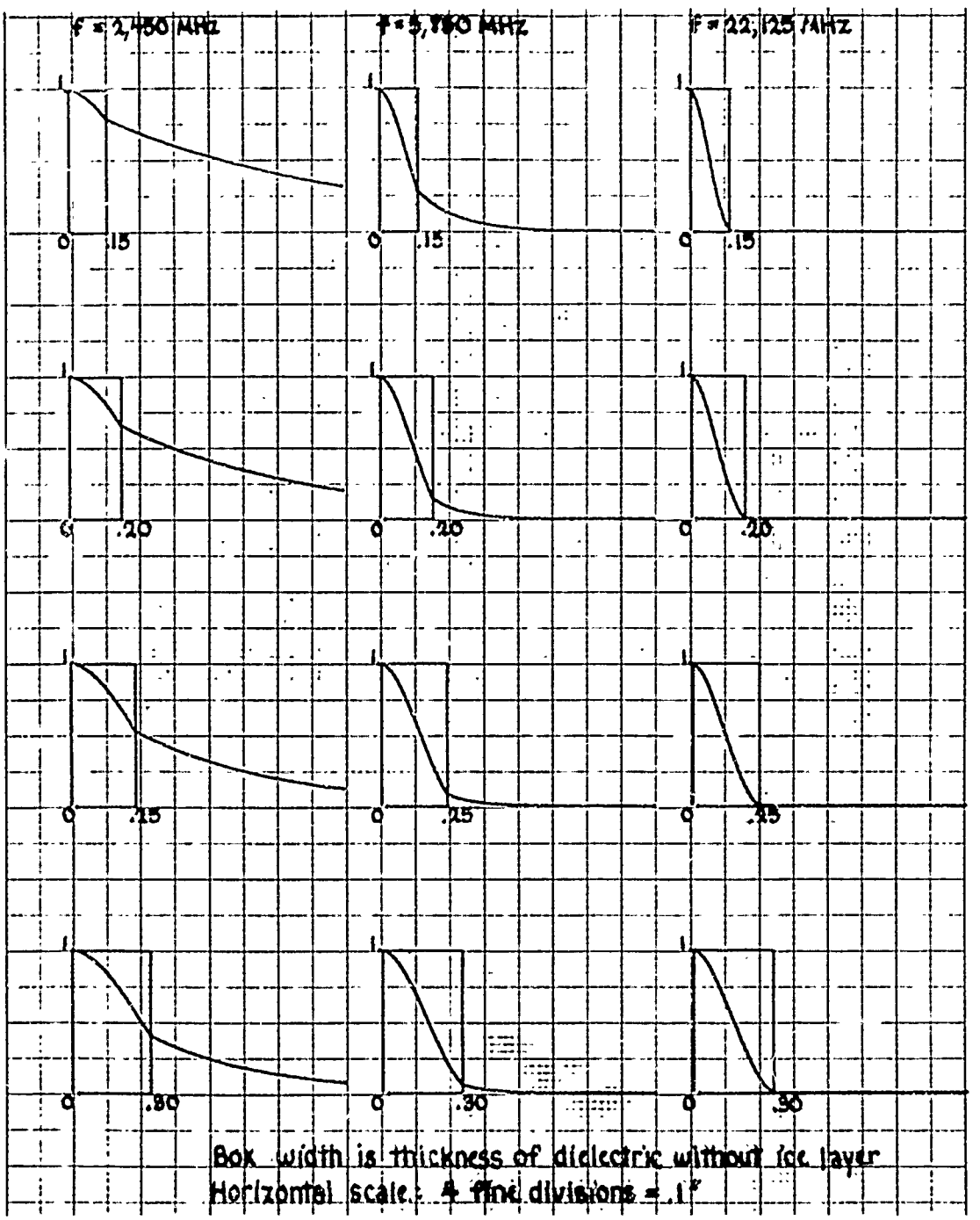

Figure F-8. Normalized power density (y-coordinate) versus vertical position (x-coordinate) for TM even mode, $\varepsilon_1 = 9.0$, $\varepsilon_2 = 1.0$

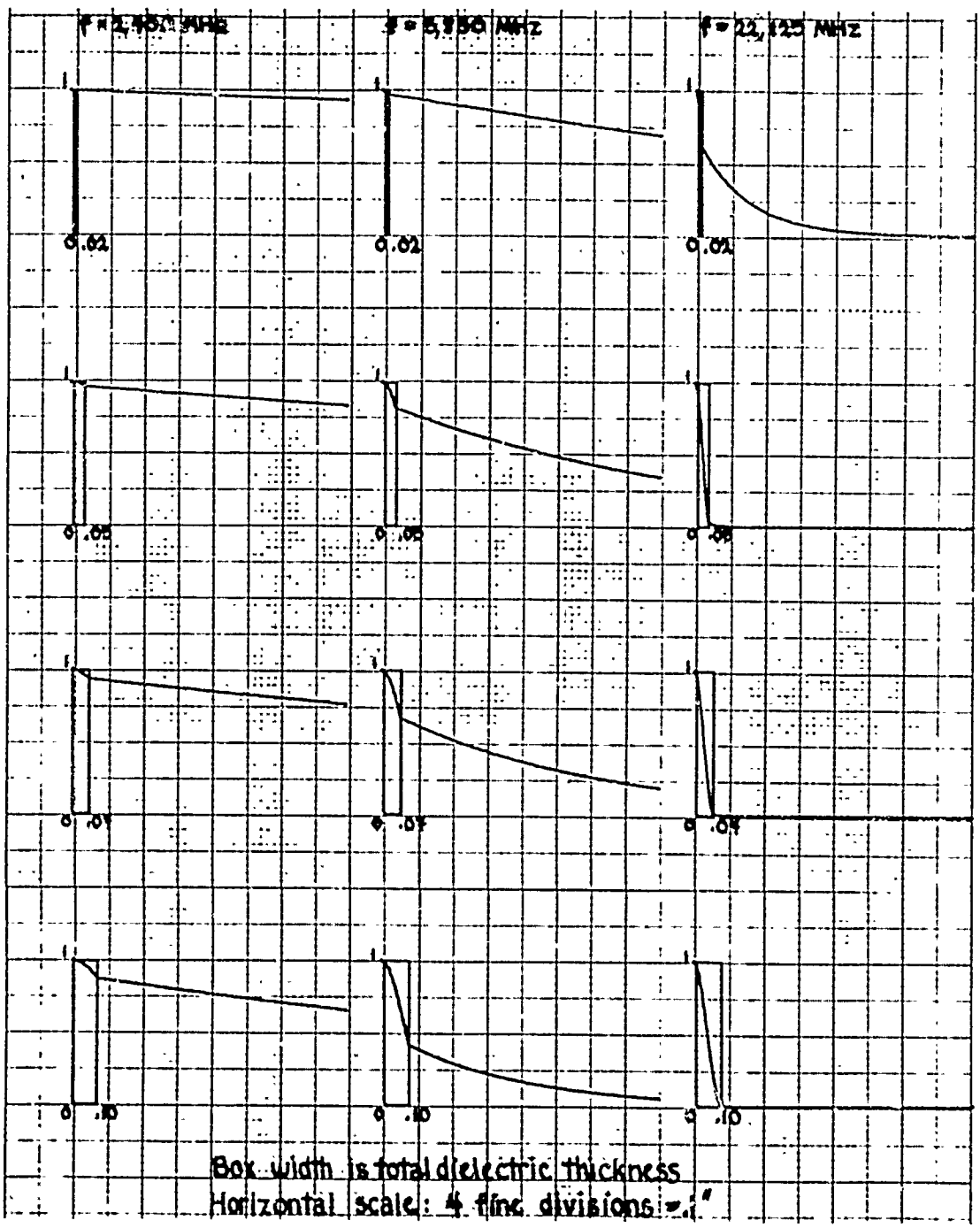

Figure F-9. Normalized power density (y-coordinate) versus vertical position (x-coordinate) for TM even mode, $\varepsilon_1 = 9.0$, $\varepsilon_2 = 3.0$

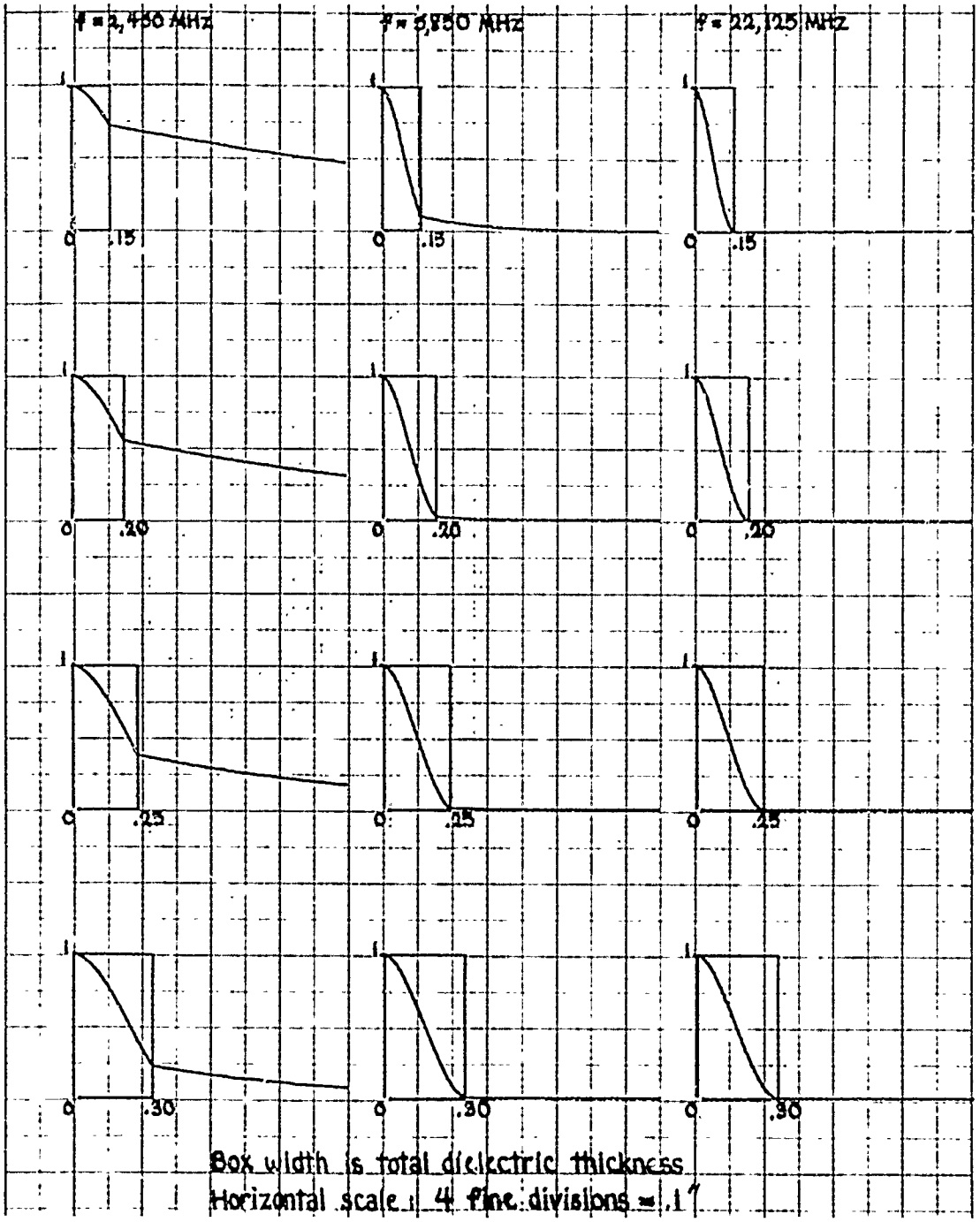

Figure F-10. Normalized power density (y-coordinate) versus vertical position (x-coordinate) for TM even mode, $\varepsilon_1 = 9.0$, $\varepsilon_2 = 3.0$

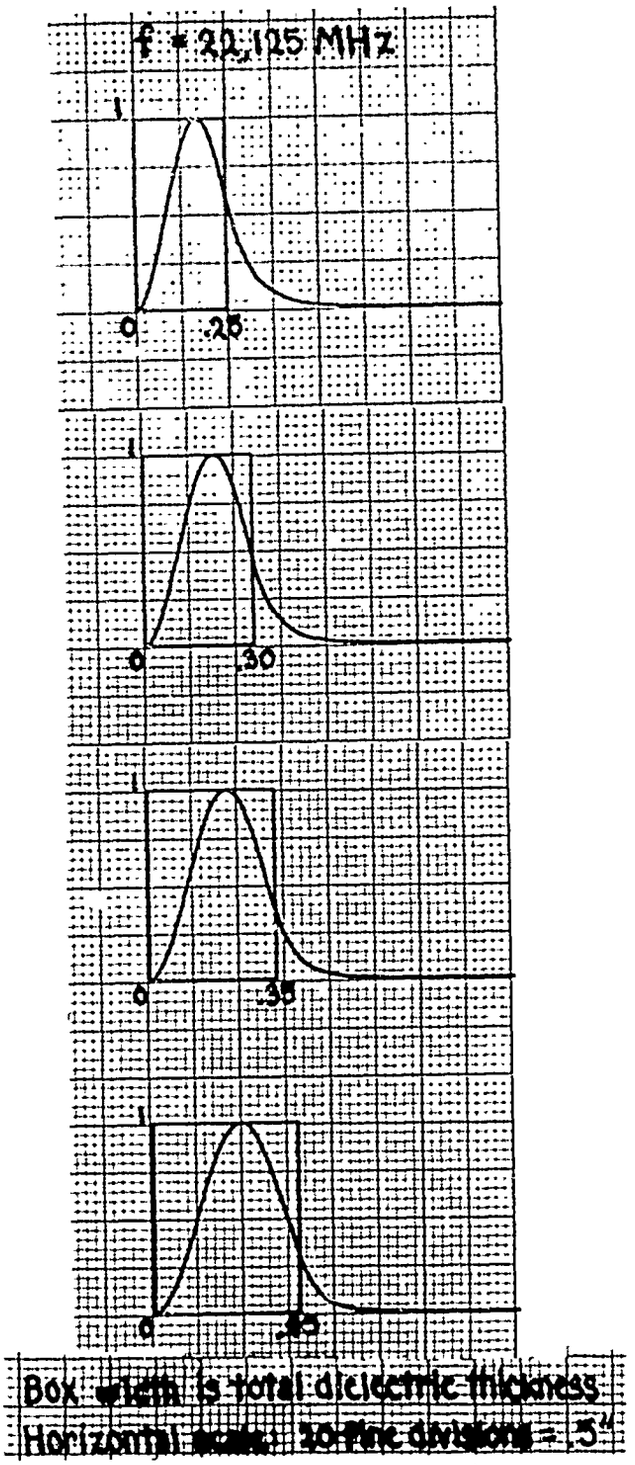

Figure F-11. Normalized power density (y-coordinate) versus vertical position (x-coordinate) for TE odd mode, $\varepsilon_1 = 2.0$

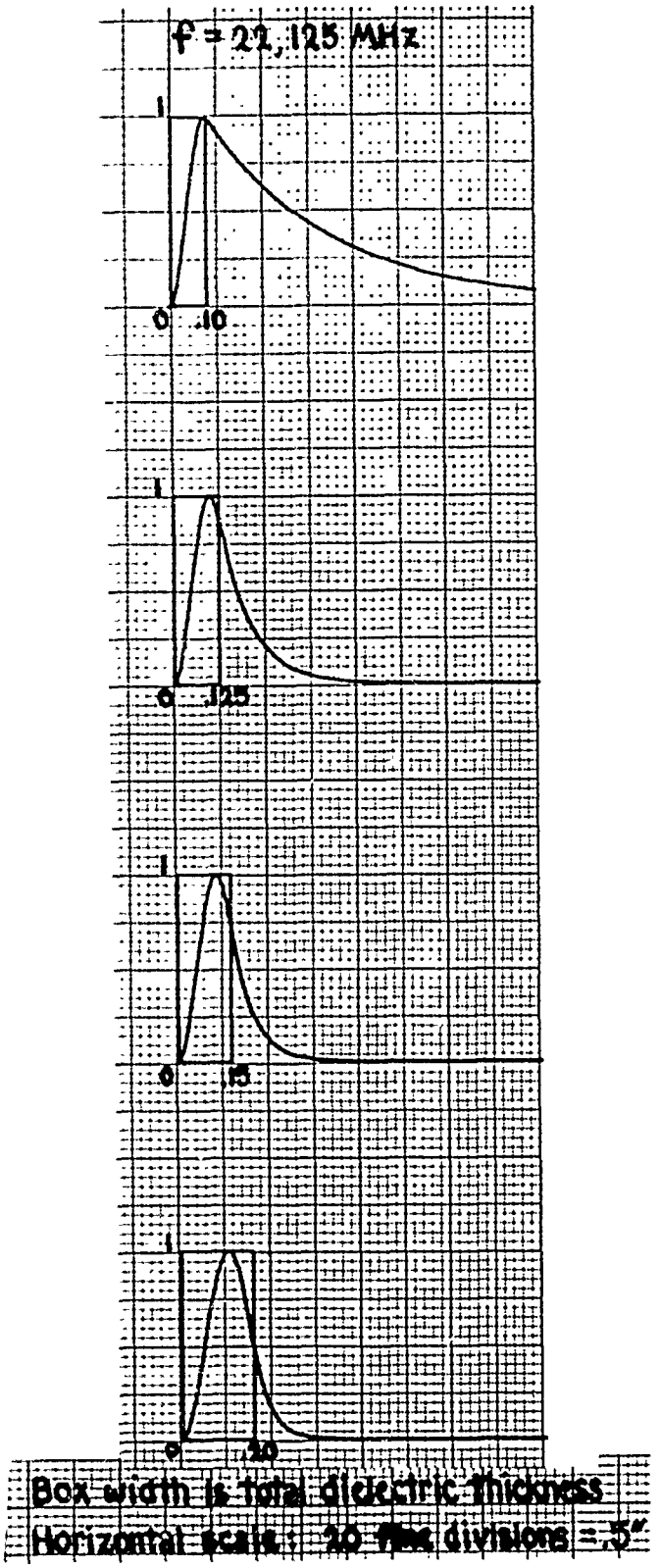

Figure F-12. Normalized power density (y-coordinate) versus vertical position (x-coordinate) for TE odd mode, $\varepsilon_1 = 3.0$

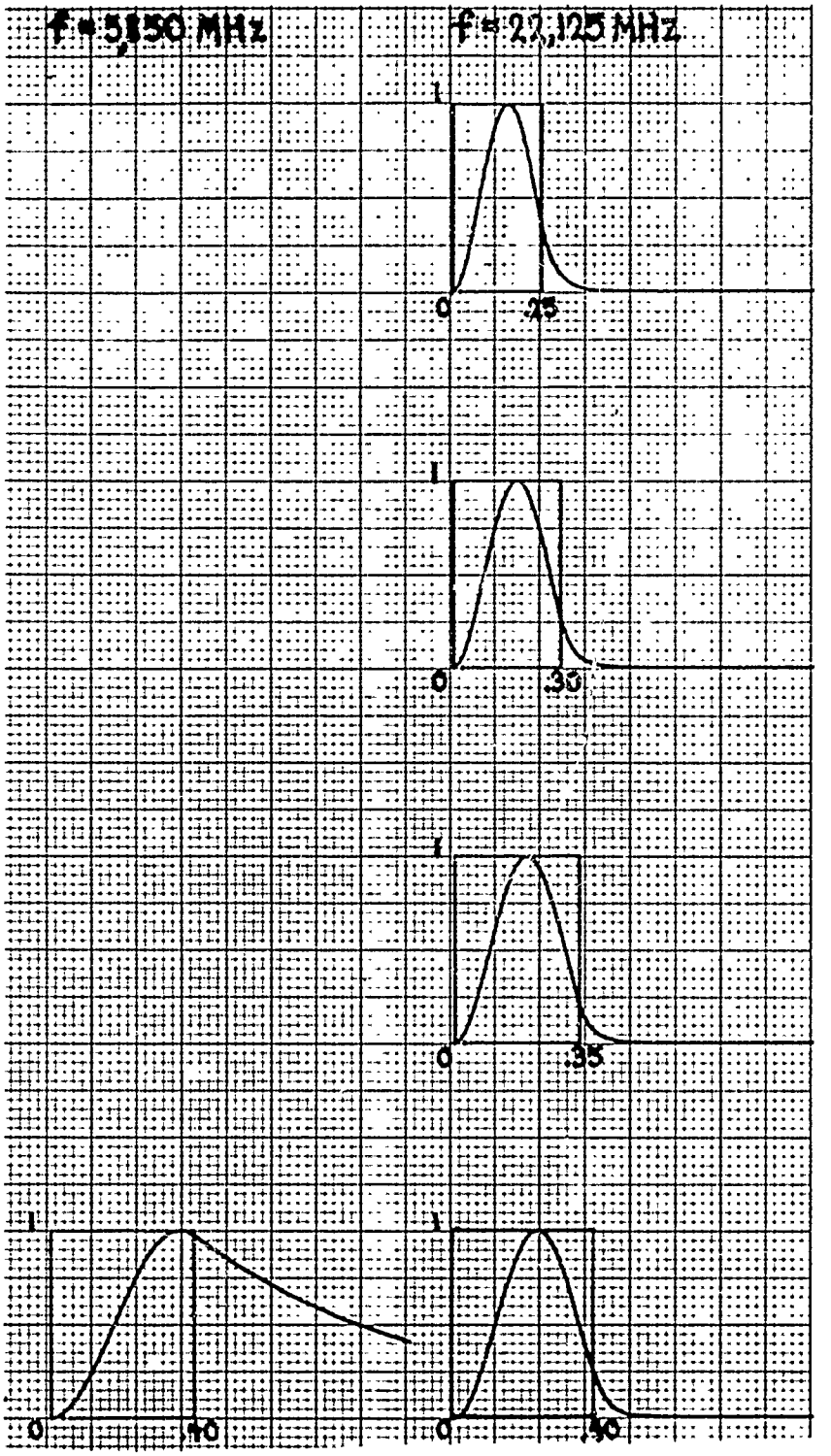

Figure F-13. Normalized power density (y-coordinate) versus vertical position (x-coordinate) for TE odd mode, $\varepsilon_1 = 3.0$

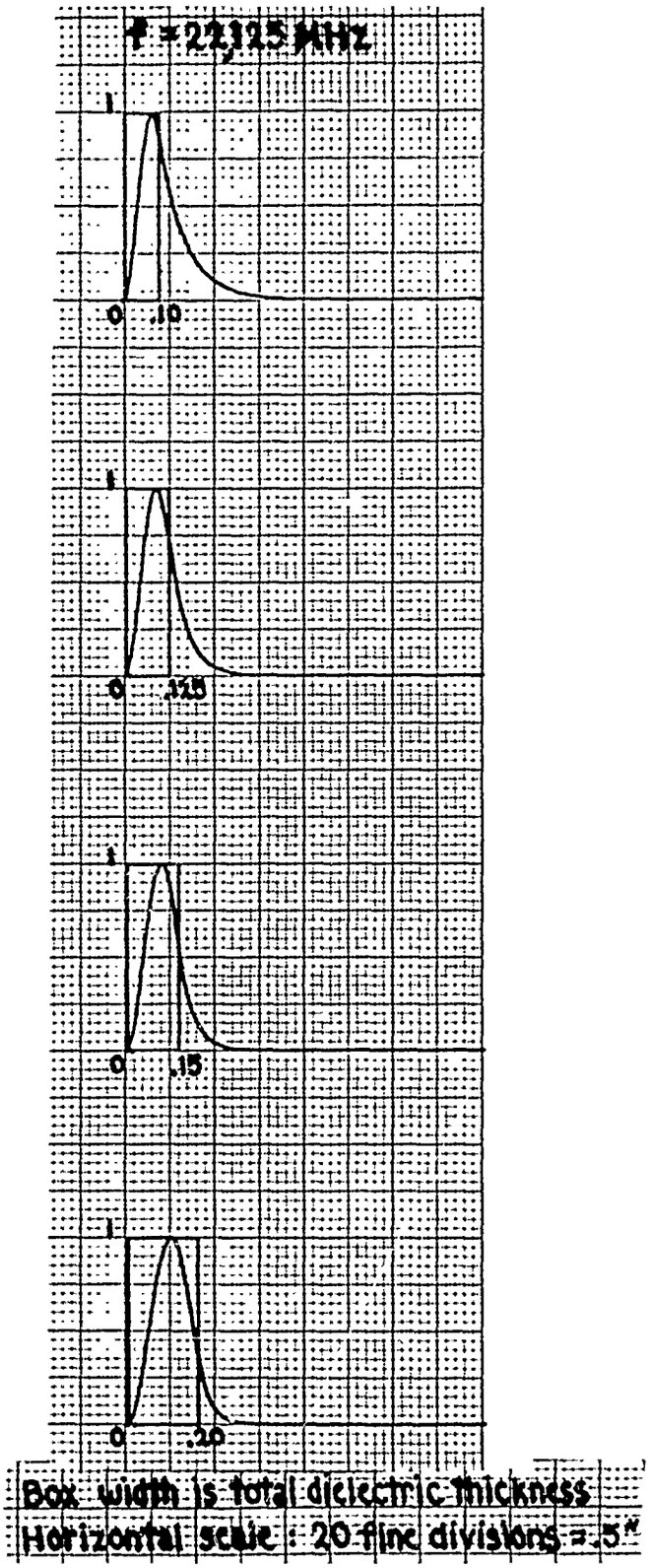

Figure F-14. Normalized power density (y-coordinate) versus vertical position (x-coordinate) for TE odd mode, $\varepsilon_1 = 4.0$

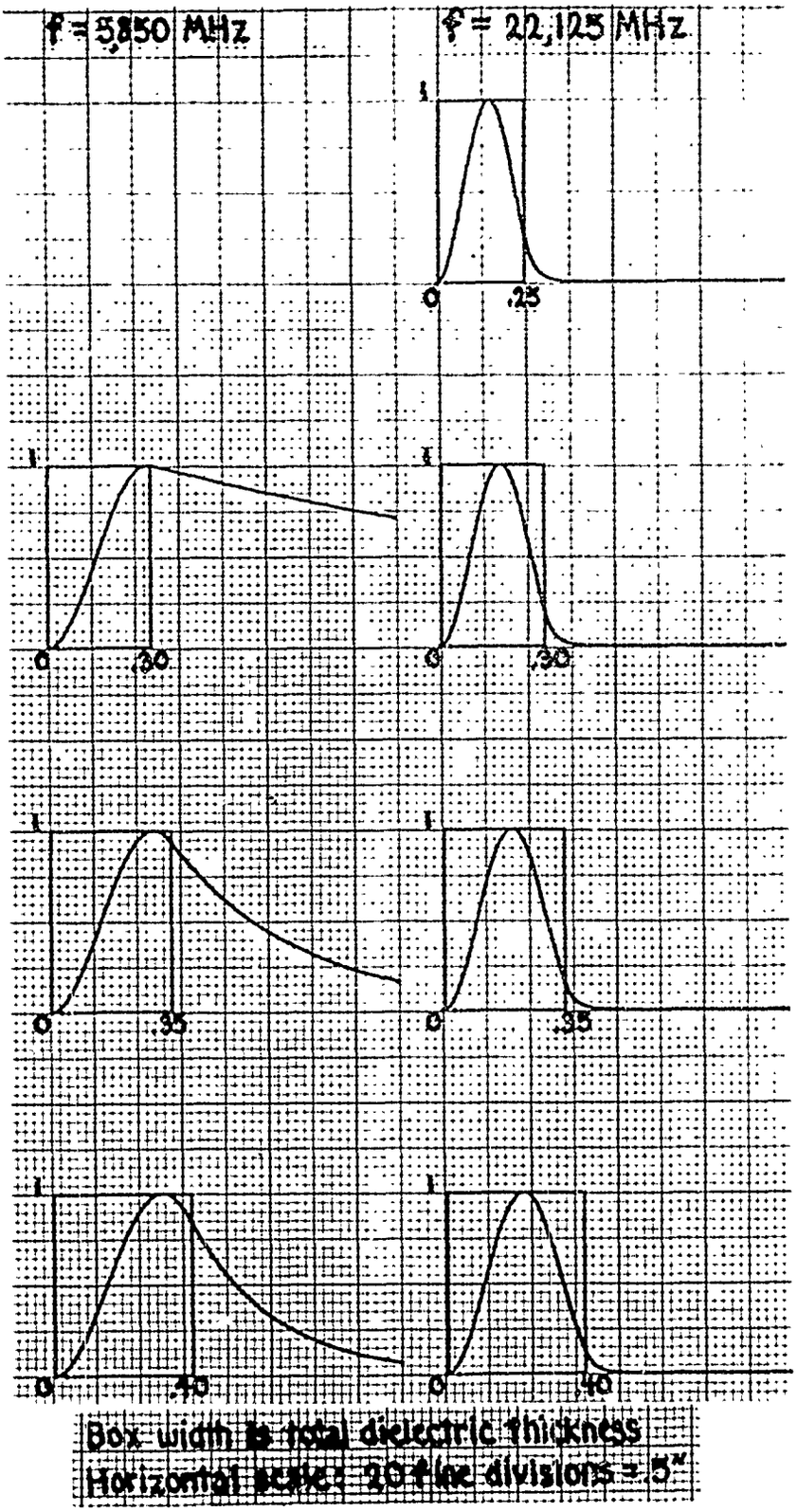

Figure F-15. Normalized power density (y-coordinate) versus vertical position (x-coordinate) for TE odd mode, $\varepsilon_1 = 4.0$

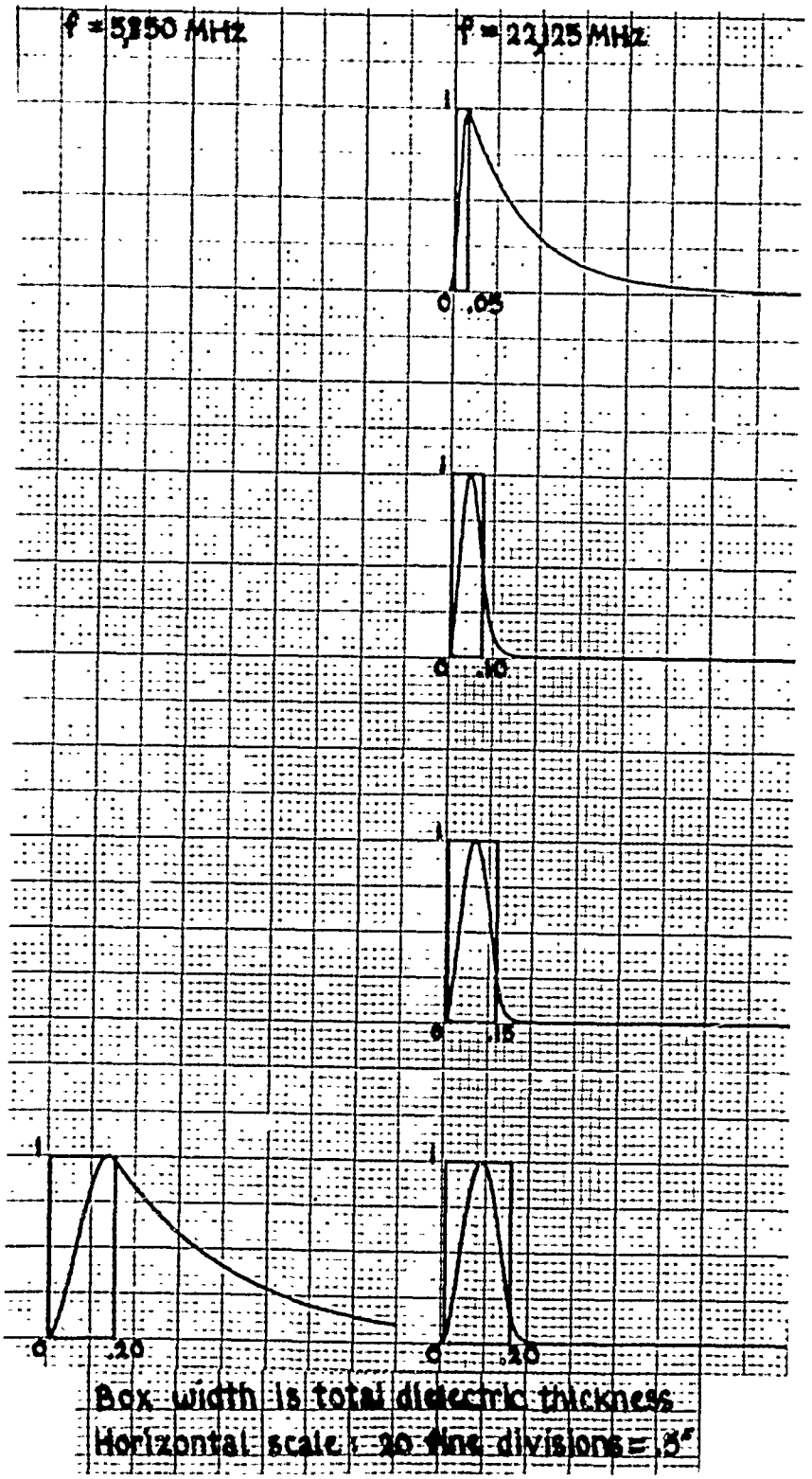

Figure F-16. Normalized power density (y-coordinate) versus vertical position (x-coordinate) for TE odd mode, $\varepsilon_1 = 9.0$

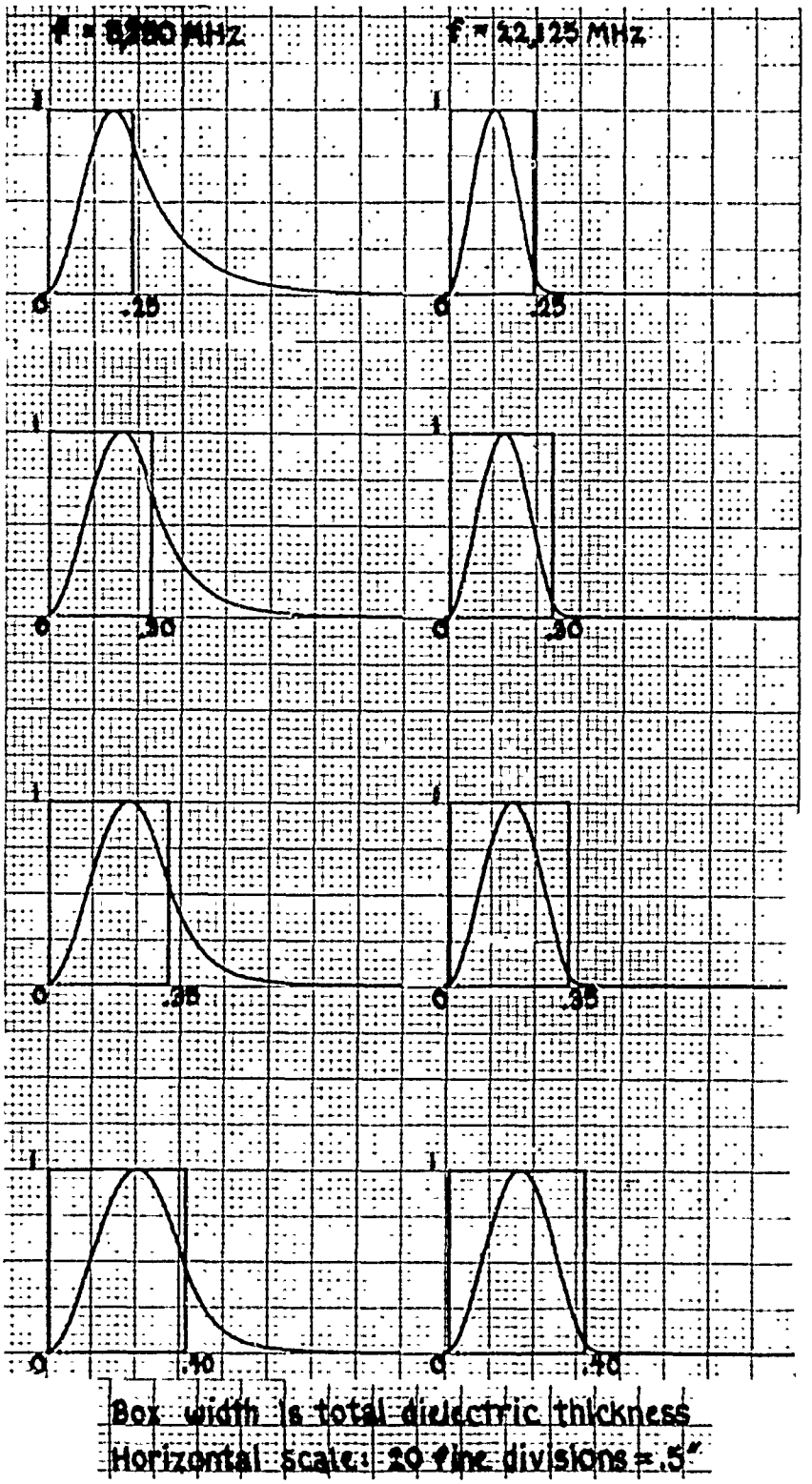

Figure F-17. Normalized power density (y-coordinate) versus vertical position (x-coordinate) for TE odd mode, ε_1 = 9.0

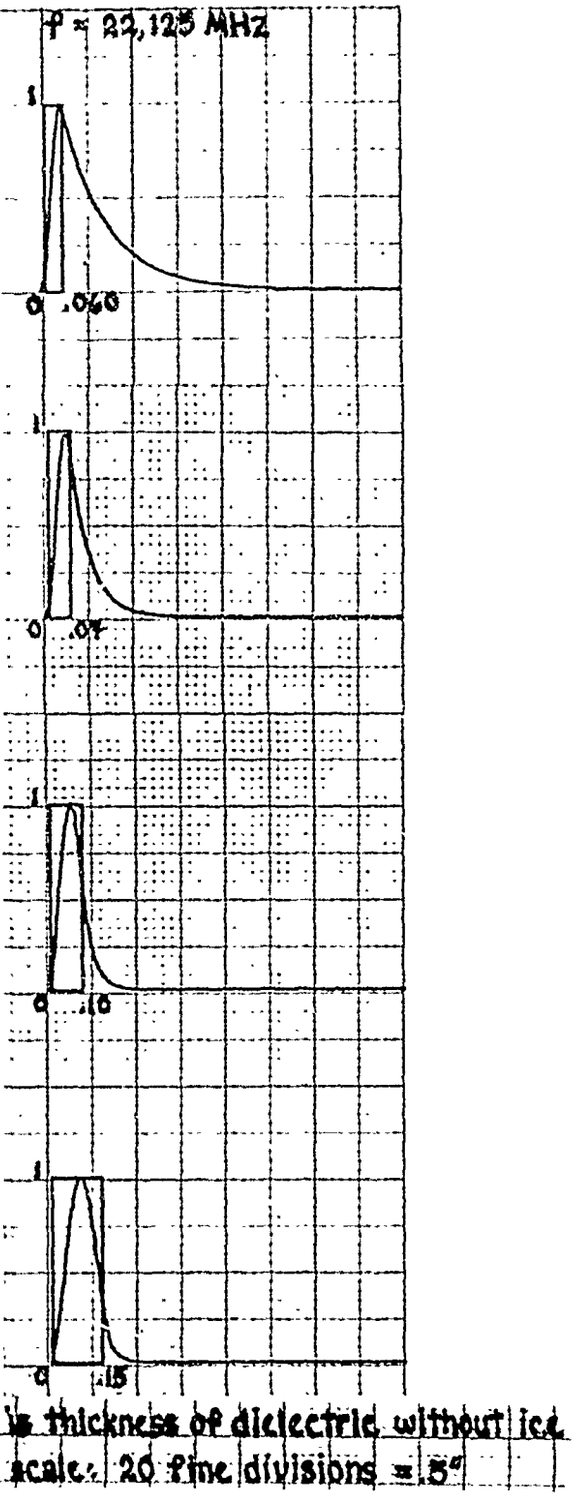

Figure F-18. Normalized power density (y-coordinate) versus vertical position (x-coordinate) for TE odd mode, $\epsilon_1 = 9.0$, $\epsilon_2 = 3.0$

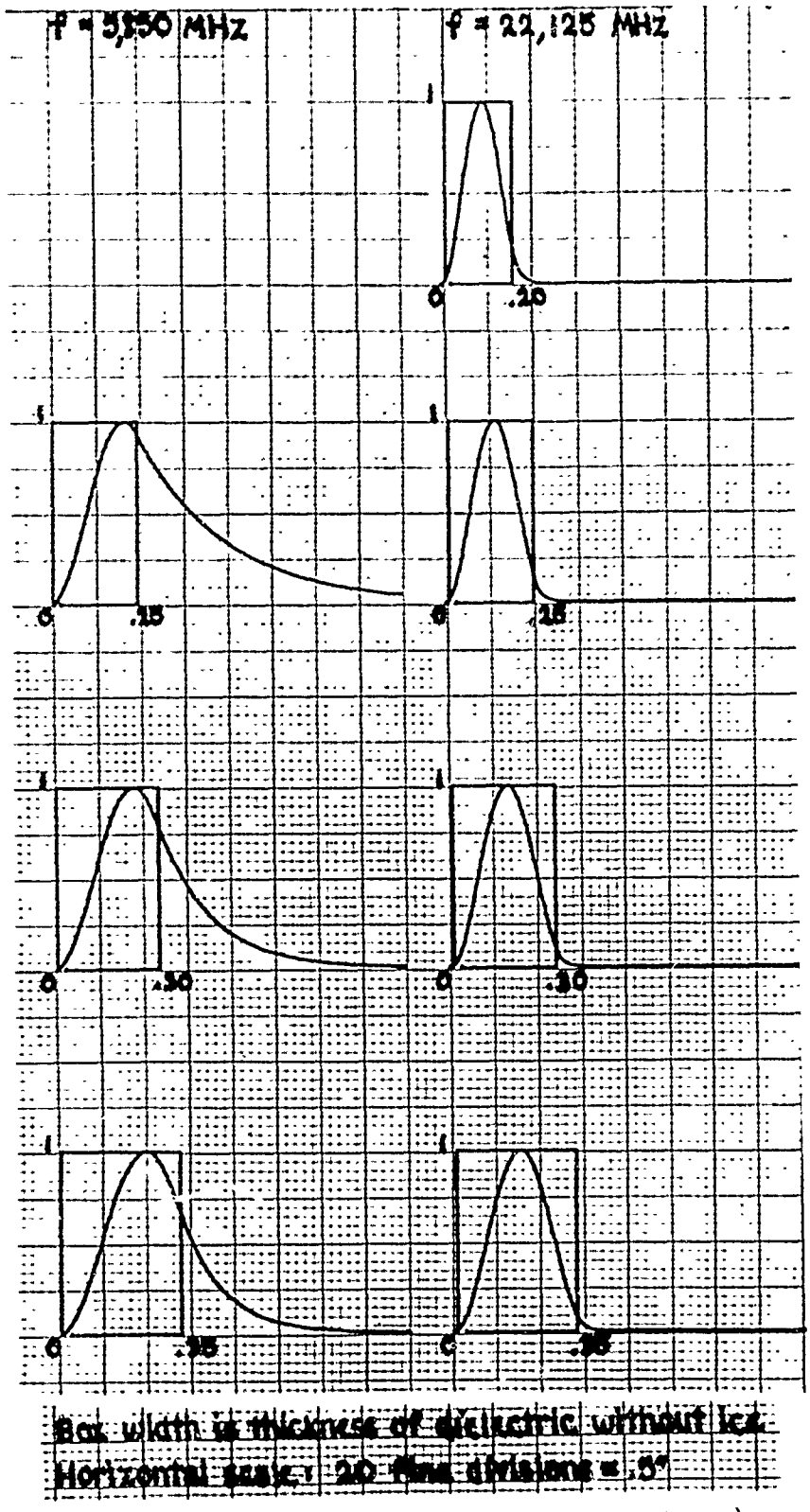

Figure F-19. Normalized power density (y-coordinate) versus vertical position (x-coordinate) for TE odd mode, $\varepsilon_1 = 9.0$, $\varepsilon_2 = 3.0$

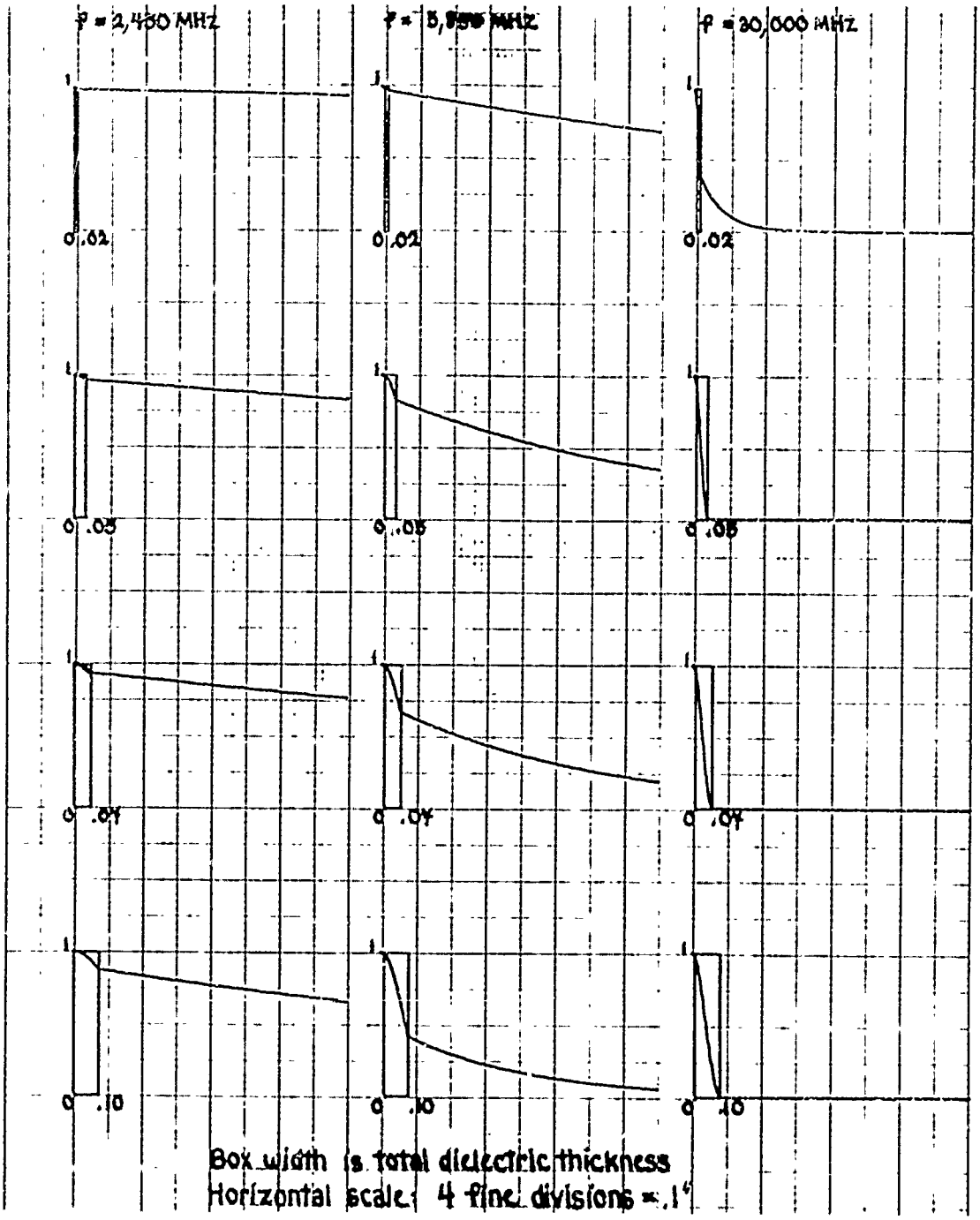

Figure F-20. Normalized power density (y-coordinate) versus vertical position (x-coordinate) for TM even mode, ε_1 = 9.0, ε_2= 1.0

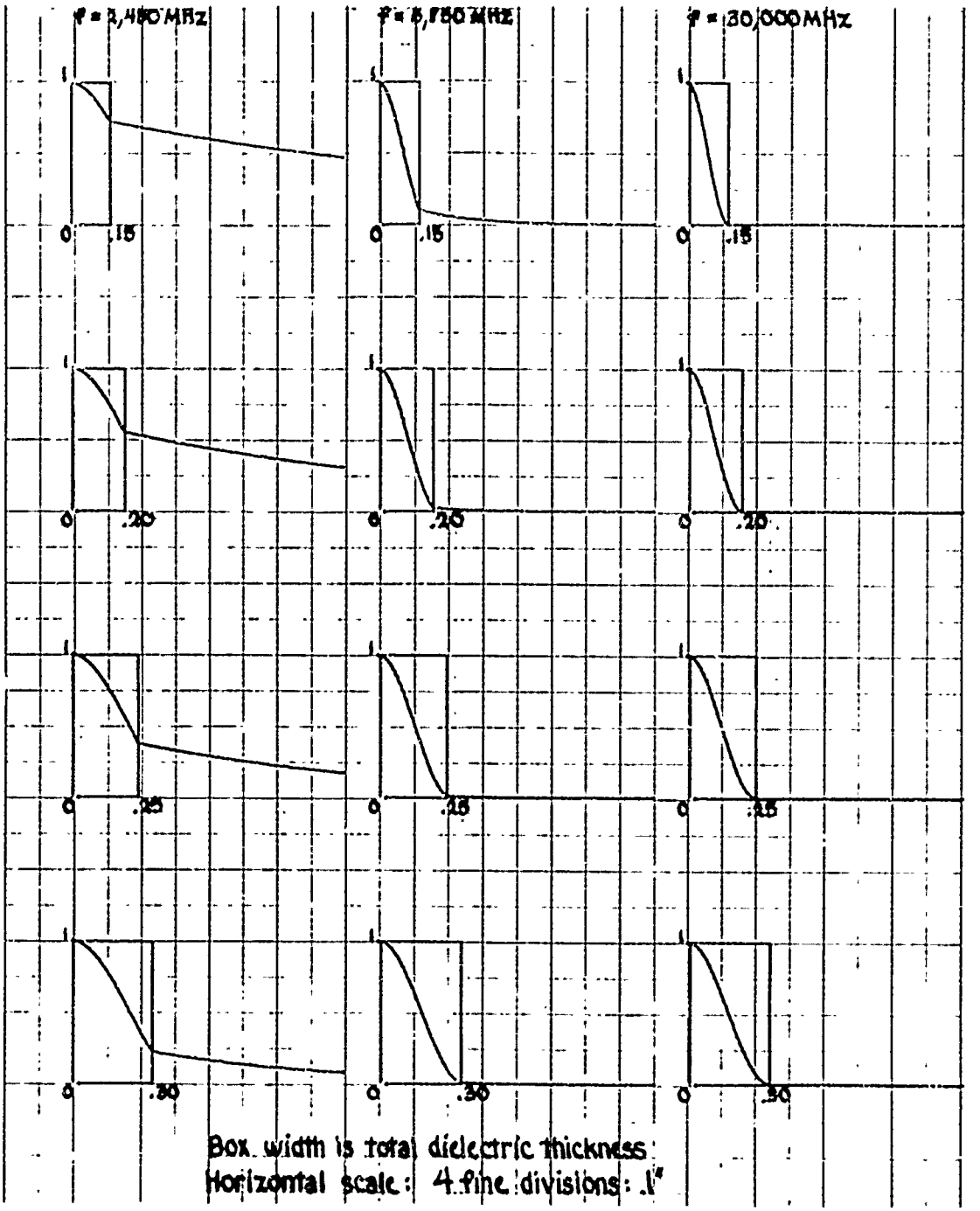

Figure F-21. Normalized power density (y-coordinate) versus vertical position (x-coordinate) for TM even mode, $\varepsilon_1 = 9.0$, $\varepsilon_2 = 1.0$

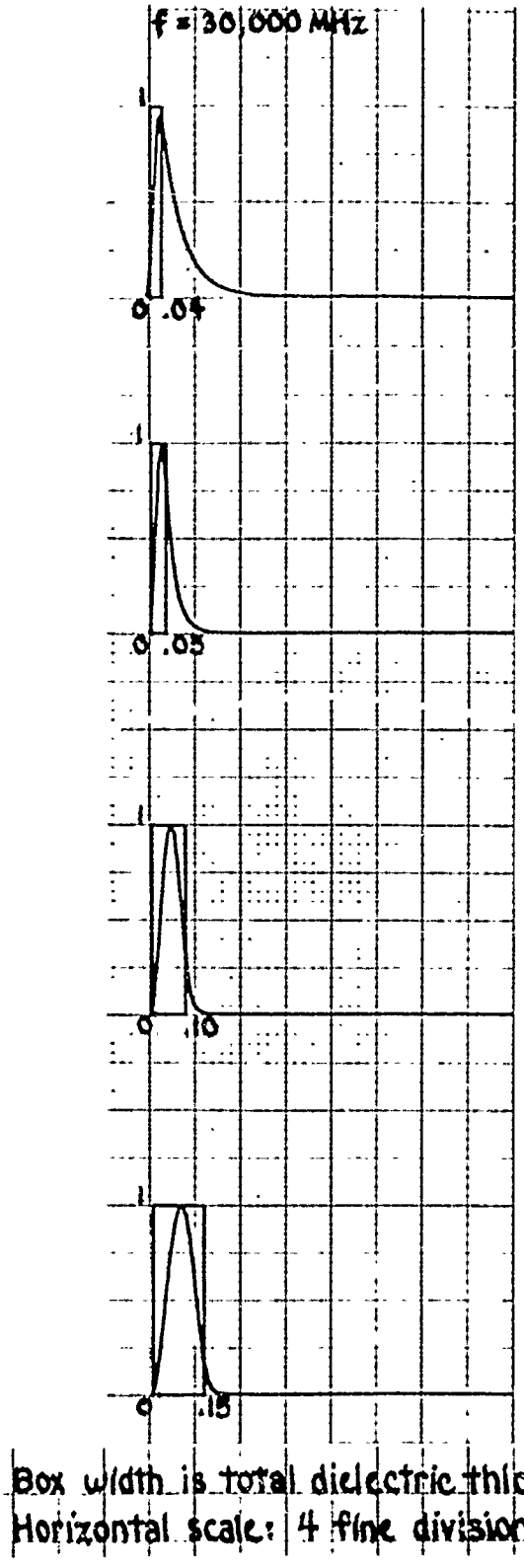

Figure F-22. Normalized power density (y-coordinate) versus vertical position (x-coordinate) for TM odd mode, $\varepsilon_1 = 9.0$, $\varepsilon_2 = 1.0$

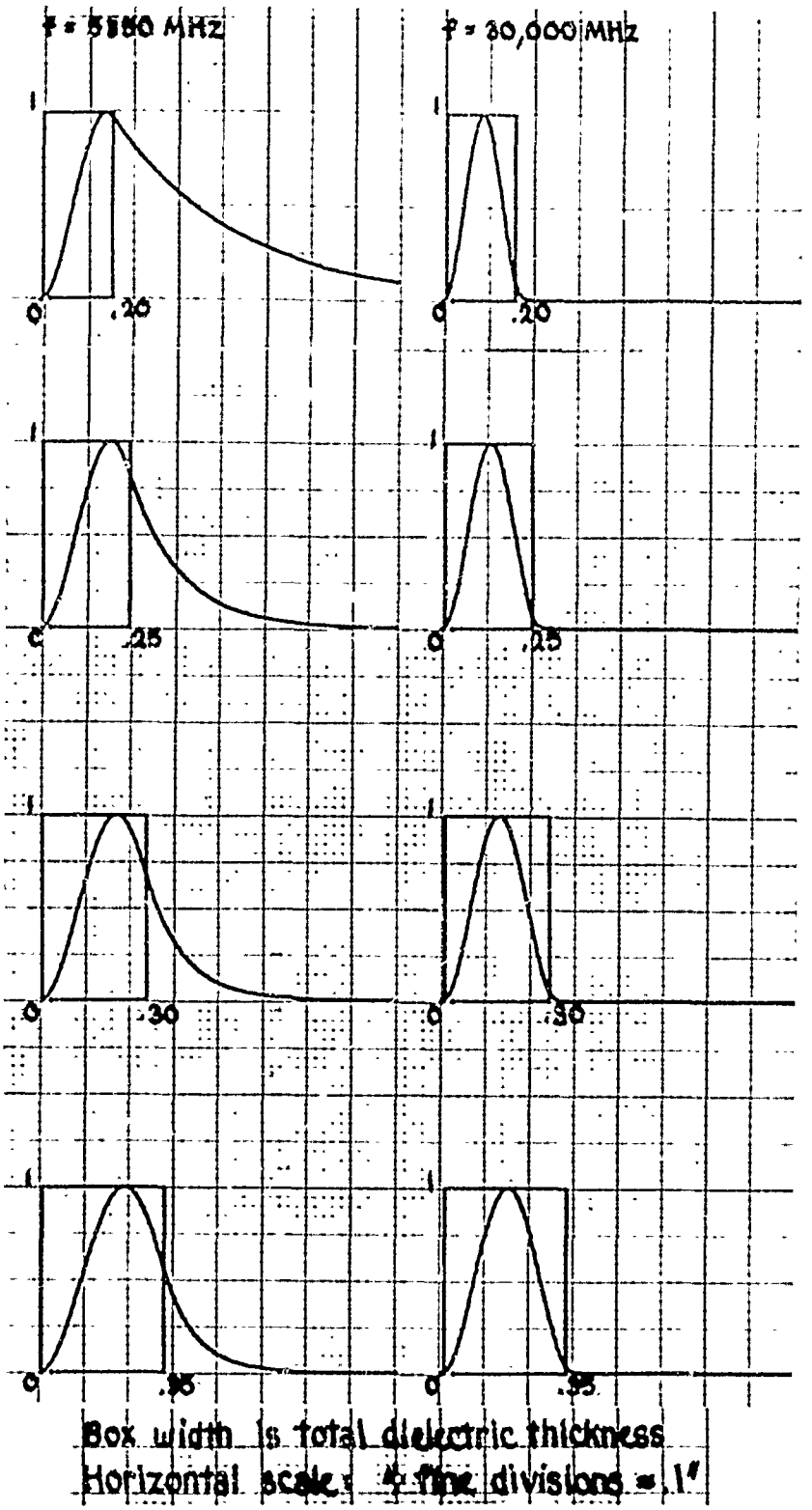

Figure F-23. Normalized power density (y-coordinate) versus vertical position (x-coordinate) for TE odd mode, $\varepsilon_1 = 9.0$, $\varepsilon_2 = 1.0$

APPENDIX G

ABSTRACTS OF LITERATURE ON SURFACE WAVEGUIDE COUPLING TECHNIQUES

PHASE III - COUPLING

Six papers describing surface wave launching experiments have been studied. All of these papers report the achievement of moderate to high coupling efficiences. The following are excerpts from these papers.

THE EXCITATION OF PLANE SURFACE WAVES[19]

"It is shown that a surface wave will be generated by a ho.izontal slot situated above a corrugated or dielectric-coated guiding surface."

"The problem of efficient launching is discussed, and it is shown that under suitable conditions a high launching efficiency is possible. Some of the theoretical predictions have been verified experimentally."

Figure G-1a illustrates the theoretical efficiency calculated by Cullen. Figure G-1b illustrates Cullen's experimental apparatus and Figure G-1c illustrates the relationship of the slot relative to the coated surface waveguide.

Cullen reports that: "With the reactive surface in position, it was soon discovered that, in accordance with theory, a field distribution resembling a surface wave was found only if the launching slot was fairly close to the reactive surface" (surface guide). One of Cullen's conclusions is that: "It has been shown that a high launching efficiency for slot excitation of surface waves is possible if the slit height is properly chosen."

---

[19]A.L. Cullen, "The Excitation of Plane Surface Waves," Proceedings of the IEE (London), Vol. 101, part IV, pp. 224-234 (February 15, 1954).

THE LAUNCHING OF A PLANE SURFACE WAVE[20]

"The subject of this paper is a theoretical and experimental investigation of surface-wave propagation over a plane conductor with dielectric coating. Special reference is made to the problem of launching such a wave." "... eventually a launcher of moderate efficiency was found."

Some conclusions drawn by Rich: "It was found to be relatively easy to excite a surface wave, almost any launching device would do that." "The efficient excitation of the surface wave was more difficult, but 50% efficiency of the double cheese launcher, which was designed on purely empirical considerations, provided a surface wave field of sufficient purity to enable more systematic investigations to be undertaken. It is found that, in theory, it is possible to get launching efficiencies of nearly 100% from apertures of no more than 2λ in extent."

TE MODE EXCITATION ON DIELECTRIC LOADED PARALLEL PLANE AND TROUGH WAVEGUIDES[21]

"A theoretical and experimental study of the launching of TE surface wave modes on dielectric loaded parallel plane and trough waveguides has been performed. The source is a linear transverse current filament perpendicular to and extending across the space between the parallel side walls. Families of curves are presented, which show the bidirectional launching efficiencies for the dominant TE modes of these two transmission lines as a function of dielectric constant, dielectric slab thickness, and current filament location. Measured bidirectional efficiencies are compared to the theoretically predicted values. Measured unidirectional launching efficiencies as high as 97 percent were obtained for the case where a short circuit is located on one side of the current

---

[20] G.J. Rich, "The Launching of a Plane Surface Wave," Proceedings of the IEE (London), Vol. 102, part B, pp. 237-246 (March 1955).

[21] Cohn, Cassedy and Kott, "TE Mode Excitation on Dielectric Loaded Parallel Plane and Trough Waveguides," IRE Transactions on Microwave Theory and Techniques, pp. 545-552 (September 1960).

(a)

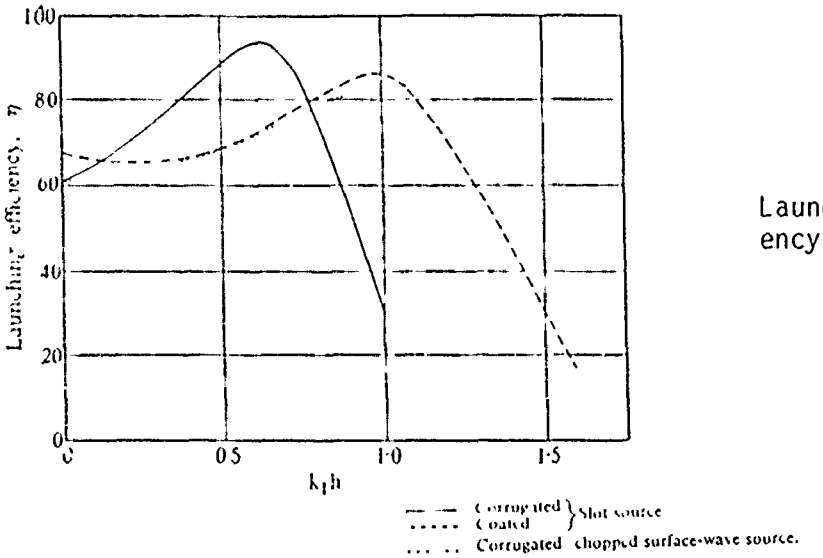

Launching efficiency curves.

(b)

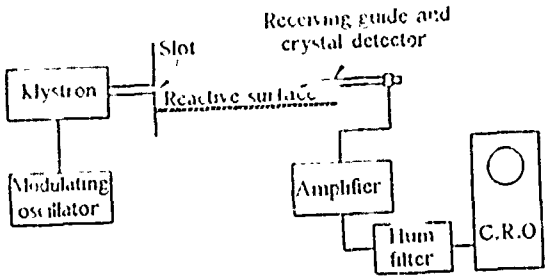

Field-measuring apparatus.

(c)

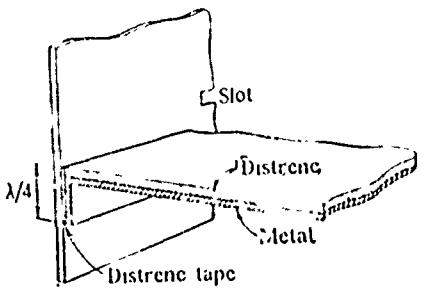

Quarter-wavelength choke connection.

Figure G-1. The Excitation of Plane Surface Waves[19]

[19]A.L. Cullen, "The Excitation of Plane Surface Waves," Proceedings of the IEE (London), Vol. 101, part IV, pp.224-234 (February 15, 1954).

filament." Computer generated plots using Cohn's technique are presented in Figures G-2 through G-6 for dielectric constants from 2.0 to 8.8.

A computer program using the analytical tools of Cohn was written to predict the bidirectional efficiency of TE_1 mode couplers to surface guides as a function of the guide thickness d, the dielectric constant ε_1, and the height of the probe above the dielectric.[21] Computer generated plots of coupling efficiency are presented in Figures G-2 through G-6 over the following range of parameters:

$$2.0 < \varepsilon_1 < 8.8$$

$$1.0 < h/d < 1.5$$

$$.3 < \frac{2d}{\lambda} < 1.0$$

The plots corroborate Cohn's original plots made fifteen years ago without the aid of the digital computer, and extend them to include dielectric constants of more interest to microwave deicing. The experimental efficiency data obtained by Cohn is plotted on graphs of theoretical predictions for $\varepsilon_1 = 2.56$ (Figure 50) to illustrate the good agreement between theory and experiment. No equivalent analytical technique for predicting TM_0 mode coupling has been identified.

THE EFFICIENCY OF EXCITATION OF A SURFACE WAVE ON A DIELECTRIC CYLINDER[23]

"This paper presents a thoeretical and experimental study of the excitation of the lowest order TM surface wave on an infinite dielectric cylinder."

"A (magnetic current) filament 0.83 wavelength in diameter will launch the TM mode with an efficiency of 95 percent." "The

[21] Cohn, Cassedy and Kott, "TE Mode Excitation on Dielectric Loaded Parallel Plane and Trough Waveguides," IRE Transactions on Microwave Theory and Techniques, pp. 545-552 (September 1960).

[23] J.W. Duncan, "The Efficiency of Excitation of a Surface Wave on a Dielectric Cylinder," IRE Transactions on Microwave Theory and Techniques, pp. 257-268 (April 1959).

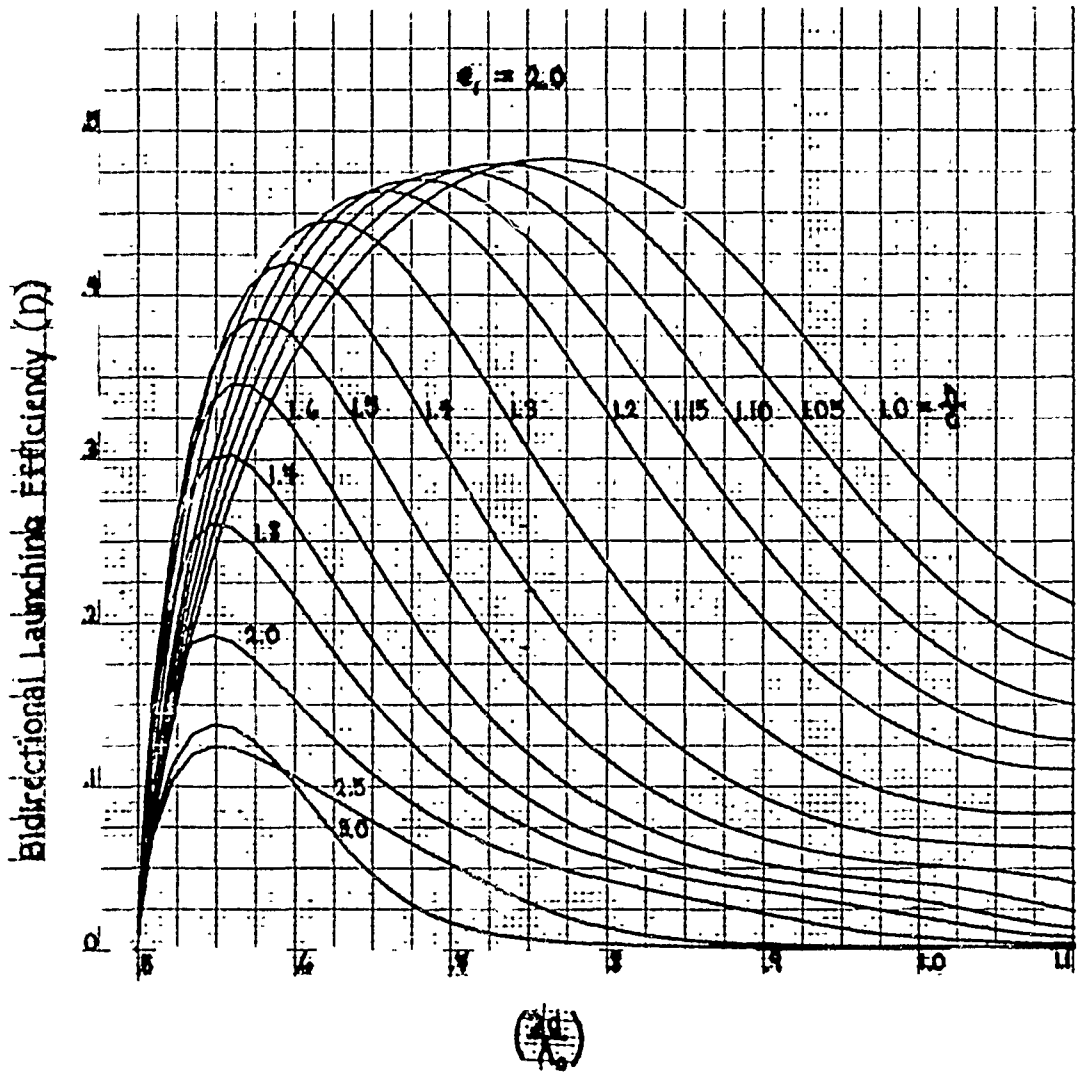

Figure G-2. Computer-generated plots of bidirectional efficiency as a function of dielectric slab thickness for various values of current filament location

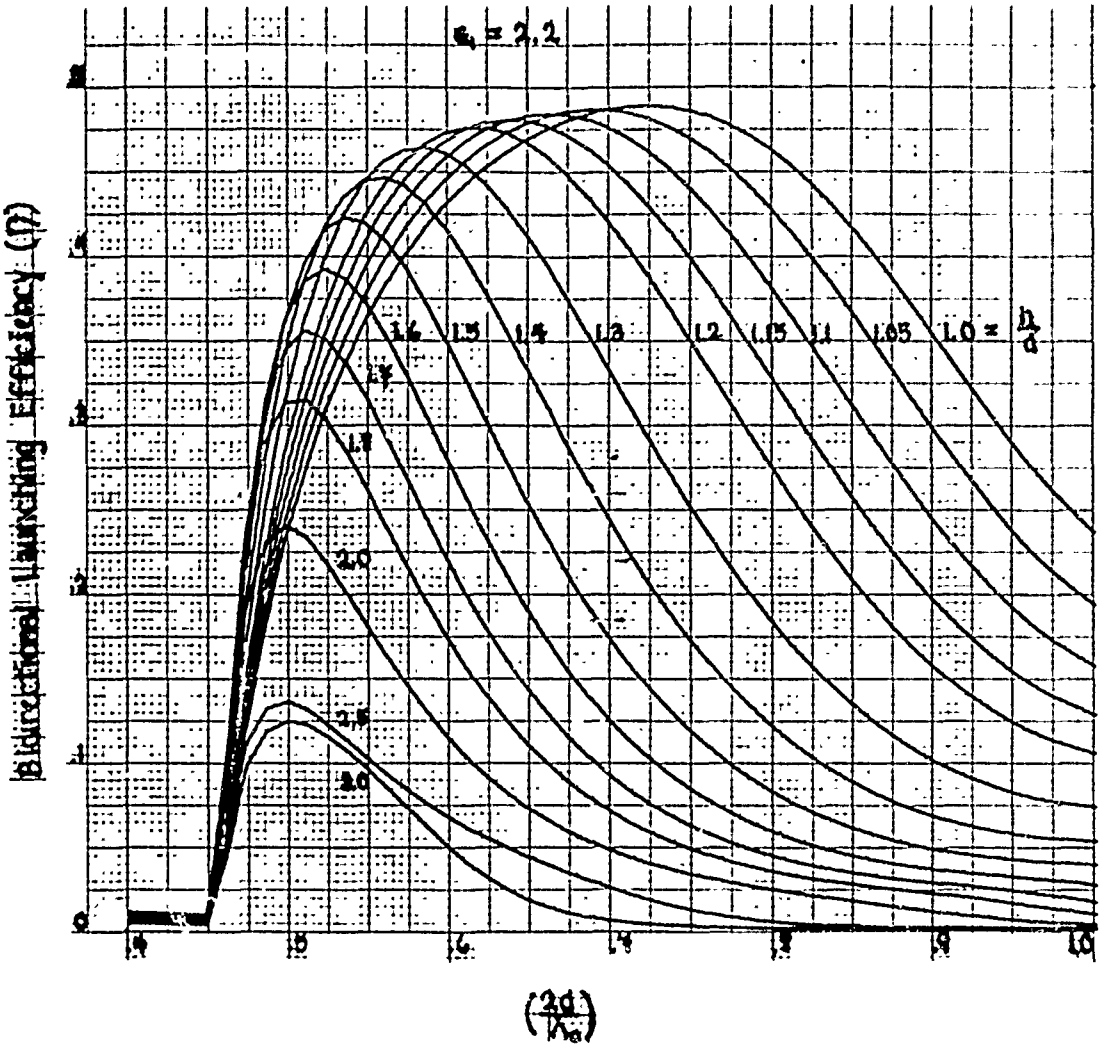

Figure G-3. Computer-generated plots of bidirectional efficiency as a function of dielectric slab thickness for various values of current filament location

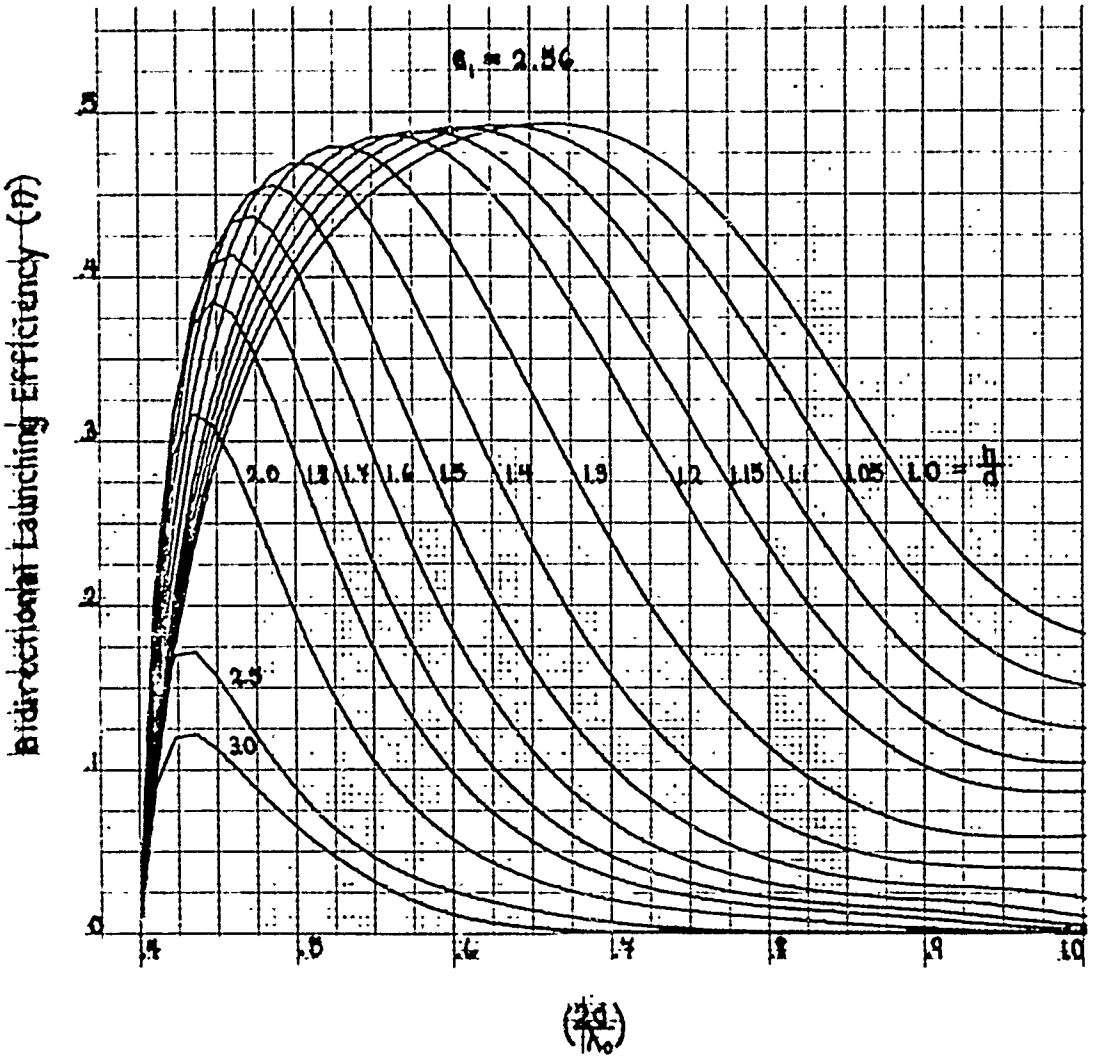

Figure G-4. Computer-generated plots of bidirectional efficiency as a function of dielectric slab thickness for various values of current filament location

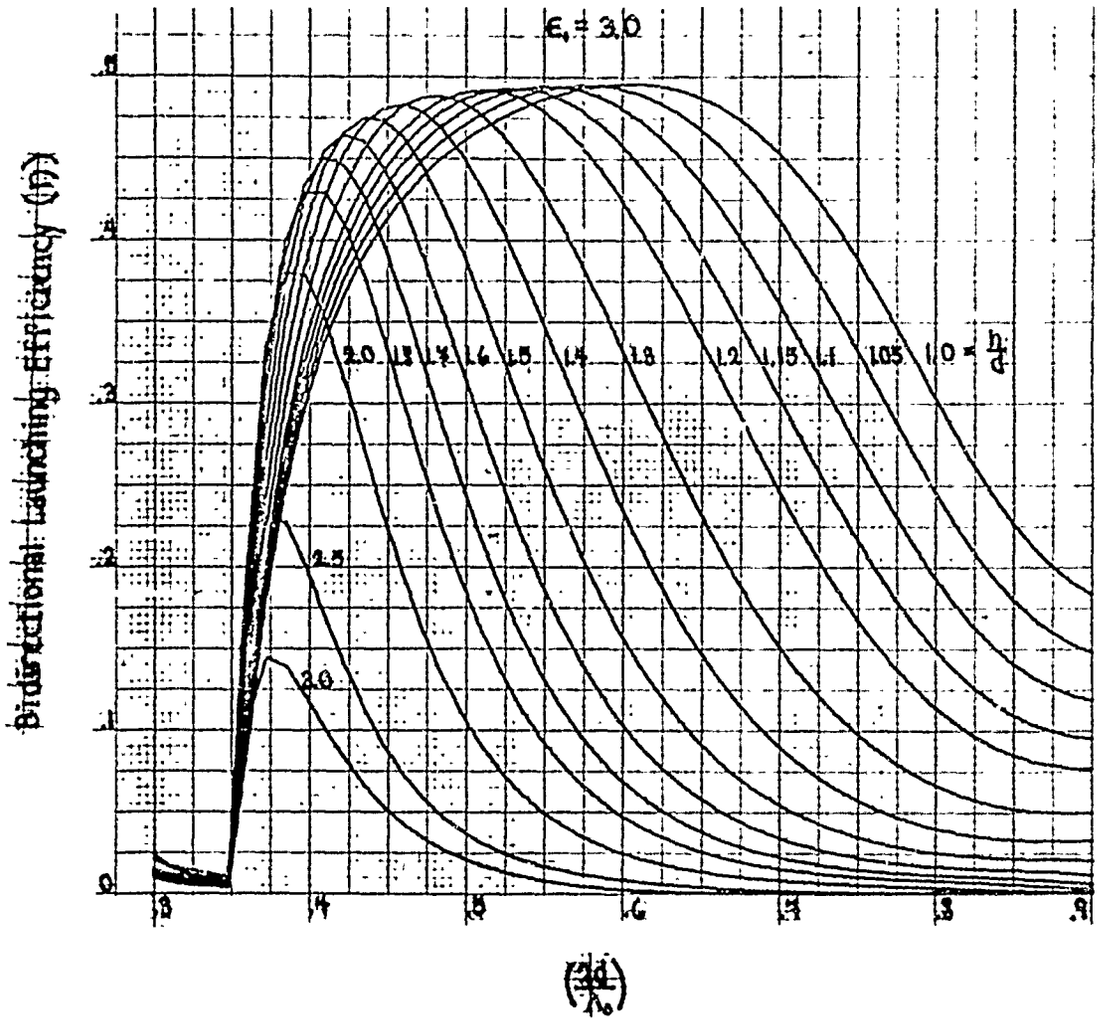

Figure G-5. Computer-generated plots of bidirectional efficiency as a function of dielectric slab thickness for various values of current filament location

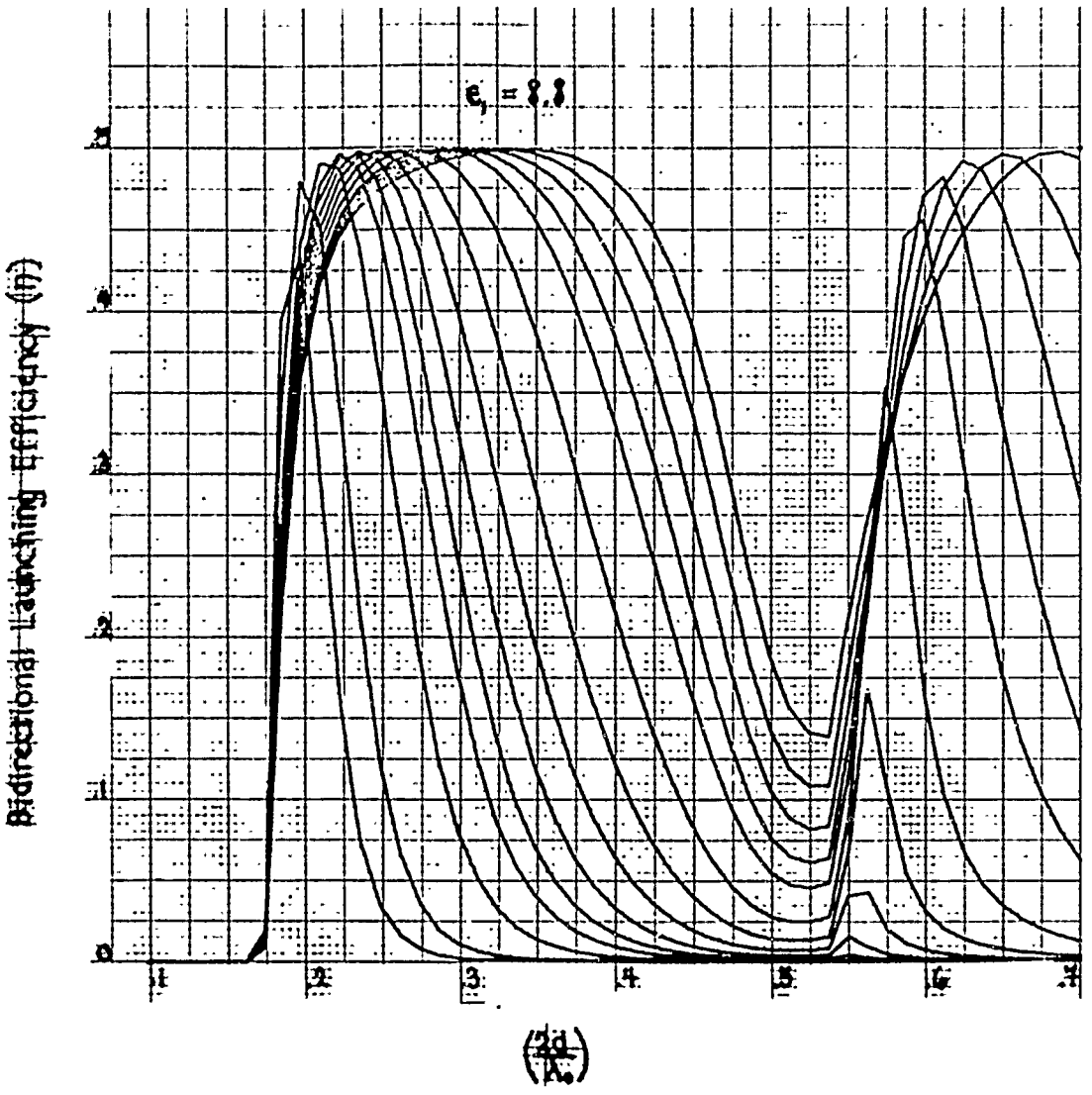

Figure G-6. Computer-generated plots of bidirectional efficiency as a function of dielectric slab thickness for various values of current filament location

experimental measurements verify the theoretical analysis. In addition, it was found that slot launching efficiency was essentially independent of ground plane dimensions." Excerpts from Reference 23 comparing theoretical and experimental efficiency are presented in Figure G-7.

It should be pointed out that Duncan's experiments were for a dielectric cylinder as opposed to a flat surface. Similar fields exist in both types of surface waveguides and it is believed that experimental results will be similar.

LAUNCHING EFFICIENCY OF WIRES AND SLOTS FOR A DIELECTRIC ROD WAVEGUIDE[24]

"This paper describes an experimental investigation of surface wave launching efficiency. Wires, rings and slots are considered as exciters of the HE_{11} mode on a dielectric rod image line. A formula is derived which relates the efficiency of a launcher to its impedance as a scatterer on the surface waveguide. Efficiency is obtained by using this formula and also by applying Deschamps' method for determining the scattering matrix coefficients of a two-port junction. Graphs are presented which illustrate the variation of efficiency with the dimensions of the launchers and with the parameter λ_g/λ, the ratio of the guide wavelength to the free space wavelength."

Again it should be pointed out that this paper deals with dielectric rod image line as opposed to a flat surface. As can be verified from the field equations, these surface waveguides are sufficiently similar to dielectric slab lines to yield similar experimental results.[1,2] Excerpts from DuHamel and Duncan are included in Figures G-8, G-9 and G-10.

---

[1] R. Collin, Field Theory of Guided Waves, New York: McGraw-Hill, 1960.

[2] Ramo, Whinnery and Van Duzer, Fields and Waves in Communication Electronics, New York: John Wiley & Sons, 1965.

[23] J.W. Duncan, "The Efficiency of Excitation of a Surface Wave on a Dielectric Cylinder," IRE Transactions on Microwave Theory and Techniques, pp. 257-268, April 1959.

[24] R.H. DuHamel and J.W. Duncan, "Launching Efficiency of Wires and Slots for a Dielectric Rod Waveguide," IRE Transactions of Microwave Theory and Techniques, July 1958.

(a)

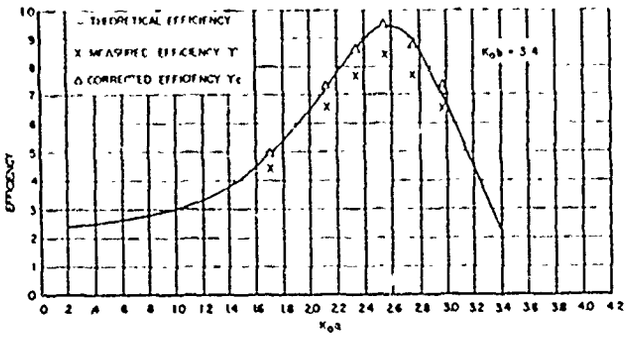

Comparison of the theoretical and measured excitation efficiency

(b)

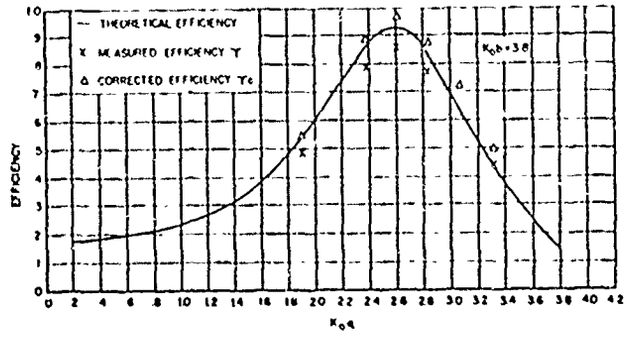

Comparison of the theoretical and measured excitation efficiency

Figure G-7. Comparing Theoretical and Measured Excitation Efficiency[23]

---

[23] J.W. Duncan, "The Efficiency of Excitation of a Surface Wave on a Dielectric Cylinder," IRE Transactions on Microwave Theory and Techniques, pp. 257-268 (April 1959).

(a)

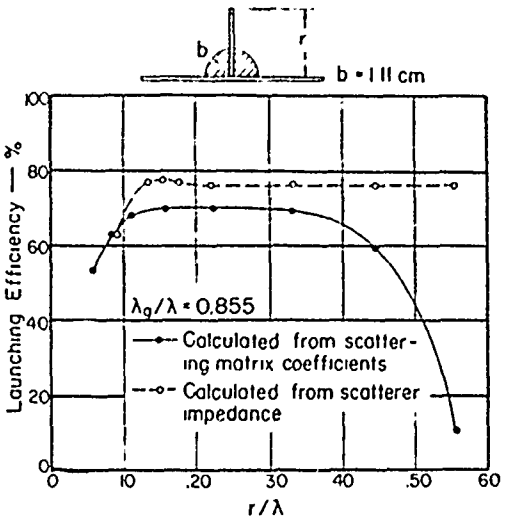

Launching efficiency of a vertical wire.

(b)

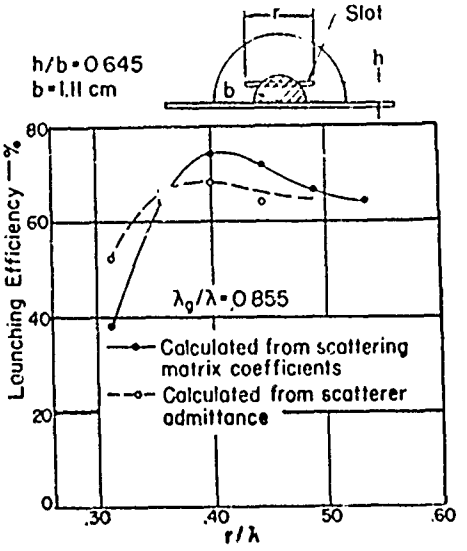

Launching efficiency of a horizontal slot above the ground plane.

Figure G-8. Excerpts from "Launching Efficiency of Wires and Slots for a Dielectric Rod Waveguide"[24]

[24] R.H. DuHamel and J.W. Duncan, "Launching Efficiency of Wires and Slots for a Dielectric Rod Waveguide," IRE Transactions of Microwave Theory and Techniques, July 1958.

(a)

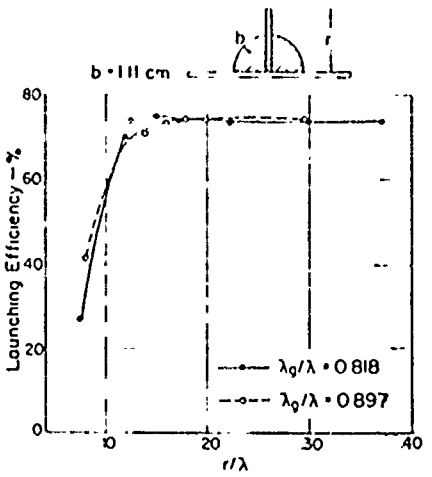

Launching efficiency of a vertical wire as a function of the normalized wire length.

(b)

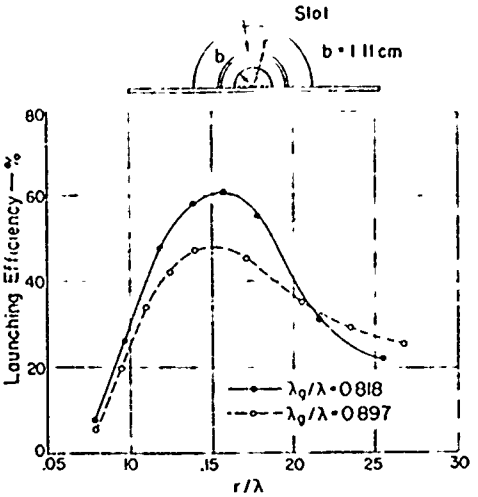

Launching efficiency of an annular slot as a function of the normalized slot radius.

(c)

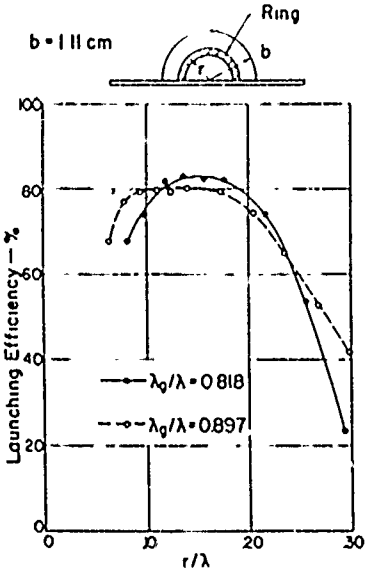

Launching efficiency of a ring as a function of the normalized ring radius.

(d)

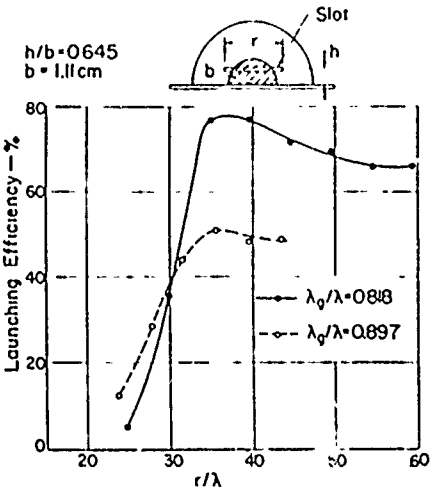

Launching efficiency of a horizontal slot as a function of the normalized slot length.

Figure G-9. Excerpts from "Launching Efficiency of Wires and Slots for a Dielectric Rod Waveguide" [24]

[24] R.H. DuHamel and J.W. Duncan, "Launching Efficiency of Wires and Slots for a Dielectric Rod Waveguide," IRE Transactions of Microwave Theory and Techniques, July 1958.

(a)

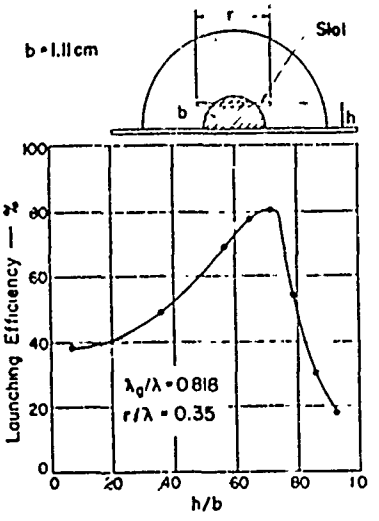

Launching efficiency of a resonant horizontal slot as a function of the normalized slot height.

(b)

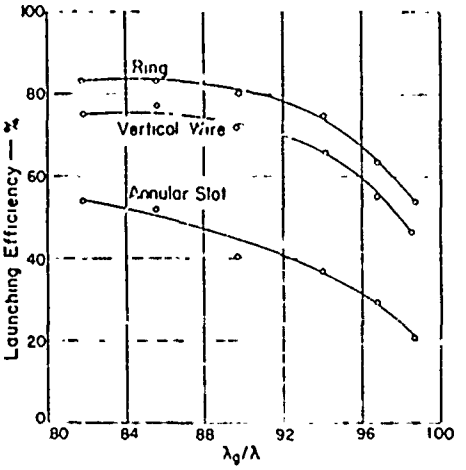

Launching efficiency of a resonant launcher as a function of the parameter λ_g/λ.

(c)

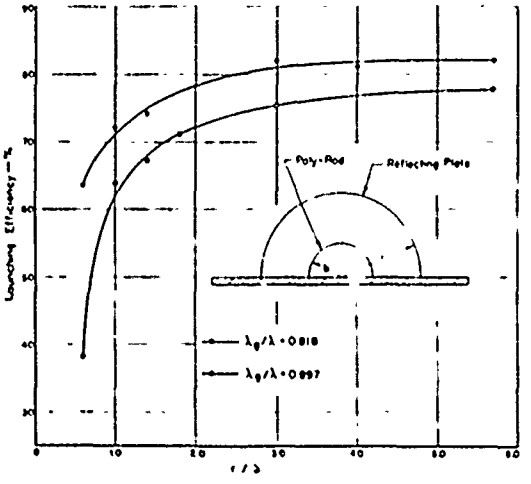

Launching efficiency of a ring exciter as a function of the normalized reflecting plate radius.

Figure G-10. Excerpts from "Launching Efficiency of Wires and Slots for a Dielectric Rod Waveguide"[24]

[24] R.G. DuHamel and J.W. Duncan, "Launching Efficiency of Wires and Slots for a Dielectric Rod Waveguide," IRE Transactions of Microwave Theory and Techniques, July 1958.

THE EXCITATION OF SURFACE WAVEGUIDES AND RADIATING SLOTS BY STRIP-CIRCUIT TRANSMISSION LINES [25]

"A variety of methods for coupling between a shielded strip-circuit transmission line, operating in the TEM coaxial mode, and a surface waveguide have been investigated. The arrangements include phased dipole arrays, series ground-plane slots and longitudinal slot excited probes. Impedance and matching conditions for each are discussed together with their relative efficiency and bandwidth. In the case of a single radiating slot, measurements on the effective equivalent circuit have been made as a function of the orientation angle of the slot with respect to the axis of the strip-line guide. Slots used ranged in length from 0.3 to 0.6 λ_g, having length/width ratios from 5 to 16".

Frost does not measure efficiency directly. Further study of Frost is required to determine the effectiveness of his methods of coupling. Frost's illustrations of his coupling techniques are in Figures G-11 and G-12.

---

[25] A.D. Frost and C.R. McGeoch and C.R. Mingins, "The Excitation of Surface Waveguides and Radiating Slots by Strip-Circuit Transmission Lines," IRE Transactions on Microwave Theory and Techniques, October 1956.

(a)

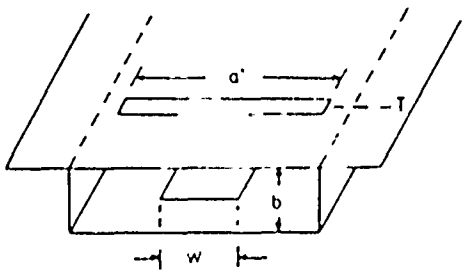

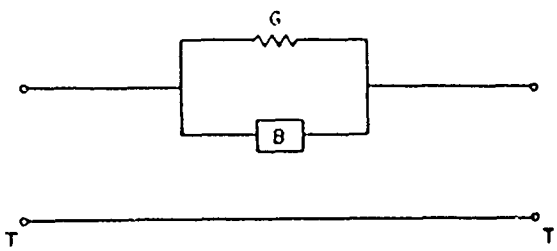

Transverse slot in equivalent strip-line guide with midplane equivalent circuit representation.

(b)

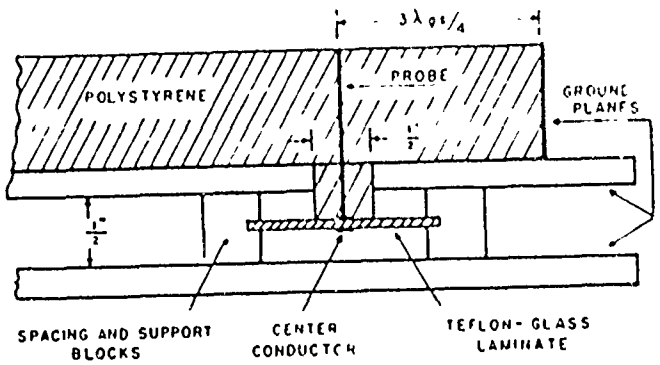

Sectional view through dielectric guide showing single single dipole coupling method.

Figure G-11. Excerpts from "The Excitation of Surface Waveguides and Radiating Slots by Strip-Circuit Transmission Lines" [25]

[25] A.D. Frost, C.R. McGeoch and C.R. Mingins, "The Excitation of Surface Waveguides and Radiating Slots by Strip-Circuit Transmission Lines," IRE Transactions on Microwave Theory and Techniques, October 1965.

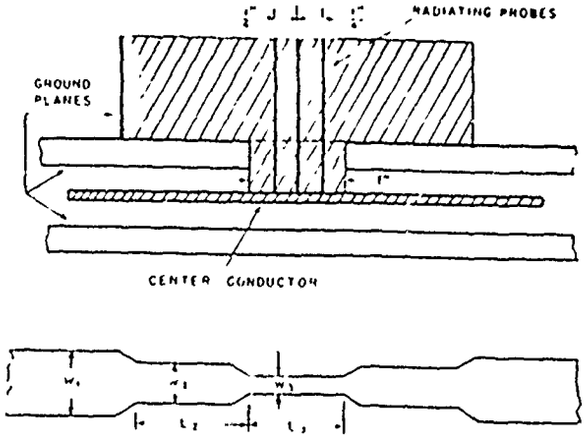

Sectional view through dielectric guide showing slot-probe coupling method and associated strip-line center conductor.

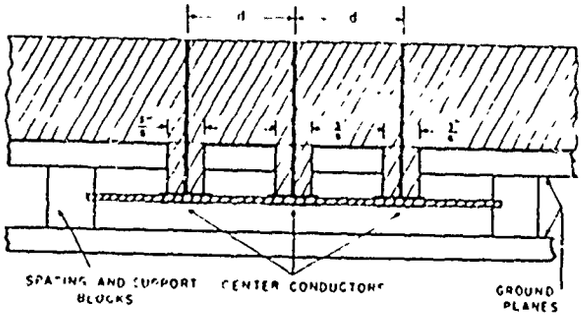

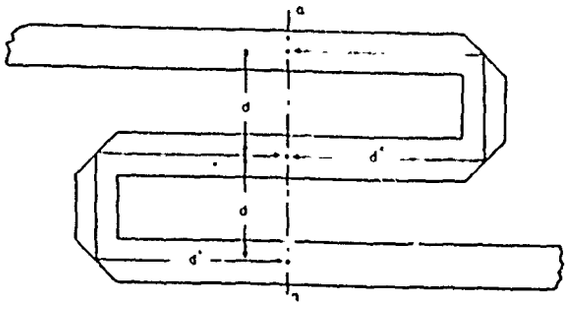

Sectional view through dielectric guide showing plane dipole array coupling method and associated strip-line center conductor.

Figure G-12. Excerpts from "The Excitation of Surface Waveguides and Radiating Slots by Strip-Circuit Transmission Lines" [25]

[25] A.D. Frost, C.R. McGeoch and C.R. Mingins, "The Excitation of Surface Waveguides and Radiating Slots by Strip-Circuit Transmission Lines," IRE Transactions on Microwave Theory and Techniques, October 1965.

APPENDIX H

BRIEF INTRODUCTION TO THE PHYSICS OF DIELECTRIC HEATING

Dielectric media such as ice and water are composed of highly polar molecules. In the presence of an applied electric field these molecules will rotate to align their axis of polarization with that of the applied field. If the applied field is alternating, the polarized molecules will attempt to follow the field by alternately rotating in synchronism with it. If the alternating frequency is low, the molecules have sufficient time to orient themselves in almost perfect alignment with the applied field. As the frequency is raised to the microwave band, the rotary motion of the molecules is not sufficiently rapid, due to viscous friction, to orient themselves in perfect alignment with the applied field, and energy is withdrawn from the applied field to overcome the friction which appears as heat. The direction of orientation of the molecules thus lags in time behind the applied field giving rise to an out or phase component.

Derivation of Loss Equation

If the applied microwave field is

$$E = E_1 \sin \omega t$$

the displacement current is

$$i_d = \frac{dD}{dt} = \varepsilon \frac{dE}{dt}$$

$$i_d = \varepsilon \omega E_1 \cos \omega t$$

If there were no loss in the dielectric, the displacement current would be in quadrature with the applied electric field, but, due to viscous friction, (requiring the dissipation of energy) the displacement current will not be exactly in quadrature with the applied field as illustrated below

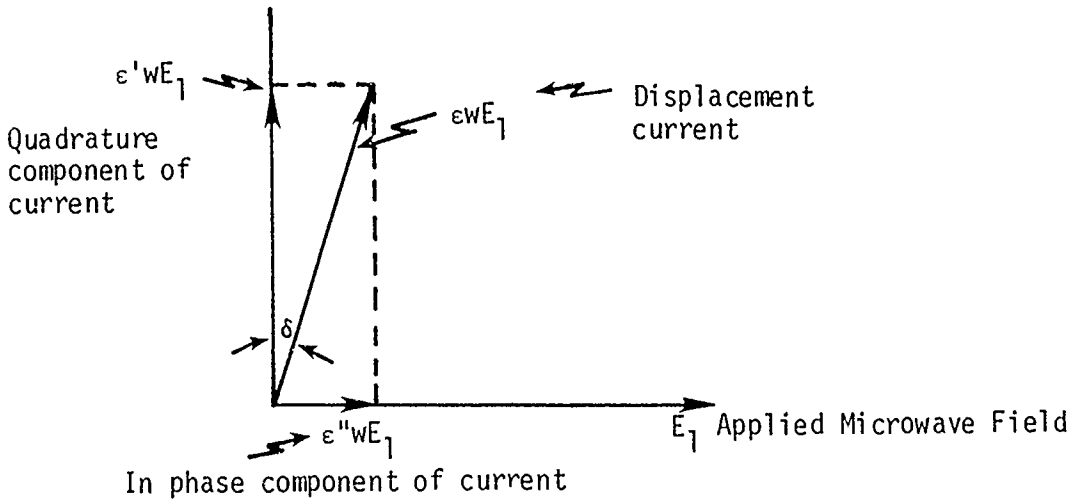

The displacement current may be thought to be composed of a quadrature component and an in-phase component. The dielectric constant may be defined as a complex quantity

$$\varepsilon \equiv \varepsilon' + j\varepsilon''$$

and the ratio of the imaginary part to the real part may be defined as the loss tangent

$$\tan\delta \equiv \frac{\varepsilon''}{\varepsilon'}$$

The power dissipated in the dielectric per unit volume is from the above diagram

$$W_d = \frac{E_1^2}{2}\omega\varepsilon'' = \frac{E_1^2}{2}\omega\varepsilon'\tan\delta$$

$$W_d = \sigma\frac{E_1^2}{2}$$

where $\sigma \equiv \omega\varepsilon'\tan\delta$ = conductivity of dielectric